

https://dspace.org/

Characterising skeletopathy in an animal model of Type 2 diabetes

Dlamini, Gcwalisile Frances

2024

https://hdl.handle.net/10539/37571

Downloaded from a DSpace repository. https://dspace.org/

CHARACTERISING SKELETOPATHY IN AN ANIMAL MODEL OF TYPE 2 DIABETES

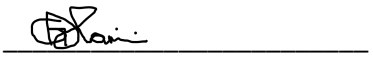
Gcwalisile Frances Dlamini

A thesis submitted to the Faculty of Health Sciences, University of the Witwatersrand, Johannesburg, in fulfilment of the requirements for the degree of Doctor of Philosophy

Johannesburg, November 2022

DECLARATION

I, Gcwalisile Frances Dlamini declare that this dissertation entitled “Characterising skeletopathy in an animal model of type 2 diabetes” is my own work. It is being submitted for the Degree of Doctor of Philosophy at the University of the Witwatersrand, Johannesburg. It has not been submitted before for any degree or examination at any other University.



10 November 2022

Gcwalisile Frances Dlamini **Date**

CONFERENCE PRESENTATIONS

1. Ndou, R., **Dlamini,** G.F., The Zucker Diabetic Sprague Dawley (ZDSD) rat as a translational rodent model of type 2 diabetes. IFAA Aug 2022 Turkey (Online)

2. **Dlamini G** and Ndou R Osteoblastogenesis and osteolysis in the Zucker Diabetic Sprague Dawley rat humerus head. Submitted to Ana Hist Embryo, 2022. (BMJD), Bangkok Thailand, 08 - 10, Nov 2018

3. Dangarembizi, R.,S. Nkosi,**G.S. Dlamini,** R. Ndou The Zucker Diabetic Sprague Dawley rat: A potential model for investigating mechanisms underlying the development of Type 2 Diabetic skeletopathy ASSA Johannesburg, 2018,

SUBMITTED ARTICLE

1. **Dlamini G** and Ndou R Osteoblastogenesis and osteolysis in the Zucker Diabetic Sprague Dawley rat humerus head. Submitted to Ana Hist Embryo, 2022

ABSTRACT

Type two diabetes (T2D) is a chronic, progressive heterogonous syndrome with a genetic and environmental origin. It is now recognized as an epidemic with a high morbidity and mortality rate. The endocrinology of type 2 diabetes (T2D) and its predisposing factors have been studied extensively, while diabetic skeletopathy has received negligible research. Previous studies report that fractures in T2D vary with specific sub regions in bones, therefore prompting our study to focus mainly on the femoral head and neck as well as the humerus head. Femoral neck fractures are the commonest, followed by the proximal femur, distal radius and proximal humerus.

Susceptibility to fracture is a sequelae of poor bone remodeling. Poor bone remodeling is established at molecular and cellular levels. It depends on the activity of osteoblasts, osteocytes and osteoclasts, which are under the influence of TGF-β1, a pro-osteogenic cytokine, together with BMP3, an anti-osteogenic cytokine.T2D induced bone marrow adipocity and the accumulation of AGEs in cortical bone have also been implicated in increasing susceptibility to fracture. It is still unclear how T2D affects molecular and cellular elements that culminate in weaker bones observed in diabetic patients. In addition, it is debatable if T2D affects the skeleton at disease onset or later in the disease. Therefore, this study aimed to characterize T2D induced skeletopathy and related it to age, in the Zucker Diabetic Sprague Dawley (ZDSD) rat, using the femur and humerus.

This study initially confirmed the diabetic state by monitoring animal weights, fasting blood glucose levels, and fasting oral glucose tolerance tests (OGTTs) every fortnight. Then triglyceride levels and quantified serum levels of osteoregulatory hormones such as insulin and osteocalcin were monitored. To assess oxidative stress, Malondialdehyde (MDA) serum levels were also determined by ELISA.

Once diabetes was successfully induced, rats were grouped according to strain and age at termination. Termination age was at 20 weeks and 28 weeks . The Sprague Dawley (SD) rats were

the controls, while the Zucker Diabetic Sprague Dawley rats (ZDSD) were the experimental groups. These were designated as SD20WK (n=8) and ZDSD20WK (n=7) respectively. Another batch was designated as SD28WK (n=8), and ZDSD (n=15) that were terminated at 28 weeks of age. The latter were further divided into moderate diabetes (ZDSD28WK-MOD) (n=9) and severe diabetes (ZDSD28WK-SVD) groups (n=6).

Bilateral humeri and femora were harvested then fixed in 10% buffered formalin. Right proximal femora and humeri were scanned using a 3D-μCT scanner (Nikon XTH 225L) to analyse trabecular morphometric parameters, cortical bone area and medullary canal area. Biomechanical strength was analyzed by three point bending tests using a universal tensile tester. Left proximal femora and humeri were processed for histology. Some sections were stained with Haematoxylin and Eosin (H&E) to assess normal histologic morphology and adipocyte quantification. Remnant sections were immunolabelled using the anti-TRAP and anti-ALP antibodies for osteocyte and osteoblast quantification respectively, to assess osteolysis and osteogenesis. Immunolocalization of AGEs, TGF-β1 and BMP3 was also conducted to investigate their role in diabetic skeletopathy.

We found that diabetes affected osteoblastogenesis as measured by ALP positive cells and bone marrow adipocytes. TRAP positive osteocytes numbers were increased in the presence of T2D, suggesting an increased osteolysis. There was reduced TGFB1 expression with increased BMP3 expression. The number of AGEs immuno-positive cells as well as its extracellular expression was increased. Our finding suggest that osteoblast and osteocyte numbers are regulated by TGFβ1 and BMP3 in both bones, under the influence of AGEs.

Our findings from osteometry, 3-point bending tests and Micro CT support that diabetes weakens bone. The diabetic effect results in lighter, shorter hollow bones that perform poorly under loading, as well as exhibit unfavourable trabeculae microarchitecture. Our findings confirm that T2D causes increased fragility in the proximal femur and humerus as well the mid-diaphysis. These perturbations occur early and late in the disease, and they are also exacerbated by the presence of hyperglycemia.

We conclude that the ZDSD rat can be used as a translational model for diabetic skeletopathy at cellular and molecular level, and it can be extrapolated to humans after consideration of other factors like, basal metabolism, age, sex and skeletal loading patterns. We recommend optimal control of blood glucose levels at all stages of the disease to reduce the incidence of fractures in diabetic patients.

ACKNOWLEDGEMENTS

It has been a long arduous journey I must say, albeit a rich learning experience on a personal and scientific spectrum. I would like to stand on the podium and acknowledge each and every person that offered their unconditional support during this journey.

My profound appreciation to my supervisor Prof Ndou, who literally held my hand, took me one step at a time, to the summit of the mountain that I now proudly stand on. Thank you for your support, your time, your vast knowledge, and most importantly your patience with me. Your guidance through this conundrum, quagmire and quicksand called scientific research and writing, is greatly appreciated.

Once more my appreciation is extended to Mrs Ali for her technical assistance in the laboratory, as well as Mr Vaughan Perry for assisting with Micro-CT analysis.

My appreciation to my friends Dudu, Gugu, Tshidi, Sif and Zandi. Thank you for your words of encouragement and support. My sister Dr SH Dlamini and hubby, Dr TC Tshepuwane for allowing me access to their house and gadgets as I navigated my way through the jungle of scientific research.

My most profound appreciation and love to my 'tribe', my children, Wawa, Nono, Una, Kusa, Stra and our four legged housemates Polka and Dot. Thank you for your understanding and patience when I had no time for you. Thank you Nono for being my 'Picasso', the illustrations and artwork are as beautiful as you are.

Lastly I thank God for the dahlias, petunias, roses, marigolds, arum lilies, tiger lilies and green grass that reside in my garden, as well as the hoopoes, red bishops, weaver birds, sparrows, hadidas, grey louries, common mynas and mouse birds that visited me, I derived much needed calm, pleasure and respite as I sat amongst these to reflect and write. Thankyou Lord. It is done.

TABLE OF CONTENTS

DECLARATION		ii
PRESENTATIONS AND PUBLICATIONS		iii
ABSTRACT		iv
ACKNOWLEDGEMENTS		vii
LIST OF FIGURES		ix
LIST OF TABLES		xi
LIST OF ABBREVIATIONS		xiii
CHAPTER 1	Introduction, Literature Review, Aims and Objectives	4
CHAPTER 2	Confirmation of diabetes	33
CHAPTER 3	Tensile strength and microarchitecture in the ZDSD rat femur	56
CHAPTER 4	Type 2 diabetes affects structural and material properties of bone in the ZDSD humerus.	84
CHAPTER 5	Osteoblast and osteocyte numbers are regulated by TGFβ1 and BMP3 in the Zucker Diabetic Sprague Dawley rat femoral head and neck	107
CHAPTER 6	Interaction of AGEs with TGFβ1 and its antagonist BMP3 in diabetes affects osteoblastogenesis and osteolysis in the Zucker Diabetic Sprague Dawley rat humerus head	140
CHAPTER 7	General discussion and conclusions	160
REFERENCES		166
APPENDICES		176

LIST OF FIGURES

Figure	Title	Page
Figure 1.1	Lipid peroxidation process	15
Figure 1.2	Macroscopic and microscopic features of bone	17
Figure 1.3	Stages in bone remodelling	20
Figure 1.4	TGFβ1 and BMP signalling pathway	25
Figure 1.5	A Force dispacement curve and 3- point bend instrument	27
Figure 2.1	Schematic presentation of study design	39
Figure 2.2	Changes in body mass from 13 to 20 weeks of age	40
Figure 2.3	Changes in body mass from 13 to 28 weeks of age	41
Figure 2.4	Oral glucose tolerance test and AUC at 20-weeks	42
Figure 2.5	Oral glucose tolerance test and AUC at 28-weeks	43
Figure 2.6	Fasting blood glucose at 12 to 20 weeks	44
Figure 2.7	Fasting blood glucose at 12 to 28 weeks	45
Figure 2.8	Serum insulin concentration	46
Figure 2.9	Blood triglyceride concentrations	47
Figure 2.10	Serum osteocalcin concentrations	48
Figure 2.11	MDA serum concentration	49
Figure 3.1	Three-dimensional reconstruction of a femoral head and neck showing parts that were investigated	58
Figure 3.2	Three-dimensional reconstruction of a femur showing various femoral head and neck diameters measured	58
Figure 3.3	Three-point bending test instrument	60
Figure 3.4	Illustration of predicted predicted group membership	75
Figure 4.1	Three-dimensional reconstruction of a humerus showing the parts that were investigated	86
Figure 4.2	Illustration of predicted predicted group membership	100
Figure 5.1	Head of the femur regions of interest	111
Figure 5.2	Adipocytes in the femoral head	113
Figure 5.3	Femoral head general histological appearance	114
Figure 5.4	Adipocytes in the femoral neck	115
Figure 5.5	Femoral neck general histological appearance	115
Figure 5.6	TRAP immunopositive cells quantity in the femoral head	116
Figure 5.7	Femoral head TRAP Immunopositive osteocytes	117
Figure 5.8	TRAP immunopositive cells in the femoral neck	118
Figure 5.9	Femoral neck TRAP Immunopositive osteocytes	119

Figure 5.10	ALP immunopositive cells quantity in the femoral head	120
Figure 5.11	Femur ALP Immunopositive osteoblasts	121
Figure 5.12	ALP immunopositive cells quantity in the femoral neck	122
Figure 5.13	Femur TGFβ1 immunopositivity grading	123
Figure 5.14	Femur BMP3 immunopositivity grading	126
Figure 5.15	Advanced glycation end products (AGEs) immunopositive cells quantity in the femoral head	128
Figure 5.16	Femoral head AGEs immunopositive cells	129
Figure 5.17	Advanced glycation end products (AGEs) immunopositive cells quantity in the femoral neck	130
Figure 5.18	Femur AGEs immunopositivity grading	130
Figure 6.1	Head of the humerus regions of interest	144
Figure 6.2	General histology and relative adipocyte infiltration in the humerus head	145
Figure 6.3	Number of adipocytes in the humerus head	146
Figure 6.4	TRAP immunopositive cells quantity in the humerus head	147
Figure 6.5	Humerus TRAP Immunopositive osteocytes	148
Figure 6.6	ALP immunopositive cells quantity in the humerus head	149
Figure 6.7	Humerus ALP Immunopositive osteoblasts	150
Figure 6.8	Humerus TGFβ1 Immunopositivity graded	151
Figure 6.9	Humerus BMP3 Immunopositivity graded	152
Figure 6.10	AGEs immunopositive cells in the humerus head	153
Figure 6.11	Humerus AGEs immunopositivity	154
Figure 6.12	Humerus AGEs Immunopositivity grading	155

LIST OF TABLES

Table	Description	Page
Table 1.1	Glucoregulatory hormones and their functions	13
Table 3.1	Scanning parameters at wee-20 and week-28	57
Table 3.2	Femur osteometric parameters	59
Table 3.3	Femur trabecular assessment parameters	59
Table 3.4	Osteometric measurements of the femur	62
Table 3.5	Osteometric measurements of the femoral midshaft	63
Table 3.6	Osteometric measurements of the femoral head and neck	65
Table 3.7	Three-point bend assessment of the femur for maximum force, break force, and yield force	66
Table 3.8	Three-point bend assessment of the femur for maximum time and maximum displacement	67
Table 3.9	Three-point bending assessment of the femur for stiffness and elastic modulus	68
Table 3.10	Micro-CT evaluation of the proximal femur at week-20 and week-28 (BV, BV/TV)	69
Table 3.11	Micro-CT evaluation of the proximal femur at week-20 and week-28 (TbTh, TbN, TbSp)	70
Table 3.12	Femur cortical area and medullary canal at week-20 and week-28	71
Table 3.13	Discriminant function analysis of the femur	73
Table 3.14	Discriminant function analysis of predicted group membership	74
Table 4:1	Scanning parameters at 20 weeks and 28 weeks	85
Table 4.2	Humerus osteometric parameters	86
Table 4.3	Humerus assessment parameters by micro-CT	87
Table 4.4	Osteometric measurements of the humerus (mass, full length, epicondylar breadth, humerus head width)	89
Table 4.5	Osteometric measurements of the humerus (mid shaft AP, ML diameter, robusticity index	91
Table 4.6	Whole bone biomechanical properties of the humerus loaded in 3-point bending (maximum force, break force, yield force)	92
Table 4.7	Whole bone biomechanical properties of the humerus loaded in 3-point bending (maximum time, maximum displacement, stiffness, elastic modulus)	94
Table 4.8	Micro-CT measurement of the humerus (BV, BV/TV)	95
Table 4.9	Micro-CT measurement of the humerus (TbTh, TbN, TbSp)	96

Table 4.10	Micro-CT measurement of the humerus (cortical area, medullary canal area)	97
Table 4.11	Discriminant function analysis of the humerus	98
Table 4.12	Discriminant function analysis of predicted group membership	99
Table 5.1	Femoral head TGFβ1 immunopositivity	123
Table 5.2	Femoral neck TGFβ1 immunopositivity	124
Table 5.3	Femoral head BMP3 immunopositivity	125
Table 5.4	Femoral neck BMP3 immunopositivity	126
Table 5.5	Femoral head AGEs immunopositivity	130
Table 5.6	Femoral neck AGEs immunopositivity	131
Table 6.1	Humerus TGFβ1 immunopositivity	151
Table 6.2	Humerus BMP3 immunopositivity	152
Table 6.3	Humerus AGEs immunopositivity	155

LIST OF ABBREVIATIONS

%:	Percentage
β:	Beta
db/db:	diabetes gene
dl:	decilitre
^{0}C:	degree celsius
g:	gram
kg:	kilogram
mm:	millimetres
mm^2:	millimetres squared
mm^3:	millimetres cubed
mmol/L:	millimole per litre
mg/dl:	milligrams per decilitre
ng/ml:	nanograms per millilitre
nmole/µL:	nanomole per microlitre
µm:	micrometre
N:	Newtons
N/mm:	Newtons per milimetre
N/mm^2:	Newtons per millimetre squared
ob/ob:	obese gene
Sec:	seconds
3D-µCT:	3 Dimensional Micro-focus X-ray Computed Tomography
AESC:	Animal Ethics Committee
AGEs:	Advanced Glycation End products
AIDS:	Acquired Immunodeficiency Syndrome
ALK5:	Anaplastic Lymphoma Kinase receptor 5
ALP:	Alkaline Phosphate
ANOVA:	Analysis of variance
AP:	Antero-posterior
AUC:	Area Under the Curve
BMD:	Bone mineral density
BMP:	Bone morphogenetic protein
BMP3:	Bone morphogenetic protein-3
BMU:	Basic multicellular units
BV/TV:	Bone tissue volume to total volume
BV:	Bone tissue volume
CAS:	Central Animal Services
CNS:	Central Nervous System
DAB:	3-3’ di-aminobenzidine
DXA:	Dual X-ray Absorptiometry
ECM:	Extra cellular matrix

EDTA:	Ethylenediamine tetraacetic acid
ELISA:	Enzyme Linked Immunosorbent Assay
FBG:	Fasting blood glucose
Fig:	Figure
FRAX:	Fracture prediction tool
GCT:	Glucose Challenge Test
GK:	Goto-Kakizaki
GLP-1:	Glucagon-like peptide 1
H&E:	Hematoxylin and Eosin
HIV:	Human Immunodeficiency Virus
HO^-:	Hydroxide ion
$HO_{2:}$	Hydroperoxyl
IDF:	International Diabetes Federation
LPO:	Lipo-oxidation end products
LSD:	Least significant difference
MDA:	Malondialdehyde
MetS:	Metabolic syndrome
ML:	Medio-lateral
MODY:	Maturity onset diabetes of the young
mRNA:	Messenger ribonucleic acid
MSC:	Mesenchymal stem cell
OGTT:	Oral Glucose Tolerance Test
PBS:	Phosphate buffer solution
PHF:	Proximal humerus fracture
PTH:	Parathyroid Hormone
RAGE:	Receptor for AGEs
ROI:	Region of interest
R-Smads:	Receptor Suppressor of Mothers against Decapentaplegic
SD:	Sprague Dawley
SD20WK:	20 Week old SDs
SI:	Supero-inferior
SMAD:	Suppressor of Mothers against Decapentaplegic
T0:	Time zero
T2D:	Type 2 diabetes
TbN:	Trabecular number
TbSp:	Trabecular spacing
TbTh:	Trabecular thickness
TGFβ:	Transforming growth factor beta
TGFβ1:	Transforming growth factor beta-1
TRAP:	Tartrate Resistant Alkaline Phosphatase
TβRI:	TGFβ type one receptor

TβRII:	TGFβ type two receptor
WHO:	World Health Organisation
ZDF:	Zucker Diabetic Fatty
ZDSD:	Zucker Diabetic Sprague Dawley
ZDSD20WK:	20 Week old ZDSDs
ZDSD28WK-MOD:	Moderately diabetic 28 week old ZDSDs
ZDSD28WK-SVD:	Severely diabetic 28 week old ZDSDs

Chapter 1

Introduction, Literature review, Aims and Objectives

CONTENTS

1.0 Introduction 4

1.1 Background to the study 4

1.2 Literature review 7

1.2.1 Diabetes 7

Type 1 diabetes ..... **Error! Bookmark not defined.**

Type 2 diabetes 7

1.2.2 History of diabetes 8

Understanding T2D pathophysiology in the last century 8

Insulin discovery 9

Distinguishing between Types 1 and 2 diabetes 9

1.2.3 Prevalence of T2D 10

Worldwide prevalence 10

T2D Prevalence in SA and its associated health burden 11

1.2.4 Abnormal glucose homeostasis as a precursor to T2D 12

1.2.5 Pathogenesis of T2D 13

1.2.6 Lipid peroxidation process 13

1.2.7 Increased skeletal fractures in T2D 15

1.2.8 Long bone structure and function 15

Cortical bone 17

Trabecular, cancellous or spongy bone 18

1.2.9 Bone remodeling 18

1.2.10 Effect of T2D on bone remodeling cells (osteocytes, osteoblasts, osteoclasts and adipocytes) 19

Osteocytes ..... **Error! Bookmark not defined.**

Adipocytes 20

Hormonal control of bone remodeling 21

1.2.11 Transforming growth factor beta (TGF-β) superfamily, from ligand to transcription for osteogenesis 22

Osteogenic cytokine TGF-beta 1 23

BMP subfamily and its antagonist BMP3 23

Anti-osteogenic cytokine BMP3 24

1.2.12 Advanced glycation end products (AGEs) affect bone homeostasis and biophysical properties 25
1.2.13 Effect of T2D on biomechanical properties of bone 25
1.2.14 Trabecular bone morphometry in T2D using 3-D micro-CT 26
1.3 Aim 28
1.4 Objectives: 28

1.0 INTRODUCTION

1.1 Background to the study

Diabetes is a chronic condition characterized by sustained hyperglycemia resulting from a syndrome of metabolic disorders (Care, 2019). In 2019, the global diabetes prevalence was estimated to be 9.3% (463 million people), expected to rise to 10.2% (578 million) by 2030 and 10.9% (700 million) by 2045 (Saeedi et al., 2019; Sun et al., 2022). Although initially prevalent in adults, it now affects adolescents and children, more especially in obese populations (Reinwald et al., 2009; Peterson et al., 2015; Cousin et al., 2022). The mortality rate is approximately 5 million annually (Cho et al., 2018). Diabetes is classified into several subtypes such as gestational, type 1, type 2, with the latter being most common at 90-95% of all those diagnosed with diabetes (Care, 2019). Although T2D is a preventable non-communicable disease, it causes a huge financial burden on health and social services especially in developing countries (Blakytny et al., 2011) due to its complications which require multidisciplinary treatment and management.

Complications arising from T2D affect multiple organs, resulting in cardiovascular disease (Hamann et al., 2011), retinopathy (Peterson et al., 2015), polyneuropathy (Starup-Linde and Vestergaard, 2016), nephropathy (Hamann et al., 2011) and skeletopathy (Reinwald et al., 2009; Hamann et al., 2011). Well known skeletal complications of T2D are Charcot's neuro-arthropathy, diabetic foot syndrome and more recently recognized, diabetic skeletopathy (Hamann et al., 2011). Despite evidence pointing towards the link between hyperglycemia and susceptibility to osteoporosis, fractures, mal-unions and non-unions (Bonds et al., 2006; Hamann et al., 2011), diabetic skeletopathy has received negligible research (Hamann et al., 2011; Oei et al., 2013). Skeletopathy is largely a result of compromised skeletal integrity at a physical and cellular as well as molecular level. Skeletal integrity is dependent on a tightly regulated bone homeostasis by:

(i) Bone turnover cells osteocytes, osteoblasts, osteoclasts (Booth et al., 2013).

(ii) Osteoregulatory hormones (parathyroid hormone, osteocalcin, and insulin (Neer et al., 2001; Ferland-McCollough et al., 2018; Ducy, 2020).

(iii) Glycemic levels as they contribute towards bone marrow adiposity (Piccinin and Khan, 2014).

(iv) Molecules such as advanced glycation end products (AGEs) (Kislinger et al., 1999; Piccinin and Khan, 2014; Singh et al., 2015) and malondialdehyde (MDA) (Del Rio et al., 2005; Tiwari et al., 2013), are elevated in T2D.

(v) The osteogenic cytokine, transforming growth factor beta-1 (TGFβ1) (Wang et al., 2018) and its antagonist bone morphogenetic protein-3 (BMP-3) (Wu et al., 2016).

Although research links T2D with compromised bone integrity, there is debate about data that points to this link (Hamann et al., 2011). This is possibly due to a lack of an appropriate animal model. Most animal studies have used various animal models such as the Goto-Kakizaki (GK) rat, a non-obese model (Castrillón et al., 2011), mouse models (db/db, ob/ob) (Chandrasekera and Pippin, 2014; Peterson et al., 2015), the Zucker Diabetic Fatty rat (ZDF) (Prisby et al., 2008; Chandrasekera and Pippin, 2014; Peterson et al., 2015) and the Zucker Diabetic Sprague Dawley (ZDSD) rat (Reinwald et al., 2009; Peterson et al., 2015). The ZDF has been a gold standard for a while but its disadvantage is that it becomes diabetic before it reaches skeletal maturity in contrast to the ZDSD rat (Fajardo et al., 2014; Peterson et al., 2015).

The widely used ZDF rat undergoes monogenetic mutations of leptin and its receptor, inducing hyperphagia that triggers hyperglycemia (Fajardo et al., 2014),and a propensity to pancreatic beta cell failure (Peterson eta al., 2015). While this results in diabetes, it often occurs prior to skeletal maturity in this rat model (Fajardo et al., 2014). Considering that leptin gene mutations are rare in humans, this makes such an animal model of diabetes inappropriate for skeletal studies (Peterson et al., 2015). In contrast, the ZDSD rat mimics a phenotype and disease progression pattern like humans whereby they develop pre-diabetic metabolic syndrome, insulin resistance and T2D diabetic complications just as in humans (Peterson et al., 2015). All this occurs without altering the leptin gene and skeletal maturity timelines in the ZDSD.

In this study, skeletal integrity is investigated using this relatively recent translational animal model of T2D, the Zucker Diabetic Sprague Dawley (ZDSD). To investigate how diabetes compromises bone quality at mechanical, cellular and molecular level, several investigative methods are undertaken. We started by monitoring body mass, fasting blood glucose levels, Oral

Glucose Tolerance Tests (OGTT) to confirm diabetes. How diabetes affected serum levels of osteoregulatory hormones osteocalcin and insulin is assessed by ELISA. The study then, employed histological means to assess trabeculae morphology and bone adiposity. We evaluated bone microarchitecture by Micro-focus X-ray Computed Tomography (Micro CT) and bone biomechanical strength was evaluated by 3-point bending tests. We then investigated how T2D affected osteolysis and osteoblastogenesis, by quantifying Tartrate Resistant Alkaline Phosphatase (TRAP) immunopositive osteocytes, and Alkaline Phosphatase (ALP) immunopositive osteoblasts respectively. The expression of the pro-osteogenic growth factor TGF-β1, and the anti-osteogenic cytokine, BMP-3 were investigated by immunohistochemistry. Finally, the intracellular and extracellular expression of advanced glycation end products (AGEs) was determined by immunohistochemistry.

1.2 LITERATURE REVIEW

1.2.1 Diabetes mellitus

Diabetes is a chronic progressive syndrome of metabolic disorders (Ozougwu et al., 2013; Hurtado and Vella, 2019), characterized by chronic hyperglycemia (Ozougwu et al., 2013). It emanates from multifactorial causes such as a sedentary lifestyle, high carbohydrate diet (Kohei, 2010) as well as genetic predisposition (Scheen, 2003). This condition exists in multiple forms (Care, 2019) that can be classified into: (i) Type 1 diabetes; (ii) Type 2 diabetes; (iii) Gestational diabetes that occurs in the third trimester when there was no prior diagnosis of diabetes; (iv) Other forms of diabetes such as neonatal, maturity onset diabetes of the young (MODY), pancreatic disease origin (pancreatitis, cystic fibrosis), organ transplant induced, or chemically induced (glucocorticoids, HIV/AIDS antivirals). The most common of these are Types 1 and 2 diabetes (Care, 2019).

T1D

Type 1 diabetes (T1D) is an autoimmune reaction to pancreatic islet cell proteins leading to their destruction and subsequent insulin deficiency (Holt, 2004; Zaccardi et al., 2016). This type has approximately 9.5% prevalence (Mobasseri et al., 2020). Autoantibodies may be directed at pancreatic beta cells (i) cytoplasmic proteins (ii) surface antigens (iii) antigens such as anti-insulin antibodies and glutamic acid decarboxylase (Ozougwu et al., 2013). Autoimmune destruction of these pancreatic beta cells leads to islet atrophy, with subsequent reduced insulin production (Ozougwu et al., 2013).

T2D

Between 90 and 95% of diagnosed diabetes is classified as T2D (Care, 2019). Its etiology is linked to multiple risk factors such as obesity, age, ethnicity, genetic predisposition, and history of gestational diabetes, smoking, heavy alcohol consumption, and metabolic syndrome (Kohei, 2010; Ozougwu et al., 2013; Zaccardi et al., 2016; Zheng et al., 2018; Care, 2019; Hurtado and Vella, 2019). T2D exhibits a multistage progression that begins with insulin resistance prior to hyperinsulinemia which compensates for the tissue resistance (Scheen, 2003), although

normoglycemia is maintained (Zheng et al., 2018). This stage is followed by pancreatic beta cell failure and apoptosis, until severe uncontrollable hyperglycemia ensues (Del Prato, 2009).

1.2.2 History of diabetes

Several researchers report how diabetes has evolved over the past 400 years (DOBSON, 1967; Jorgens, 2006; Polonsky, 2012; Lakhtakia, 2013; Blaslov et al., 2018; Zheng et al., 2018). As narrated by Baslov et al., (2018) and Polonsky K, (2012) its initial discovery was in 1552 B.C by ancient Egyptians. It was first described as a disease that is characterized by polyuria, emaciation and death. Other authors report the initial discovery of diabetes in the 1600s as a disease with an excessively sweet tasting urine (Minkowski, 1890; Polonsky, 2012; Lakhtakia, 2013; Zaccardi et al., 2016).

The term 'diabetes insipidus' is derived from the Greek language 'diabainen' which means 'to go through' implying excessive passing of urine by the kidneys, and the Latin word 'insapere' meaning tasteless (DOBSON, 1967; Zajac et al., 2010). The term 'diabetes mellitus' meaning 'honey' and 'siphon' was later introduced by Greek physician Aretaeus, to reflect the sweet taste of urine (Blaslov et al., 2018). In the 1600s the term 'mellitus' replaced the term 'insipidus' to confirm that the urine had a sweet taste (DOBSON, 1967). Years later, between 1735-1784, Mathew Dobson of Liverpool actually measured the concentration of glucose in urine to demonstrate that the 'sweet taste' was due to sugar in the urine (Polonsky, 2012).

Understanding T2D pathophysiology in the last century

At the beginning of the 19th century, French physicist, Claude Bernard and other researchers demonstrated that diabetes was due to abnormal glucose homeostasis that was under the control of the liver, hormones and the central nervous system (Polonsky, 2012; Zaccardi et al., 2016; Blaslov et al., 2018). During the same period, Claude Bernard observed that a puncture on the floor of the 4th ventricle in the brain induces diabetes, thus confirming the brain as a glucoregulatory organ (Morton and Schwartz, 2011). This observation was later validated by the discovery of the leptin pathway that explains how the hormone leptin interacts with the central nervous system (CNS) in regulating glucose homeostasis (Morton and Schwartz, 2011). In the

1920s, a French physician Jean Vague, observed that upper body obesity was associated with a cluster of risk factors (hypertension, low levels of high-density lipoprotein cholesterol, dyslipidemia) that seemed to predispose individuals to diabetes (Morton and Schwartz, 2011; Polonsky, 2012; Blaslov et al., 2018). The term metabolic syndrome was introduced in the 1950s to describe this cluster of risk factors (Blaslov et al., 2018). In 1988 Gerald Reaven postulated that insulin resistance was the underlying factor to metabolic syndrome, and he renamed it syndrome 'X' (Reaven, 2005; Blaslov et al., 2018).

Insulin discovery

The link between diabetes and insulin was clarified in 1889 when a pancreotomy was performed on a dog that later died from diabetes (Minkowski, 1890; Polonsky, 2012; Blaslov et al., 2018). In 1910, Edward Albert Sharpey-Schafer hypothesized that diabetes was caused by a deficiency in a substance produced by the pancreas islets, and named it insulin (Polonsky, 2012). This was later identified in 1869 by Langerhans (Zaccardi et al., 2016). Insulin is derived from the Latin word 'insula', meaning an 'island' when referring to the islets of Langerhans (Polonsky, 2012). In 1921 Frederick Banting and Charles Best reversed diabetes in dogs, using an extract from pancreatic islets (Polonsky, 2012; Blaslov et al., 2018). James Collip and John Macleod extracted purified insulin from bovine pancreases that was used to treat diabetic patients (Polonsky, 2012).

After the discovery of insulin, diabetes research focused on insulin secretion and its effect on peripheral tissues (Morton and Schwartz, 2011). The role of insulin in regulating glucose metabolism was only demonstrated in the 1920s, where a distinction between insulin dependent and non-insulin-dependent diabetes was suggested (Allan, 1972). However, it was only in the 1950s that reliable tests for circulating blood insulin levels were developed, thus confirming the differences between the two types of diabetes (Zaccardi et al., 2016).

Distinguishing between T1D and T2D

In 1936 Harold Himsworth postulated that most patients with diabetes have insulin resistance rather than insulin deficiency (Himsworth, 1936; Polonsky, 2012). The next 30 years developed immunologic techniques which identified autoimmune diseases that destroy pancreatic beta

cells in insulin dependent diabetes (Zaccardi et al., 2016). During the same period, more experiments were conducted to demonstrate insulin resistance by peripheral insulin sensitive tissues to further distinguish the two types of diabetes (Zaccardi et al., 2016). Differences between the two types of diabetes were formally adopted around 1979 where new definitions of type I diabetes (replacing insulin dependent diabetes) and type II diabetes (replacing non-insulin-dependent diabetes) were introduced (Zaccardi et al., 2016). As cellular and molecular understanding of T2D advances, there is a drive to depart from a glucocentric classification of T2D to a more pathophysiologic classification that will encompass a description of the patient phenotype as well (Zaccardi et al., 2016).

1.2.3 Prevalence of T2D

Worldwide prevalence

The International Diabetes Federation (IDF) estimated that 1 in 11 adults aged between 20 to 79 years had diabetes mellitus in 2015, a total of 415 million people (Zheng et al., 2018). The global diabetes prevalence in 2019 is estimated to be 9.3% (463 million people), rising to 10.2% (578 million) by 2030 and 10.9% (700 million) by 2045 (Sun et al., 2022). The prevalence is higher in urban (10.8%) than rural (7.2%) areas, and in high-income (10.4%) than low-income countries (4.0%) (Saeedi et al., 2019; Sun et al., 2022). One in two (50.1%) people living with diabetes do not know that they have diabetes (Saeedi et al., 2019; Sun et al., 2022). Amongst the population diagnosed with diabetes, 90-95 % have T2D (Cho et al., 2018; Pheiffer et al., 2018; Zheng et al., 2018; Care, 2019). The escalating epidemic is compounded by an explosive population growth, ageing populations, urbanization, poor eating habits, leading to obesity due to a sedentary lifestyle (Zheng et al., 2018).

Although T2D was initially thought to be an adulthood disease, it has become more prevalent among obese adolescents in their second decade, where it coincides with adolescent insulin resistance (D'Adamo and Caprio, 2011). In the past two decades, T2D only affected 3% of the adolescent population but of late it has escalated to 40% of newly diagnosed cases of adolescent T2D (D'Adamo and Caprio, 2011).

China and India are the leading epicenters for T2D, with the USA having the 3rd highest number of diabetic persons, in addition, North America, the Caribbean islands and Pacific nations also experience a high incidence of T2D (Zheng and Wang, 2001; Abubakar et al., 2015). The Middle East is another emerging epicenter with a prevalence ranging between 9.5% and 25.4% of the general population (Al-Rubeaan et al., 2015).

The Global Burden of Disease Study conducted in 2013 classified T2D as the 9th major cause of reduced life expectancy (Abubakar et al., 2015). In 2010 it was estimated that 3.96 million adults aged between 20 to 79 years died from T2D, whereas in 2015 the International Diabetes Federation (IDF) raised the estimate to 5 million deaths (Abubakar et al., 2015; Cho et al., 2018). Medical costs for diabetics are three times higher, the IDF estimated that in 2015 alone 12% ($673 billion) of the global health budget was spent on the treatment of diabetes and its complications (Abubakar et al., 2015). Latin America spends an average of 25% on treatment of T2D, thus causing the heaviest financial burden on health budgets, in fact T2D is considered as the leading cause of mortality in Mexico and Brazil (Arredondo, 2014).

T2D Prevalence in SA and its associated health burden

South Africa experiences the same risk factors for T2D that predisposes every country to an increased prevalence of T2D. About 50% of diabetics in the world remain undiagnosed with roughly 60.2% being found in low and middle class income brackets in Africa which includes South Africa (Cho et al., 2018; Pheiffer et al., 2018; Zheng et al., 2018). The prevalence of T2D in South Africa increased from 5.5 % to 9% between 2000 and 2009 (Bradshaw et al., 2007; Manyema et al., 2015; Pheiffer et al., 2018). In 2000 it was estimated that 87% of diabetic cases were due to obesity, in 2013, 38% of men and 69% of women were classified as overweight (Bradshaw et al., 2007; Pheiffer et al., 2018).

In 2015 the Global Burden of Disease Study ranked a high Body Mass Index (BMI) and hyperglycemia as the second and third contributors of mortality and disability in South Africa (Abubakar et al., 2015; Pheiffer et al., 2018). Here, (in South Africa) 76% of deaths of individuals below 60 years are due to T2D, this poses an economic challenge in the country because it

appears T2D affects the most economically productive sector of the population (Pheiffer et al., 2018). Other than the disease itself, multiple diabetic complications (macro/microvascular disease, neuropathy, retinopathy, renal disease, hypertension, amputations) exacerbate the economic burden on the health system (Bertram et al., 2013), leading to increased morbidity and mortality. In 2009, T2D related amputations were estimated at 2000 procedures annually (Manyema et al., 2015; Pheiffer et al., 2018).

The economic burden is related to hospital costs, chronic medication, disability grants and absenteeism from work of both the diabetic individual and the caretaker (Manyema et al., 2015; Pheiffer et al., 2018). Health expenditure for diabetics is projected to increase by 50% between 2010 and 2030 with a capital spend ranging from $1.1 billion to $2.2 billion by 2030 (Manyema et al., 2015). Average hospitalization costs in 2009 were R27 000 for diabetics compared to R18 000 for none diabetic patients (Manyema et al., 2015). Therefore, it is imperative to undertake more studies to assess the link between T2D and compromised bone integrity, in order to reduce mortality, morbidity and financial implications related to skeletal complications caused by T2D.

1.2.4 Abnormal glucose homeostasis as a precursor to T2D

The aim of glucose homeostasis is to maintain serum glucose concentrations within a narrow physiological range while sustaining a balance between glucose utilization, dietary glucose delivery and endogenous glucose production (Aronoff et al., 2004; Giugliano et al., 2008). To maintain homeostasis, glucoregulatory hormones such as pancreatic hormones (insulin, glucagon, and amylin), adipocyte hormone (leptin), gut hormones, glucose dependent insulinotropic hormones, epinephrine, cortisol and growth hormone (Aronoff et al., 2004; Giugliano et al., 2008; Morton and Schwartz, 2011) work in tandem as summarized in Table 1. The functions and levels of glucoregulatory hormones depend on the fed or fasting state. The fed state results in glycolysis, glycogen synthesis, lipid synthesis, fructose/galactose metabolism. The fasting state results in gluconeogenesis, glycogenolysis, protein catabolism and ketone body metabolism (Nakrani et al., 2020). A disruption in glucose homeostasis results in hyperglycemia associated with T2D (Morton and Schwartz, 2011).

Table 1:1 **Glucoregulatory hormones and their functions**

Hormone	Organ	Function	Effect on Plasma Glucose Levels
Glucagon	Pancreatic alpha-cells	• Glycogenolysis • Hepatic gluconeogenesis • Hepatic ketogenesis	Increase
Insulin	Pancreatic beta-cells	• Promotes cellular glucose uptake • Suppresses post prandial glycogen secretion • Promotes protein and fat synthesis	Decrease
Amylin	Pancreatic islet amyloid deposits	• Suppresses post prandial glucagon secretion • Reduces gastric emptying • Suppresses food ingestion and body weight	Decrease
GLP-1	Intestinal L-cells	• Enhances post prandial insulin secretion • Suppresses post prandial glucagon secretion • Reduces gastric emptying • Suppresses food ingestion and body weight • Promotes pancreatic beta cell integrity	Decrease

1.2.5 Pathogenesis of T2D

Insulin facilitates the uptake of glucose by insulin sensitive target tissues such as the liver, muscle and adipose tissue (Kowalski and Bruce, 2014; Adeva-Andany et al., 2019). Impaired insulin sensitivity by target tissues and pancreatic beta cell dysfunction are the main precusors to T2D (Kahn, 2003; Scheen, 2003; Zaccardi et al., 2016). T2D exhibits a multistage progression beginning with target tissue resistance as well as excessive insulin secretion to compensate for insulin resistance (Scheen, 2003). At this stage, subjects are normoglycemic but hyperinsulinemic, as pancreatic beta cells adapt to the demand (Scheen, 2003). This stage is followed by a decline in pancreatic beta cell numbers and loss of body mass. Finally, a period of overt uncontrollable hyperglycemia ensues (Del Prato, 2009).

1.2.6 Lipid peroxidation process

Hyperglycaemia, hyperlipidaemia and hypercholesterolaemia found in T2D, create an environment that stimulates lipid peroxidation. This process (Del Prato, 2009; Li et al., 2011; Ayala et al., 2014; Xu and Porter, 2015) follows these steps (Fig. 1) : (1) **Initiation**: Pro-oxidants like HO_2 (Hydroperoxyl) $^{\cdot}$and $HO^{\cdot}$(hydroxide ion) abstract hydrogen atoms close to the carbon-carbon double bonds of unsaturated lipids to form lipid centered radicals. (2) **Propagation**: The

lipid centered radicals react with oxygen to form lipid peroxy radicals. The lipid perox yradicals abstract hydrogen from other unsaturated lipid molecules to form other lipid centered radicals that will again react with oxygen to form more peroxy radicals. This process initiates a sequence of chain reactions that generate even more reactive radicals. (3) **Termination**: The progression of the chain reaction proceeds until advanced lipo-oxidation end products (LPO) are formed. Anti- oxidants like Vitamin C and Vitamin E donate hydrogen to the lipid peroxy radical to form a non- radical lipid hydroperoxide. The end products are primary hydroperoxides and secondary carbonyl compounds such as malondialdehyde (MDA) (Paul and Snyder, 2010; Tiwari et al., 2013; Ayala et al., 2014) (Fig 1).

Malondialdehyde (MDA) serum levels are elevated in diabetic patients (Del Rio et al., 2005; Tiwari et al., 2013). This molecule is cytotoxic and permeates cell membranes to react with intracytoplasmic and intranuclear macromolecules, and adversely affects gene expression, causing irreversible protein damage (Slatter et al., 2000; Negre-Salvayre et al., 2010; Tiwari et al., 2013). MDA cross links collagen and elastin making these proteins resistant to proteolysis by enzymes (Slatter et al., 2000; Tiwari et al., 2013), therefore affects skeletal integrity.

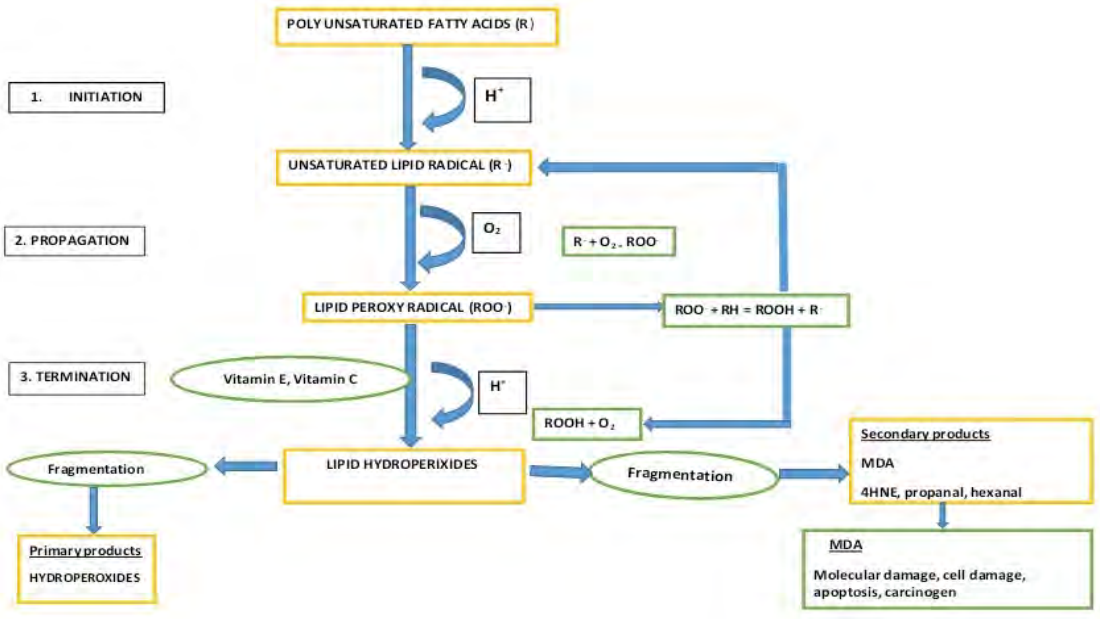


Figure 1.1: Lipid peroxidation process (Illustration G.F Dlamini)

1.2.7 Increased skeletal fractures in T2D

Treatment of diabetes is mainly targeted at the endocrinology aspect of the diseases. This is despite multiple scientific reports in both humans (Karim et al., 2019; Lekkala et al., 2019) and rats (Prisby et al., 2008; Reinwald et al., 2009; Castrillón et al., 2011; Creecy et al., 2016) highlighting the link between T2D and its effect on bone mass, bone mineral density (BMD) (Vestergaard et al., 2009), bone turnover (Lekkala et al., 2019), bone microarchitecture, bone strength, bone resistance and susceptibility to fractures (Dobnig, 2006; Reinwald et al., 2009; Vestergaard et al., 2009; Creecy et al., 2016; Lekkala et al., 2019).

A large cohort study (Rotterdam study) of 6655 men and women aged 55 years and older found that non vertebral fractures were higher in patients with T2D, likewise other studies on osteoporotic fractures found that women with T2D aged 65 years or older, had an increased risk for hip, proximal humerus and foot fractures respectively (Moseley, 2012). A women's health initiative cohort observational study found that women above 40 years of age with T2D have 82% risk for hip fractures (Valderrabano and Linares, 2018). Another systemic review and meta-analysis of diabetic subjects showed an increased risk of hip and proximal humerus fractures (Schwartz, 2003; Dobnig, 2006; Hamann et al., 2011; Creecy et al., 2016; Valderrabano and Linares, 2018). Proximal humerus fractures (PHF) are the most frequent after femoral neck and wrist fractures (Chu et al., 2004). This risk of fractures is often underestimated using Dual X-ray absorptiometry (DXA), BMD, T-score, Fracture prediction tool (FRAX) (Schwartz, 2003).

Studies on the ZDF rat distal femur using Micro CT, and immunohistochemistry, found lower trabeculae numbers thinner trabecular, lower mineralized bone tissue volume, impaired osteoblast differentiation and less mineralized matrix formation in diabetics compared to controls (Ahmad et al., 2003; Blakytny et al., 2011; Hamann et al., 2011).

1.2.8 Long bone structure and function

To understand diabetic skeletopathy, knowledge of long bone structure and function is crucial. Long bones have a diaphysis, proximal and distal epiphysis (Fig.2). The diaphysis is made of

cortical bone that surrounds a central marrow cavity while both epiphysis are comprised of a trabeculae bone lattice that is surrounded by cortical bone (Junqueira and Carneiro, 2003).

Bone is comprised of a mineralized inorganic and organic multicellular specialized connective tissue. The organic content (type I collagen), the inorganic component (hydroxyapatite crystals), bone turnover cells (osteoblasts, osteocytes, osteoclasts, bone lining cells) are all embedded in a proteoglycan and glycoprotein ground substance, to form bone tissue (Junqueira and Carneiro, 2003). Bone tissue forms discrete morphologically diverse bones (Florencio-Silva et al., 2015) that are joined together by tendons, ligaments and muscle to form the skeleton (Junqueira and Carneiro, 2003). Skeletal function is to maintain stature, provide support, locomotion, attachment sites (muscles, tendons, ligaments) protect vital organs, and act as a metabolic organ (calcium and phosphate homeostasis) (Feng and McDonald, 2011). The skeleton is comprised of flat, short and long bones (Junqueira and Carneiro, 2003). Long bones such as the femur and humerus consist of a middle marrow filled hollow called the diaphysis, this is made up of cortical bone. At the extreme ends of the diaphysis, are the proximal and distal epiphysis, made of trabecular bone, that is covered by a thin layer of cortical bone (Chapurlat and Confavreux, 2016) (Fig. 2).

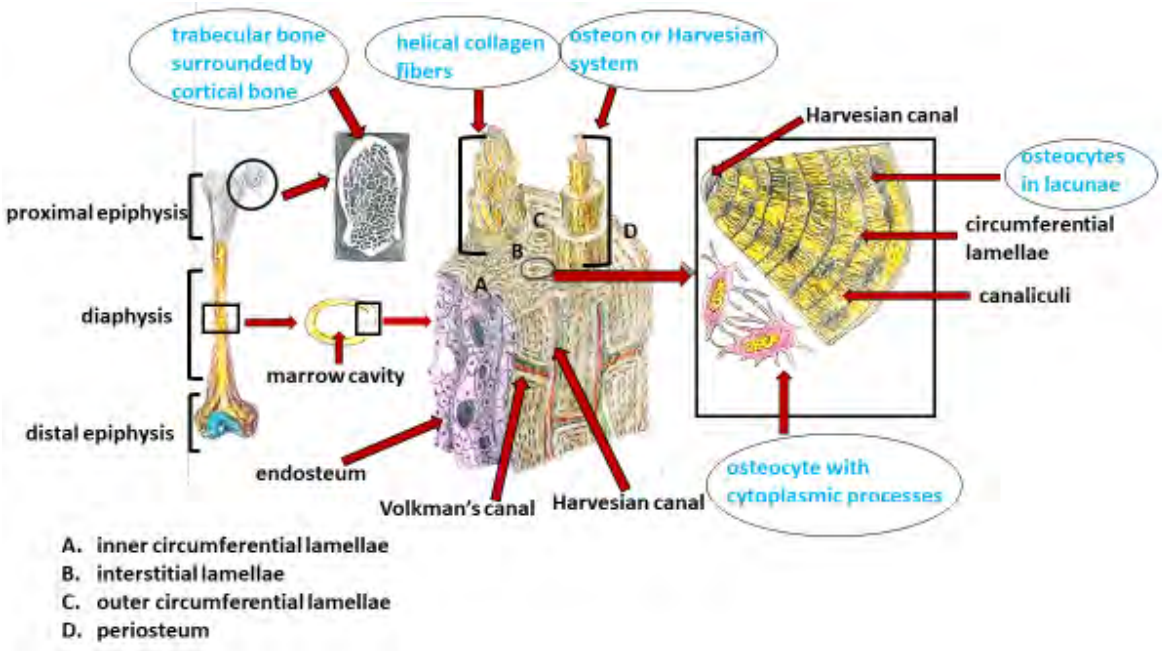


Figure 1.2: Macroscopic and microscopic features of bone. The epiphysis and diaphysis are shown. Circumferential and interstitial lamellae as well as multiple Harvesian systems are visible. Illustrated by N. Gulubane and G. Dlamini. Modified from Junqueira and Carneiro, 2003; Kierszenbaum and Tres, 2015.

Cortical bone

Cortical bone or compact bone characteristically exhibits parallel, calcified collagen fibers arranged into layers or lamellae (Junqueira and Carneiro, 2003). These lamellae can be concentric, surrounding a Harvesian canal to form an osteon or Harvesian system (Kierszenbaum and Tres, 2015). The central Harvesian canal contains nerves, lymphatics, blood vessels, it branches laterally to form Volkman's canals (Junqueira and Carneiro, 2003). In the diaphysis of long bones lamellae are typically arranged into outer circumferential lamellae (adjacent to the periosteum), inner circumferential (adjacent to the endosteum), between the outer and inner circumferential lamellae are interstitial lamellae, plus multiple osteons or Harvesian systems (Junqueira and Carneiro, 2003) (Fig 2). Interstitial lamellae are remnants of old Harvesian systems that were destroyed during remodeling and growth, and each discrete Harvesian system is surrounded by a cement line (Junqueira and Carneiro, 2003).

Interspersed between the lamellae are osteocytes. These (osteocytes) are cell which were initially osteoblasts that got trapped in their own calcified matrix. Osteoblasts originate from osteoprogenitor cells found in the periosteum and endosteum, these osteoblasts secrete osteoid that gets mineralized on a helical scaffold of parallel collagen fibers giving bone tissue its lamellate appearance (Kierszenbaum and Tres, 2015). Collagen fibers allow for flexibility in bone while the mineral content gives bone its strength. Osteocytes are the most abundant and long lived bone cells that reside in lacunae (Florencio-Silva et al., 2015). They project their cytoplasmic processes in small tunnels within the bone called canaliculi, and communicate with each other via gap junctions (Kierszenbaum and Tres, 2015). This chain of communication eventually reaches the Harvesian and Volkman's canals housing nerves, lymphatics and blood vessels (Junqueira and Carneiro, 2003; Kierszenbaum and Tres, 2015), to facilitate nutrition and gaseous exchange. This osteocyte perilacunae and pericanaliculi network has been found to be

responsible for localized bone remodeling, mechanosensing and mechanotransduction (Qing et al., 2012; Dole et al., 2017).

Trabecular, cancellous or spongy bone

Cancellous bone is found at the epiphyseal ends of hollow long bones, and inner surfaces of marrow cavities (Junqueira and Carneiro, 2003). Epiphyseal cancellous bone is covered by a thin layer of cortical bone (Kierszenbaum and Tres, 2015; Chapurlat and Confavreux, 2016). It forms a lattice of interconnected rod-like and plate like partitions called trabeculae (Hsu et al., 2013), hence it is sometimes called trabeculae bone. The inter-trabeculae spaces are filled with bone marrow and bone marrow cells (Hsu et al., 2013). Trabeculae lamellae are arranged as an irregular network due to the non-parallel orientation of its collagen fibers. Cancellous or trabecular bone is highly porous (40-95%) depending on age (Lin and Dass, 2018). The highly porous architecture allows for the transmission of stress loads to the stronger cortical bone, therefore provides structural support regardless of lower bone density (Feng and McDonald, 2011). Trabeculae bone has the same cell types as cortical bone, and is a major site of bone remodeling, therefore prone to most bone diseases (Feng and McDonald, 2011) Fig. 2.

1.2.9 Bone remodeling

The purpose of adult bone remodeling is to maintain optimal bone strength by repairing micro cracks during skeletal adaptation, as well as maintain calcium homeostasis (Raggatt and Partridge, 2010; Kierszenbaum and Tres, 2015). Bone remodeling is a physiologic process described as mineral deposition by osteoblasts, resorption by osteoclasts and matrix maintenance by osteocytes, (Feng and McDonald, 2011; Booth et al., 2013). It is tightly regulated and coordinated by osteoregulatory hormones (Seibel, 2005; Feng and McDonald, 2011; Henneicke et al., 2014), cytokines, and growth factors (Seibel, 2005). It occurs in anatomical structures known as basic multicellular units (BMU), and requires a coordinated sequence by bone lining cells, osteocytes, osteoclasts and osteoblasts (Feng and McDonald, 2011). Osteocytes act a mechanosensors of these micro cracks and initiate the bone remodeling cascade (Feng and McDonald, 2011; Florencio-Silva et al., 2015). An imbalance in bone remodeling results in either osteoporotic or osteopetrotic bone diseases (Florencio-Silva et al., 2015), and an increased bone

fragility. The remodeling cascade follows four major distinct and overlapping processes (Feng and McDonald, 2011; Kierszenbaum and Tres, 2015) as outlined below (Fig 3):

1. **Activation**: where osteoclast precursors are recruited to a specific site, then differentiates into osteoclasts.
2. **Resorption**: bone resorption is initiated and additional mesenchymal stem cells and osteoprogenitors are recruited to resorption sites.
3. **Reversal**: osteoblasts reverse the resorption process, by lining the resorption cavity and initiate osteoid secretion.
4. **Formation**: at this final stage, osteoblasts continue to secrete osteoid that is then mineralized. Osteoblasts are trapped in the mineralized matrix and are now referred to as osteocytes. Osteocytes maintain the bone matrix, while acting as mechanosensors for future micro cracks.

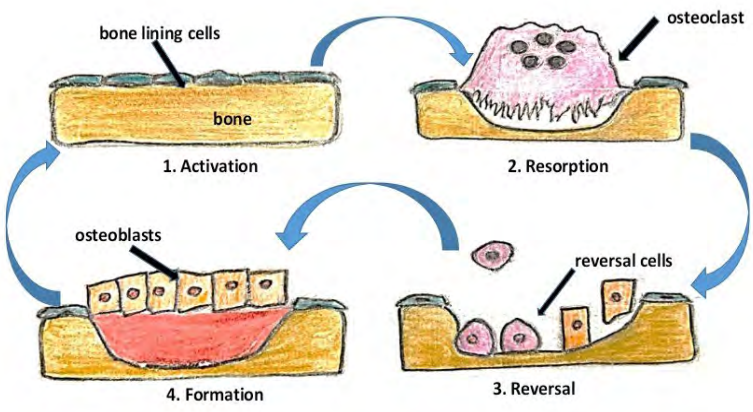


Figure 1.3: Stages in bone remodelling. Illustrated by N. Gulubane and G.Dlamini

1.2.10 Effect of T2D on bone remodeling cells (osteocytes, osteoblasts, osteoclasts and adipocytes)

Osteocytes

Osteocytes comprise 95 % of the total bone cell population (Bellido, 2014), they are interconnected via a network of canaliculi and gap junctions to exchange nutrients, oxygen and waste material (Picke et al., 2019). Initially, osteocytes were considered as inactive cells, but are now regarded as active cells that undertake bone remodeling in their vicinity via peri-lacunae and

peri-canaliculi networks (Qing et al., 2012; Abubakar et al., 2015; Dole et al., 2017). This network facilitates their function as mechanosensors and mechanotransductors in response to bone overload, fatigue and micro damage (Burger, 1998; Kaya et al., 2017). This network is impaired in T2D, resulting in an impaired mechanosensing and mechanotransduction response (Picke et al., 2019). Osteocytes regulate osteoblasts, osteoclasts and bone lining cell activity, via osteocyte osteolysis or peri lacuna-canaliculi remodeling (Burger, 1998; Dole et al., 2017). This causes direct resorption and deposition of the bone matrix in their immediate environment, in response to lactation, hibernation and pathologic conditions like diabetes (Qing et al., 2012; Dole et al., 2017).

Apoptotic osteocytes are increased in T2D (Picke et al., 2019), these apoptotic osteocytes attract osteoclast precursors to their vicinity, and increase bone matrix resorption, therefore, increased bone fragility (Burger, 1998; Bellido, 2014). Osteocytes express the bone matrix catabolic enzyme TRAP (a standard marker for osteoclasts) intracellularly, where its presence is further confirmed by the expression of TRAP mRNA signals in osteocytes (Nakano et al., 2004; Qing et al., 2012; Kaya et al., 2017)(Nakano et al., 2004; Qing et al., 2012; Kaya et al., 2017).

Osteoblasts are significant in bone formation, they synthesize collagen, secrete osteoid and mineralize the organic matrix under the influence of ALP (Picke et al., 2019). ALP is produced by several tissues including bone, moreover, bone specific alkaline phosphatase expressed by osteoblasts, and promotes osteoid formation and bone mineralization (Leung et al., 1993). Immunohistochemistry studies on the distal femur of the ZDF rat, found impaired osteoblast differentiation, less osteoblast numbers and less mineralized matrix formation in diabetic rats (Ahmad et al., 2003; Blakytny et al., 2011; Hamann et al., 2011). Some studies report a reduction in osteoid volume and thickness in the iliac crest of individuals with T2D (Picke et al., 2019).

Adipocytes

Bone marrow adipocytes originate from pluripotent skeletal stem cells, (previously called bone marrow mesenchymal stromal cells) capable of differentiating into osteoblastic, chondrogenic and hematopoietic cell lineages (Kim and Schafer, 2016; Ferland-McCollough et al., 2018). T2D increases bone marrow adipocytes in both humans (Kim and Schafer, 2016) and rats (Piotrowska

and Tarnowski, 2021). These increased bone marrow adipocytes are associated with an increased prevalence of hip fractures (Kim and Schafer, 2016). T2D favors the differentiation of skeletal stem cells into adipogenic cell lineages while suppressing the differentiation of osteogenic cell lineages (Gillet et al., 2017; Ferland-McCollough et al., 2018). In addition, the molecule sclerostin secreted by osteocytes, induces bone marrow adiposity (Fairfield et al., 2018). Pathologic conditions like oxidative stress, dyslipidemia, hypoinsulinemia and hyperinsulinemia that are common in T2D, also increase bone marrow adiposity (Piccinin and Khan, 2014). These studies suggest that bone marrow adiposity in T2D functions as an adverse contributor to bone remodeling, and increases skeletal fragility.

Hormonal control of bone remodelling

Under normal physiologic processes, bone homeostasis is tightly regulated by multiple osteoregulatory hormones such as parathyroid hormone (PTH), osteocalcin and insulin (Neer et al., 2001; Seibel, 2005; Feng and McDonald, 2011). Insulin is an osteo-anabolic hormone that increases osteoblast numbers, osteoblast function, reduces osteoblast apoptosis and osteoclast activity (Huang et al., 2010). It acts directly on bone via insulin receptors (Huang et al., 2010), or synergistically with other anabolic agents such as PTH (Thrailkill et al., 2005).

The hormone PTH is necessary for controlling serum calcium and phosphate levels, therefore regulates bone homeostasis (Thrailkill et al., 2005; Raggatt and Partridge, 2010; Goettsch et al., 2014; Florencio-Silva et al., 2015). An imbalance in PTH levels results in either osteoporotic or osteopetrotic bone diseases (Florencio-Silva et al., 2015). Hyperactive parathyroid glands release excessive calcium from bones resulting in osteoporosis (Neer et al., 2001; Goettsch et al., 2014). In T2D, poor glycemic control leads to excessive urinary loss of calcium, this stimulates hypersecretion of PTH, causing accelerated bone resorption and increased bone fragility (Cipriani et al., 2020). Serum levels of PTH and osteocalcin are used as bone turnover markers in diseases such as diabetes induced skeletopathy (Kemink et al., 2000; Thrailkill et al., 2005; Huang et al., 2010).

Osteocalcin, is an osteoblast derived hormone that is exclusively found in bone tissue (Booth et al., 2013; Ferron and Lacombe, 2014). Its serum levels are used to assess glucose metabolism (Im et al., 2008) and bone turnover (Kemink et al., 2000). It increases pancreatic beta cell proliferation, insulin secretion, and increases insulin sensitivity by peripheral tissues (Lee et al., 2007; Booth et al., 2013; Kanazawa, 2015; Cipriani et al., 2020). Studies on osteocalcin receptor knockout mice exhibited reduced islet numbers, hyperglycemia, glucose intolerance, and reduced osteoblast mediated bone mineralization (Fulzele and Clemens, 2012; Ferron and Lacombe, 2014).

Calcitriol, Calcitonin and Sex Hormones

Calcitriol action is to increase intestinal absorption of calcium and phosphorus, thus supplying minerals for the skeleton. Calcitonin can block bone breakdown by inactivating osteoclasts, Calcitonin may be more important for maintaining bone development and normal blood calcium levels in early life. Oestrogen and testosterone both have effects on bone. Oestrogen acts on both osteoclasts and osteoblasts to inhibit bone breakdown at all stages in life. Oestrogen and testosterone may also stimulate bone formation.

Type I collagen is the most abundant protein component of bone, and C- and N-terminal telopeptides of type I collagen (CTX and NTX) are both fragments of type I collagen from the telopeptide region. CTX is the product of cathepsin K-mediated bone resorption, as direct digestion of bone with cathepsin K, causes CTX release. Hence is usable as a bone turnover marker.

1.2.11 Transforming growth factor beta (TGF-β) superfamily, from ligand to transcription for osteogenesis.

Members of the TGF superfamily of growth factors, consist of TGFβs, activins and bone morphogenetic proteins (BMPs) (Massaous and Hata, 1997). These growth factors and cytokines function as local mediators in bone homeostasis, to maintain a balance between bone resorption and deposition (Seibel, 2005). For this to occur, the TGF-β superfamily of growth factors that include TGF-β1 and BMPs are crucial in encoding for cell cycles, cell differentiation, proliferation, migration, adhesion and survival, via SMAD dependent or non-SMAD dependent signaling

pathways (Massaous and Hata, 1997; Horbelt et al., 2012; Yang et al., 2014). Transcriptional or signaling aberrations of the TGF-β and BMP superfamily are one of the causes of multiple diseases that include skeletal pathology (Horbelt et al., 2012). The subfamilies of TGF-β1, and BMP-3 that will be investigated in this study, are significant in bone remodeling and the maintenance of bone homeostasis.

Osteogenic cytokine TGF-beta 1

The cytokine TGF-β1 is an abundant cytokine found in bone matrix (Ehnert et al., 2010; Horbelt et al., 2012; Wu et al., 2016). It is responsible for regulating the differentiation, proliferation and migration of osteoprogenitor cells (Tang et al., 2009; Ehnert et al., 2010). TGF-β1 stimulates osteoblast proliferation and chemotaxis (Janssens et al., 2005; Wu et al., 2016). It exists as a latent extracellular complex that gets activated by proteases and subsequently binds to type I receptors (TβRI,ALK5) and type II receptors (TβRII) to trigger the intracellular signalling cascade (Ehnert et al., 2010; Yang et al., 2014; Wu et al., 2016) (Fig 4). TβRII induces the transphosphorylation of TβRI which then phosphorylates receptor-activated Smads (R-Smad) Smad 2 and 3, and other non-Smad receptors within the cytoplasm (Horbelt et al., 2012) (Fig. 4). At this stage, Smad 7 negatively regulates R-Smad signalling by blocking the phosphorylation of the Smad receptors (Wu et al., 2016). Phosphorylated R-Smad 2 and 3 bind to their common partner Smad-4, or bind other non Smad receptors, to form co-Smad complexes that migrate to the nucleus (Ehnert et al., 2010). These co-Smad complexes bind co-factors that trigger the regulation of gene expression to promote osteoprogenitor cell differentiation, proliferation, and chemotaxis, increasing osteoblast activity (Janssens et al., 2005; Ehnert et al., 2010; Yang et al., 2014; Wu et al., 2016). Again Smad 6 and 7 regulates the Smad signaling cascade by blocking the translocation of co-Smad complexes into the nucleus (Wu et al., 2016).

BMP subfamily and its antagonist BMP3

The BMP subfamily influences the commitment of mesenchymal precursor cells to differentiate into osteoprogenitor cells that will eventually mature into osteoblasts and osteocytes (Oei et al., 2013; Matzelle et al., 2016; Wu et al., 2016). It regulates bone homeostasis via Smad or non-Smad BMP signalling pathways. Extracellular BMP binds to type II receptors that transphosphorylate type I receptors, that subsequently phosphorylate R-Smads, 1, 5 and 8 (Horbelt et al., 2012; Yang et al., 2014) (Fig. 4). Phosphorylated R-Smads (1, 5, and 8) form

complexes with Smad 4, translocate to the nucleus and co-opt other co-factors and mediate gene expression associated with osteogenesis (Ehnert et al., 2010; Horbelt et al., 2012; Yang et al., 2014; Wu et al., 2016). Smad 6 and 7 act as negative regulators of the Smad dependent signalling pathways whereby they block the phosphorylation of R-Smads as well as the translocation of co-Smad complexes into the nucleus (Wu et al., 2016).

Anti-osteogenic cytokine BMP3

BMP3 is an anti-osteogenic cytokine (Wu et al., 2016) secreted by osteoblasts and osteocytes (Kokabu and Rosen, 2018). It is the most abundant BMP within the bone matrix, accounting for approximately 65% of the total BMP content in demineralized bone (Kokabu and Rosen, 2018). BMP-3 is a non-signalling molecule that antagonizes the BMP signalling pathway, it competes via the TGFβ-Activin common pathway (Bahamonde and Lyons, 2001). It binds competitively to the activin receptor (ActRIIB), and opposes R-Smad 2 and 3 signalling (Wu et al., 2016; Kokabu and Rosen, 2018). It suppresses osteoblastogenesis by repressing BMP-Smad signalling (Wu et al., 2016; Kokabu and Rosen, 2018). Its effect manifests as reduced BMD, reduced trabeculae volume and thinner cortical bone (Gamer et al., 2009; Horbelt et al., 2012; Wu et al., 2016; Kokabu and Rosen, 2018) therefore increased bone fragility Fig.4.

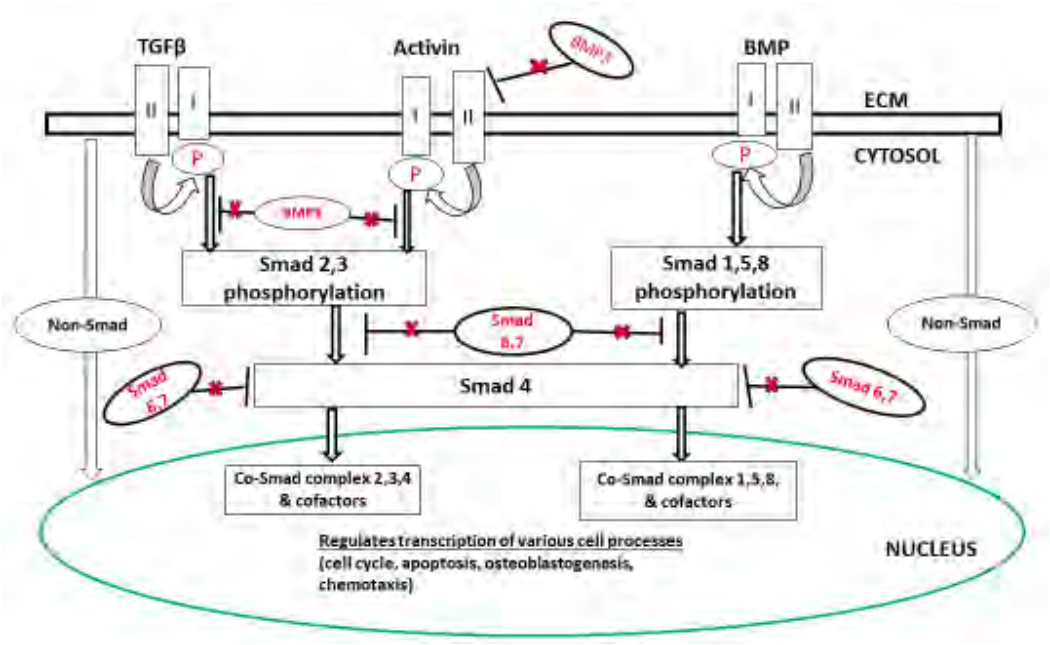


Figure 4:TGFβ1 and BMP signalling pathway. Illustrated by G.F Dlamini

1.2.12 Advanced glycation end products (AGEs) affect bone homeostasis and biophysical properties

Bone matrix AGEs are active biomolecules formed by an abnormal, non-enzymatic (Yamamoto and Sugimoto, 2016) glycation of proteins, lipids, nucleic acids and proteins (Sun et al., 2012; Sanguineti et al., 2014; Yamamoto and Sugimoto, 2016; Thomas et al., 2018). Long standing diabetic hyperglycemia facilitates the formation of AGEs that compromise skeletal integrity (Singh et al., 2015). The longstanding hyperglycemia causes the glycation of bone collagen and compromises the biophysical properties of bone (Thomas et al., 2018). About 95% of the organic content of bone is comprised of type I collagen which contributes its material strength (Yamamoto and Sugimoto, 2016) therefore, the accumulation of AGEs in bone matrix collagen affects bone toughness and increases fragility, increased bone fragility is proportional to the duration of T2D (Creecy et al., 2016).

In addition, AGEs accumulation also occurs in bone cells (Creecy et al., 2016) that express a surface receptor for AGEs called RAGE, thus enabling the binding of AGEs to osteocytes, osteoblasts and osteoclasts, adversely compromising their function (Kislinger et al., 1999; Singh et al., 2015; Plotkin et al., 2019). Alterations of bone proteins by AGEs, inhibits osteoblast proliferation, differentiation, induces osteoblast apoptosis, increases bone resorption by osteoclasts (Sanguineti et al., 2014; Singh et al., 2014; Yamamoto and Sugimoto, 2016)and osteocytes (Plotkin et al., 2019). The effect of AGEs on bone cells affect bone remodelling, therefore compromises skeletal integrity (Thomas et al., 2018).

1.2.13 Effect of T2D on biomechanical properties of bone

T2D affects structural and material properties of trabecular and compact bone, leading to reduced mechanical strength and increased fragility (Fajardo et al., 2014; Creecy et al., 2016). Usually, bone mechanical tests are performed on cortical bone of whole long bone diaphysis, (Jepsen et al., 2015), these include compression testing (push) (McCalden et al., 1997; Yeni et al., 2004), tensile testing (pull) (Kotha and Guzelsu, 2007), torsion (twist) (Turner and Burr, 1993) and bending testing (Margolis et al., 2006; Lekkala et al., 2019). A widely used method to assess

biomechanical properties of long bones is the three-point bending test (Leppanen et al., 2006). This involves securing a whole bone onto a material testing machine that is gradually loaded until broken.

The three-point bending test provides various parameters that describe different aspects of bone fragility (Jepsen et al., 2015). These parameters are derived from the force displacement curve (Fig. 5), and describes the following: i) Displacement (Deflection) – the amount of vertical deviation from the horizontal plane required to fracture the bone. ii) Maximum force- the amount of force required to cause deformation. Iii) Break Force – the amount of force required to fracture the bone. iv) Yield Point-indicates the value of the load at the yield point which is where the load-displacement plot deviates from linearity. v) Time - the duration that the bone withstands the force until a fracture. v) Work to fracture (Energy-to-fracture) is defined as the total area under the curve. It represents the work that must be done to fracture the bone. A tough bone requires more work to fracture (Jepsen et al., 2015).

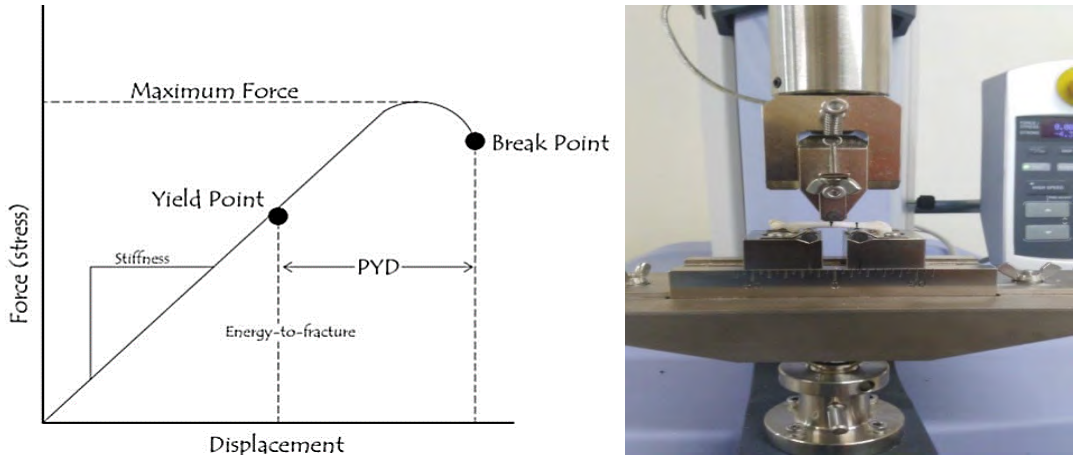


Figure 5: A Force dispacement curve. B 3- point bend instrument

1.2.14 Trabecular bone morphometry in T2D using 3-D micro-CT

Whole bone or structural biomechanics as described by the 3-poing bend test, depend on bone size, whereas micro-CT (μCT) morphologic tests are independent of bone size (Jepsen et al., 2015). For this reason, minimum bone test standards dictate that these two tests must be

combined when analyzing bone biomechanical properties (Jepsen et al., 2015). Micro-CT assesses quantitative trabecular bone morphometric indices such as bone tissue volume to total volume (BV/TV), Trabecular thickness (TbTh) trabecular number (TbN) and trabecular spacing (TbSp) (Bouxsein et al., 2010; Jepsen et al., 2015; Creecy et al., 2016). In the cortex, parameters such as cross-sectional area (area enclosed by the periosteum), medullary cavity area (area enclosed by the endosteum) and cortical thickness (difference between the cross sectional area and medullary area) are reported in long bones (Bouxsein et al., 2010; Jepsen et al., 2015). Cortical bone thickness measurements reflect cellular activity on the endosteal surface and periosteal surfaces therefore bone remodelling (Jepsen et al., 2015). Studies on ZDF and ZDSD rat femora and tibiae report loss of trabecular bone, reduced bone mechanical properties and increased bone fragility with the progression of T2D (Prisby et al., 2008; Reinwald et al., 2009; Creecy et al., 2016).

1.3 AIM

To characterise the skeletopathy of the femur and humerus of ZDSD rats

1.4 OBJECTIVES:

1.4.1 To confirmation the development of diabetes in an experimental of diabetes by measuring the following parameters.

i) Rats were weighed weekly

ii) Fasting blood glucose levels were recorded once a week

iii) Fasting oral glucose tolerance tests (OGTTs) were measured monthly.

1.4.2 To provide a biochemical analysis in and experimental model of diabetes mellitus by measuring the following parameters.

i) Triglyceride levels were measured with a TG meter

ii) To assess how diabetes affects hormones that are involved in bone homeostasis. Serum concentrations of osteocalcin, and insulin were quantified using ELISA.

iii) To assess oxidative stress, Malondialdehyde (MDA) serum levels were determined by ELISA

1.4.3 To characterize bone strength and trabecular morphometric parameters in an experimental model of diabetes mellitus by analysing the following parameters

i) The biomechanical strength was analyzed by three point bending tests using a universal tensile tester

ii) Cortical bone area, medullary area, trabeculae thickness, trabeculae volume and trabeculae numbers were analyzed using Three Dimensional Micro-focus X-ray Computed Tomography (3D-µCT)

1.4.4 To characterize bone by histological and Immunohistochemical analysis in an experimental model of diabetes mellitus.

a) Histological analysis of bone trabecular morphology and adiposity was performed using hematoxylin and Eosin (H&E) stain.
b) Immunohistochemical analysis
    i) Expression of the osteogenic growth factor (TGF-β1) and the antagonistic growth factor (BMP-3) were evaluated to understand whether T2D compromises bone quality through altering osseous tissue cytokine expression.
    ii) To assess osteolysis and osteogenesis, osteocytes and osteoblasts were immunolabelled using the anti-TRAP and anti-ALP antibodies, respectively.
    iii) Immunolocalization of AGEs was conducted to investigate their role in diabetic skeletopathy.

1.5 Hypothesis

Diabetes negatively affects skeletogenic cytokines, increases bone marrow adiposity and increases bone fragility irrespective of severity and duration.

Chapter 2

Confirmation of Diabetes

TABLE OF CONTENTS

2.0 Introduction 33
2.1 Materials and methods 36
2.1.1 Ethics Clearance 36
2.1.2 Rats 36
Grouping 36
Dietary Scheme 37
2.1.3 Blood tests 37
Fasting blood glucose and triglycerides monitoring 37
Oral glucose tolerance tests (OGTTs) 37
2.1.4 Biochemical tests 38
Insulin, malondialdehyde (MDA), and osteocalcin 38
2.1.5 Statistical analysis 38
2.2 Results 40
2.2.1 Body mass 40
Body mass: 13-20-weeks 40
Body mass: 13-28-weeks 41
2.2.2 Oral glucose tolerance tests 42
OGTT: 20-week-old 42
OGTT: 28-week-old 43
2.2.3 Fasting blood glucose 44
Fasting blood glucose: 12 to 20-weeks 44
Fasting blood glucose: 12-28-weeks 45
Insulin levels 46
Triglyceride levels 47
Osteocalcin serum concentration 48
Malondialdehyde (MDA) serum concentration 49
2.3 Discussion 50
Body mass changes 50
Glucose handling (OGTTs and FBG) 50
Triglycerides, insulin and osteocalcin interaction 51

Oxidative stress (MDA) 52
2.4 Conclusions 52

2.0 INTRODUCTION

Type two diabetes (T2D) is a chronic, progressive heterogonous syndrome with a genetic and environmental origin (Zaccardi et al., 2016; Care, 2019). It is now recognized as an epidemic with a high morbidity and mortality rate (Mohan et al., 2007). In 2019, the prevalence of this disease was 9.3% (463 million people), estimated to rise to 10.2% (578 million) by 2030 and 10.9% (700 million) by 2045, with one in two (50.1%) people living with diabetes being unaware of their diabetic state (Cho et al., 2018; Saeedi et al., 2019; Sun et al., 2022).

The main feature of T2D is sustained hyperglycemia with tissue resistance to insulin, and subsequent pancreatic beta cell failure that results in hypoinsulinemia (Giugliano et al., 2008; Del Prato, 2009; Ozougwu et al., 2013; Zaccardi et al., 2016). According to the WHO, metabolic syndrome (MetS) or prediabetes precedes T2D (Organization, 2006). Prediabetes is as a cluster of risk factors (central obesity, insulin resistance, hyperlipidemia, and raised fasting glucose levels) that establish an intermediate state between asymptomatic hyperglycemia and fully blown symptomatic T2D (Garber et al., 2008; Giugliano et al., 2008; Alberti, 2009; Del Prato, 2009; Peterson et al., 2015).

Several animal models of T2D that describe chemically induced (streptozocin; alloxan) (Chandrasekera and Pippin, 2014), surgically induced, (Reinwald et al., 2009; Chandrasekera and Pippin, 2014), genetically induced (ZDF; knockout mice (ob/ob; db/db) (Chandrasekera and Pippin, 2014; Peterson et al., 2015) and combined diet and genetic induced (ZDSD) (Reinwald et al., 2009; Peterson et al., 2015) diabetes, and its skeletal complications (Reinwald et al., 2009; Chandrasekera and Pippin, 2014) exist in the literature. ZDF rat has monogenetic mutation that is responsible for the initiation of obesity and subsequent insulin resistance. The ZDSD rat does not have these mutations but still has obesity metabolic syndrome and diabetes. Produced by crossing diet induced obese (DIO) rats derived from the Crl:CD(SD) strain (exhibiting polygenetic obesity and insulin resistance) with homozygous lean ZDF/Crl rats (which expresses beta cell failure with the Leprfa/Leprfa genotype). Was addressed in chapter 11

In this study, this relatively new model of T2D, the ZDSD rat as our translational model for diabetes. The ZDSD was chosen because it shares similar characteristics of T2D progression as

humans, therefore, studies performed on the ZDSD rat can be extrapolated to humans (Peterson et al., 2015). Initially, ZDSDs develop prediabetes prior to overt diabetes just like humans (Peterson et al., 2015). ZDSDs are daytime feeders, a trait they share with humans as opposed to other species that are nocturnal feeders (Reinwald et al., 2009; Creecy et al., 2016).

Another advantage of the ZDSD rat is that obesity and diabetes develop between 15 and 17 weeks in both sexes, which coincides with skeletal maturity in male rats (Fajardo et al., 2014; Creecy et al., 2016). However, development of diabetes and skeletal maturity in females is variable (Fajardo et al., 2014; Peterson et al., 2015), hence the decision to use males only in our study.

Tissue resistance to insulin exacerbates hyperglycemia, this causes hyperinsulinemia, followed by hypoinsulinemia as the disease the progresses, due to pancreatic beta cell death (Aronoff et al., 2004; Giugliano et al., 2008; Del Prato, 2009). Physiologically, insulin inhibits lipolysis of visceral and subcutaneous fat, but T2D induced hypoinsulinemia triggers lipolysis of these fat stores, causing dyslipidemia (Morigny et al., 2016). Dyslipidemia is characterized by constant hypertriglyceridemia and hypercholesterolemia as disease and age progress (Boden and Laakso, 2004; Peterson et al., 2015). Another adverse effect of insulin resistance is sarcopenia, caused by abnormal protein synthesis in muscle tissue, leading to reduced muscle mass (Boden and Laakso, 2004; Gougeon, 2013). The combined effect of sarcopenia and lipolysis leads to drastic weight loss as the disease progresses. It is proposed that weight loss and reduced insulin levels will be observed once rats are diabetic and as the disease progresses.

Hyperglycemia and hyperlipidemia accelerate the production of reactive oxygen species (ROS) that feed into toxic lipid peroxidation processes, to produce bio toxic molecules like MDA (Jaganjac et al., 2013; Wang et al., 2018). Elevated MDA serum/plasma levels were observed in diabetic patients and hyperglycemic mice in previous studies (Del Rio et al., 2005; Tiwari et al., 2013). MDA causes oxidative stress in various tissues and adversely affects cell cycles (Slatter et al., 2000; Negre-Salvayre et al., 2010; Ayala et al., 2014).

A diagnosis of T2D in humans is reached when fasting blood glucose (FBG) levels are >126 mg/dL (>7.0 mmol/L), where fasting is defined as no caloric intake for at least 8 hours. Random glucose

tests are >200 mg/dL (11.1 mmol/L), and blood glucose levels are >200 mg/dL (>11.1 mmol/L), two hours following an oral glucose tolerance test (OGTT) (Organization, 2006; Vijan, 2010; Care, 2019). The global prevalence of impaired OGTTs is estimated to be 7.5% (374 million) in 2019 and projected to reach 8.0% (454 million) by 2030 and 8.6% (548 million) by 2045 (Saeedi et al., 2019; Sun et al., 2022).

Peterson et al., (2014) defines the diabetic state in ZDSDs as fed glucose levels >13.88mmol/L, with more than 200% increase in the area under the curve (AUC) following an OGTT. These authors (Peterson et al., 2015) further qualify diabetes as overt if there is weight loss, reduced insulin levels, and diabetes defining parameters are exceeded.

To confirm the development of diabetes and provide a biochemical analysis in and experimental model of diabetes mellitus, fasting glucose were monitored levels every 2 weeks, and performed OGTT monthly. Triglyceride levels were also be monitored every 2 weeks. Rats were weighed weekly, while MDA, osteocalcin and insulin were recorded at 20-weeks and 28-weeks.

2.1 MATERIALS AND METHODS

2.1.1 Ethics Clearance

Ethics approval for the study has been granted by the University of the Witwatersrand Animal Ethics Committee (AESC 2015/07/28/C).

2.1.2 Rats

In this study, 38 male rats consisting of 16 Sprague Dawley (SD) and 22 Zucker Diabetic Sprague Dawley (ZDSD) rats were used. The SD rats, which served as controls were sourced from the Central Animal Services (CAS) University of the Witwatersrand. The ZDSD rats came from PreClinomics, Indianapolis, Indiana, USA. The SD rats were used as the non-diabetic controls because they are the parental strains of the ZDSD rats (Creecy et al., 2016). All rats were housed one per cage, maintained under pathogen free conditions, in a temperature-controlled environment of $23^0C \pm 2^0C$ under a 12-hour light and dark cycle.

Grouping

The rats were grouped according to strain and age at termination. SD (n=8) and ZDSD (n=7) rats were terminated at 20 weeks of age. These were designated as SD20WK and ZDSD20WK, respectively (Fig. 2.1). Another batch of SD rats (n=8) designated SD28WK, and 15 ZDSD rats were terminated at 28 weeks of age. The latter were further divided into moderate diabetes (ZDSD28WK-MOD) (n=9) and severe diabetes (ZDSD28WK-SVD) groups (n=6) (Fig 2.1). Because of variations in experimental designs, definitions of diabetes may differ. This study has defined the diabetic groups based on oral glucose tolerance test (OGTT) as follows:

(i) ZDSD20WK rats terminated at 20 weeks of age with >7.0 mmol/L fasting blood glucose (FBG) prior to glucose load and >10.0 mmol/L two hours after glucose loading.

(ii) moderately diabetic (ZDSD28WK-MOD) rats terminated at 28 weeks of age that had >8.0 mmol/L fasting blood glucose (FBG) prior to glucose load and > 12 .5 mmol/L two hours after glucose loading, more than 50% increase in area under the curve (AUC) after oral glucose tolerance test (OGTT).

(iii) Severely diabetic rats (ZDSD28WK-SVD) had >11.2 mmol/L fasting blood glucose (FBG) prior to glucose load and >23.0 mmol/L two hours after glucose loading, and more than 200% increase in AUC.

The ZDSDs terminated at the age of 28 weeks showed differences in glucose handling, hence the subdivision into ZDSD28WK-MOD and ZDSD28WK-SVD group.

Dietary Scheme

All rats were fed ad libitum a standard Purina 5008 chow (Lab diet, St Louis, MO) and given water, ad libitum. At 15 weeks, the ZDSD rats were changed into a high fat diet (5SCA, Test diet, Richmond, IN), where 47.7% of the kilocalories is derived from fat. These rats were switched back to the standard Purina 5008 chow after 6 weeks. The high fat diet was used to synchronize the onset of hyperglycemia in the ZDSD rats (Creecy et al., 2016).

2.1.3 Blood tests

Fasting blood glucose and triglycerides monitoring

Rats were fasted for 12 hours overnight prior to blood glucose measurements. A glucometer (Performa Accutrend, Roche Diagnostics, Germany) was used to measure fasting blood glucose weekly. The blood was obtained by lancing the tail vein. Rats showing a sustained fasting blood glucose above >8.0 mmol/L were classified as moderately diabetic (ZDSD28WK-MOD), while rats measuring >11.2 mmol/L were considered severely diabetic (ZDSD28WK-SVD). Fasting blood triglycerides measurements were obtained by GCT meter (Accutrend Plus, Roche Diagnostics, Germany). Both tests were performed every 2 weeks.

Oral glucose tolerance tests (OGTTs)

Oral glucose tolerance tests (OGTTs) were performed monthly following a 12 hour fast. Fasting glucose levels were recorded at time zero (T0) before receiving an oral glucose load (2 g/kg). Glucose levels were measured from blood collected from the tail vein at 15, 30, 60 and 120 min intervals after the glucose load.

2.1.4 Biochemical tests

Insulin, malondialdehyde (MDA), and osteocalcin

Intracardiac blood was aspirated at termination and collected into serum separating tubes, then centrifuged at relative centrifugal force (RFC) of 1409 for 10 minutes. Serum was decanted into aliquots that were stored at minus 80◦C for serum analysis of insulin, MDA and total osteocalcin concentrations. All biochemical tests were performed by ELISA. Rat OC/BGP (Osteocalcin) ELISA Kit, (Insulin) ELISA Kit, MDA E-BC-K025-M, all from Elabscience Houston Texas USA.

2.1.5 Statistical analysis

The data were managed in Microsoft Excel Office 365 (Microsoft Corporation) and analysed using SPSS® version 28 (IBM®). ANOVA with LSD post-hoc was used for multiple group comparisons of means. Significance level was set at $p < 0.05$.

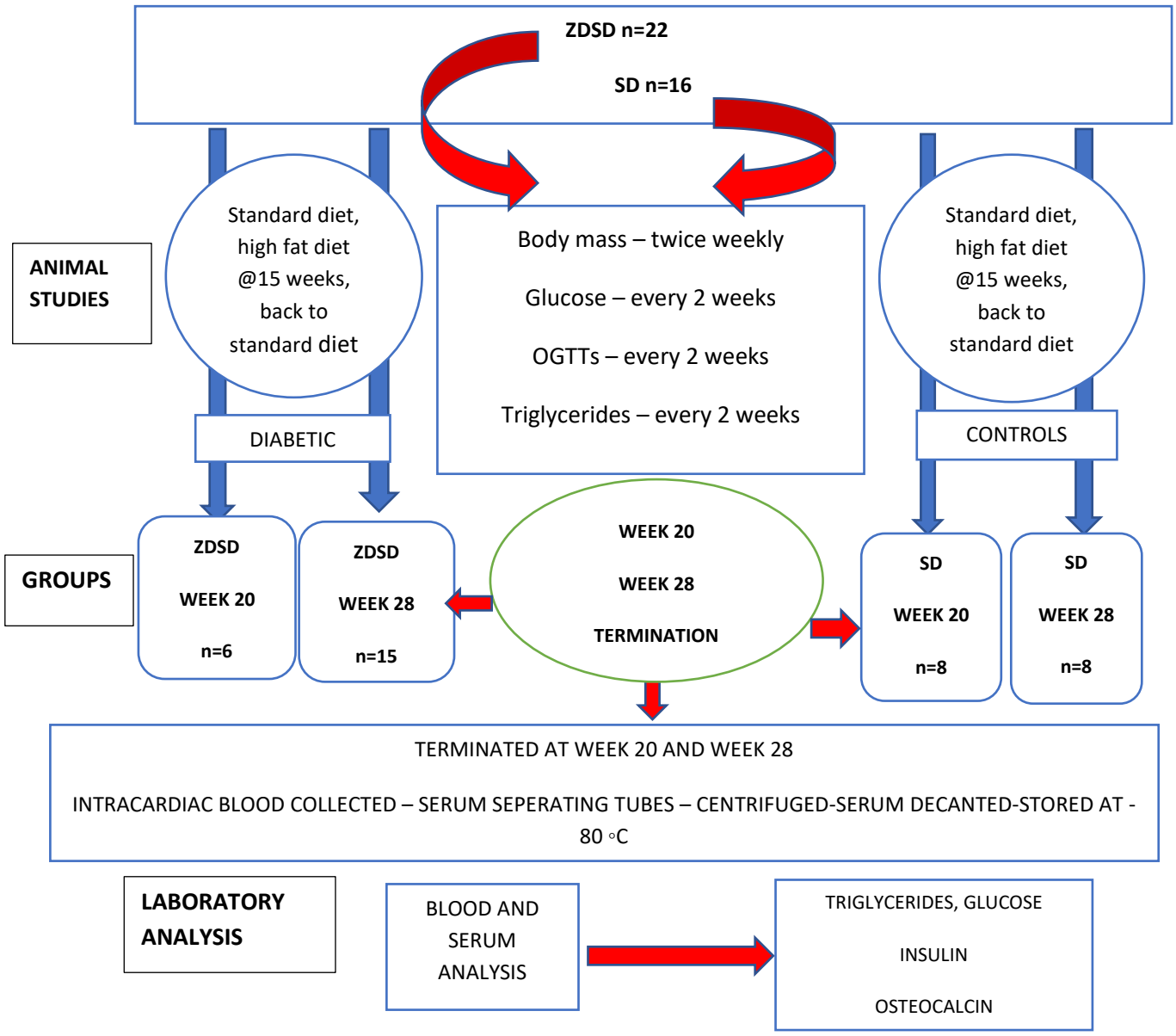


Figure 2.1: Schematic presentation of study design

2.2 RESULTS

2.2.1 Body mass

Body mass: 13-20-weeks

Both study groups showed a steady body mass gain until week 16 where the ZDSD body mass started to decline (SD, 570.33 ±33.48g; ZDSD, 510.66 ± 12.11g) (Fig. 2.2). Significant differences between the SD20WK and ZDSD20WK ($p<0.001$) were observed from week 18 onwards with the continued body mass decline among ZDSD rats (Fig. 2.2). By week-20 the SDs (590.83 ± 6.69g) had gained 20.5g compared to the ZDSDs (450.00 ± 66g) that had lost 60.66g (Fig. 2.2).

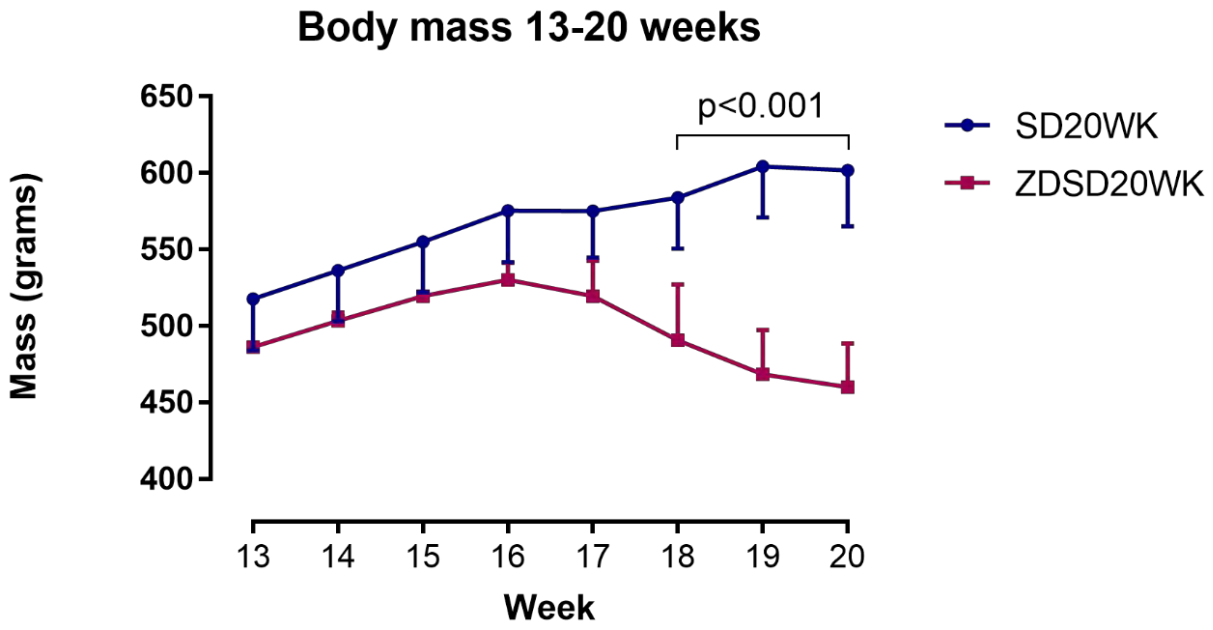


Figure 2.2: Changes in body mass from 13 to 20 weeks of age. A reduction in body mass in the ZDSD20WK is observed from week-18 until week-20 ($p<0.001$). SD20WK; Sprague Dawley rats aged 20 weeks. ZDSD20WK; Zucker Diabetic Sprague Dawley rats aged 20 weeks. Errors bars represent standard deviation

Body mass: 13-28-weeks

Rats in all the study groups showed a steady body mass gain up to week -17 (Fig. 2.3). By week-18, the ZDSD-MOD (530.31 ± 22.50g) and ZDSD-SVD (519.67 ± 10.45g) had a lower body mass compared to SD (540 ± 12.18g) controls (Fig. 2.3). As such, significant differences were observed between SD28WK and both ZDSD28WK-MOD and ZDSD28WK-SVD ($p<0.001$) from week 18 until termination (Fig. 2.3). At 28 weeks the SDs (610.75 ± 20.66) had gained 70.63g compared to both ZDSD-MOD (521.45 ± 11.23g) and ZDSD-SVD (490 ± 20.15g) that had lost 8.86g and 29.47g respectively (Fig. 2.3).

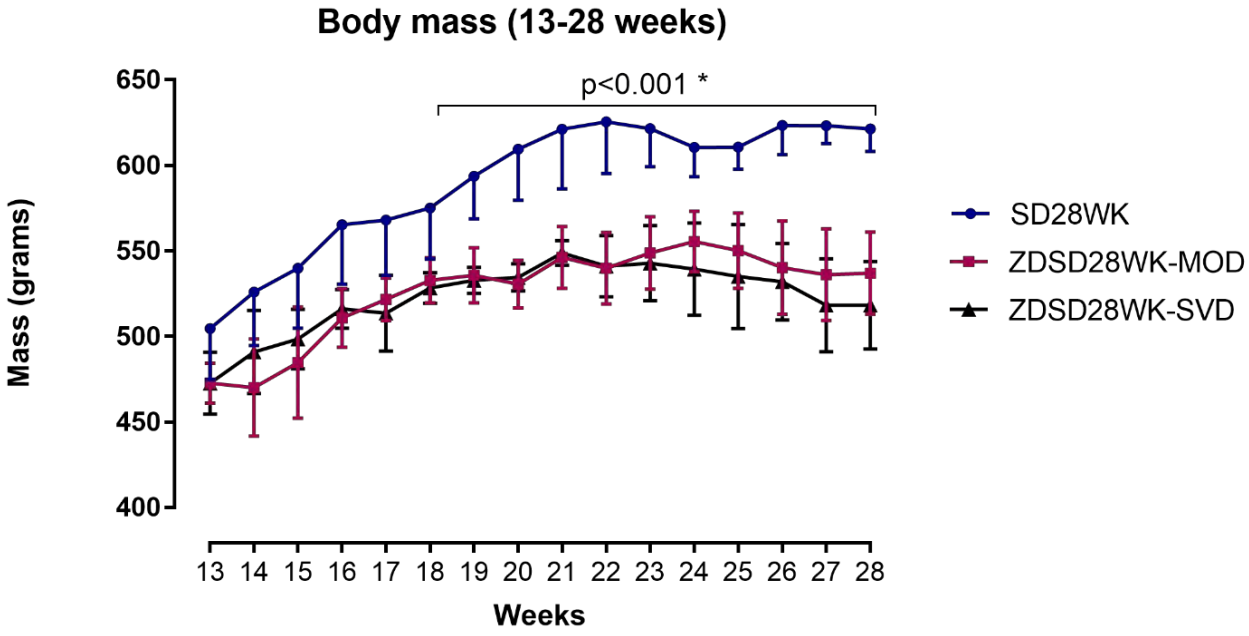


Figure 2.3: Changes in body mass from 13 to 28 weeks of age. A gradual reduction in mass is exhibited from week 18 in ZDSD28WK-MOD and ZDSD28WK-SVD when compared to SD28WK (*$p<0.001$ for both). SD20WK and SD28WK; Sprague Dawley rats aged 20 and 28 weeks, respectively. ZDSD20WK, ZDSD28WK-MOD and ZDSD28WK-SVD; Zucker Diabetic Sprague Dawley rats aged 20 weeks, and aged 28 weeks moderately diabetic and severely diabetic, respectively. Errors bars represent standard deviation.

2.2.2 Oral glucose tolerance tests

OGTT: 20-week-old

Average glucose levels at time zero were significantly higher in ZDSD20WK (19.28 ± 6.31 mmol/L) compared to SD20WK (4.6 ± 0.57 mmol/L controls) ($p<0.001$) (Fig. 2.4). The same trend was observed 2 hours post administration of the glucose load, with ZDSD20WK exhibiting significantly higher glucose values (24.08 ± 1.88mmol/L) than SD20WK (6.81 ± 0.61 mmol/L) controls ($p<0.001$) (Fig. 2.4). ZDSD20WK exhibited a 270% increase in the mean AUC (2999±159.80 mmol min/dL) compared to SD20WK (812. 40 ± 40.44 mmol min/dL).

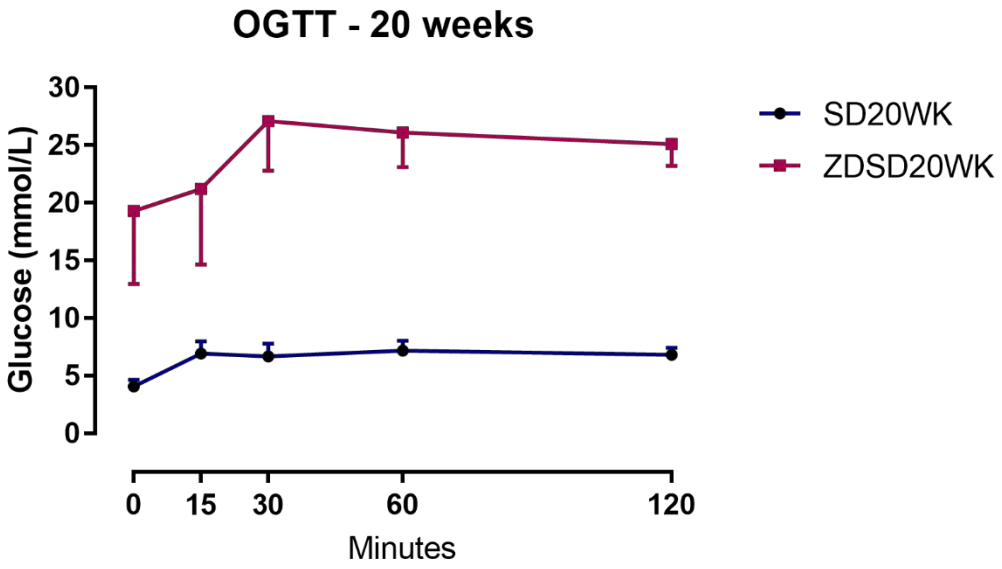


Figure 2.4: Oral glucose tolerance test and AUC at 20-weeks. Average values of the glucose tolerance exhibited abnormal glucose disposal by ZDSD20WK, and optimal glucose handling by the SD20WK ($p<0.001$). After 2 hours following administration of glucose, the ZDSD20WK had the highest area under the curve compared to SD20WK ($p<0.001$). SD20WK; Sprague Dawley rats aged 20 weeks. ZDSD20WK; Zucker Diabetic Sprague Dawley rats aged 20 weeks. Errors bars represent standard deviation

OGTT: 28-week-old

The SD28WK (4.70 mmol/L) controls exhibit lower glucose values at time zero compared to ZDSD-MOD (8.25 mmol min/dL) and ZDSD-SVD (11.20 mmol/L) ($p=0.014$, $p<0.001$ respectively) (Fig. 2.5). This significant trend is maintained 2hrs post administration of the glucose bolus, with SD28WK controls (6.53 mmol/L) showing lower values than ZDSD-MOD (12.97 mmol/L) together with the ZDSD-SVD (23.27 mmol/L) ($p<0.001$) for both (Fig. 2.5). The ZDSD-MOD (1314 ± 136.5 mmol min/dL) and ZDSD-SVD (2434 ± 320.60 mmol min/dL) show an increase (71.2% and 217% respectively) in mean AUC when compared to SD28WK (767.50 ± 29.64 mmol min/dL) controls.

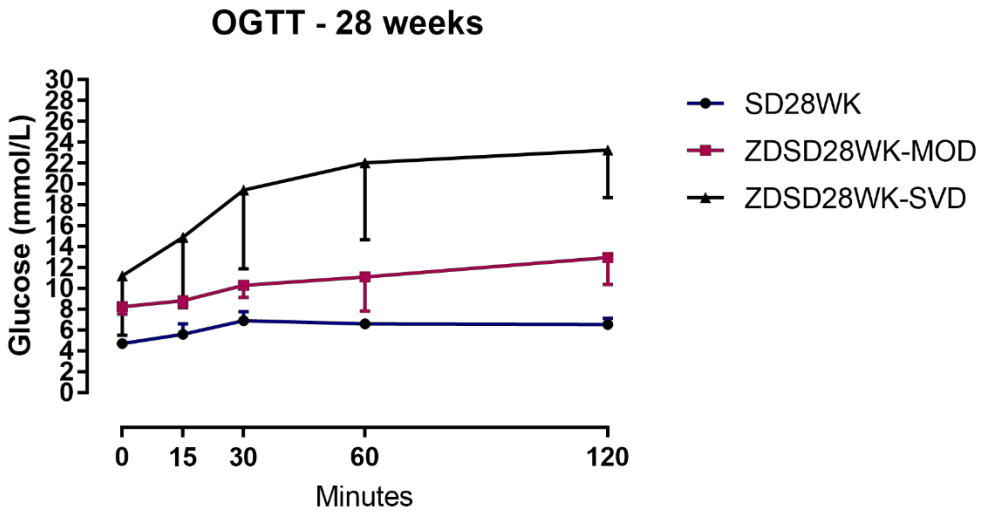


Figure 2.5: Oral glucose tolerance test and AUC at 28-weeks. Average glucose tolerance values show inefficient glucose disposal by the ZDSD28WK-SVD and ZDSD28WK-MOD compared to the SD28WK ($p=<0.001$, $p=0.014$ respectively). The ZDSD28WK-SVD had the largest mean AUC ($p<0.001$), followed by the ZDSD28WK-MOD ($p=0.014$) when compared with the SD28WK controls. SD20WK and SD28WK; Sprague Dawley rats aged 20 and 28 weeks, respectively. ZDSD20WK, ZDSD28WK-MOD and ZDSD28WK-SVD; Zucker Diabetic Sprague Dawley rats aged 20 weeks, and aged 28 weeks, moderately diabetic and severely diabetic, respectively. Errors bars represent standard deviation

2.2.3 Fasting blood glucose

Fasting blood glucose: 12 to 20-weeks

Significant differences were observed between the SD20WK (5.7mmol/L) controls and ZDSD20WK (7.70 mmol/L) from week 12 (p=0.001) until week 20, with the ZDSD20WK (22.07 mmol/L) exhibiting higher numbers compared to SD20WK (4.07 mmol/L) (p<0.001) (Fig. 2.6).

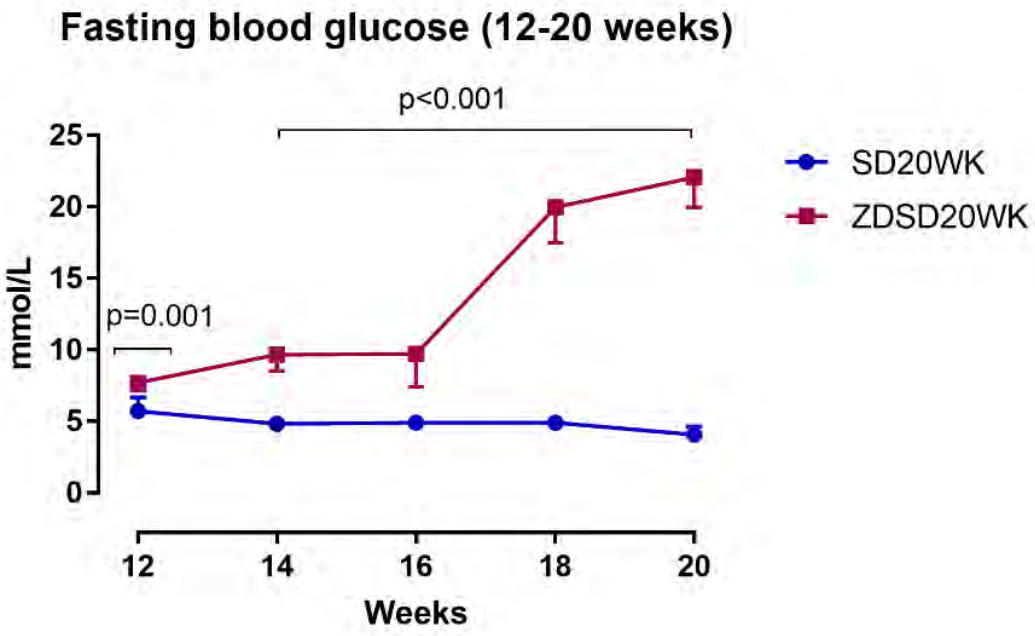


Figure 2.6: Fasting blood glucose at 12 to 20 weeks. SD20WK vs ZDSD20WK. p= 0.001 at week-12. p<0.001 from week-14 to week- 20. SD20WK and SD28WK; Sprague Dawley rats aged 20 and 28 weeks, respectively. ZDSD20WK, ZDSD28WK-MOD and ZDSD28WK-SVD; Zucker Diabetic Sprague Dawley rats aged 20 weeks, and aged 28 weeks, moderately diabetic and severely diabetic, respectively. Errors bars represent standard deviation

Fasting blood glucose: 12-28-weeks

The SD28WK (5.1 ± 0.41 mmol/L) controls exhibit lower values compared to ZDSD-MOD (8.1 ±0.57 mmol min/dL) and ZDSD-SVD (8.55 ± 1.66 mmol/L) ($p<0.001$ for both) at week-12 (Fig. 2.7). The same trend is shown at week 28, with SD28WK (4.99 ± 0.31 mmol/L) controls recording lower glucose levels compared to ZDSD-MOD (7.11 ± 0.13 mmol/L) and ZDSD-SVD (13.38 ± 1.61 mmol/L) ($p=0.019$; $p<0.001$ respectively) (Fig. 2.7).

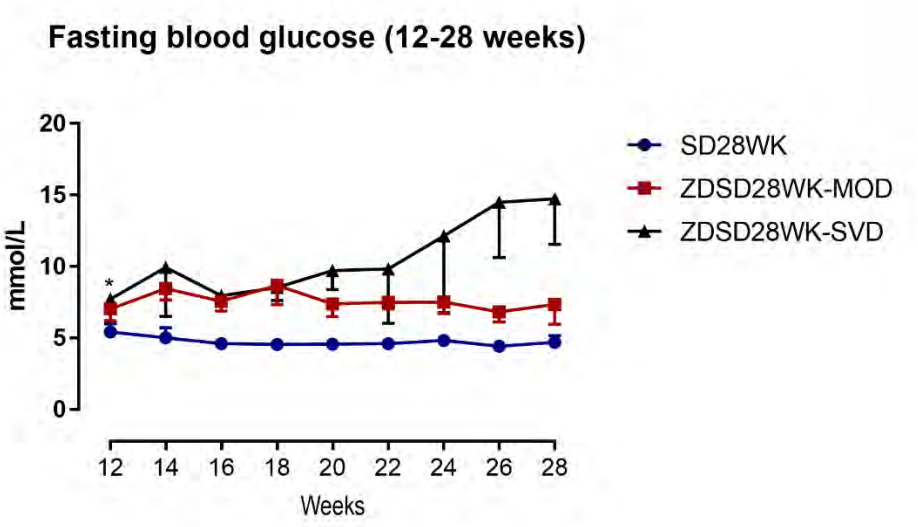


Figure 2.7: Fasting blood glucose at 12 to 28 weeks. SD28WK vs ZDSD28WK-MOD and ZDSD28WK-SVD ($p=0.019$, $p<0.001$ respectively). ZDSD28WK-MOD vs ZDSD28WK-SVD ($p<0.001$). SD20WK and SD28WK; Sprague Dawley rats aged 20 and 28 weeks, respectively. ZDSD20WK, ZDSD28WK-MOD and ZDSD28WK-SVD; Zucker Diabetic Sprague Dawley rats aged 20 weeks, and aged 28 weeks moderately diabetic and severely diabetic, respectively. Errors bars represent standard deviation

Insulin levels

SD20WK controls (10.45ng/ml ± 3.66) exhibited significantly higher insulin levels compared to ZDSD20WK (1.70 ± 0.48 10.45ng/ml) ($p<0.001$) (Fig .2.8). This trend is repeated at 28 weeks, with the SD28WK controls (13.24 ± 3.63) recording higher insulin levels relative to ZDSD28WK-MOD (4.07 ± 1.20 10.45ng/ml) and ZDSD28WK-SVD (3.10 ± 0.70 10.45ng/ml) ($p<0.001$ respectively) (Fig. 2.2). Age differences were observed between the ZDSD20WK when compared with ZDSD28WK-SVD ($p=0.003$) but not the ZDSD28WK-MOD ($p= 0.007$) (Fig .2.8).

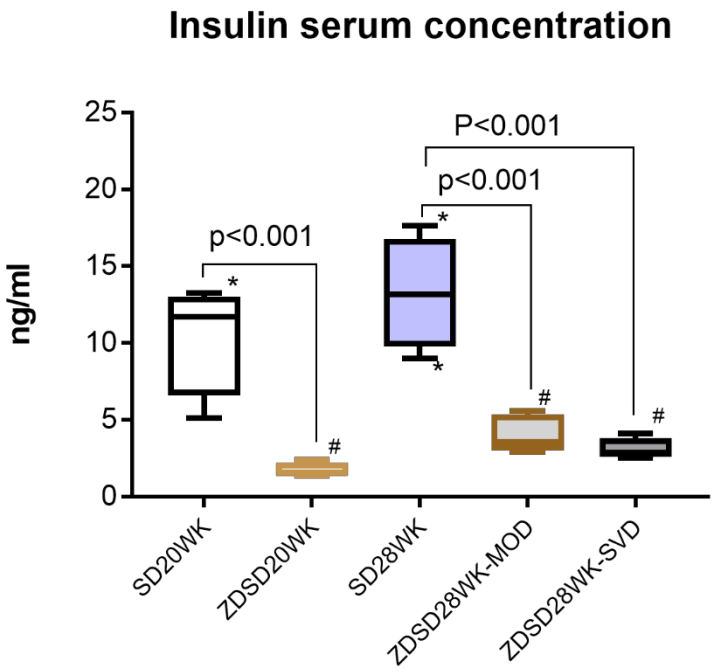


Figure 2.8: Serum insulin concentration. Box-and-whisker plots show insulin levels in various study groups. The line inside the box represents the mean, whereas the bottom and top lines of the box show the 25th and 75th percentiles, respectively. The whiskers below and above the box show the minimum and maximum values, respectively.

SD20WK and SD28WK; Sprague Dawley rats aged 20 and 28 weeks, respectively. ZDSD20WK, ZDSD28WK-MOD and ZDSD28WK-SVD; Zucker Diabetic Sprague Dawley rats aged 20 weeks, and aged 28 weeks moderately diabetic and severely diabetic, respectively. *; p=0.469 comparing SD20WK against SD28WK and #; p=0.007, p=0.003, comparing ZDSD20WK against ZDSD28WK-MOD and ZDSD28WK-SVD respectively.

Triglyceride levels

Triglyceride levels were higher in ZDSD20WK (2.06 mmol/L ±0.33) than SD20WK controls (1.70 ± 0.53 mmol/L) but differences were not significant (p=0.789) (Fig. 2.9). Significance is observed at 28 weeks, with SD28WK (1.40 ± 0.28 mmol/L) controls exhibiting lower numbers relative to the ZDSD28WK-MOD (2.62 ± 0.33 mmol/L) and ZDSD28WK-SVD (2.95 ± 0.31 mmol/L) (p=0.005, p<0.001 respectively) (Fig. 2.9). No age differences were observed when comparing ZDSD20WK, with ZDSD28WK-MOD and ZDSD28WK-SVD (p=0.414, p=0.062 respectively) (Fig. 2.9).

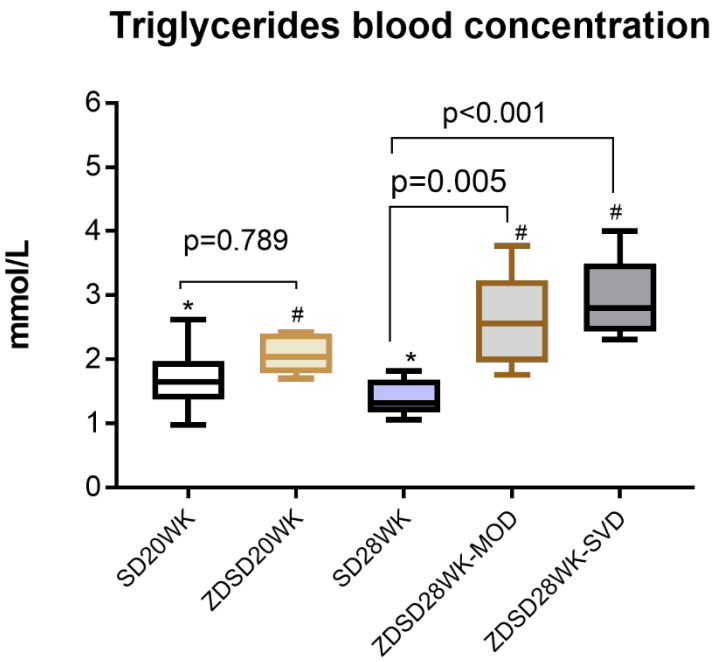


Figure 2.9: Blood triglyceride concentrations. Box-and-whisker plots show triglyceride levels in various study groups. The line inside the box represents the mean, whereas the bottom and top lines of the box show the 25th and 75th percentiles, respectively. The whiskers below and above the box show the minimum and maximum values, respectively.

SD20WK and SD28WK; Sprague Dawley rats aged 20 and 28 weeks, respectively. ZDSD20WK, ZDSD28WK-MOD and ZDSD28WK-SVD; Zucker Diabetic Sprague Dawley rats aged 20 weeks, and aged 28 weeks moderately diabetic and severely diabetic, respectively. *; p=0.873 comparing SD20WK against SD28WK, and #; p=0.414, p=0.062, comparing ZDSD20WK against ZDSD28WK-MOD and ZDSD28WK-SVD respectively.

Osteocalcin serum concentration

At 20 weeks, there were insignificant differences in osteocalcin levels between the SD20WK controls (9.38 ± 3.26 ng/ml) and ZDSD20WK (10.89 ± 5.87 ng/ml) (p=0.999) (Fig. 2.10). A similar trend is observed at 28 weeks where SD28WK controls (18.29 ± 1.10 ng/ml) did not exhibit any significant differences to ZDSD28WK-MOD (15.59 ± 2.49 ng/ml) and ZDSD28WK-SVD ZDSDs (34.25 ± 2.33 ng/ml) (p= 0.999; p= 0.5022) (Fig. 2.10). Similarities were observed between ZDSD20WK when contrasted with ZDSD28WK-MOD and ZDSD28WK-SVD (p=0.999; p=0.502 respectively) (Fig. 2.10).

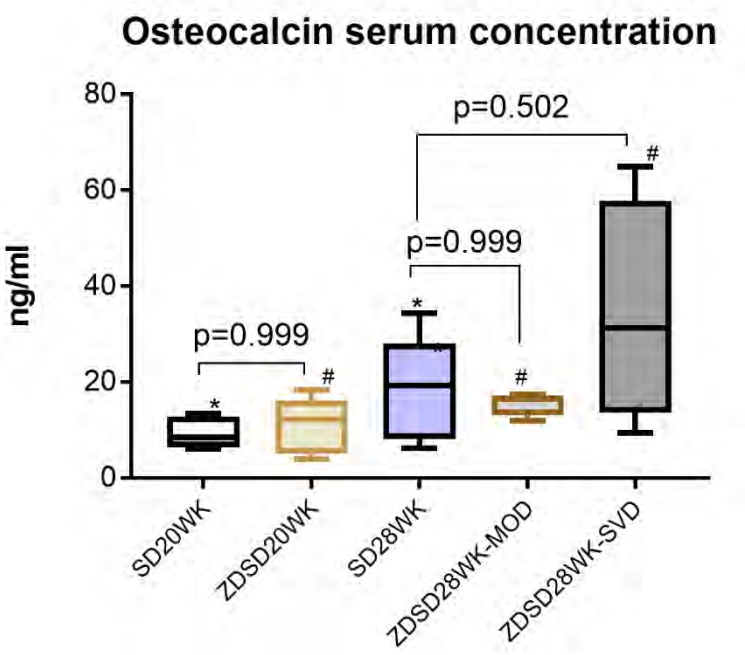


Figure 2.10: Serum osteocalcin concentrations. Box-and-whisker plots show serum osteocalcin levels in various study groups. The line inside the box represents the mean, whereas the bottom and top lines of the box show the 25th and 75th percentiles, respectively. The whiskers below and above the box show the minimum and maximum values, respectively.

SD20WK and SD28WK; Sprague Dawley rats aged 20 and 28 weeks, respectively. ZDSD20WK, ZDSD28WK-MOD and ZDSD28WK-SVD; Zucker Diabetic Sprague Dawley rats aged 20 weeks, and aged 28 weeks moderately diabetic and severely diabetic, respectively. *; p=0.999 comparing SD20WK against SD28WK and #; p=0.999, p=0.065 comparing ZDSD20WK against ZDSD28WK-MOD and ZDSD28WK-SVD respectively.

Malondialdehyde (MDA) serum concentration

Significant differences were observed between SD20WK (4.1 nmol/µL) and ZDSD20WK (19.11 nmol/µL) ($p<0.001$) (Fig.2.11). At week-28, significance was again observed when contrasting SD28WK (6.2 nmol/µL) with ZDSD28WK-MOD (17.8 nmol/µL) and ZDSD28WK-SVD (11.5 nmol/µL) ($p=0.007$, $p<0.001$ respectively) (Fig. 2.11). Age changes are observed between the ZDSD20WK and ZDSD28WK-SVD ($p=0.008$) but not the ZDSD28WK-MOD ($p=0.103$) (Fig. 2.11).

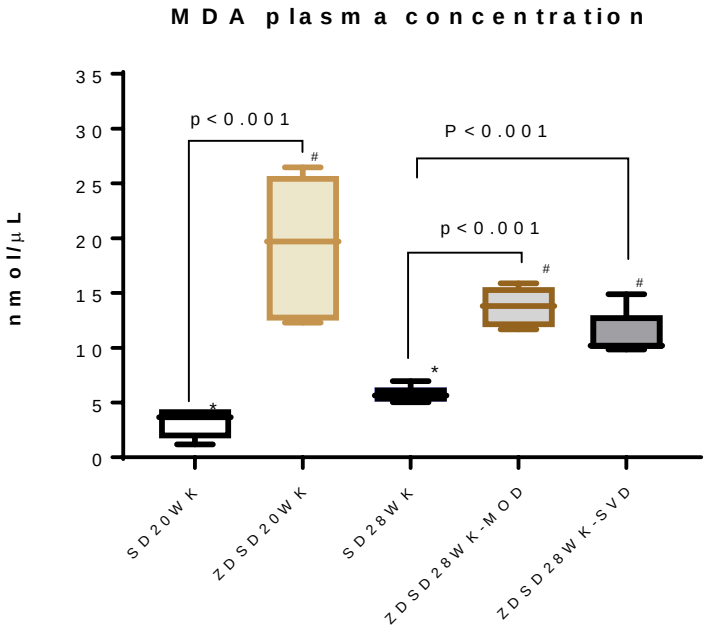


Figure 2.11: MDA serum concentration. Box-and-whisker plots show MDA serum levels in various study groups. The line inside the box represents the mean, whereas the bottom and top lines of the box show the 25th and 75th percentiles, respectively. The whiskers below and above the box show the minimum and maximum values, respectively.

SD20WK and SD28WK; Sprague Dawley rats aged 20 and 28 weeks, respectively. ZDSD20WK, ZDSD28WK-MOD and ZDSD28WK-SVD; Zucker Diabetic Sprague Dawley rats aged 20 weeks, and aged 28 weeks moderately diabetic and severely diabetic, respectively. *; $p=0.746$ comparing SD20WK against SD28WK, and #; $p=0.103$, $p=0.008$, comparing ZDSD20WK against ZDSD28WK-MOD and ZDSD28WK-SVD respectively.

2.3 Discussion

Multiple models of T2D (Zucker fatty rat, ZDF rat; knockout mice (ob/ob, db/db, Goto-Kakizaki, streptozocin induced) have been used in the past (Reinwald et al., 2009; Castrillón et al., 2011; Chandrasekera and Pippin, 2014; Peterson et al., 2015). While these have proved useful in diabetes studies, this study demonstrates the polygenetic ZDSD as an ideal animal model for T2D that can be extrapolated to humans. We have successfully synchronized the onset of diabetes with a high fat diabetogenic diet (Creecy et al., 2016). Following introduction of the diabetogenic diet, all ZDSD rats developed symptoms that are typical of T2D such as loss of mass, low insulin levels, high triglyceride levels, high FBG and abnormal OGTTs (Peterson et al., 2015).

Body mass changes

We observed a gradual loss of body mass between week-18 and week-19 that progressed until week-28 in the ZDSDs. As the rats were introduced to the diabetogenic diet at 15 weeks of age, this mass loss is consistent with the induction of diabetes. Creecy et al. 2016, reports that ZDSD rats become diabetic within 2 weeks of switching to the high fat diet. The 28-week severely diabetic group exhibits the highest loss in body mass. Lipolysis and sarcopenia that leads to weight loss is well documented in subjects with T2D (Boden and Laakso, 2004; Gougeon, 2013; Morigny et al., 2016).

Glucose handling (OGTTs and FBG)

Further confirmation of the diabetic state is demonstrated by abnormal OGTTs and FBG levels. All ZDSDs exhibited FBG levels of > 7mmol/L and readings of >11.1 mmol/L after 2 hours from the time of receiving a glucose load (Turner and Burr, 1993; Organization, 2006; Association, 2010). Increases in area under the curve following OGTTs again confirm the diabetic state and suggest an inefficient disposal of glucose by diabetic rats. Multiple studies have confirmed the development of T2D in the ZDSD rat after switching to the high fat diet (Reinwald et al., 2009; Fajardo et al., 2014; Creecy et al., 2016).

Triglycerides, insulin and osteocalcin interaction

The diabetic state as confirmed by OGTTs and FBG levels facilitated the development of hypoinsulinemia for both 20-week and 28-week-old rats. Hypoinsulinemia in T2D is a result of persistent hyperglycemia that causes pancreatic beta cell failure and apoptosis (Kahn, 2003; Scheen, 2003; Thrailkill et al., 2005). The low insulin levels observed at 20 weeks suggest beta cell failure must have occurred much earlier in the disease, in contrast with other studies that report compensatory hyperinsulinemia at disease onset, followed by hypoinsulinemia as the disease progresses (Aronoff et al., 2004; Giugliano et al., 2008; Del Prato, 2009). In the present study, insulin levels were tested upon termination at 20 and 28 weeks of age. It is possible that the characteristic hyperinsulinemia may have been missed. Peterson et al., (2015) reports peak insulin levels at week-19 before levels decline with disease progression.

Insulin acts synergistically with the hormone osteocalcin, to regulate glucose metabolism, increase tissue sensitivity to insulin, increase pancreatic beta cell proliferation and increase insulin secretion (Lee et al., 2007; Booth et al., 2013; Kanazawa, 2015). Both carboxylated and uncarboxylated osteocalcin directly increase glucose transport in adipocytes and muscle cells. Our study reports similarities in total osteocalcin levels across all experimental groups when contrasted with age matched controls. This suggests that serum osteocalcin levels were not affected by the diabetic state. This is in contrast with other studies on osteocalcin receptor knockout mice and untreated diabetic mice (Thrailkill et al., 2005) that exhibit low osteocalcin levels, reduced islet numbers, hyperglycemia, and glucose intolerance (Fajardo et al., 2014; Ferron and Lacombe, 2014).

Hypoinsulinemia triggers lipolysis to cause elevated serum triglycerides (Morigny et al., 2016). Hypertriglyceridemia is linked to age and disease progression (Boden and Laakso, 2004; Peterson et al., 2015). We observed higher triglyceride levels in older diabetic rats (28-week-old groups) suggesting that long standing hyperglycemia facilitates serum accumulation of triglycerides. Fasted triglyceride levels were reported to peak at 19 weeks in ZDSDs, then decline and remain stable after 21 weeks (Peterson et al., 2015), contrary to Reinwald et al., (2009) who reported

elevated triglyceride levels in diabetic ZDSDs compared to controls. Our findings agree with Reinwald et al, (2009) that reported elevated triglyceride levels later in the disease (33-weeks).

Oxidative stress (MDA)

Here, elevated MDA levels early in the disease and as the disease progresses similar to reports on diabetic patients and hyperglycemic mice are reported (Del Rio et al., 2005; Tiwari et al., 2013). MDA plasma levels are used as markers of oxidative stress in clinical settings (Slatter et al., 2000; Negre-Salvayre et al., 2010; Ayala et al., 2014).The high glucose levels recorded from OGTTs and fasting blood glucose together with triglycerides may have triggered the development of ROS that feed into toxic lipid peroxidation processes, to produce bio toxic molecules like MDA (Jaganjac et al., 2013; Wang et al., 2018). These abnormal MDA levels from week 20 signify that oxidative stress is established once the diabetic state is present.

2.4 Conclusions

In this study diabetes was successfully induced in a relatively new polygenetic model of T2D, as indicated by various markers that confirm the presence of T2D. There was loss of body mass, abnormal OGTTs and FBG that are in line with definitions of T2D by the WHO. There was reduced insulin levels in diabetic rats, a feature that is a symptom pancreatic beta cell failure due to long standing hyperglycemia. Other abnormal biochemical tests include elevated MDA levels in diabetic rats. Levels of the hormone osteocalcin that acts in synergy with insulin remained unchanged irrespective of hyperglycemia and hypoinsulinemia in ZDSD rats.

Chapter 3

Tensile strength and microarchitecture of the ZDSD rat femur

TABLE OF CONTENTS

3.0 Introduction 56
3.1 MATERIALS AND METHODS 57
3.1.1 Rat model for diabetes type 2 57
3.1.2 Bone harvesting 57
3.1.3 Micro-focus X-ray Computed Tomography (Micro CT) 57
3.1.5 Data analysis 60
3.2 Results 61
3.2.1 Femur osteometry at week-20 and week-28 61
Femur Bone mass 61
Femur Full bone length 61
Femur Biomechanical length 61
Femur bicondylar width 62
Femur midshaft anteroposterior (AP) diameters 62
Femur midshaft mediolateral (ML) diameters 63
Femur robusticity Index 63
Femur head width 64
Femoral neck superoinferior (SI) length 64
Femoral neck anteroposterior (AP) length 64
Femur maximum force 65
Femur break force 65
Femur yield force 66
Femur maximum time 66
Femur maximum displacement 67
Femur stiffness 67
Femur elastic modulus 68
3.2.3 Proximal femur trabecular morphometry at week-20 and week-28 68
Femur bone tissue volume (BV) 68
Femur bone tissue volume to bone tissue volume ratio (BV/TV) 69
Femur trabecular thickness (TbTh) 69
Femur trabecular number (TbN) 69
Femur trabeculae spacing (TbSp) 70

3.2.4 Femoral mid diaphysis cortical area and medullary canal area at week-20 and week-28 71
Femur cortical area 71
Femur medullary canal area 71
3.2.5 Parameters of the femur most affected by age, diabetes and is duration 72
3.3 Discussion 76
Osteometric aspects 76
3-point bending parameters 77
Trabecular morphometry 78
3.3.1 Conclusions 80

3.0 INTRODUCTION

Fractures of the proximal femur, also described as hip fractures, are very common. In 1990, hip fractures were estimated to be 1.26 million globally, this number is expected to double in 2025, and increase to 4.5 million by 2050 (Gullberg et al., 1997; Emmerson et al., 2022). Hip fractures can occur at various points of the proximal femur such as the acetabulum of the pelvis, femoral head, intertrochanteric area and the femoral neck (Emmerson et al., 2022). Fractures of the femoral neck are the most common (Monzem et al., 2022) hence our study was focused on the proximal femur.

There seems to be a link between T2D and increased fracture risk. Multiple, but inconclusive studies elucidate the association between T2D and increased fracture risk (Janghorbani et al., 2007; Vestergaard et al., 2009; Valderrabano and Linares, 2018). These studies analyse bone strength using three point bending tests, micro-CT and various osteometric tools to study the effect if T2D on the femur (Prisby et al., 2008; Reinwald et al., 2009; Creecy et al., 2016). However, these studies tend to omit correlating bone geometry with its robusticity when assessing bone strength. This study, collates the geometry of the femur with its robusticity, to determine if the bones are long, and thin or short and thick, then evaluate how these bones perform when subjected to 3-point bend testing until fracture. Whole bone structural strength is influenced by its geometry (mass, shape and size), robusticity, and micro architectural organization (Patel et al.; Prisby et al., 2008; Martin and Correa, 2010; Jepsen et al., 2015).

This chapter aimed to evaluate the tensile strength and the microarchitecture of the femur of ZDSD rats. This was done by assessing femur load (force) handing properties, osteometry, midshaft cortical and medullary canal areas as well as femoral head trabecular morphological parameters. Further investigations were undertaken understand if perturbations caused by T2D are age dependent, by comparing femora of 20-week with those from 28-week-old rats.

3.1 MATERIALS AND METHODS

3.1.1 Rat model for diabetes type 2

Rats were handled as described in section 2.1.2

3.1.2 Bone harvesting

Rats were immersed in 10% buffered formalin after abdominal and limb incisions were made to facilitate penetration of the fixative. Posterior left and right limbs were removed, and muscles were cleaned out of the femur. Individual bones were then stored in 10% buffered formalin to continue fixation until further processing. Right femora were used for biomechanical investigations by 3-D micro-CT and 3-point bend tests.

3.1.3 Micro-focus X-ray Computed Tomography (Micro CT)

For Micro-focus X-ray Computed Tomography (Micro CT), bilateral femora from rats terminated aged 20 and 28-weeks were scanned using a Nikon XTH 225/320 LC X-ray microtomograph. To keep the samples steady during scanning, the bones were placed in plastic tubes and mounted in low density Styrofoam that allows X-rays to penetrate the sample with negligible absorption. The plastic container with the sample inside was positioned on a rotating manipulator in the scanning chamber for the scanning process. Scanning parameters as listed in table 3.1.

Table 3.1: Scanning parameters at week-20 and week-28

Parameter	Value
X-ray voltage	70kv
X-ray current	400µA
Filter	1 mm aluminium
Scanning resolution	20µ
Tomographic rotation	360 degrees
Rotation step	1 degree
Frame averaging	4
Scan duration	8 minutes

Parts of the femora and trabecular morphometry parameters studied

Bones were weighed and a digital handheld calliper was used to determine femoral osteometric parameters. Full bone length, biomechanical length, bicondylar width and various femoral head and neck diameters, were measured, robusticity index (Patel et al.) was calculated. (Fig. 3.1 and Table 3.2). Following reconstruction, VG studio Max ®3.2 was used for data analysis as previously described (Bouxsein et al., 2010). The trabecular morphometric parameters were studied in the proximal epiphysis of the bone. The following parameters were determined, the trabecular number, thickness, spaces and volume (Table 3.3).

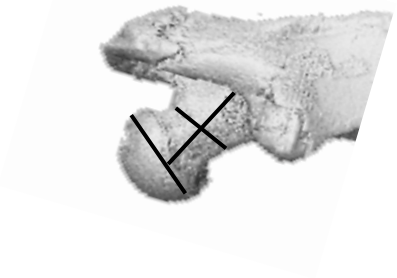


Figure 3.1. Three-dimensional reconstruction of a femur showing the various femoral head and neck diameters, were measured

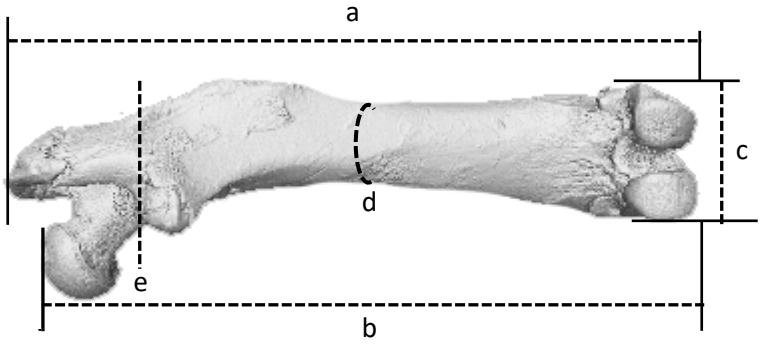


Figure 3.2. **Three-dimensional reconstruction of a femur showing the parts that were investigated**. (a), full femur length; (b), biomechanical length; (c), bicondylar breadth; (d), 50th (midshaft) mark; (e), proximal ROI for trabeculae morphological assessment. (Image courtesy of R. Ndou and G.F Dlamini).

Table 3.2: Femur osteometric parameters

Parameter	Description
Full femur length	The maximum length measured between the top of the greater trochanter and the bottom of the farthest condyle
Biomechanical length	The distance between the medial most and lateral most points on the epicondyles
Bicondylar width	The distance between the medial most and lateral most points on the epicondyles
Midshaft AP diameter	Distance between bulgiest parts in an antero-posterior direction at the 50th percentile
Midshaft ML diameter	Distance between bulgiest parts in a medio-lateral direction at the 50th percentile
Robusticity index	Sum of the ML and AP midshaft diameter multiplied by 100 and divided by physiological length of the femur
Femoral head width	Distance between bulgiest part in an anteroposterior, medio-lateral, supero-inferior direction when viewed from the top
Femoral neck SI length	Between the highest and lowest point on the articular margin, taken at right angles to the AP length
Femoral neck AP length	Distance between bulgiest part in an anterio-posterior direction

Table 3.3: Femur trabecular assessment parameters (adapted from (Bouxsein et al., 2010)

Parameter	Definition
$\frac{\mathbf{BV}}{\mathbf{TV}}$ (bone tissue volume to total volume)	Represents the ratio of material (bone) volume to total volume.
TbTh (mean trabecular thickness)	The material (bone), calculated as follows: **TbTh =2/BS/BV** Where **BS/BV** is the ratio of material (bone) surface (**BS**) to material (bone) volume (**BV**)
TbN (mean trabecular number)	Shows the mean number of trabecular (column-like) structures per unit length, calculated as follows: **TbN=BV/TV/TbTh**
TbSp (mean trabecular spacing)	Indicates the mean distance between trabecular (column-like) structures, calculated as follows: **TbSp=1/TbN−TbTh**
Medullary cavity area	The area of a slice taken from the outer margins encompassing the medullary canal at the 50th percentile mark
Cross-sectional area	The area of a slice taken from the outer margins encompassing the shaft at the 50th percentile marks

3.1.4 Three-point bending test

The right femora were subjected to a three-point bending test. The load was applied at the midshaft, midway between two supports that were 15mm apart. (Fig. 3.3). The femora were positioned such that bending occurred in an anteroposterior plane. Load-displacement curves were recorded at a constant speed of 5mm/min until failure.

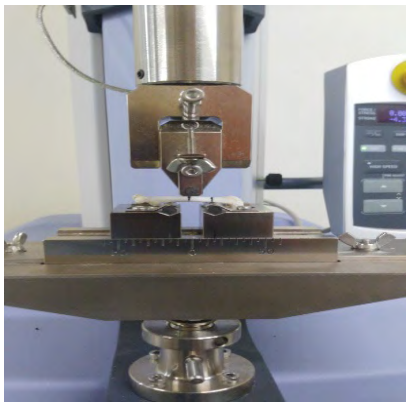


Figure 3.3: **Three-point bending test instrument**. The load is applied to the midshaft of the femur between two supports 15mm part in the mediolateral plane.

3.1.5 Data analysis

The data were managed in Microsoft Excel 2016 (Microsoft Corporation) and analyzed using SPSS® version 25 (IBM®). ANOVA with LSD post-hoc was used for multiple group comparisons of means. Significance level was set at $p < 0.05$.

3.2 RESULTS

3.2.1 Femur osteometry at week-20 and week-28

Femur Bone mass

At 20 weeks of age, the ZDSD femora weighed significantly less than their SD controls ($p<0.001$) (Table 3.4). The same trend was observed at week-28, with ZDSD28WK-MOD and ZDSD28WK -SVD recording significantly lower values than their SD controls ($p<0.001$ for both comparisons). The SD controls exhibited age related differences, with bones of older rats (age of 28 weeks) weighing significantly less than the 20-week-olds ($p<0.001$) (Table 3.4). Similarly, ZDSD femora weighed less at 28 weeks (ZDSD28WK-MOD and ZDSD28WK-SVD) compared to those of 20 week old ZDSDs ($p=0.020$ and $p=0.014$, respectively).

Femur Full bone length

Similarities in full femoral length were observed among 20-week-old rats between the ZDSDs and SD controls ($p=0.596$) (Table 3.4). In contrast, at the age of 28 weeks, both ZDSD28WK-MOD and ZDSD28WK-SVD exhibited significantly shorter lengths compared to their SD controls ($p<0.001$, for both comparisons). Age differences were observed in SD controls between rats aged 20 and those aged 28 weeks, younger (20 weeks) SDs had shorter bones than older rats ($p=0.001$ (Table 3.4). In contrast, ZDSD full femoral length was similar at 20 weeks of age compared to the 28-week-old groups (ZDSD28WK-MOD #$p=0.354$ and ZDSD28WK-SVD $p=0.059$).

Femur Biomechanical length

There were similarities in biomechanical length values between 20-week-old rats when comparing SD controls with ZDSDs ($p=0.584$) (Table 3.4). In contrast, among the 28-week-old rats, ZDSD28WK-MOD and ZDSD28WK-SVD exhibited shorter biomechanical lengths than their SD controls ($p<0.001$ for both comparisons). Similarities in biomechanical length were observed in 20-week-old SDs and 28-week-old SDs ($p=0.105$) (Table 3.4). On the contrary, age differences were observed between ZDSD28WK-MOD and ZDSD28WK-SVD ($p=0.024$ and $p<0.001$ respectively), with younger (20-week-old) ZDSDs having longer biomechanical lengths.

Femur bicondylar width

At week-20, ZDSDs exhibited significantly shorter bicondylar widths compared to SD controls ($p<0.001$) (Table 3.4). This significant trend of shorter bicondylar widths continued and was observed at week-28 when comparing ZDSD28WK-MOD ($p=0.003$) and ZDSD28WK-SVD ($p<0.001$) with their SD controls. Age related differences were observed between the SD groups, where younger SDs (20-week-olds) had wider condyles than the 28-week-old SDs ($p<0.001$) (Table 3.4). Similarly, younger ZDSDs (20-week group) also exhibited wider condyles compared to older ZDSD28WK-MOD and ZDSD28WK-ZVD groups ($p=0.003$ and $p= 0.020$, respectively).

Table 3.4: Osteometric measurements of the femur

		Week-20			***Week 28***		
Property	**SD (n=12)**	**ZDSD (n=12)**	**p value**	**SD (n=12)**	**ZDSD-MOD (n=12)**	**ZDSD-SVD (n=12)**	**p value**
Mass (g)	1.35±0.09	1.19±0.04	<0.001	1.26±04	1.25±0.06	1.16±0.11	^[0.005, 0.001], *<0.001 #0.001 (both)
Full length (mm)	39.71±0.83	39.57±0.37	0.545	40.45±0.31	39.37±0.28	39.13±0.85	^[<0.001(both),] *0.001 #0.354, 0.059
Biomechanical length (mm)	38.59±0.53	38.43±0.41	0.584	39.03± 0.53	37.85±0.68	37.18±0.47	^[<0.001,0.003] *<0.105 #0.024,<0.001(both)
Bicondylar width (mm)	7.78±0.26	6.91±0.19	<0.001	7.14±0.21	7.11±0.07	6.85±0.25	^[0.003, <0.001], *<0.001 #0.003,0.020

^ Respective comparison of ZDZD28Wk with ZDSD28WK-MOD and ZDSD28WK-SVD: *; p-value comparing SD20WK against SD28WK, and #; p-value comparing ZDSD20WK against ZDSD28WK-MOD and ZDSD28WK-SVD respectively

Femur midshaft anteroposterior (AP) diameters

There were similarities in midshaft AP diameters between SD controls and ZDSDs at 20-weeks of age ($p=0.063$) (Table 3.5). In contrast, at week-28, differences were observed when comparing SD controls with ZDSD28WK-MOD and ZDSD28WK-SVD ($p<0.001$ for both comparisons). No age related differences were observed between 20-week-old and 28-week-old SD controls ($p=0.188$) (Table 3.5). On the contrary, 20-week-old ZDSDs exhibited wider AP diameters when compared with ZDSD28WK-MOD and ZDSD28WK-SVD ($p<0.001$ for both comparisons).

Femur midshaft mediolateral (ML) diameters

At 20 weeks of age, midshaft mediolateral diameters were significantly larger in ZDSDs compared to SD controls ($p<0.001$) (Table 3.5). Similarly, 28 weeks old rats showed that both the ZDSD28WK-MOD and ZDSD28WK-SVD exhibited larger measurements when compared with 28-week-old SD controls ($p<0.001$ for both comparisons). No age-related differences were observed between 20-week-old and 28-week SD controls (Table 3.5). On the contrary, 20-week-old ZDSDs exhibited wider ML diameters when compared with ZDSD28WK-MOD and ZDSD28WK-SVD in this region ($p<0.001$ for both comparisons).

Femur robusticity Index

At week-20, the SD controls were significantly more robust than the ZDSDs ($p=0.002$) (Table 3.5). This trend was maintained at week-28, where SD controls were more robust than ZDSD28WK-MOD and ZDSD28WK-SVD ($p<0.001$ for both comparisons). Younger (20-week-old) SDs were significantly more robust than older (28-week-old) SDs ($p=0.002$) (Table 3.5). The same trend was observed in the ZDSD group, where younger (20-week-old) ZDSDs were more robust than older (28-week-old) ZDSD28WK-MOD and ZDSD28WK-SVD ($p<0.001$ for both comparisons).

Table 3.5: Osteometric measurements of the femoral midshaft

	Week 20			***Week 28***			
Property	**SD (n=12)**	**ZDSD (n=12)**	**p value**	**SD (n=12)**	**ZDSD-MOD (n=12)**	**ZDSD-SVD (n=12)**	**p value**
Mid shaft AP diameter (mm)	3.80±0.15	3.61±0.09	0.063	3.69±0.20	3.61±0.35	3.83±0.44	^[<0.001(both)] *0.188 #<0.001(both)
Mid shaft ML diameter (mm)	5.13±0.17	4.75±0.17	<0.001	5.05±0.0.26	3.61±0.35	3.83±0.44	^[<0.001(both)] *0.188 #<0.001(both)
Robusticity Index (%)	22.49±1.17	21.13±0.44	0.002	21.21±0.85	16.65±1.39	16.71±1.04	^[0.001(both)] *0.003 #<0.001(both

^ Respective comparison of ZDZD28Wk with ZDSD28WK-MOD and ZDSD28WK-SVD: *; p-value comparing SD20WK against SD28WK, and #; p-value comparing ZDSD20WK against ZDSD28WK-MOD and ZDSD28WK-SVD respectively

Femur head width

The 20-week-old ZDSDs had shorter femoral head width measurements when compared with their SD controls ($p<0.001$) (Table 3.6). In contrast, similarities with SD controls were observed in 28-week-old rats for both ZDSD28WK-MOD and ZDSD28WK-SVD ($p=0.403$ and $p= 0.188$, respectively). Older (28-week) SDs had significantly smaller head widths when compared with 20-week-old SD controls ($p<0.001$) (Table 3.6). On the other hand, ZDSD28WK-MOD did not show any age differences ($p=0.706$), while the ZDSD28WK-SVD ($p=0.019$) had smaller heads when compared with 20-week-old ZDSDs.

Femoral neck superoinferior (SI) length

The 20-week-old ZDSDs had shorter femoral neck SI length measurements when compared with their SD controls ($p=0.001$) (Table 3.6). In contrast, similarities with SD controls were observed in 28-week-old rats for both ZDSD28WK-MOD and ZDSD28WK-SVD ($p=0.573$, $p= 0.172$ respectively). Older (28-week-old) SDs had shorter femoral neck SI lengths when compared with 20-week-old SD controls ($p=0.008$) (Table 3.6). On the contrary, ZDSD femoral neck SI lengths were similar at 20-weeks of age compared to the 28-week-old groups (ZDSD28WK-MOD $p=0.668$ and ZDSD28WK-SVD $p=0.665$).

Femoral neck anteroposterior (AP) length

The 20-week-old ZDSDs had similar femoral neck AP length measurements when compared with their SD controls ($p=0.664$) (Table 3.6). The same trend was observed in 28-week-old rats when comparing SD controls with ZDSD28WK-MOD and ZDSD28WK-SVD ($p=0.253$, $p= 0.618$ respectively)). No age-related differences were observed in femoral neck AP length between 20-week-old and 28-week SD controls ($p=0.420$) (Table 3.6). This trend of similar femoral neck AP lengths was also observed in ZDSD groups, when comparing 20-week-old ZDSDs with 28-week-old ZDSD groups (ZDSD28WK-MOD $p=0.883$ and ZDSD28WK-SVD $p=0.089$).

Table 3.6: Osteometric measurements of the femoral head and neck

	Week-20			*Week 28*			
Property	**SD (n=12)**	**ZDSD (n=12)**	**p value**	**SD (n=12)**	**ZDSD-MOD (n=12)**	**ZDSD-SVD (n=12)**	**p value**
Femoral head width (mm)	4.59±0.20	4.03±0.33	<0.001	4.14±0.30	4.06±0.21	4.28±0.32	^[0.403,0.188], *<0.001 #0.706,0.019
Femoral neck SI length (mm)	3.43±0.63	2.81±0.37	0.001	2.97±0.42	2.88±0.39	2.73±0.28	^[0.573,0.172], *0.008 #0.668,0.665
Femoral neck AP length (mm)	2.22±0.18	2.18±0.07	0.664	2.30±0.34	2.20±0.10	2.35±0.43	^[0.253,0.618], *0.420 #0.883,0.089

^ Respective comparison of ZDZD28Wk with ZDSD28WK-MOD and ZDSD28WK-SVD: *; p-value comparing SD20WK against SD28WK, and #; p-value comparing ZDSD20WK against ZDSD28WK-MOD and ZDSD28WK-SVD respectively

3.2.2 Three-point bending assessment of the femur mid-diaphysis in 20- and 28-week-old rats

Femur maximum force

The 20-week-old SD controls displayed higher values for maximum force (p=0.050), when compared with age matched ZDSDs (Table 3.7). On the contrary, at week-28, similarities were observed between 28-week-old SD controls when compared with ZDSD28WK-MOD and ZDSD28WK-SVD (p=0.170 and p= 0.364, respectively). No age-related differences were observed for maximum force between 20-week-old and 28-week SD controls (p=0.841) (Table 3.7). On the other hand, when younger (20-week-old) ZDSDs were compared with older (28-week-old) groups, the ZDSD28WK-MOD did not show any age differences (p=0.318), while the ZDSD28WK-SVD (p=0.003) exhibited lower maximum force values.

Femur break force

At week-20, there were similarities in break force (Table 3.7) between 20-week-old rats when comparing SD controls with ZDSDs (p=0.584). In contrast, among the 28-week-old rats, ZDSD28WK-MOD and ZDSD28WK-SVD exhibited a lower break force than their SD controls (p<0.001 for both comparisons). No age-related differences were observed in break force

between 20-week-old and 28-week-old SD controls (Table 3.7). On the other hand, when younger (20-week-old) ZDSDs were compared with older (28-week-old) groups, the ZDSD28WK-MOD did not show any age differences (p=0.790), while the ZDSD28WK-SVD (p=0.014) exhibited lower break force values.

Femur yield force

At week-20, there were similarities in yield force between 20-week-old rats when comparing SD controls with ZDSDs (p=0.584) (Table 3.7). This similar trend was observed again at week-28 between SD controls when compared with ZDSD28WK-MOD and ZDSD28WK-SVD (p=0.343, p= 0.911 respectively). Older (28-week-old) SDs had lower yield force values when compared with 20-week-old SD controls (p<0.038) (Table 3.7). On the contrary, ZDSD yield force values were similar at 20-weeks of age compared to the 28-week-old groups (ZDSD28WK-MOD #p=0.158 and ZDSD28WK-SVD #p=0.307).

Table 3.7: Three-point bend assessment of the femur for maximum force, break force, and yield force.

	Week-20			***Week 28***			
Property	**SD (n=12)**	**ZDSD (n=12)**	**p value**	**SD (n=12)**	**ZDSD-MOD (n=12)**	**ZDSD-SVD (n=12)**	**p value**
Maximum force (N)	171.09±37.40	150.56±10.45	0.052	182.53±16.55	173.16±30.31	160.11±26.32	^[0.170, 0.364] *0.841 #0.318,0.003
Break force (N)	170±27.12	150.46±10.45	0.071	175.08±27.12	153.08±10.45	152.09±10.01	^[0.025(both)] *0.628 #0.790,0.014
Yield force (N)	119.28±26.30	118.84±14.86	0.969	104.31±32.31	94.49±12.88	93.21±43.59	^[0.343,0.911] *0.038 #0.158,0.307

^ Respective comparison of ZDZD28Wk with ZDSD28WK-MOD and ZDSD28WK-SVD: *; p-value comparing SD20WK against SD28WK, and #; p-value comparing ZDSD20WK against ZDSD28WK-MOD and ZDSD28WK-SVD respectively

Femur maximum time

There were similarities in maximum time to fracture when comparing 20-week-old rats SD controls with age matched ZDSDs (p=0.384) (Table 3.8). In contrast, among the 28-week-old rats, ZDSD28WK-MOD and ZDSD28WK-SVD exhibited shorter maximum times to fracture than their SD controls (p<0.001 for both comparisons). Age differences were observed in SD controls

between rats aged 20 weeks and those aged 28 weeks (p<0.001), where younger (20 weeks) had shorter times (Table 3.8). On the contrary, age differences were observed between ZDSD28WK-MOD and ZDSD28WK-SVD (p=0.012, p<0.001 respectively), with younger (20-week-old) ZDSDs having shorter maximum times to fracture.

Femur maximum displacement

At week-20, there were similarities in yield force between 20-week-old rats when comparing SD controls with ZDSDs (p=0.584) (Table 3.8). This similar trend was observed again at week-28 between SD controls when compared with ZDSD28WK-MOD and ZDSD28WK-SVD (p=0.225, p= 0.427 respectively). Age related differences were observed between the SD controls, where younger SDs (20 week olds) exhibited lower maximum displacement values than 28 week old SDs (p<0.001) (Table 3.8). Similarly, among the ZDSD groups, younger ZDSDs (20-week group) exhibited lower maximum displacement values compared to older ZDSD28WK-MOD and ZDSD28WK-ZVD groups (p=0.040 and p=0.028, respectively).

Table 3.8: Three-point bend assessment of the femur for maximum time and maximum displacement.

	Week-20			Week 28			
Property	**SD (n=12)**	**ZDSD (n=12)**	**p value**	**SD (n=12)**	**ZDSD-MOD (n=12)**	**ZDSD-SVD (n=12)**	**p value**
Maximum time (sec)	13.69±2.58	12.73±2.39	0.384	18.94±2.87	13.69±2.58	11.07±3.30	^[<0.001(both)] *<0.001 #0.012,<0.001
Maximum displacement (mm)	0.71±0.24	0.69±0.13	0.682	0.89±0.15	0.84±0.19	0.82±0.16	^[0.225,0.427] *0.012 #0.040,0.028

^ Respective comparison of ZDZD28Wk with ZDSD28WK-MOD and ZDSD28WK-SVD: *; p-value comparing SD20WK against SD28WK, and #; p-value comparing ZDSD20WK against ZDSD28WK-MOD and ZDSD28WK-SVD respectively

Femur stiffness

There were similarities in stiffness between 20-week-old rats when comparing SD controls with ZDSDs (p=0.384) (Table 3.9). This similar trend was observed again at week-28 when comparing SD controls with ZDSD28WK-MOD and ZDSD28WK-SVD (p=0.900, p=0.360 respectively). Age related differences were observed between the SD controls, where younger SDs (20-week-olds) exhibited higher values for stiffness compared to 28-week-old SDs (p=0.019) (Table 3.9). On the

contrary, stiffness values and ZDSDs were similar at 20-weeks of age compared to the 28-week-old groups (ZDSD28WK-MOD p=0.408 and ZDSD28WK-SVD p=0.980).

Femur elastic modulus

Similarities in elastic modulus were observed in 20-week-old rats, when comparing ZDSDs and SD controls (p=0.0.938) (Table 3.9). In contrast, at the age of 28 weeks, both ZDSD28WK-MOD and ZDSD28WK-SVD exhibited lower elastic modulus values when compared to their SD controls (p<0.001, for both comparisons). Age differences were observed in SD controls between rats aged 20 weeks and those aged 28 weeks, with older (28 weeks) having higher values than younger (20 weeks) SDs (p<0.001) (Table 3.9). In contrast, ZDSD values for elastic modulus were similar when comparing the 20 weeks old with the 28-week-old groups (ZDSD28WK-MOD p=0.969 and ZDSD28WK-SVD p=0.926).

Table 3.9: Three-point bending assessment of the femur for stiffness and elastic modulus.

	Week 20			Week 28			
Property	**SD (n=12)**	**ZDSD (n=12)**	**p value**	**SD (n=12)**	**ZDSD-MOD (n=12)**	**ZDSD-SVD (n=12)**	**p value**
Stiffness (N/mm)	278.64±18.87	226.67±45.41	0.136	227.46±56.47	200.76±39.13	196.93±35.70	^[0.900,0.360] *0.019 #0.408,0.980
Elastic modulus (N/mm^2)	2709.95±433.86	2591.06±384.45	0.938	2537.08±423.90	2728.88±614.05	2372.37±414.12	^[<0.001(both)] *<0.001 #0.969,0.926

^ Respective comparison of ZDZD28Wk with ZDSD28WK-MOD and ZDSD28WK-SVD: *; p-value comparing SD20WK against SD28WK, and #; p-value comparing ZDSD20WK against ZDSD28WK-MOD and ZDSD28WK-SVD respectively

3.2.3 Proximal femur trabecular morphometry at week-20 and week-28

Femur bone tissue volume (BV)

At 20 weeks of age, the ZDSDs exhibited lower BV ratios than their SD controls (p<0.039) (Table 3.10). The same trend was observed with ZDSD28WK-MOD and ZDSD28WK-SVD recording significantly lower values than their SD controls (p=0.002 for both comparisons) No age-related differences were observed in BV between 20-week-old and 28-week SD controls (p=0.116) (Table 3.10). This trend of similar BV ratios was also observed in ZDSD groups, when comparing 20-week-old ZDSDs with 28-week-old ZDSD groups (ZDSD28WK-MOD p=0.505 and ZDSD28WK-SVD p=0.604).

Femur bone tissue volume to bone tissue volume ratio (BV/TV)

The 20-week-old ZDSDs had lower BV/TV ratios when compared with their SD controls (p<0.001) (Table 3.10). In contrast, similarities with SD controls were observed in 28-week-old rats for both ZDSD28WK-MOD and ZDSD28WK-SVD (p=0.944, p= 0.955 respectively). Older (28-week-old) SDs had lower BV/TV ratios when compared with 20-week-old SD controls (p<0.001) (Table 3.10). On the contrary, ZDSD BV/TV ratios were similar at 20-weeks of age compared to the 28-week-old groups (ZDSD28WK-MOD p=0.828 and ZDSD28WK-SVD p=0.936).

Table 3.10: Micro-CT evaluation of the proximal femur at week-20 and week-28 (BV, BV/TV)

	Week 20			**Week 28**			
Parameter	**SD (n=12)**	**ZDSD (n=12)**	**p value**	**SD (n=12)**	**ZDSD-MOD (n=12)**	**ZDSD-SVD (n=12)**	**p value**
BV (mm^3)	30.90±8.45	26.69±3.55	0.039	34.08±2.96	27.93±3.01	27.73±2.87	^[0.002(both)] *0.116 #0.505,0.604
BV/TV (%)	26±2	18±5	<0.001	19±9	19±2	18±2	^[0.944,0.955] *<0.001 #0.828,0.936

^ Respective comparison of ZDZD28Wk with ZDSD28WK-MOD and ZDSD28WK-SVD: *; p-value comparing SD20WK against SD28WK, and #; p-value comparing ZDSD20WK against ZDSD28WK-MOD and ZDSD28WK-SVD respectively. BV, bone tissue volume; BV/TV, bone bone tissue volume to total volume

Femur trabecular thickness (TbTh)

Similarities were observed in trabeculae thickness when comparing 20-week-old ZDSDs with their age matched SD controls (p=0.692) (Table 3.11). In contrast, among the 28-week-old rats, ZDSD28WK-MOD and ZDSD28WK-SVD exhibited thinner trabeculae than their SD controls (p=0.002 and p=0.001, respectively). Age differences were observed in SD controls between rats aged 20 and those aged 28 weeks), with younger (20 weeks) having thinner trabeculae (p=0.001) (Table 3.11). On the contrary, trabecular thickness was similar among ZDSDs when comparing 20-weeks with 28-week-old groups (ZDSD28WK-MOD p=0.403 and ZDSD28WK-SVD p=0.842).

Femur trabecular number (TbN)

The 20-week-old ZDSDs had fewer trabeculae numbers when compared with their SD controls (p<0.001) (Table 3.11). In contrast, similarities with SD controls were observed in 28-week-old

rats for both ZDSD28WK-MOD and ZDSD28WK-SVD (p=0.884, p= 0.368 respectively). Older (28-week-old) SDs had fewer trabeculae when compared with 20-week-old SD controls (p<0.001) (Table 3.11). On the contrary, ZDSD trabeculae numbers were similar at 20-weeks of age compared to the 28-week-old groups (ZDSD28WK-MOD p=0.639 and ZDSD28WK-SVD p=0.740).

Femur trabeculae spacing (TbSp)

The 20-week-old ZDSDs had similar trabeculae spaces when compared with their SD controls (p=0.053) (Table 3.11). In contrast, similarities with SD controls were observed in 28-week-old rats for both ZDSD28WK-MOD and ZDSD28WK-SVD (p=0.851, p= 0.858 respectively). Older (28-week-old) SDs had more trabeculae spaces when compared with 20-week-old SD controls (p<0.001) (Table 3.11). On the contrary, ZDSD trabeculae numbers were similar at 20-weeks of age compared to the 28-week-old groups (ZDSD28WK-MOD p=0.115 and ZDSD28WK-SVD p=0.143).

Table 3.11: Micro-CT evaluation of the proximal femur at week-20 and week-28 (TbTh, TbN, TbSp)

		Week-20			***Week 28***		
Property	**SD (n=12)**	**ZDSD (n=12)**	**p value**	**SD (n=12)**	**ZDSD-MOD (n=12)**	**ZDSD-SVD (n=12)**	**p value**
TbTh (mm)	0.33±0.14	0.31±0.04	0.692	0.46±0.10	0.35±0.08	0.32±0.07	^[0.002,0.001] *0.001 #0.403,0.842
TbN (numerals)	2.40±1.25	0.57±0.18	<0.001	0.39±0.20	0.43±0.21	0.67±0.98	^[0.884,0.368] *<0.001 #0.639,0.740
TbSp (mm)	0.39±0.62	1.59±.0.61	0.050	2.50±1.66	2.50±1.66	2.61±1.36	^[0.851,0.858] *0.001 #0.115,0.143

^ Respective comparison of ZDZD28Wk with ZDSD28WK-MOD and ZDSD28WK-SVD: *; p-value comparing SD20WK against SD28WK, and #; p-value comparing ZDSD20WK against ZDSD28WK-MOD and ZDSD28WK-SVD respectively. TbTh, trabecular thickness; TbN, trabecular number; TbSp, trabecular spacing

3.2.4 Femoral mid diaphysis cortical area and medullary canal area at week-20 and week-28

Femur cortical area

The 20-week-old ZDSDs had a similar cortical area when compared with their SD controls (p=0.056) (Table 3.12). The same trend was observed in 28-week-old SD controls when compared with ZDSD28WK-MOD and ZDSD28WK-SVD (p=0.164, p= 0.635 respectively). No age-related differences were observed in cortical area between 20-week-old and 28-week SD controls (p=0.420) (Table 3.12). This trend of a similar area was also observed in when comparing 20-week-old ZDSDs with 28-week-old ZDSD28WK-MOD (p=0.226), but not the ZDSD28WK-SVD (p=0.005) that had a larger cortical area.

Femur medullary canal area

At week 20, the ZDSDs had a larger medullary canal area when compared with their SD controls (p=0.001) (Table 3.12). The same trend was observed when comparing 28-week-old SD controls with ZDSD28WK-MOD (p=0.145), however, ZDSD28WK-SVD exhibited larger medullary canal areas than 28-week-old SD controls (p=0.011) (Table 3.12). No age related differences were observed in medullary canal area between 20-week-old and 28-week SD controls (p=0.420) (Table 3.12). This trend of similar medullary canal area was also observed in ZDSD groups, when comparing 20-week-old ZDSDs with 28-week-old ZDSD groups (ZDSD28WK-MOD (p=0.733) and ZDSD28WK-SVD, (p=0.202)

Table 3.12: Femur cortical area and medullary canal area at week-20 and week-28

	Week-20			*Week 28*			
Property	**SD (n=12)**	**ZDSD (n=12)**	**p value**	**SD (n=12)**	**ZDSD-MOD (n=12)**	**ZDSD-SVD (n=12)**	**p value**
C-area 50th percentile (mm^2)	19.97±2.58	18.26±0.71	0.056	20.41±2.09	19.26±2.37	20.83±1.56	^[0.164,0.635] *0.619 #0.226,0.005
Medullary area 50th percentile (mm^2)	9.39±0.67	12.48±2.66	<0.001	9.39±0.67	10.34±1.02	11.43±1.34	^[0.146,0.011] *0.161 #0.733,0.202

^ Respective comparison of ZDZD28Wk with ZDSD28WK-MOD and ZDSD28WK-SVD: *; p-value comparing SD20WK against SD28WK, and #; p-value comparing ZDSD20WK against ZDSD28WK-MOD and ZDSD28WK-SVD respectively

3.2.5 Parameters of the femur most affected by age, diabetes and is duration

Discriminant function analysis was conducted to determine the femoral variables that are influenced by age, diabetes, and its duration. The structure matrix showed that bicondylar width, TbN, femoral weight, femoral neck superoinferior diameter and maximum time(s) to fracture were the main factors influenced (Table 3.13).

The discriminant analysis yielded 4 functions, although the Wilk's lambda results indicate a good fit for only Functions 1, 2 and 3 (Wilk's lambda = 0,008; 0,074; 0,443 for Functions 1, 2 and 3, respectively) ($p<0.001$). Function 4 was not significant ($p=0.67$). Function 1 accounted for 56.5% of the variability, Function 2 accounted for 35.1% whereas Function 3 accounted for only 8%. For the cross-validated classification, 76.7% of femora were correctly classified according to their diabetic (ZDSD) and control (SD) group status as well as age in the respective groupings. Among the SD control groups, the model correctly classified 100% of the femora as belonging to the SD20WK group and 75% as belonging to the SD28WK group. Among the diabetic groups, the model could only correctly classify half (50%) of the femora as belonging to the ZDSD20WK group. However, this improved with 3 quarters (75%) of the femora being correctly classified as belonging to the ZDSD28WK-MOD group and 83% for the ZDSD28WK-SVD (Table 3.14 and Fig. 3.4)

Table 3.13: Discriminant function analysis of the femur. The contributing variables are arranged in descending order according to component 1, 2, 3, and 4, with major contributors in bold (above ±0.3).

Structure Matrix				
Parameter	**Function**			
	1	**2**	**3**	**4**
Bicondylar width	**0,586**	0,092	0,153	-0,506
Trabeculae number (TbN	**0,329**	0,245	0,207	0,139
Mass	**0,308**	-0,119	0,087	-0,144
Superoinferior (SI) length	**0,302**	-0,055	0,229	0,173
Bone tissue volume to total volume (BV/TV)	**0,356**	0,242	0,173	0,388
Midshaft medullary canal area	0,123	-0,102	0,305	-0,371
Maximum displacement	0,117	0,185	0,113	0,118
Biomechanical length	0,108	-0,25	0,062	-0,093
Full length	0,102	-0,040	0,223	-0,003
Femur midshaft (ML) mediolateral diameter	0,073	0,023	0,070	-0,093
Femoral head width	0,072	0,097	-0,057	0,035
Femur midshaft (AP) anteroposterior diameter	0,069	0,139	0,167	-0,152
Femoral neck anteroposterior diameter	0,046	-0,006	0,258	-0,030
Break force	0,015	0,041	0,542	0,314
Bone tissue volume (BV)	0,005	-0,146	0,074	-0,232
Midshaft cortical area	-0,017	-0,002	0,538	-0,405
Maximum force	-0,081	-0,027	0,358	0,157
Elastic modulus	-0,129	0,190	0,219	-0,53
Yield force 0.5mm N	-0,154	-0,152	-0,216	0,001
Trabeculae thickness (TbTh)	-0,183	-0,025	-0,229	0,203
Stiffness	-0,185	-0,011	0,269	0,013
Trabeculae spacing (TbSp)	-0,191	-0,057	-0,154	-0,228
Maximum time	-0,231	**0.632**	0,016	0,165
Function loading %	56,5	35,1	8,0	0,4

Table 3.14: Discriminant function analysis of predicted group membership

Classification Results[a,c]

		Group	Predicted Group Membership					Total
			SD20WK	SD28WK	ZDSD20WK	ZDSD28WK-MOD	ZDSD28WK-SVD	
Original	Count	SD20WK	12	0	0	0	0	12
		SD28WK	0	10	2	0	0	12
		ZDSD20WK	0	0	10	2	0	12
		ZDSD28WK-MOD	0	0	2	10	0	12
		ZDSD28WK-SVD	0	0	0	1	11	12
	%	SD20WK	100.0	.0	.0	.0	.0	100.0
		SD28WK	.0	83.3	16.7	.0	.0	100.0
		ZDSD20WK	.0	.0	83.3	16.7	.0	100.0
		ZDSD28WK-MOD	.0	.0	16.7	83.3	.0	100.0
		ZDSD28WK-SVD	.0	.0	.0	8.3	91.7	100.0
Cross-validated[b]	Count	SD20WK	12	0	0	0	0	12
		SD28WK	0	9	2	0	1	12
		ZDSD20WK	0	1	6	5	0	12
		ZDSD28WK-MOD	0	0	3	9	0	12
		ZDSD28WK-SVD	1	0	0	1	10	12
	%	SD20WK	100.0	.0	.0	.0	.0	100.0
		SD28WK	.0	75.0	16.7	.0	8.3	100.0
		ZDSD20WK	.0	8.3	50.0	41.7	.0	100.0
		ZDSD28WK-MOD	.0	.0	25.0	75.0	.0	100.0
		ZDSD28WK-SVD	8.3	.0	.0	8.3	83.3	100.0

a. 88,3% of original grouped cases correctly classified.

b. Cross validation is done only for those cases in the analysis. In cross validation, each case is classified by the functions derived from all cases other than that case.

c. 76,7% of cross-validated grouped cases correctly classified.

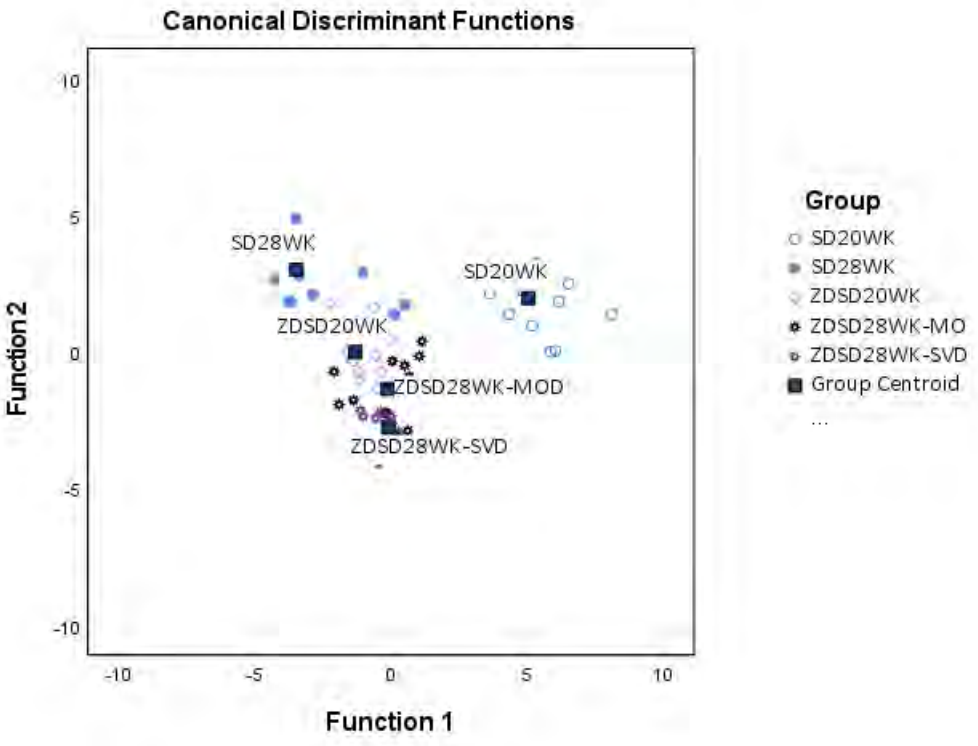


Figure 3.4: Illustrated discriminant function analysis of predicted group membership

3.3 Discussion

The femur was selected for this study because most long bone fractures affect this bone. This study investigated whether diabetes would affect osteometric measurements, midshaft cortical and medullary canal areas as well as proximal femoral epiphysis trabecular morphological parameters. We studied 3-poing bending properties to ascertain the effect of diabetes on the femur load (force) handing properties. Further investigations assessed whether perturbations caused by T2D were diabetes severity, status or age dependent. Older diabetic rats had shorter, lighter, and less robust bones compared to SD controls that exhibited stronger, robust bones. This observation suggests a diabetes induced loss of growth in length and girth of the femur with progression of diabetes. Although severely diabetic rats reported larger cortical areas, their medullary canal areas were the largest, suggesting a short, light and hollow bone phenotype. The younger diabetic bones (20-week) also exhibited a lighter hollow phenotype but showed similarities in bone length, biomechanical length and cortical area. Diabetic rats had reduced trabeculae thickness with more spacing (TSp) and lower bone tissue volume fractions. Discriminant function analysis revealed that osteometric, 3-point bending, and trabecular morphometric parameters of the rat femur were affected by age, diabetes, and its duration.

Osteometric aspects

The femora had similar biomechanical and full lengths at the age of 20 weeks when comparing the diabetic group with controls, even although the ZDSDs had a smaller bicondylar width. More pronounced changes occurred among the 28-week-old groups in which femora were shorter in the diabetic groups, smaller biomechanical and full lengths, as well as smaller bicondylar widths. This suggests that the effect of diabetes on osteometric measurements worsened with prolonged untreated hyperglycemia. The osteometric measurements gave an estimate of size which was corroborated by mass, that was lower in both diabetic rats, at the age of 20 weeks and later at 28 weeks. This means that diabetes adversely affected bone size. Previous studies on diabetic ZDSD and ZDF rats also observed similarities in bone structure for younger rats (early stages of diabetes) (Creecy et al., 2016), and reduced femoral bone size and mass with disease progression (Reinwald et al., 2009; Creecy et al., 2016).

Robusticity is here was considered as referring to the thickness of the femurs relative to respective lengths. An extensive review of the scientific literature, has indicated that this is the first study that has investigated the robusticity of diabetic rat humeri. The rational for assessing femoral robusticity is our supposition that a shorter bone with a wide shaft would be stronger than a thin long bone. Our results showed a lower robusticity index in diabetic bones at both 20 and 28 weeks. This supports previous literature that has shown that diabetic bones are weaker (Reinwald et al., 2009). The low robusticity could be a contributing factor to the diabetic bone weakness.

3-point bending parameters

No detectable differences in 3-point bending parameters occurred in younger rats (20 weeks old). In contrast, the 28-week-old rats showed that break force and maximum time to fracture were both lower in the diabetic rats. This lack of significant differences at the early stages could suggest that diabetes may not have affected bone strength at the early stages of the disease. On the other hand, the observation of low break force and maximum time to fracture in ZDSD rats at the age of 28 suggest that the bones became weaker with progression of diabetes. Therefore, it is recommended that diabetes screenings should be increased and interventions to control hyperglycemia be implemented early to prevent deterioration of bone quality.

Among 20-week-old rats, elastic modulus was similar between the diabetic group and controls. Therefore, the initial phases of the diabetic state did not affect the ability of bone to deform (elastically). Perhaps, it would be possible to maintain this status if diabetic interventions start early. In 28-week-old rats, elastic modulus was higher in controls and lower in both ZDSD groups. This means the duration and severity of diabetes (hyperlycemia) had a crucial role in how much elastic deformation was possible as this deterioration in elastic modulus was observed in both the moderately diabetic (ZDSD28WK-MOD) and the severely diabetic group (ZDSD28WK-SVD). However, other studies did not find differences in elastic modulus even at 29 and 33 weeks (Reinwald et al., 2009; Creecy et al., 2016). These differences in study findings may be due to the

classification of severity of diabetes in each study. Differences may have not have been picked had the present study considered the moderately diabetic group (ZDSD28WK-MOD) combined as one with the rats belonging to the severely diabetic group (ZDSD28WK-SVD. Alternatively, using different glycemic threshold points to assign groups into moderately and severely diabetic groups would have yielded a different finding as well.

When comparing stiffness at 20 and 28 weeks in each respective group, this parameter reduced as age increased from 20 to weeks among the SD rats. This suggests that the amount of force a femur absorbed, was reduced as the animal got older. Therefore, this stiffness reduction is an age effect. On the other hand, no significant change occurred in the ZDSDs when comparing 20- and 28-week-old rats. This is an indication that diabetes reduces the amount of force a femur absorbs before fracture is affected from the onset of diabetes and persists as the disease progresses.

Trabecular morphometry

The BV was consistently lower at the age of 20 weeks and among 28-week-old rats. however, bone tissue volume ratio (BV/TV) was lower in the diabetic group at only 20 weeks of age. This shows that diabetic groups had smaller femora, meaning that diabetes had reduced overall femoral size. The lack of significant difference in BV/TV among 28-week-old rats suggests that there may have been compensatory means to maintain osseous tissues quantity as diabetes progressed. This is possibly because of prolonged mechanical loading as age progressed. Bone tissue adapts by consolidating under prolonged mechanical loading (Turner and Burr, 1993; Tyrovola and Odont, 2015; Iwaniec and Turner, 2016).

Among the trabecular morphometric parameters, trabeculae thickness remained unaffected in both 20 and 28-week diabetic rats compared to their controls. Trabecular thickness (TbTh) was reduced in late stages of diabetes as shown by the lower TbTh in 28-week-old diabetic groups, while unaffected in 20-week-old diabetes groups. In contrast, trabeculae number (TbN) was significantly lower in 20-week-old diabetic rats, but similar among the 28-week-old groups. This

means that while diabetes resulted in a reduction in trabecular thickness, the trabecular number was not affected. Instances when trabecular number was reduced, the thickness was unaffected. This observation may be related to compensatory mechanisms in an attempt to maintain bone structural integrity in the diabetic state. This would ensure a situation where trabeculae thickness and trabeculae number are reduced simultaneously. Otherwise, the bone quality would be quickly compromised in diabetes. This observation suggests that T2D affects trabeculae microarchitecture independent of age in ZDSDs, whereas in SDs, there is an age-related pattern, where older rats exhibit fewer, more spaced, and thinner trabeculae. Previous studies report an unchanged bone tissue volume fraction and trabeculae thickness in 22-week old ZDSDs, but significantly reduced trabeculae thickness in 29-week old ZDSDs (Creecy et al., 2016). Studies on male Fischer rats reported a decrease in trabeculae numbers, increase in trabeculae spacing, and increased trabeculae thinning with age (Uppuganti et al., 2016).

The ZDSDs and SD controls had a similar midshaft cortical area when compared with their SD controls irrespective of age group. Controls showed no age-related differences in cortical area between 20-week-old and 28-week rats. However, among the ZDSDs this trend of a similar area was only observed in when comparing 20-week-old ZDSDs with 28-week-old ZDSD28WK-MOD but not the severely diabetic group (ZDSD28WK-SVD), that had a larger cortical area. This is an indication that the severity of diabetes had a major role in reducing cortical area, which may explain the observed reduction in cortical area reported in previous studies (Reinwald et al., 2009). This phenomenon is thought to contribute the diabetic bone weakness (Jepsen et al., 2015).

At week 20 of age, the ZDSDs and SD controls had a larger medullary canal area. Among the 28-week-old rats, only the severely diabetic group (ZDSD28WK-SVD) exhibited larger medullary canal areas. The observed increased medullary canal area may be attributed to T2D induced endosteal bone resorption as bone marrow area expansion is linked to increased bone resorption by endosteal cells (Jepsen et al., 2015) that is possibly accelerated in diabetes. A reduction in cortical area combined with an increased medullary canal area, would compromise the structural

strength of the bone. These results support the observed bone weakness reported in human studies (Janghorbani et al., 2007; Vestergaard et al., 2009; Valderrabano and Linares, 2018).

Aspects of femoral parameters most affected by age, diabetes, and its duration

Parameters related to osteometry, 3-point bending and trabecular morphometry were among the most affected by age, diabetes and its duration as shown by the outcome of the discriminant function analysis (DFA). These parameters were, bicondylar width, TbN, femoral mass, femoral neck superoinferior diameter and maximum time(s) to fracture were the main factors influenced. Some of these parameters were also significantly different in the diabetic groups when ANOVA was conducted before DFA. These were: lower mass, smaller bicondylar width, less time to fracture and fewer trabecular in the diabetic rats.

3.3.1 Conclusions

This study confirms that T2D affects femoral osteometry, mid-diaphyseal loading, and trabeculae microarchitectural parameters. The diabetic effect results in lighter, shorter hollow bones that perform poorly under loading, as well as exhibit unfavourable trabeculae microarchitecture. These perturbations occur early and late in the disease, and they are also exercebated by the presence of hyperglycemia. These findings confirm that T2D causes increased femoral fragility in the proximal femoral head and neck as well as its mid-diaphysis, in an age dependent manner. Early interventions is recommended in controlling hyperglycemia, to reduce femoral head and neck fractures in diabetic patients. The ZDSD rat is also recommended as a suitable translational model that can be extrapolated to humans, as it shares a similar diabetes progression as humans.

Chapter 4

Type 2 diabetes affects structural and material properties of bone in the ZDSD humerus.

TABLE OF CONTENTS

4.0 Introduction 84
4.1 Materials and methods 85
4.1.1 Rat model for diabetes type 2 85
4.1.2 Termination and bone harvesting 85
4.1.3 Three-dimensional Micro-focus X-ray Computed Tomography (3D- μCT) 85
Parts of the humerus trabecular parameters studied 86
4.2 Results 88
4.2.1 Humerus osteometry at age 20 and 28 weeks 88
Humerus bone mass 88
Humerus length 88
Humerus epicondylar breadth 88
Humerus head width 89
Humerus midshaft anteroposterior (AP) diameters 90
Humerus midshaft mediolateral (ML) diameters 90
Humerus robusticity index 90
Humerus maximum force 91
Humerus break force 91
Humerus yield force 92
Humerus maximum time 92
Humerus maximum displacement 93
Humerus stiffness 93
Humerus elastic modulus 93
Humerus bone tissue volume (BV) 94
Humerus bone tissue volume to bone tissue volume ratio (BV/TV) 94
Humerus trabecular thickness (TbTh) 95
Humerus trabecular number (TbN) 95
Humerus trabecular spacing (TbS) 96
Humerus cortical area 96
Humerus medullary canal area 97
4.3 Discussion 101

Osteometric characterization 101
3-point bending and force loading limits 102
Aspects of humerus head trabecular morphometry 103
Midshaft cortical and medullary canal properties 104
4.3.1 Conclusions 104

4.0 INTRODUCTION

Most research has neglected diabetic skeletopathy despite evidence that links diabetes with susceptibility to fractures (Bonds et al., 2006; Oei et al., 2013), especially humerus fractures. Proximal humerus fractures (PHF) are the most frequent after the femoral neck and wrist fractures (Chu et al., 2004). A large cohort study (Rotterdam study) of 6655 men and women aged 55 years and older found that appendicular skeletal fractures that include the proximal humerus, were higher in patients with T2D, after the exclusions of risk factors for falls due to declining vision, a history of stroke, walking speed, neuropathy and medications that cause drowsiness (Schwartz, 2003). There is still a paucity of studies that link T2D with humerus fractures, as most studies have mainly focused on the femur.

Biomechanical properties that determine whole bone strength such as its geometry (mass, size, shape) (Prisby et al., 2008; Martin and Correa, 2010; Jepsen et al., 2015), together with bone tissue properties that are determined at molecular, cellular, matrix composition and micro architectural level have been reported (Forestier-Zhang and Bishop, 2016; Uppuganti et al., 2016). It is still unclear if T2D affects these properties in isolation or concurrently.

This study profiled humerus geometry, investigated trabeculae architecture by micro-CT and assessed bone strength using 3-point bend till fracture, to ascertain if T2D compromises whole bone strength in the humerus. We investigated the proximal epiphysis and mid-diaphysis because the risk of fracture in diabetes varies with specific sub regions of a bone (Ahmad et al., 2003). A study on spontaneously diabetic Goto-Kakizaki rat humeri found a significant loss of trabeculae bone, due to diabetic osteopenia (Ahmad et al., 2003). This osteopenia led to impaired function of bone turn over cells, that resulted in increased bone fragility in T2D (Hamann et al., 2011).

4.1 MATERIALS AND METHODS

4.1.1 Rat model for diabetes type 2

The rat model for diabetes mellitus was established as described in section 2.1.2

4.1.2 Humerus harvesting

The humeri were collected and processed in the same manner as described in section 3.12. Left and right humeri were used for biomechanical investigations by 3-D micro-CT and 3-point bend tests.

4.1.3 Three-dimensional Micro-focus X-ray Computed Tomography (3D- µCT)

The scanning procedure used for the humerus is described in section 3.13. The scanning parameters used are shown in table 4.1.

Table 4:1: Scanning parameters at 20 weeks and 28 weeks

Parameter	Value
X-ray voltage	70kv
X-ray current	400µa
Filter	1 mm aluminium
Scanning resolution	18µ
Tomographic rotation	360 degrees
Rotation step	1 degree
Frame averaging	4
Scan duration	8 minutes

Parts of the humerus trabecular parameters studied

Bones were weighed and a digital handheld calliper was used to determine femoral osteometric parameters. Full bone length, bicondylar length, bicondylar breadth and various hunerus head diameters were measured. (Fig. 4.1 and Table 4.2). Following reconstruction, VG studio Max ®3.2 was used for data analysis as previously described (Bouxsein et al., 2010). The trabecular morphometric parameters were studied in the proximal and distal epiphysis of the bone. The following parameters were determined, trabecular number, thickness, spaces and volume (Table 4.3). A cross-sectional slice from each percentile mark was captured then saved for further analysis on Fiji image J. From the slices, cortical area and medullary canal area of the shaft were measured at the 50th percentile mark of the humerus (Fig. 4.1 and Table 4.3).

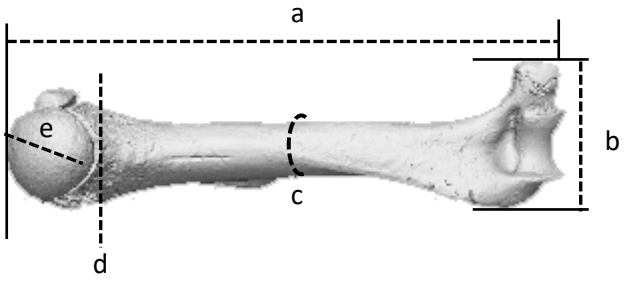


Figure 4.1: **Three-dimensional reconstruction of a humerus showing the parts that were investigated**. (a), full humerus length; (b), epicondylar breadth; (c), 50th (midshaft) mark; (f), proximal ROI for trabeculae morphological assessment. (Image R. Ndou and G.F Dlamini).

Table 4.2: Humerus osteometric parameters

Parameter	Description
Full humerus length	The maximum length that can be measured between the top of the humeral head and the most distant point on the distal humerus
Epicondylar breadth	the greatest distance between the medial and lateral epicondyles
Humerus head diameter	Distance between bulgiest part in an anteroposterior, medio-lateral, supero-inferior direction when viewed from the top
Mid diaphysis AP diameter	Distance between bulgiest parts in an antero-posterior direction at the 50th percentile
Mid diaphysis ML diameter	Distance between bulgiest parts in a medio-lateral direction at the 50th percentile
Robusticity index	Sum of the ML and AP midshaft diameter multiplied by 100 and divided by physiological length of the femur

Table 4.3: Humerus assessment parameters by micro-CT (adapted from (Bouxsein et al., 2010).

Parameter	Definition
$\frac{\mathbf{BV}}{\mathbf{TV}}$ (bone tissue volume to total volume)	Represents the ratio of material (bone) volume to total volume.
TbTh (mean trabecular thickness)	The material (bone), calculated as follows: **TbTh =2/BS/BV** Where **BS/BV** is the ratio of material (bone) surface (**BS**) to material (bone) volume (**BV**)
TbN (mean trabecular number)	Shows the mean number of trabecular (column-like) structures per unit length, calculated as follows: **TbN=BV/TV/TbTh**
TbSp (mean trabecular spacing)	Indicates the mean distance between trabecular (column-like) structures, calculated as follows: **TbSp=1/TbN−TbTh**
Cross-sectional area	The area of a slice taken from the outer margins encompassing the shaft at the 50th percentile marks
Medullary cavity area	The area of a slice taken from the inner margins encompassing the medullary canal at the 50th percentile marks

4.1.4 Three-point Bending

The right humeri were subjected to a three-point bending test. The load was applied at the midshaft, midway between two supports that were 13 mm apart for the humerus (Fig. 4.2). The humeri were positioned such that bending occurred at the mediolateral plane. Load-displacement curves were recorded at a constant speed of 5mm/min until failure.

4.1.5 Data, statistics and discriminant function component analysis

The data were managed in Microsoft Excel 2016 (Microsoft Corporation) and analysed using SPSS® version 28 (IBM®). ANOVA with LSD post-hoc was used for multiple group comparisons of means. Discriminant function analysis analysis was conducted to assess how femur and humerus morphology parameters clustered. Significance level was set at $p < 0.05$.

4.2 RESULTS

4.2.1 Humerus osteometry at age 20 and 28 weeks

Humerus bone mass

At 20 weeks of age, the ZDSD humeri weighed significantly less than their SD controls ($p<0.001$) (Table 4.4). The same trend was observed with ZDSD28WK-MOD and ZDSD28WK–SVD, recording significantly lower values than their SD controls ($p<0.001$, for both comparisons). The SD controls exhibited age related differences, with bones of older rats (age of 28 weeks) weighing significantly less than those of 20-week-olds ($p<0.001$) (Table 4.4). Similarly, ZDSD humeri weighed less at 28 weeks (ZDSD28WK-MOD and ZDSD28WK-SVD) compared to their 20-week-old counterparts ($p=0.002$ and $p=0.003$, respectively compared to 20-week-olds).

Humerus length

At 20 weeks of age, ZDSD humerus lengths were significantly shorter than their SD controls ($p=0.009$) (Table 4.4). Similarly, among the 28-week-old rats, ZDSD28WK-MOD and ZDSD28WK-SVD exhibited shorter humerus lengths than their SD controls ($p<0.001$ for both comparisons). Age similarities in full humerus lengths were observed when comparing 20 and 28-week-old SDs ($p=0.794$) (Table 4.4). On the contrary, there were ZDSD age differences as younger (20-week-old) ZDSDs had longer humerus lengths than the ZDSD28WK-MOD and ZDSD28WK-SVD ($p<0.001$ for both comparisons).

Humerus epicondylar breadth

At 20 weeks of age, epicondylar breadth measurements were significantly wider in SD controls compared to ZDSDs ($p<0.001$) (Table 4.4). Similarly, at the age of 28 weeks, SD controls exhibited wider epicondylar breadth values when compared to ZDSD28WK-MOD and ZDSD28WK-SVD ($p<0.001$, for both comparisons). Age differences were observed in SD controls between 20-week-old and those aged 28 weeks ($p=<0.001$), with younger (20-weeks) rats exhibiting narrower epicondylar breadths (Table 4.4). In contrast, ZDSDs exhibited similarities when comparing 20-week-old ZDSDs with the 28-week-old groups (ZDSD28WK-MOD $p=0.542$ and ZDSD28WK-SVD $p=0.207$).

Humerus head width

At 20 week of age, humerus head width measurements were wider in SD controls than ZDSDs (p<0.001) (Table 4.4). In contrast, similarities with SD controls were observed in 28-week-old rats, for both ZDSD28WK-MOD and ZDSD28WK-SVD (p=0.083 and p= 0.107 respectively). Older (28-week-old) SDs had narrower head widths when compared to their younger 20-week-old counterparts (p=0.001) (Table 4.4). On the contrary, ZDSD humerus head widths were similar at 20-weeks of age compared to the 28-week-old groups (ZDSD28WK-MOD p=0.762), but the ZDSD28WK-SVD, had significantly smaller head widths (p=0.002).

Table 4.4: Osteometric measurements of the humerus (mass, full length, epicondylar breadth, humerus head width).

	Week 20			**Week 28**			
Parameter	**SD (n=12)**	**ZDSD (n=14)**	**p value**	**SD (n=14)**	**ZDSD-MOD (n=17)**	**ZDSD-SVD (n=12)**	**p value**
Mass (g)	0.65±0.04	0.57±0.02	<0.001	0.61±0.05	0.55±0.04	0.55±0.02	^[<0.001, (both)] *<0.001 #0.002,0.003
Full length (mm)	31.66±1.55	30.81±0.35	0.009	31.58±0.34	28.88±1.26	28.84±1.00	^[<0.001, (both)] *0.794 #0.001, (both)
Epicondylar breadth (mm)	7.68±0.19	7.24±0.26	<0.001	7.37±0.24	7.31±0.15	6.70±0.48	^[<0.001(both)] *<0.001 #0.542.0.207,
Humerus head width (mm)	5.56±0.24	5.11±0.25	<0.001	5.38±0.26	5.23±0.17	5.08±0.23	^[0.083,0.107] *0.001 #0.762,0.002

^ Respective comparison of ZDZD28Wk with ZDSD28WK-MOD and ZDSD28WK-SVD: *; p-value comparing SD20WK, against SD28WK, and #; p-value comparing ZDSD-20WK against ZDSD28WK-MOD and ZDSD28WK-SVD respectively

Humerus midshaft anteroposterior (AP) diameters

At 20 weeks of age, midshaft anteroposterior diameters were significantly larger in ZDSDs compared to SD controls ($p<0.001$) (Table 4.5). Similarly, 28 weeks old rats showed that the 28-week-old SD controls had larger measurements when compared with ZDSD28WK-MOD and ZDSD28WK-SVD ($p<0.001$, for both comparisons). No age-related differences were observed between 20-week-old and 28-week SD controls ($p=0.876$) (Table 4.5). On the contrary, 20-week-old ZDSDs exhibited larger midshaft anteroposterior diameters when compared with ZDSD28WK-MOD and ZDSD28WK-SVD in this region ($p=0.009$ and $p<0.001$, respectively).

Humerus midshaft mediolateral (ML) diameters

The 20-week-old ZDSDs had similar midshaft mediolateral diameters when compared with their SD controls ($p=0.195$) (Table 4.5). The same trend was observed in 28-week-old rats when comparing SD controls with ZDSD28WK-MOD and ZDSD28WK-SVD ($p=0.851$ and $p=0.462$, respectively). No age-related differences were observed in midshaft mediolateral diameters between 20-week-old and 28-week SD controls ($p=0.163$) (Table 4.5). This trend of similar midshaft mediolateral diameters was also observed in ZDSD groups, when comparing 20-week-old ZDSDs with 28-week-old ZDSD groups (ZDSD28WK-MOD $p=0.766$ and ZDSD28WK-SVD $p=0.403$).

Humerus robusticity index

At week-20, the SD controls were significantly more robust than the ZDSDs ($p<0.001$) (Table 4.5). This trend was maintained at week-28, where SD controls were more robust than ZDSD28WK-MOD and ZDSD28WK-SVD ($p<0.001$, for both comparisons). No age-related differences were observed in robusticity between 20-week-old and 28-week SD controls ($p=0.656$) (Table 4.5). This trend of similarities in robusticity was also observed in ZDSD groups, when comparing 20-week-old ZDSDs with 28-week-old ZDSD groups (ZDSD28WK-MOD $p=0.867$), but not in the ZDSD28WK-SVD that were less robust ($p=0.018$).

Table 4.5: Osteometric measurements of the humerus (mid shaft AP, ML diameter, robusticity index)

	Week 20			Week 28			
Parameter	**SD (n=12)**	**ZDSD (n=14)**	**p value**	**SD (n=14)**	**ZDSD-MOD (n=17)**	**ZDSD-SVD (n=12)**	**p value**
Mid shaft AP diameter (mm)	6.26±0.25	4.75±0.49	<0.001	6.23±0.23	4.31±0.58	3.77±0.50	^[<0.001, (both)] *0.876 #0.009,<0.001
Mid shaft ML diameter (mm)	2.62±0.28	2.71±0.13	0.195	2.72±0.22	2.73±0.11	2.77±0.09	^[0.851,0.462] *0.163 #0.766,0.403
Robusticity Index (%)	28.04±1.28	24.36±1.43	<0.001	28.35±1.17	24.46±2.45	22.68±1.86	^[<0.001(both)] *0.656 #0.867,0.018

^ Respective comparison of ZDZD28Wk with ZDSD28WK-MOD and ZDSD28WK-SVD: *; p-value comparing SD20WK, against SD28WK, and #; p-value comparing ZDSD-20WK against ZDSD28WK-MOD and ZDSD28WK-SVD respectively

4.2.2 Humerus mid-diaphysis 3-point bending parameters

Humerus maximum force

The 20-week-old SD controls displayed higher values for maximum force when compared with age matched ZDSDs (p=0.001) (Table 4.6). On the contrary, at week-28, similarities were observed between 28-week-old SD controls when compared with ZDSD28WK-MOD and ZDSD28WK-SVD (p=0.347 and p= 0.113, respectively). No age-related differences were observed for maximum force between 20 and 28-week SD controls (p=0.257) (Table 4.6. On the contrary, age differences occurred between 28-week-old ZDSD groups (ZDSD28WK-MOD and ZDSD28WK-SVD (p=0.001 and p<0.001, respectively), where younger (20-week-old) ZDSDs exhibited lower maximum force values).

Humerus break force

The 20-week-old SD controls displayed higher values for break force when compared with age matched ZDSDs (p=0.032) (Table 4.6). Similarly, among the 28-week-old rats, SD controls exhibited higher break force than ZDSD28WK-MOD and ZDSD28WK-SVD (p=0.032 and p=0.017, respectively). No age-related differences were observed in break force between 20 and 28-week-old SD controls (p=0.386) (Table 4.6). On the contrary, age differences were observed between

20-week-old ZDSD groups when compared with (ZDSD28WK-MOD and ZDSD28WK-SVD (p=0.001 and p<0.001, respectively) with younger (20-week-old) ZDSDs, recording lower values for break force

Humerus yield force

Among the 20-week-old groups, yield force values were significantly higher in SD controls than ZDSDs (p=0.003) (Table 4.6). On the contrary, at week-28, similarities were observed only between 28-week-old SD controls and ZDSD28WK-MOD (p=0.123), but not in ZDSD28WK-SVD that showed significantly lower yield force (p=0.006). No age-related differences were observed in yield force between 20-week-old and 28-week-old SD controls (p=0.085) (Table 4.6). On the contrary, age differences were observed between ZDSD28WK-MOD and ZDSD28WK-SVD (p=0.004 and p<0.001, respectively), with younger (20-week-old) ZDSDs showing lower values for yield force.

Table 4.6: Whole bone biomechanical properties of the humerus loaded in 3-point bending (maximum force, break force, yield force)

	Week 20			Week 28			
Parameter	**SD (n=12)**	**ZDSD (n=14)**	**p value**	**SD (n=14)**	**ZDSD-MOD (n=17)**	**ZDSD-SVD (n=12)**	**p value**
Maximum force (N)	97.36±8.13	75.08±7.20	0.001	100.72±18.37	95.35±20.22	89.00±13.60	^[0.347,0.113] *0.257 #0.001,<0.001
Break force (N)	87.56±15.59	73.37±8.15	0.032	96.38±6.78	93.86±12.62	82.71±21.81	^[0.032,0.017] *0.386 #0.001,<0.001
Yield force (N)	74.14±13.70	52.78±15.56	0.003	82.01±12.013	71.96±20.17	61.93±22.97	^[0.123,0.006] *0.085 #0.004,<0.001

^ Respective comparison of ZDZD28Wk with ZDSD28WK-MOD and ZDSD28WK-SVD: *; p-value comparing SD20WK, against SD28WK, and #; p-value comparing ZDSD-20WK against ZDSD28WK-MOD and ZDSD28WK-SVD respectively

Humerus maximum time

At week-20, there were similarities in maximum time to fracture the humerus between SD controls and ZDSDs (p=0.135) (Table 4.7). On the contrary, among the 28-week-old rats, SD controls, exhibited higher break force values than ZDSD28WK-MOD and ZDSD28WK-SVD (p=0.032 and p=0.017, respectively). No age-related differences were observed in maximum time between 20-week-old and 28-week-old SD controls (p=0.878) (Table 4.7). Similarly, no age differences were observed between ZDSD28WK-MOD and ZDSD28WK-SVD (p=0.435 and p<0.400, respectively).

Humerus maximum displacement

The 20-week-old ZDSDs had similar maximum displacement measurements when compared with their SD controls (p=0.139) (Table 4.7). On the contrary, at week-28, similarities were only observed between 28-week-old SD controls and ZDSD28WK-MOD (p=0.084), but not in ZDSD28WK-SVD that showed significantly lower values (p=0.037). No age-related differences were observed in maximum displacement between 20-week-old and 28-week SD controls (p=0.879) (Table 4.7).This trend of similar maximum displacement was also observed in ZDSD groups, when comparing 20-week-old ZDSDs with 28-week-old ZDSD groups (ZDSD28WK-MOD (p=0.967) and ZDSD28WK-SVD (p=0.633).

Humerus stiffness

The 20-week-old SD controls displayed similar values for stiffness when compared with age matched ZDSDs (p=0.263) (Table 4.7). On the contrary, among the 28-week-old rats SD controls, exhibited a higher stiffness than ZDSD28WK-MOD and ZDSD28WK-SVD (p=0.041 and p=0.008, respectively). No age-related differences were observed in stiffness between 20-week-old and 28-week-old SD controls (p=0.543) (Table 4.7). In contrast, age differences were observed between ZDSD28WK-MOD and ZDSD28WK-SVD (p=0.010 and p=0.002, respectively), with younger (20-week-old) ZDSDs showing lower stiffness values.

Humerus elastic modulus

At week-20, the elastic modulus was significantly higher in ZDSDs than SD controls (p=0.026) (Table 4.7). Similarly, at the age of 28 weeks, both ZDSD28WK-MOD and ZDSD28WK-SVD exhibited significantly lower elastic modulus values compared to their SD controls (p=0.001 and p=0.005, respectively). Age differences were observed in SD controls between rats aged 20 and those aged 28 weeks (p=0.026), where younger SDs (20 weeks) had lower values for elastic modulus compared to those aged 28 weeks (Table 4.7). In contrast, there were similarities in elastic modulus values at 20 weeks of age when compared with 28-week-old groups (ZDSD28WK-MOD #p=0.719 and ZDSD28WK-SVD p=0.918).

Table 4.7: Whole bone biomechanical properties of the humerus loaded in 3-point bending (maximum time, maximum displacement, stiffness, elastic modulus)

	Week 20			Week 28			
Parameter	**SD (n=12)**	**ZDSD (n=14)**	**p value**	**SD (n=14)**	**ZDSD-MOD (n=17)**	**ZDSD-SVD (n=12)**	**p value**
Maximum time (sec)	14.09±3.49	12.35±3.04	0.135	14.27±3.61	11.42±2.16	11.38±2.05	^[0.016,0.014] *0.878 #0.435,0.400
Maximum displacement (N)	0.71±0.17	0.62±0.15	0.139	0.71±0.18	0.62±0.11	0.59±0.08	^[0.084,0.037] *0.879 #0.967,0.633
Stiffness (N/mm)	140.10±28.69	123.02±26.95	0.263	153.79±55.68	150.84±33.22	141.85±33.11	^[0.041,0.008] *0.543 #0.010,0.002
Elastic modulus (N/mm^2)	2104.76±493.35	1630±760.09	0.026	2173.60±459.90	2126.10±282.05	1529.84±55.59	^[0.001,0.005} *0.026 #0.719,0.918

^ Respective comparison of ZDZD28Wk with ZDSD28WK-MOD and ZDSD28WK-SVD: *; p-value comparing SD20WK, against SD28WK, and #; p-value comparing ZDSD-20WK against ZDSD28WK-MOD and ZDSD28WK-SVD respectively

4.2.3 Proximal humerus trabecular morphometry at week-20 and week-28

Humerus bone tissue volume (BV)

There were similarities in BV between SD controls and ZDSDs at 20-weeks of age (p=0.121) (Table 4.8). This similar trend is observed, at week-28, when comparing 28-week old SD controls with ZDSD28WK-MOD and ZDSD28WK-SVD (p=0.586 and p=0.804, respectively). No age-related differences in BV ratios were observed between 20-week-old and 28-week-old SD controls (p=0.541) (Table 4.8). Similarly, 20-week-old ZDSDs did not show any age differences when compared with ZDSD28WK-MOD and ZDSD28WK-SVD (p=0.632 and p=0.232, respectively).

Humerus bone tissue volume to bone tissue volume ratio (BV/TV)

The 20-week-old ZDSDs had lower BV/TV ratios when compared with their SD controls (p<0.001) (Table 4.8). The 28-week-olds showed that SD controls had similarities with 28-week-old ZDSD28WK-MOD (p=0.066), but not in the ZDSD28WK-SVD that had significantly lower BV/TV rations (p=0.043). Older (28-week) SDs had significantly lower BV/TV ratios when compared with 20-week-old SD controls (p<0.001) (Table 4.8). On the other hand, ZDSD28WK-MOD and ZDSD28WK-SVD did not show any age differences when compared with 20-week-old ZDSDs (p=0.485 and p=0.775, respectively).

Table 4.8: Micro-CT measurement of the humerus (BV, BV/TV)

	Week 20			Week 28			
Parameter	**SD (n=12)**	**ZDSD (n=14)**	**p value**	**SD (n=14)**	**ZDSD-MOD (n=17)**	**ZDSD-SVD (n=12)**	**p value**
BV (mm^2)	24.99±1.97	21.19±2.22	0.121	23.51±3.02	22.27±3.38	24.11±3.67	^[0.586,0.804] *0.541 #0.632,0.232
BV/TV (%)	27.60±9.97	11.74±4.50	<0.001	22.24±8.92	14.40±4.57	12.93±3.59	^[0.066,0.043] *<0.001 0.485,0.775

^ Respective comparison of ZDZD28Wk with ZDSD28WK-MOD and ZDSD28WK-SVD: *; p-value comparing SD20WK, against SD28WK, and #; p-value comparing ZDSD-20WK against ZDSD28WK-MOD and ZDSD28WK-SVD respectively. BV, bone tissue volume; BV/TV, bone tissue volume to total volume

Humerus trabecular thickness (TbTh)

At week-20 the ZDSDs exhibited similar trabeculae thickness when compared with SD controls (p=0.171) (Table 4.9). This similar trend was observed, at week-28, when comparing 28-week-old SD controls with ZDSD28WK-MOD and ZDSD28WK-SVD (p=0.476 and p=0.145, respectively). No age-related differences in trabeculae thickness were observed between 20-week-old and 28-week-old SD controls (p=0.076) (Table 4.9). Similarly, 20-week-old ZDSDs did not show any age differences when compared with older (28-weeks) ZDSD28WK-MOD (p=0.056). However, the older (28-week) ZDSD28WK-SVD exhibited significantly thinner trabeculae than 20-week old ZDSDs (p=0.016).

Humerus trabecular number (TbN)

At week-20, there were fewer trabeculae in 20-week old ZDSDs than age matched SD controls (p<0.001) (Table 4.9). On the contrary, 28-week-old ZDSDs did not show any age differences when compared with ZDSD28WK-MOD and ZDSD28WK-SVD (p=0.615 and p=0.132, respectively). Older (28-week) SDs had significantly fewer trabeculae when compared with 20-week-old SD controls (p<0.001) (Table 4.9). On the contrary, 20-week-old ZDSDs did not show any age differences when compared with older (28-week) ZDSDs (ZDSD28WK-MOD and ZDSD28WK-SVD (p=0.632 and p=0.232, respectively).

Humerus trabecular spacing (TbS)

At 20 weeks of age, the ZDSDs exhibited more trabeculae spacing than their SD controls (p<0.001) (Table 4.9). The same trend was observed at 28-weeks of age where ZDSD28WK-MOD and ZDSD28WK–SVD had more trabeculae spaces than their SD controls (p=0.020 and p=0.001, respectively). The SD controls exhibited age related differences, with bones of older rats (age of 28 weeks) having more trabeculae spaces than the 20-week-olds (p<0.001) (Table 4.9). On the contrary, older (28- weeks) ZDSD28WK-MOD showed similarities when compared with 20-week-old ZDSDs (p=0.326), whereas 28-week-old ZDSD28WK-SVD exhibited increased trabeculae spacing when compared with 20-week old ZDSDs. (p=0.008)

Table 4.9: Micro-CT measurement of the humerus (TbTh, TbN, TbSp)

	Week 20			Week 28			
Parameter	**SD (n=12)**	**ZDSD (n=14)**	**p value**	**SD (n=14)**	**ZDSD-MOD (n=17)**	**ZDSD-SVD (n=12)**	**p value**
TbTh (mm)	0.25±0.08	0.21±0.02	0.171	0.30±0.05	0.28±0.04	0.26±0.08	^[0.476,0.145] *0.076 #0.056,0.016
TbN (number)	1.31±0.86	0.78±0.30	<0.001	0.76±0.31	0.59±0.23	0.47±0.14	^[0.615,0.132] *<0.001 #0.575,0.402
TbSp (mm)	0.19 ±0.22	1.29 ±0.71	<0.001	1.21 ±0.57	1.54 ±0.71	2.03 ±0.77	^[0.020,0.004] *<0.001 #0.326,0.008

^ Respective comparison of ZDZD28Wk with ZDSD28WK-MOD and ZDSD28WK-SVD: *; p-value comparing SD20WK against SD28WK, and #; p-value comparing ZDSD20WK against ZDSD28WK-MOD and ZDSD28WK-SVD respectively. TbTh, trabecular thickness; TbN, trabecular number; TbSp, trabecular spacing

4.2.4 Humerus cross-sectional area and medullary canal area at week-20 and week-28

Humerus cortical area

At week 20, the cortical area was similar in ZDSDS when compared with their SD controls (p=0.335) (Table 4.9). The same trend was observed in 28-week-old rats when comparing SD controls with ZDSD28WK-MOD and ZDSD28WK-SVD (p=0.665, p= 0.619 respectively). No age-related differences were observed in cortical area between 20-week-old and 28-week SD controls (p=0.694) (Table 4.9). This trend of a similar cortical area at 20 and 28 weeks of age was also observed in ZDSD groups, when comparing 20-week-old ZDSDs with 28-week-old ZDSD groups (ZDSD28WK-MOD and ZDSD28WK-SVD (p=0.063 and p=0.915, respectively).

Humerus medullary canal area

At week-20, the medullary canal area was similar in 20-week-old ZDSDs and SD controls (p=0.930) (Table 4.9). The same trend was observed in 28-week-old rats when comparing SD controls with ZDSD28WK-MOD and ZDSD28WK-SVD (p=0.714, p=0.582 respectively). No age-related differences were observed in medullary canal area between 20-week-old and 28-week SD controls (p=0.420) (Table 4.9). This trend of a similar medullary canal area was also observed in ZDSD groups, when comparing 20-week-old ZDSDs with 28-week-old ZDSD groups (ZDSD28WK-MOD p=0.677 and ZDSD28WK-SVD p=0.812).

Table 4.10: Micro-CT measurement of the humerus (cortical area, medullary canal area)

		Week 20			Week 28			
Parameter	**Unit**	**SD (n=12)**	**ZDSD (n=14)**	**p value**	**SD (n=14)**	**ZDSD-MOD (n=17)**	**ZDSD-SVD (n=12)**	**p value**
Cortical area 50th percentile (mm^2)	mm^2	16.00 ±2.59	15.11 ±1.47	0.338	16.74 ±1.60	16.82 ±2.35	16.28 ±2.16	^[0.665,0.619] *0.694 #0.063,0.915
Medullary area 50th percentile (mm^2)	mm^2	5.52 ±1.17	5.46 ±1.29	0.930	5.59 ±1.61	5.73 ±2.09	5.97 ±1.53	^[0.714,0.582] *0.522 #0.677,0.812

^ Respective comparison of ZDZD28Wk with ZDSD28WK-MOD and ZDSD28WK-SVD: *; p-value comparing SD20WK against SD28WK, and #; p-value comparing ZDSD20WK against ZDSD28WK-MOD and ZDSD28WK-SVD respectively. C-area, cross sectional area

4.2.5 Discriminant function analysis of femur factors influenced by age, diabetes, and its duration in the humerus

Discriminant function analysis was conducted to determine the humerus variables that are influenced by age, diabetes, and its duration. The structure matrix showed that epicondylar breadth, midshaft anteroposterior diameter, maximum force bone length, Robusticity Index, and TbN were the main factors influenced (Table 4.11).

The discriminant analysis yielded 4 functions, although the Wilk's lambda results indicate a good fit for only Functions 1, 2 and 3 (Wilk's lambda = 0,007; 0,135; 0,547 for Functions 1, 2 and 3, respectively) (p<0.001). Function 4 was not significant (p=0.064). Function 1 accounted for 82.4%

of the variability, Function 2 accounted for 14.2% whereas Function 3 accounted for only 2.5%. For the cross-validated classification, 88.4% of humeri were correctly classified according to their diabetic (ZDSD) and control (SD) status as well as age in the respective groupings. Among the SD control groups, the model correctly classified 100% of the humeri as belonging to the SD20WK or SD28WK group. Among the diabetic groups, the model correctly classified 92.9 of the humeri as belonging to the ZDSD20WK group. However, this was slightly less with older age, the model correctly classified humeri as belonging to the ZDSD28WK-MOD group (76.5%) and ZDSD28WK-SVD (75%) (Table 4.12 and Fig. 4.3)

Table 4.11: Discriminant function analysis of the humerus. The contributing variables are arranged in descending order according to component 1, 2, 3, and 4, with major contributors in bold (above ±0.3).

Structure Matrix

	Function			
Parameter	**1**	**2**	**3**	**4**
Humerus midshaft (AP) anteroposterior diameter	**0,542**	-0,258	0,236	-0,263
Full length	**0,348**	-0,193	**-0,496**	**0,692**
Robusticity index	**0,340**	-0,158	**0,327**	**-0,594**
Trabeculae number (TbN)	0,241	**0,403**	-0,026	-0,023
Humerus head diameter	0,124	-0,035	-0,068	0,120
Humerus midshaft (ML) mediolateral diameter	0,105	-0,051	-0,167	**-0,355**
Yield Force 0.5 mm N	0,102	0,072	0,285	0,170
Elastic modulus	0,097	0,026	0,14	-0,068
Maximum force	0,068	**-0,312**	0,034	0,061
Bone tissue volume (BV)	0,029	0,057	0,218	0,211
Maximum force	0,023	0,083	0,265	0,078
Trabeculae thickness (TbTh)	0,021	-0,207	0,108	0,231
Epicondylar breadth	0,004	**0,608**	-0,273	**-0,437**
Maximum time	-0,022	-0,3	0,022	0,075
Bone tissue volume to total volume (BV/TV)	-0,027	-0,133	0,063	0,043
Mass	-0,037	0,31	0,003	-0,193
Break force	-0,067	0,173	0,495	-0,207
Stiffness	-0,107	0,266	0,152	0,094
Trabeculae spacing (TbSp)	-0,217	-0,165	0,222	0,4
Function Loading %	82,4	14,2	2,5	0,8

Table 4.12: Predicted group membership

Classification Results[a,c]

Group			Predicted Group Membership					Total
			SD20WK	ZDSD20WK	SD28WK	ZDSD28WK-MOD	ZDSD28WK-SVD	
Original	Count	SD20WK	12	0	0	0	0	12
		ZDSD20WK	0	14	0	0	0	14
		SD28WK	0	0	14	0	0	14
		ZDSD28WK-MOD	0	0	0	15	2	17
		ZDSD28WK-SVD	0	0	0	2	10	12
	%	SD20WK	100,0	0,0	0,0	0,0	0,0	100,0
		ZDSD20WK	0,0	100,0	0,0	0,0	0,0	100,0
		SD28WK	0,0	0,0	100,0	0,0	0,0	100,0
		ZDSD28WK-MOD	0,0	0,0	0,0	88,2	11,8	100,0
		ZDSD28WK-SVD	0,0	0,0	0,0	16,7	83,3	100,0
Cross-validated [b]	Count	SD20WK	12	0	0	0	0	12
		ZDSD20WK	0	13	0	1	0	14
		SD28WK	0	0	14	0	0	14
		ZDSD28WK-MOD	0	1	0	13	3	17
		ZDSD28WK-SVD	0	0	0	3	9	12
	%	SD20WK	100,0	0,0	0,0	0,0	0,0	100,0
		ZDSD20WK	0,0	92,9	0,0	7,1	0,0	100,0
		SD28WK	0,0	0,0	100,0	0,0	0,0	100,0
		ZDSD28WK-MOD	0,0	5,9	0,0	76,5	17,6	100,0
		ZDSD28WK-SVD	0,0	0,0	0,0	25,0	75,0	100,0

a. 94,2% of original grouped cases correctly classified.

b. Cross validation is done only for those cases in the analysis. In cross validation, each case is classified by the functions derived from all cases other than that case.

c. 88,4% of cross-validated grouped cases correctly classified.

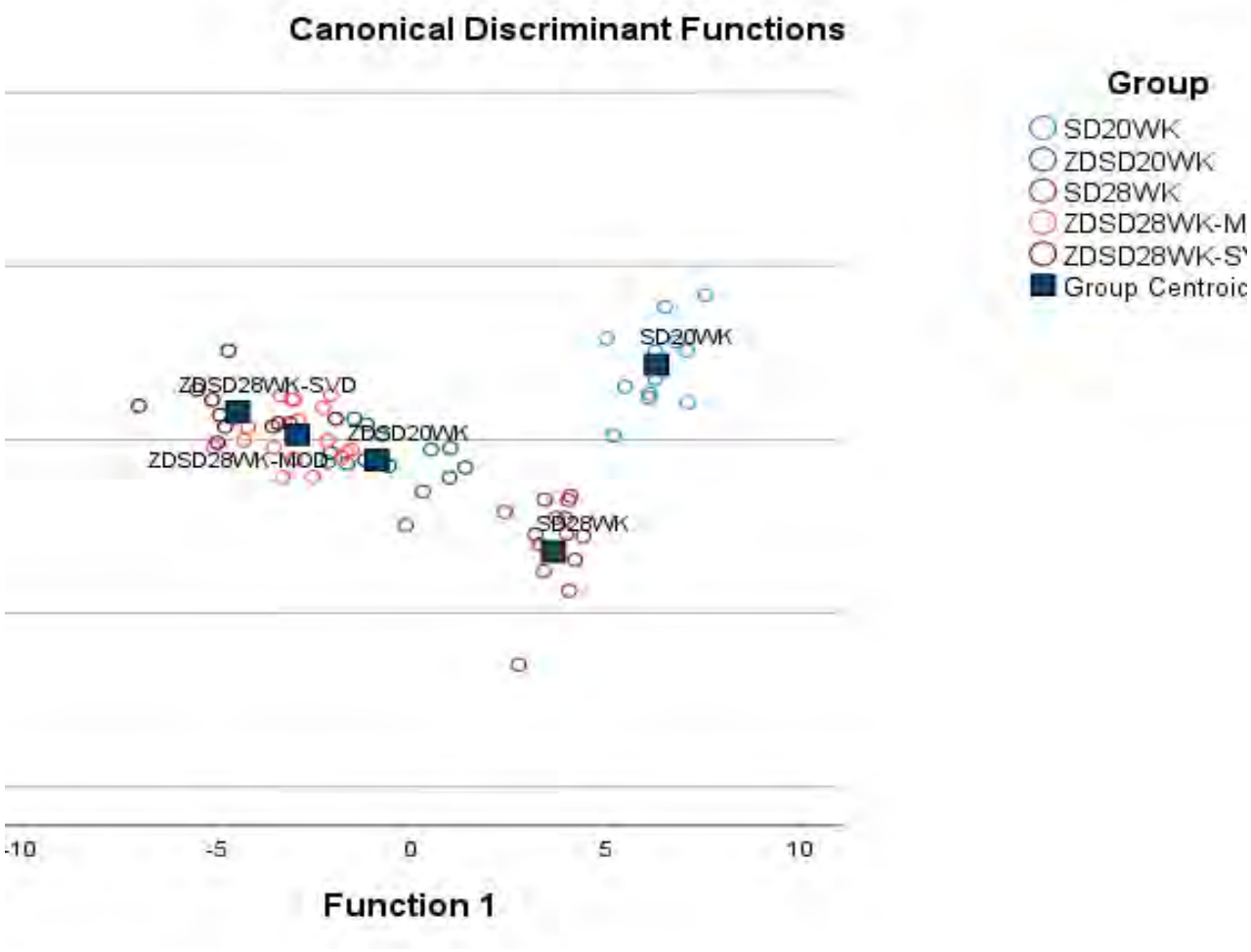


Figure 4.3: Illustration of predicted group membership.

4.3 DISCUSSION

The current study profiled humerus geometry, investigated trabeculae architecture by micro-CT and assessed bone strength using three point bend till fracture, to ascertain if T2D compromises whole bone strength in the humerus. We investigated the proximal epiphysis and mid-diaphysis because the risk of fracture in diabetes varies with specific sub regions of a bone (Ahmad et al., 2003). Because unfavourable alterations in bone biomechanics occur at disease onset and progress with disease (Prisby et al., 2008), bone biomechanics of the humerus in 20-week and 28-week-old diabetic rats was analysed. We used the male ZDSD as an animal model as it reaches skeletal maturity before the onset of T2D (Fajardo et al., 2014; Peterson et al., 2015). We further classified the older rats into diabetic or severely diabetic groups, to ascertain if disease severity has an impact on bone fragility.

Osteometric characterization

The SD and ZDSDs exhibited age related differences, with bones of older rats (age of 28 weeks) weighing significantly less than those of 20-week-olds. This shows that bone mass decreases with age advancement. ZDSD humeri weighed significantly less than their SD controls at both 20 and 28 weeks of age. This finding supports the phenomenon that diabetes causes a decrease bone mass (Prisby et al., 2008).

The humerus length, epicondylar breadth and head diameter as well as robusticity were all smaller in ZDSD rats than the SDs at 20 weeks of age. This was also seen at 28 weeks, except for the head diameter which was similar between the groups among rats of this age. The fact that most of these parameters were lower in the diabetic groups suggest a growth impairment effect of diabetes as supported by the finding of lower humerus mass in this study (Ahmad et al., 2003; Prisby et al., 2008). The humerus length and its robusticity did not change with age when comparing the 20 with the 28 weeks old SDs. This may mean that these control rats were better able to proportionally adjust the length and shaft width (components of robusticity) as the rats grew older. When comparing the ZDSDs aged 20 with those ages 28 weeks, these parameters were both smaller in the severely diabetic (ZDSD28WK-SVD) at an older age of 28 weeks old. This

shows that severe diabetes that remains untreated for a prolonged duration may render the rat humerus unable to match its length with shaft girth as represented by their poor robusticity in the ZDSDs. Robusticity is herein studied in the rat humerus of ZDSD rats for the first time based on our best knowledge of the English scientific literature.

3-point bending and force loading limits

Both maximum force and break force were lower in the ZDSDs than the SDs at the age of 20 weeks with this pattern continuing for break force among the 28-week-old rats. These respective parameters reflect the amount of energy the humerus could take before fracture (maximum force) and the energy required to fracture bone (break force) once the absorbable energy limit is exceeded. The lower load required to fracture ZDSD rat bones corroborates previous reports which document that diabetes increases bone propensity to fracture (Ahmad et al., 2003; Reinwald et al., 2009; Creecy et al., 2016).

The mean time it took to fracture diabetic bones (maximum time to fracture) was less than that for the controls in the 28-week-old groups while no significant differences occurred in the 20-week-old rats. This finding is not due the aging of bones as no age-related differences were observed (in maximum time to fracture) between 20-week-old and 28-week-old SD controls as well as ZDSD rats. Taking less time to fracture only among the 28-week-old ZDSD rats means that, with prolonged diabetes, it became easier to fracture the bones whereas that was not the case in the early stages of diabetes. Again, this demonstrates the validity of our proposition that diabetes interventions are required at disease onset to minimize bone deterioration.

The yield force among the 20-week-old groups, was significantly lower in ZDSDs than SD controls. In older rats, only the ZDSD28WK-SVD showed significantly lower yield force. This demonstrates that diabetes lowered the load limit to forces that could be applied without causing permanent deformation. Therefore, diabetic bones could take less load prior to deformation in the present study. These findings corroborate previous studies (Reddy et al., 2001). No age-related differences were observed in yield force between 20-week-old and 28-week-old SD controls. This

contrasted with the ZDSDs in which older rats (28 weeks) showed lower values for yield force than younger (20-week-old) ZDSDs. The lack of age differences in yield force among controls suggest that the lower yield force on the ZDSD28WK-SVD was due to prolonged diabetes and its severity and not a consequence of aging bone. In support of this, maximum displacement was affected only in the in the ZDSD28WK-SVD group which showed significantly less displacement. Since this parameter reflects bone flexibility, it means that both the duration and severity of diabetes may affect bone flexibility causing it to bend less under load. This may explain the observed higher fracture rate among diabetics as reported in human studies (Janghorbani et al., 2007; Vestergaard et al., 2009; Valderrabano and Linares, 2018). Diabetic rats exhibited significantly lower elastic modulus values compared to their SD controls at both 20 and 28 weeks of age. Therefore, diabetes reduced the amount of load (force) that could be absorbed per unit area of bone without permanent deformation (ability of bone to deform elastically) (Reddy et al., 2001; Jepsen et al., 2015).

Aspects of humerus head trabecular morphometry

In the present study, no bone tissue volume (BV) differences were observed between controls and the ZDSD, and no age-related differences occurred in both 20- and 28-weeks-old rats. However, in 20-week-old rats the bone tissue volume to bone tissue volume ratio (BV/TV) *w*as lower in ZDSDs. Among the 28-week-old rats, the severity of hyperglycemia played a role as only the severely diabetic group (ZDSD28WK-SVD) had significantly lower BV/TV ratios. Older (28-week) SDs had significantly lower BV/TV ratios when compared with 20-week-old SDs whereas the diabetic groups did not show any age differences when comparing the 20 and 28-week-old ZDSDs. In normal SDs as expected and in accordance with previous literature (Uppuganti et al., 2016). In respect of the ZDSDs, the lack of age-related changes suggests that bone tissue volume ratios decreased due to hyperglycemia and not the effect of aging. This is consistent with the findings of (Prisby et al., 2008).

While there were no group differences in trabecular thickness (TbTh) among 20-week-old rats, the ZDSDs had lower trabeculae number (TbN) and greater trabecular spacing (TSp). The latter was also observed in older rats (20 weeks). This implies fewer and more widely spaced trabeculae

in the diabetic group. It suggests that there may have been less trabecular bone deposition and more resorption, reducing thickness while increasing spacing. This finding is in support of the reports that diabetes weakens bone by disturbing the balance of bone resorption and new bone deposition (Ahmad et al., 2003).

Midshaft cortical and medullary canal properties

The midshaft cortical and medullary canal areas showed no detectable differences between controls and the ZDSDs, and no age-related differences occurred in both 20- and 28-weeks-old rats. This was unexpected in the present study as most 3-point bending and robusticity results indicated weaker diabetic bones. It is possible that despite the lack of differences in cortical and medullary canal areas, the quality of the bone material forming the cortical area may be compromised by diabetes. The lighter (lower mass) in diabetic bones in the present study further support this proposition.

Hormonal influences

Studies on osteocalcin receptor knockout mice exhibited reduced islet numbers, hyperglycemia, glucose intolerance, and reduced osteoblast mediated bone mineralization (Fulzele and Clemens, 2012; Ferron and Lacombe, 2014). While both carboxylated and uncarboxylated osteocalcin impact bone, the present study did not distinguish between the two. Additionally, in this study osteocalcin remain unaffected. An imbalance in PTH levels results in either osteoporotic or osteoporotic bone diseases (Florencio-Silva et al., 2015). Hyperactive parathyroid glands release excessive calcium from bones resulting in osteoporosis. It is possible that PTH had a role in the trabecular morphometry in the present study.

4.3.1 Conclusions

Osteometry findings of micro CT and there-point bending tests shows that the severity and the duration of diabetes plays a major role in compromising bone integrity in diabetes. This humerus data should be interpretedwith caution in respect of its translationability to humans as this bone is weight bearing in rats but not in humans.

Chapter 5

Osteoblast and osteocyte numbers are regulated by TGFβ1 and BMP3 in the Zucker Diabetic Sprague Dawley rat femoral head and neck

TABLE OF CONTENTS

5.0 Introduction 107

5.1 MATERIALS AND METHODS 109

5.1.1 Rat model for diabetes type 2 109

5.1.2 Termination and bone harvesting 109

5.1.3 Tissue processing for immunohistochemical techniques 109

5.1.4 Haematoxylin and Eosin (H&E) stain 109

5.1.5 Immunohistochemistry for TRAP, ALP, BMP3, TGFβ1, AGE in the femoral head and neck 110

5.1.6 Photography, quantification, and staining intensity of ROI (region of interest) 111

5.1.7 Data analysis 111

5.2 Results 113

5.2.1 General histology and adipocyte infiltration in the femur head and neck 113

Estimate of adipocyte numbers in the femoral head of 20 and 28-week-old rats 113

Estimate of adipocyte numbers in the femoral neck of 20 and 28-week-old rats 114

5.2.2 Estimate of osteocyte quantity in the femoral head of 20 and 28-week-old rats 116

Cells expressing TRAP (Osteocytes) 116

5.2.3 Estimate of osteocyte quantity in the femoral neck of 20 and 28-week-old rats 118

Cells expressing TRAP (Osteocytes) 118

5.2.4 Estimate of osteoblast quantities in the femoral head of 20 and 28-week-old rats 120

Cells expressing ALP (Osteoblasts) 120

5.2.5 Estimate of osteoblast quantities in the femoral neck of 20 and 28-week-old rats 122

Cells expressing ALP (Osteoblasts) 122

5.2.10 TGFβ1 expression in the femoral head of 20-week-old and 28 week old rats 123

5.2.11 TGFβ1 expression in the femoral neck of 20 week old and 28 week old rats 124

5.2.12 BMP3 expression in the femoral head of 20 week old and 28 week old rats 124

5.2.13 BMP3 expression in the neck of 20-week-old and 28 week old rats 126

5.2.6 Percentage estimate of cells expressing AGE in the femoral head of 20 and 28-week-old rats . 127

5.2.7 Percentages estimate of cells expressing AGE in the femoral neck of 20 and 28-week-old rats 130

5.3 Discussion 133

5.3.1 Conclusions 137

5.0 INTRODUCTION

Type 2 diabetes (T2D) is now recognized as an epidemic and has a high morbidity and mortality rate (Mohan et al., 2007). This condition affects about 387 million people (Zaccardi et al., 2016) worldwide, with a high prevalence in adults, and may affect adolescents and children (Reinwald et al., 2009; Peterson et al., 2015). The predisposing factors and the endocrinology of T2D have been studied extensively (Del Prato, 2009) while its effect on the skeleton has received negligible research despite evidence linking hyperglycemia with compromised bone structural integrity (Bonds et al., 2006; Hamann et al., 2011). Focus in this study is on the femoral head and neck in a relatively new model of diabetes, the Zucker Diabetic Sprague Dawley rat (ZDSD) as these regions are vulnerable to fracture in T2D (Moseley, 2012).

Susceptibility to fracture is consequential from poor bone remodeling resulting from disturbances in the expression of cytokines and growth factors (Seibel, 2005). Bone remodeling depends on the activity of osteoblasts, osteocytes and osteoclasts which are under the influence of TGF-β1, a pro-osteogenic cytokine (Yang et al., 2014), together with BMP3, an anti-osteogenic cytokine (Wu et al., 2016). TGFβ1 is an abundant cytokine found in the bone matrix (Ehnert et al., 2010; Wu et al., 2016). It is responsible for regulating the differentiation, proliferation and migration of osteoprogenitor cells (Janssens et al., 2005; Jian et al., 2006). In contrast, BMP3 negatively regulates osteoblastogenesis, its effect manifests as reduced BMD, reduced trabeculae volume and thinner cortical bone (Gamer et al., 2009; Horbelt et al., 2012).

Hyperglycemia, such as in T2D facilitates the accumulation of AGEs in bone tissue and bone cells. AGEs bind to bone turnover cells, adversely compromising their function (Kislinger et al., 1999; Singh et al., 2014; Plotkin et al., 2019). T2D favours the differentiation of skeletal stem cells into adipogenic cell lineages while suppressing the proliferation of osteogenic cell lineages in both human and animal models (Kim and Schafer, 2016; Gillet et al., 2017; Ferland-McCollough et al., 2018). A previous study reports T2D that increases bone marrow adiposity in both humans (Sheu et al., 2017) and obese animal models (Devlin et al., 2014) where bone marrow fat was associated with an increased prevalence of hip fractures (Kim and Schafer, 2016).

The aim of the study was to determine if osteoblast and osteocyte numbers are regulated by TGFβ1 and BMP3 in ZDSD rat femoral head and neck in a relatively new animal model of T2D, the ZDSD rat. While the ZDSD is fast becoming the golden standard of T2D research, this study questioned whether it is appropriate for diabetic skeletopathy investigations. We will quantitatively assess T2D effects on adipocytes, osteoblast, osteocyte numbers, and evaluate the impact of T2D on TGFB1 and BMP3 expression in bone tissue. Finally, the extracellular expression of AGEs, and quantify AGEs immunopositive cells will be assessed.

5.1 MATERIALS AND METHODS

5.1.1 Rat model for diabetes type 2.

Rats were handled as described in section 2.1.2

5.1.2 Termination and bone harvesting

Rats were injected with a lethal intraperitoneal dose of 1 ml sodium pentobarbital (Euthanase, 200 mg/ml; Kyron Laboratories (Pty) Ltd, South Africa), then immersed in 10% buffered formalin, after abdominal and limb incisions were made, to facilitate penetration of the fixative. Posterior left and right limbs were removed, and muscles were cleaned out of the femur. Individual bones were then stored in 10% buffered formalin to continue fixation until further processing. Left femora were used for immunohistochemical investigations.

5.1.3 Tissue processing for immunohistochemical techniques

Bone samples were fixed in 10% buffered formalin for a minimum of 14 days, then decalcified in 20% w/v ethylenediaminetetraacetic acid (EDTA, pH 7.4) for 10 days in an incubator with regular gentle shaking at 45˚C. The bones were then rinsed, and their proximal epiphysis severed about 3mm below the inferior trochanter, then immersed in 10% buffered formalin for 24 hours before processing for histology. An automatic processor (Citadel 2000, Thermo Fischer Scientific) was used to take the samples through ascending grades of ethanol prior to embedding in paraffin wax. During embedding, bone samples were orientated longitudinally to minimize differences in the sectioning angle. Bone sections were cut at 5µm thickness using a microtome (Leica RM2125 RTS, Leica Biosystems, USA) and mounted on silane-coated glass slides. Section sequences were mounted in order for specific stains, namely; Hematoxylin and Eosin to assess femoral head and neck morphology, and to quantify adipocyte number as well as immunolocalization of TRAP, ALP, BMP3, TGFβ1 and AGEs for the same regions.

5.1.4 Haematoxylin and Eosin (H&E) stain

This method is also used to determine normal tissue structure (Totty, 2002). Sections were dewaxed in xylene for 10 minutes and hydrated by passing through 3 changes (1 minute each) of

absolute alcohol followed by 90% and 70% alcohol (1 minute each) and eventually into running tap water for 1 minute. The sections were then stained for 10 min in haematoxylin, differentiated in periodic acid for 10 seconds, rinsed in tap water for a minute, blued in Scott's tap water for 2 minutes, and rinsed again in tap water. The cytoplasm was stained with eosin by immersing the sections in 70% alcohol followed by eosin for 2 minutes. The sections were then dehydrated in increasing concentrations of alcohol before they were mounted in entellen.

5.1.5 Immunohistochemistry for TRAP, ALP, BMP3, TGFβ1, AGE in the femoral head and neck

Immunohistochemistry was conducted using the anti-TRAP antibody (ab185716) for osteocytes detection, anti-ALP antibody (ab108337) for osteoblasts and anti-AGE antibody (ab23722) AGEs, anti-BMP3 antibody (ab134724) and anti-TGF beta 1 antibody (ab92486). All antibodies were sourced from Abcam. Sections were placed in an incubator at 40^0C for 30 minutes and then deparaffinized and rehydrated in a series of graded alcohols. They were then immersed in a citrate buffer (pH=6) and placed in a water bath set at 60^0C for 24 hours, to facilitate antigen retrieval. After 24 hours sections were cooled at room temperature for 20 minutes then rinsed 3 x 5minutes times in PBS (pH=7.4). Endogenous peroxidase was blocked with 1% hydrogen peroxide (H_2O_2) and then the sections were washed in PBS 3 x 5 minutes. Sections were transferred to a perspex plate and incubated with the primary antibodies at appropriate dilutions (TRAP; 1: 100, ALP; 1:200, AGE; 1: 10 000, TGFβ1, 1:400, BMP3 1: 75) and placed at 4^0C overnight. After 24 hours, sections were left on the benchtop for 20 minutes to reach room temperature before washing in PBS 3 x 5 minutes. The slides were then incubated in biotinylated secondary antibody (Biotinylated Goat Anti-Rabbit IgG (H+L) (ab64256) for 10 minutes, and again washed in PBS 3 x 5 minutes. Sections were then incubated in streptavidin HRP for 10 minutes (ab64269) for detection and to enhance the binding of the antibodies. This was followed by 3 x 5 minutes rinses in PBS (pH=7.4). The slides were then incubated with 3-3' di-aminobenzidine (DAB) working solution while monitoring color development under a light microscope. Once optimal staining was achieved the sections were, rinsed in running tap water for 5 minutes, then dehydrated through graded alcohol, cleared in xylene and eventually mounted in entellen.

5.1.6 Photography, quantification, and staining intensity of ROI (region of interest)

A light microscope (Zeiss Axioscope 2 plus) fitted with an axiocam HRC digital camera (Zeiss, Germany) connected to a PC (Hewlett-Packard, South Africa) was used to take photomicrographs of the stained slides. Photomicrographs were taken under different magnification scales, 50x, 200x and 400x for anatomical orientation, quantification and cellular detail respectively. Anatomical landmarks were determined for both the femoral head and neck, using the H&E stained slides, to create consistency in quantification and staining analysis. Non adjacent fields were selected, two above and two below the epiphyseal growth plate for the femoral head, and three non-adjacent fields were selected in the femoral neck (Fig. 5.1). Photomicrographs were imported into Fiji Image-J software (National Institute of Health USA) for further analysis. TRAP positive osteocytes (Nakano et al., 2004; Dole et al., 2017), ALP positive osteoblasts (Miao and Scutt, 2002), AGEs positive bone cells and adipocytes were identified as specified in previous literature (Ferland-McCollough et al., 2018). Cells were counted manually by the investigator at different times in the same region to check for consistency. Immunolocalization for anti-AGEs antibody, anti-BMP3 antibody, and anti-TGFβ1 antibody was performed. These were graded as no stain, mild, moderate and intense staining.

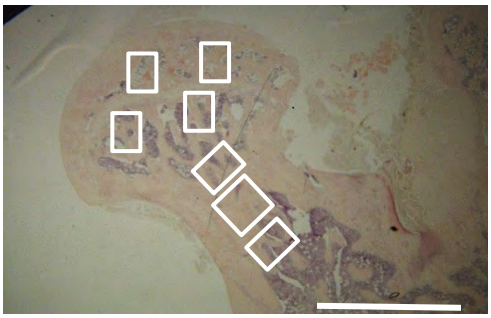


Figure 5.1: Head of the femur regions of interest. Scale bar represents 100µm

5.1.7 Data analysis

The data were managed in Microsoft Excel 2016 (Microsoft Corporation) and all data were analyzed using SPSS® version 28 (IBM®) The data was tested for normality using the Shapiro Wilks

test, the data was found to be normally distributed, and a One-Way ANOVA with LSD post-hoc test was applied for multiple group comparisons. Ordinal data for staining intensity were assigned grading scales of no stain (0), mild (1), moderate (2) and intense (3). All data (ordinal and numeric), significance level was set at $p < 0.05$.

5.2 RESULTS

5.2.1 General histology and adipocyte infiltration in the femur head and neck

Estimate of adipocyte numbers in the femoral head of 20 and 28-week-old rats

Controls exhibited normal bone marrow cells as opposed to diabetic groups that had extensive adipocyte infiltration (Fig. 5.3, (a, c; b, d, e respectively)**.** The SD20WK controls mean=31.00±9.98) had fewer adipocyte numbers compared to ZDSD20WK (mean=55.83±9.26) ($p<0.001$) in the femoral head (Figs. 5.2 and 5.3, a-b). This trend of fewer adipocytes in SD28WK controls (mean=24.64±8.32) was maintained when compared with ZDSD28WK-MOD (mean=89.74±14) and ZDSD28WK-SVD (mean=71.33±6.79) ($p<0.001$) (Fig. 5.2 and Fig. 5.3, c-e). No age differences were observed in the SD controls ($p=0.281$) in this femoral region. In contrast, the ZDSD groups had more adipocytes at 28 weeks ($p<0.001$; $p=0.015$ respectively) (Fig. 5.2).

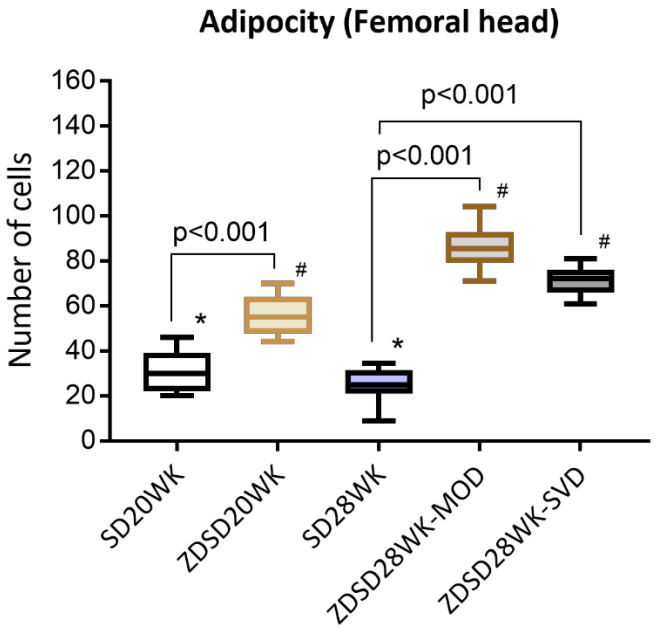


Figure 5.2 Adipocytes in the femoral head. Box-and-whisker plots of adipocyte estimation in various study groups. The line inside the box represents the mean, whereas the bottom and top lines of the box show the 25th and 75th percentiles, respectively. The whiskers below and above the box show the minimum and maximum values, respectively.

SD20WK and SD28WK, Sprague Dawley rats aged 20 and 28 weeks, respectively. ZDSD20WK, ZDSD28WK-MOD and ZDSD28WK-SVD, Zucker Diabetic Sprague Dawley rats aged 20 weeks, and aged 28 weeks moderately diabetic and severely diabetic, respectively. *; p=0.573 and #; p=0.742; p=0.668 comparing ZDSD20WK against the ZDSD28WK-MOD and ZDSD28WK-SVD, respectively.

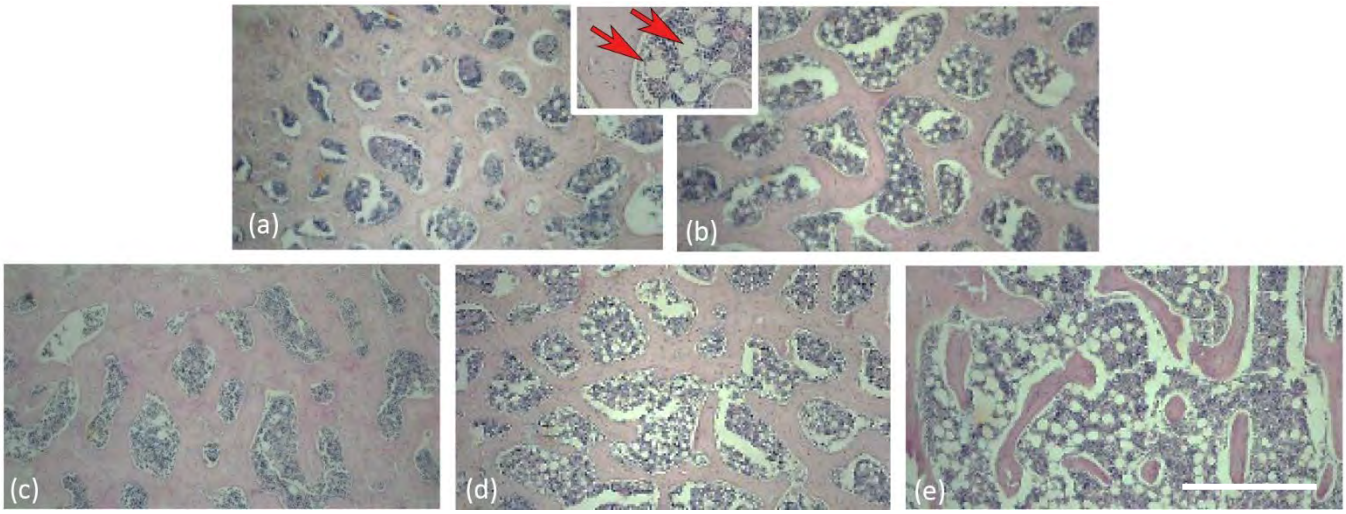


Figure 5.3: Femoral head general histological appearance. Adipocytes are the large round cells with a clear cytoplasm as depicted by the arrows in the insert Scale bar represents 100µm and applies to all.

Estimate of adipocyte numbers in the femoral neck of 20 and 28-week-old rats

In the femoral neck, there was an even distribution of adipocytes (Fig. 5.5). No statistical differences were detected in adipocyte numbers between the SD20WK controls (mean=5.50±3.78) and ZDSD20WK (mean=6.50±4.42) (p=0.633) (Figs. 5.4 and 5.5, a-b). Similarly, no differences in adipocyte quantities were observed between the SD28WK controls (mean=5.57±3.46) when contrasted ZDSD28WK-MOD (mean=4.89±3.72) and ZDSD28WK-SVD ZDSDs (mean= 5.17±2.14) (p=0.709; p=0.884 respectively) (Figs. 5.4 and 5.5, c-e). No age differences were observed for both 20 and 28-week SD controls (p=0.972) and ZDSD groups (p=0.402; p=0.525 respectively) (Fig. 5.4).

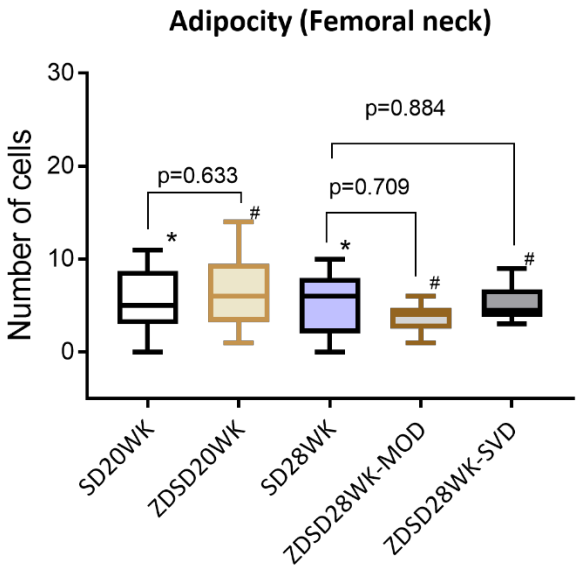


Figure 5.4: Adipocytes in the femoral neck. Box-and-whisker plots of adipocyte estimation in various study groups. The line inside the box represents the mean, whereas the bottom and top lines of the box show the 25th and 75th percentiles, respectively. The whiskers below and above the box show the minimum and maximum values, respectively.

SD20WK and SD28WK, Sprague Dawley rats aged 20 and 28 weeks, respectively. ZDSD20WK, ZDSD28WK-MOD and ZDSD28WK-SVD, Zucker Diabetic Sprague Dawley rats aged 20 weeks, and aged 28 weeks moderately diabetic and severely diabetic, respectively. *; p=0.573 and #; p=0.742; p=0.668 comparing ZDSD20WK against the ZDSD28WK-MOD and ZDSD28WK-SVD, respectively.

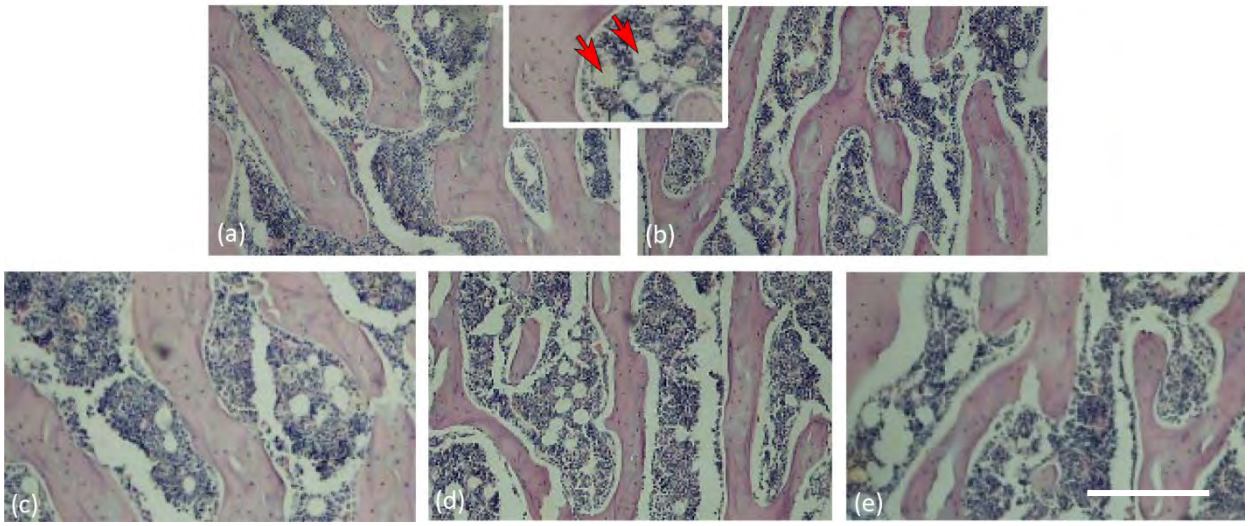


Figure 5.5: Femoral neck general histological appearance. Adipocytes are the large round cells with a clear cytoplasm as depicted by the arrow in the insert Scale bar represents 100µm and applies to all.

5.2.2 Estimate of osteocyte quantity in the femoral head of 20 and 28-week-old rats

Cells expressing TRAP (Osteocytes)

The ZDSD20WK rats (mean=96.50±24.11) showed significantly more TRAP positive cells than SD20WK controls (mean=65.79±6.70) in the femoral head (p=0.001) (Figs. 5.6 and 5.7 a-d). A similar trend was observed at 28 weeks, where the ZDSD28WK-MOD (mean=72.51 ±12.43) and ZDSD28WK-SVD (mean=73.60 ±15.58) demonstrated significantly more TRAP positive cells than SD28WK controls (mean=44.90 ±12.91) (p=0.001; p=0.002, respectively) (Figs. 5.6 and 5.7 e-j). Age differences were observed for both SDs and ZDSDs, with fewer TRAP positive cells expressed at 28 weeks compared to 20 weeks (p=0.019; p= 0.005 respectively) (Fig. 5.6).

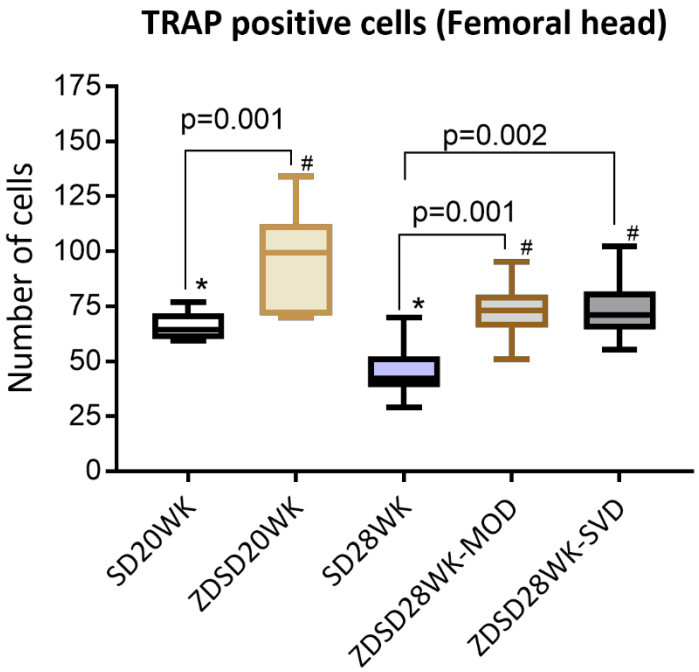


Figure 5.6: TRAP immunopositive cells quantity in the femoral head. Box-and-whisker plots of osteocyte estimation in various study groups. The line inside the box represents the mean, whereas the bottom and top lines of the box show the 25th and 75th percentiles, respectively. The whiskers below and above the box show the minimum and maximum values, respectively.
SD20WK and SD28WK, Sprague Dawley rats aged 20 and 28 weeks, respectively. ZDSD20WK, ZDSD28WK-MOD and ZDSD28WK-SVD, Zucker Diabetic Sprague Dawley rats aged 20 weeks, and aged 28 weeks moderately diabetic and severely diabetic, respectively. *; p=0.019 and #; p=0.005, comparing ZDSD20WK against ZDSD28WK-MOD and ZDSD28WK-SVD.

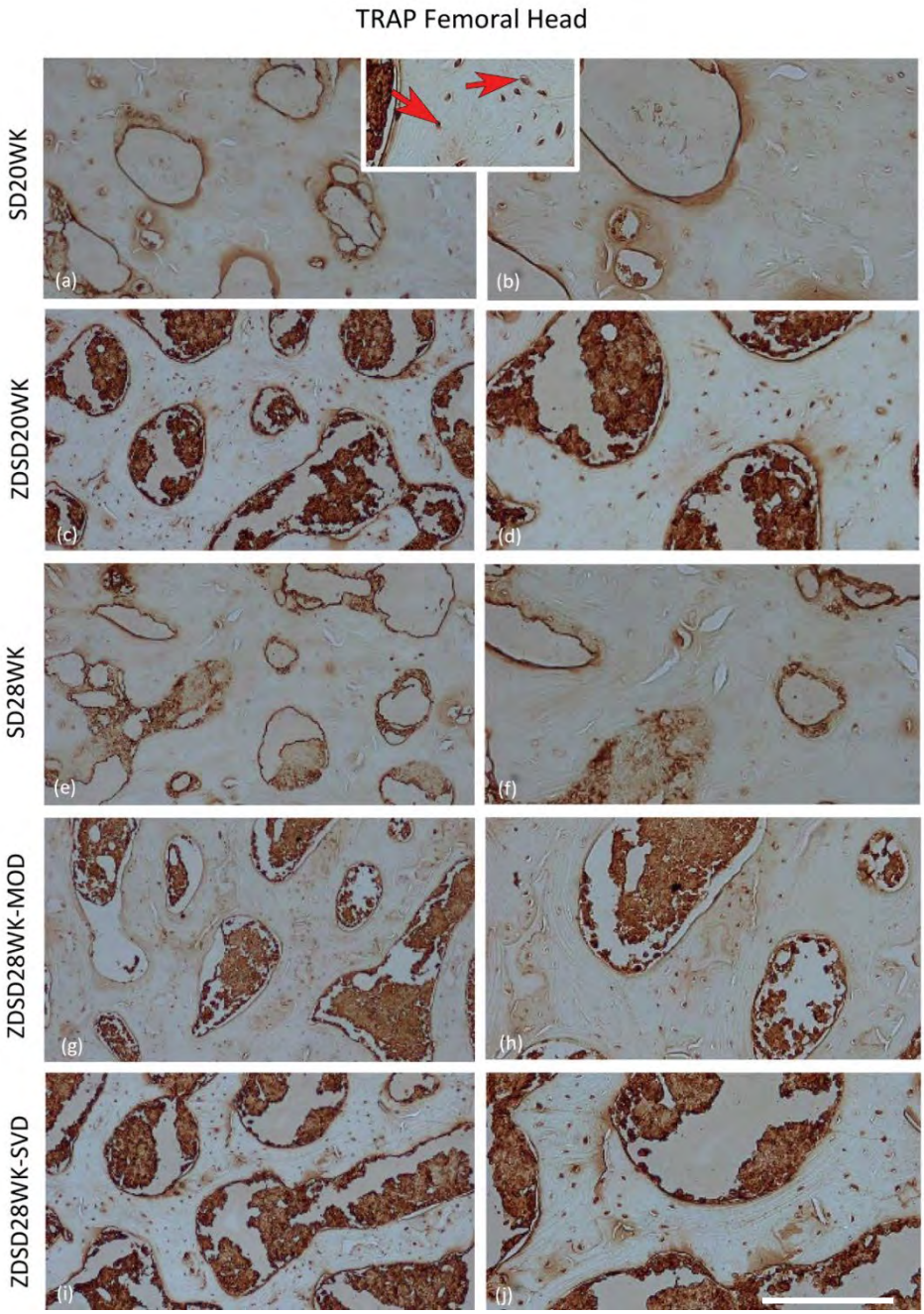


Figure 5.7: Femoral head TRAP Immunopositive osteocytes. The osteocytes are embedded in the bone matrix as depicted by the arrows in the insert and are found throughout a-j. Scale bar represents 100µm and applies all photomicrographs.

5.2.3 Estimate of osteocyte quantity in the femoral neck of 20 and 28-week-old rats

Cells expressing TRAP (Osteocytes)

At 20 weeks, SD20WK (mean=50.61±10.16) and ZDSD20WK (mean=46.45±12.84) exhibited similarities in the number of TRAP positive cells in the femoral neck (p=0.44) (Figs. 5.8 and 5.9 a-d). At 28 weeks these cell numbers were similar for the SD28WK controls (mean=39.31 ±9.03) and ZDSD28WK-MOD (mean= 40.44±7.93) (p=0.809) but not the ZDSD28WK-SVD group (mean=54.11±4.75) (p=0.007) (Figs. 5.8 and 5.9 e-j). Age differences were observed in the expression of TRAP positive cells in both SD controls and ZDSDs. With the exception of the ZDSD28WK-SVD, all other groups had fewer cells at 28 weeks compared to 20 weeks (p<0.001; for all comparisons). The ZDSD28WK-SVD showed more TRAP positive cells than the ZDSD20WK comparison (p<0.001) (Fig. 5.8).

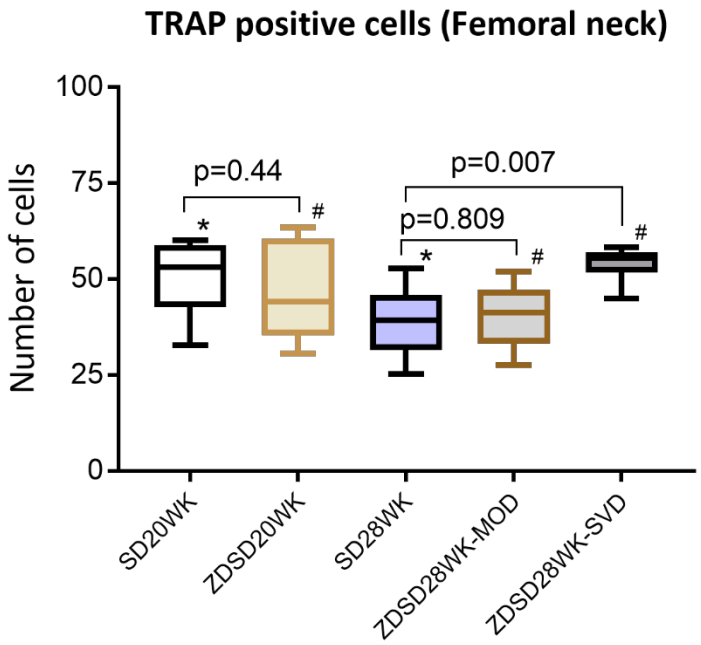


Figure 5.8: TRAP immunopositive cells in the femoral neck. Box-and-whisker plots of osteocyte estimation in various study groups. The line inside the box represents the mean, whereas the bottom and top lines of the box show the 25th and 75th percentiles, respectively. The whiskers below and above the box show the minimum and maximum values, respectively.
SD20WK and SD28WK, Sprague Dawley rats aged 20 and 28 weeks, respectively. ZDSD20WK, ZDSD28WK-MOD and ZDSD28WK-SVD, Zucker Diabetic Sprague Dawley rats aged 20 weeks, and aged 28 weeks, moderately diabetic and severely diabetic, respectively. *, #; p<0.001 for respective age comparisons.

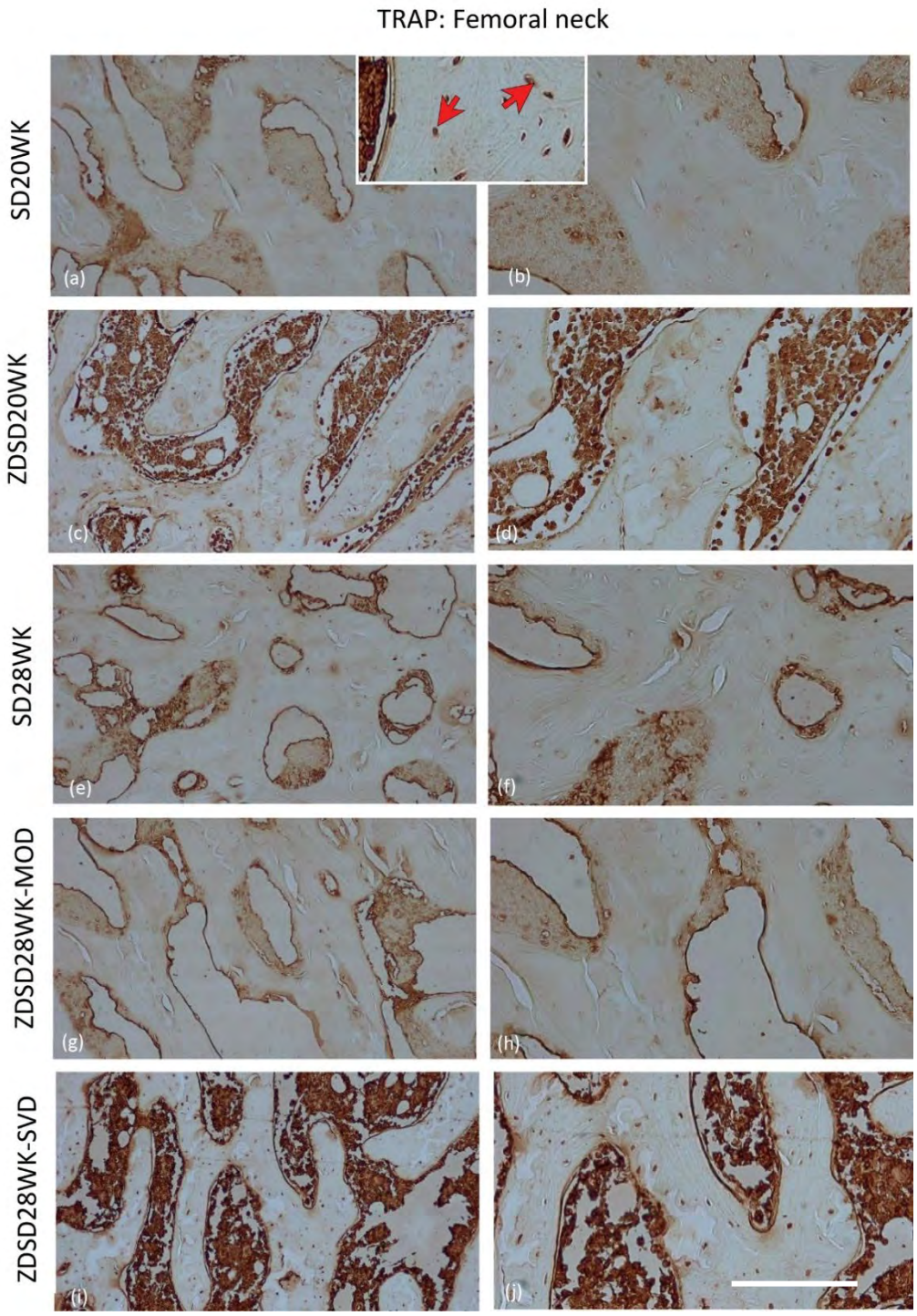


Figure 5.9: Femoral neck TRAP Immunopositive osteocytes . The osteocytes are embedded in the bone matrix as depicted by the arrows in the insert and are found throughout a-j. Scale bar represents 100µm and applies all photomicrographs.

5.2.4 Estimate of osteoblast quantities in the femoral head of 20 and 28-week-old rats

Cells expressing ALP (Osteoblasts)

The SD20WK (mean=20.34±4.51) showed higher numbers of ALP positive cells than ZDSD20WK (mean=3.65±1.00) in the femoral head ($p<0.001$) (Figs. 5.10 and 5.11 a-d). This trend was maintained at 28 weeks, where SD28WK controls (mean=19.10±3.83) recorded higher ALP positive cell numbers than ZDSD28WK-MOD (mean=5.34±1.09) and ZDSD28WK-SVD (mean=4.65±0.77) ($p<0.001$) (Figs. 5.10 and 5.11 e-j). Age similarities were observed in the expression of ALP positive cells between SD20WK and SD28WK ($p=0.413$) as well as both ZDSD groups in this region ($p=0.241$; $p=0.524$ respectively) (Fig. 5.10).

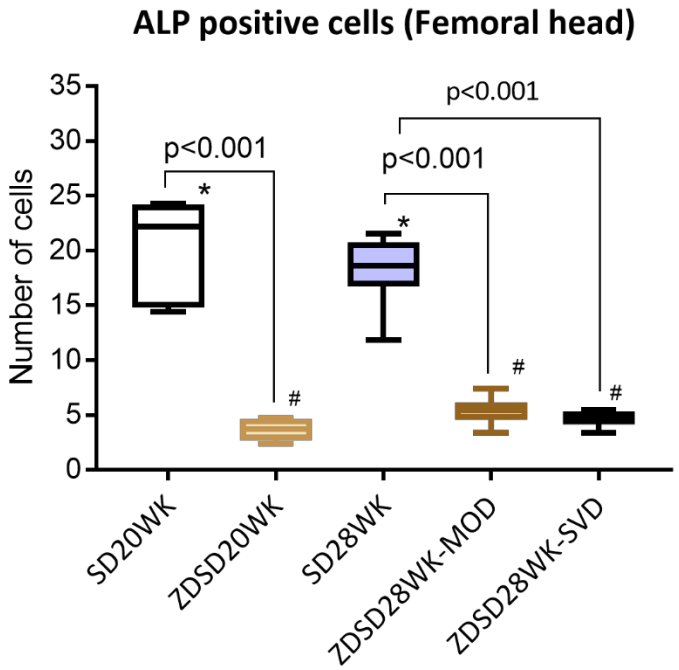


Figure 5.10: ALP immunopositive cells quantity in the femoral head. Box-and-whisker plots of osteoblast estimation in various study groups. The line inside the box represents the mean, whereas the bottom and top lines of the box show the 25th and 75th percentiles, respectively. The whiskers below and above the box show the minimum and maximum values, respectively.
SD20WK and SD28WK, Sprague Dawley rats aged 20 and 28 weeks, respectively. ZDSD20WK, ZDSD28WK-MOD and ZDSD28WK-SVD, Zucker Diabetic Sprague Dawley rats aged 20 weeks, and aged 28 weeks moderately diabetic and severely diabetic, respectively. *; $p=0.413$ and #; $p=0.241$; $p=0.524$ comparing ZDSD20WK against ZDSD28WK-MOD and ZDSD28WK-SVD respectively.

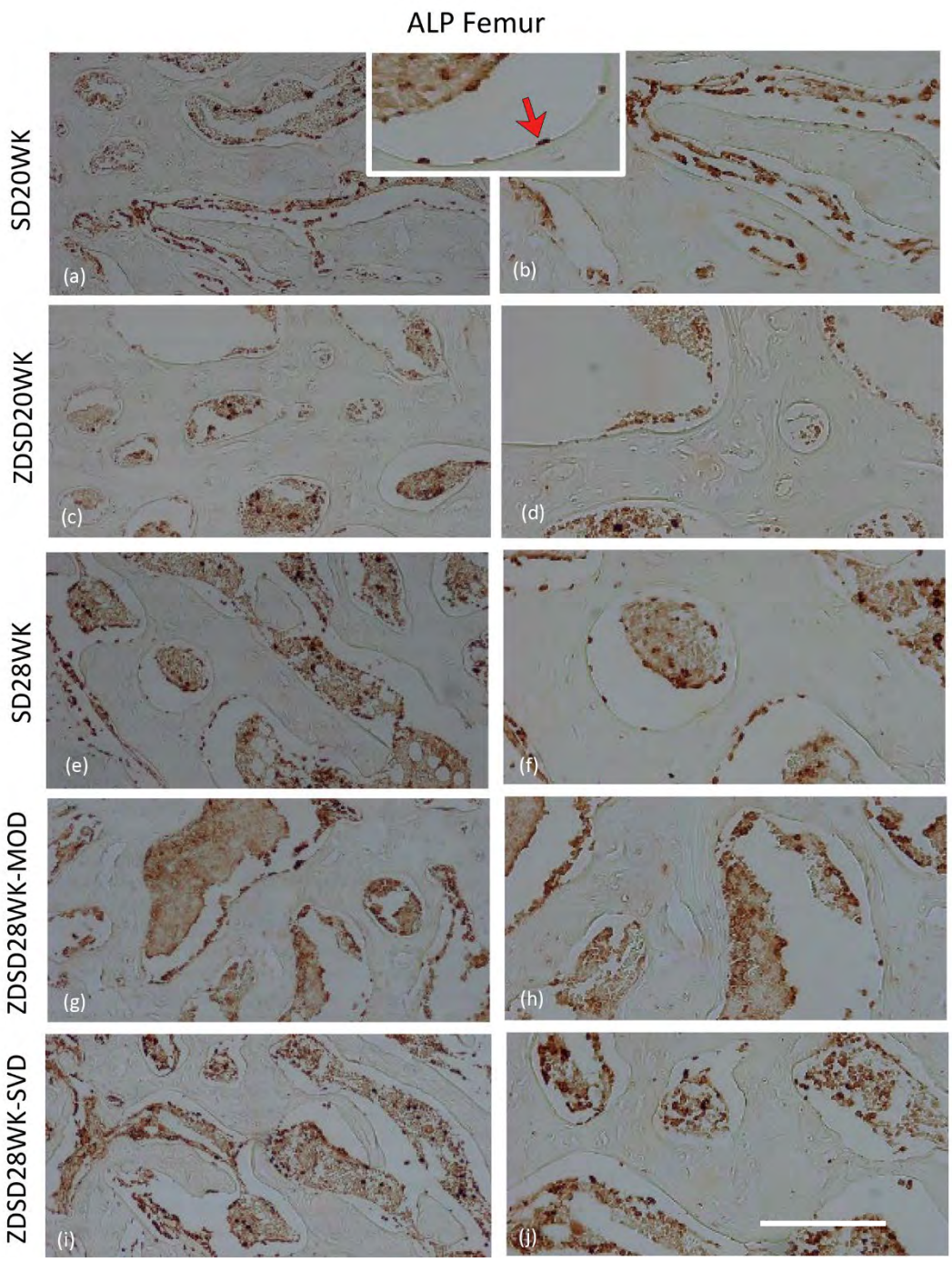


Figure 5.11: Femur ALP Immunopositive osteoblasts The osteoblasts lining bone marrow spaces are depicted by arrows in the insert and are found throughout a-j. Scale bar represents 100µm and applies all photomicrographs.

5.2.5 Estimate of osteoblast quantities in the femoral neck of 20 and 28-week-old rats

Cells expressing ALP (Osteoblasts)

In the femoral neck, SD20WK (mean=7.63±1.36) exhibited more ALP positive cells than ZDSD20WK (mean=2.74±0.65) (p=0.001) (Figs. 5.12 and 5.11 a-d). This trend was maintained at 28 weeks with SD28WK controls (mean=17.08 ±4.27) recording higher numbers than the ZDSD28WK-MOD (mean=3.41±0.95) and ZDSD28WK-SVD (mean=3.64±1.42) (p<0.001; p<0.001 respectively) (Figs. 5.12 and 5.11 e-j). Age differences in the number of ALP positive cells were only observed in the comparison of SD20WK and SD28WK controls, being more in the latter (p<0.001). In contrast, ZDSD groups had a similar number of these cell irrespective of age (p=0.241; p=0.524 respectively) (Fig. 5.12).

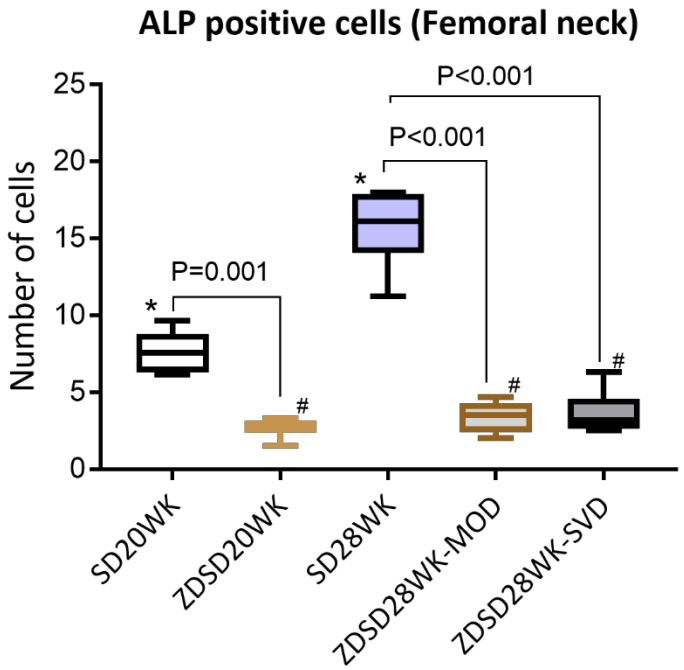


Figure 5.12: ALP immunopositive cells quantity in the femoral neck. Box-and-whisker plots of osteoblast estimation in various study groups. The line inside the box represents the mean, whereas the bottom and top lines of the box show the 25th and 75th percentiles, respectively. The whiskers below and above the box show the minimum and maximum values, respectively.
SD20WK and SD28WK, Sprague Dawley rats aged 20 and 28 weeks, respectively. ZDSD20WK, ZDSD28WK-MOD and ZDSD28WK-SVD, Zucker Diabetic Sprague Dawley rats aged 20 weeks, and aged 28 weeks moderately diabetic and severely diabetic, respectively. *; p<0.001 and #; p=0.241; p=0.524 comparing ZDSD20WK against the ZDSD28WK-MOD and ZDSD28WK-SVD, respectively.

5.2.10 TGFβ1 expression in the femoral head of 20-week-old and 28 week old rats

Majority of the SD20WK controls (n=4; 66.67%) had moderate staining, with 2 rats (33.33%) exhibiting moderate staining to TGFβ1 (Table 5.1 and Fig 5.13). In comparison, all the ZDSD20WK had mild staining (n=6; 100%). Statistical significance was observed between the two groups (p=0.002) (Table 5.3). All SD28WK controls (n=7; 100%) showed mild staining, while there was no staining in the majority of ZDSD28WK-MOD (n=6; 66.67%) with 3 rats that exhibited mild staining (33.33%) (Table 5.1 and Fig 5.13). All the ZDSD28WK-SVD (n=6; 100%) had zero staining. Differences between the SD28WK controls and both groups of age matched ZDSDs showed statistical significance (p<0.001). Age differences were observed in both the SDs (p=0.001) and ZDSD groups (p<0.001; for both) (Table 5.1).

Table 5.1: Femoral head TGFβ1 immunopositivity

Femur head TGFB1

Group	No stain			Mild		Moderate		Intense		p value
	N	Count	%	Count	%	Count	%	Count	%	
SD20WK	6	0	0	2	33.33	4	66.67	0	0	
ZDSD20WK	6	0	0	6	100	0	0	0	0	p=0.002
SD28WK	7	0	0	7	100	0	0	0	0	
ZDSD28WK-MOD	9	6	66.67	3	33.33		0	0	0	p=0.001
ZDSD28WK-SVD	6	6	100	0	0	0	0	0	0	#p,0.001

Comparison of SD28WK with ZDSD-SVD

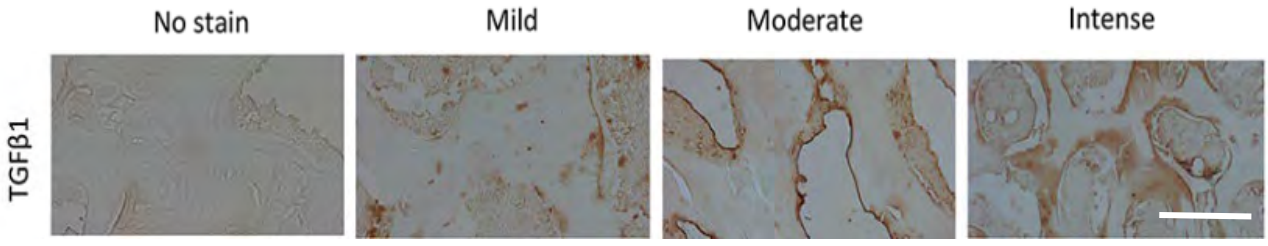


Figure 5.13: Femur TGFβ immunopositivity grading. Scale bar represents 100µm and applies all photomicrographs.

5.2.11 TGFβ1 expression in the femoral neck of 20 week old and 28 week old rats

All SD20WK (n=6; 100%) exhibited mild immunopositivity, while all the ZDSD20WK (n=6; 100%) displayed zero immunopositivity, with statistical significance (p<0.001) (Table 5.2 and Fig 5.13). At 28 weeks, all SD28WK controls (n=7; 100%) exhibited mild immunopositivity, the majority of ZDSD28WK-MOD (n=6; 66.67%) had zero immunopositivity, and 3 rats (33.33%) showed mild immunopositivity (Table 5.2 and Fig 5.13). All ZDSD28WK-SVD (n=6; 100%) had zero immunopositivity. Statistical significance was observed between the SD28WK and ZDSD28WK-MOD and ZDSD28WK-SVD (p<0.001, for both) (Table 5.2). No age differences were observed in the SD controls (p=1.000), whereas differences were observed in the ZDSD28WK-MOD (p=0.023) but not the ZDSD28WK-SVD (p=1.000) (Table 5.2).

Table 5.2: Femoral neck TGFβ1 immunopositivity

Femur neck TGFB1

Group	No stain			Mild		Moderate		Intense		p value
	N	Count	%	Count	%	Count	%	Count	%	
SD20WK	6	0		6	100	0	0	0	0	p<0.001
ZDSD20WK	6	6	100	0		0	0	0	0	
SD28WK	7	0	0	7	100	0	0	0	0	
ZDSD28WK-MOD	9	6	66.67	3	33.33	0	0	0	0	p<0.001
ZDSD28WK-SVD	6	6	100	0	0	0	0	0	0	#p<0.001

Comparison of SD28WK with ZDSD-SVD

5.2.12 BMP3 expression in the femoral head of 20 week old and 28 week old rats

A higher proportion of the SD20WK (n=4; 66.67%) rats in the study showed no BMP3 expression, with only few rats showing (n=2; 33.33%) a mild expression. In contrast, mild expression was detected in the majority of ZDSD20WK (n=5; 83.33%) with 1 animal exhibiting moderate expression (16.78%) (p=0.002) (Table 5.3 and Fig 5.14). All SD28WK controls had mild immunopositivity (n=7; 100%), again the majority of ZDSD28WK-SVD had mild immunopositivity (n=5; 83.33%) with 1 animal exhibiting moderate immunopositivity (16.67%) (p=0.486), whereas the majority of ZDSD28WK-SVD exhibited moderate immunopositivity (n=5; 55.67%) with mild immunopositivity shown by the rest of the rats (n=4; 44.44%) (p=0.015) (Table 5.3 and Fig 5.14).

Age differences were observed in BMP3 expression in SDs (p=0.008) whereas similarities were observed in the ZDSD groups (p=0.093; p=1.000 respectively) (Table 5.3).

Table 5.3: Femoral head BMP3 immunopositivity

Femur Head BMP3

Group	No stain			Mild		Moderate		Intense		p value
	N	Count	%	Count	%	Count	%	Count	%	
SD20WK	6	4	66.7	2	33.3	0	0	0	0	p=0.002
ZDSD20WK	6	0	0	5	83.3	1	16.7	0	0	
SD28WK	7	0	0	7	100	0	0	0	0	
ZDSD28WK-MOD	9	0	0	4	44.4	5	55.6	0	0	p=0.015
ZDSD28WK-SVD	6	0	0	5	83.3	1	16.7	0	0	#p=0.486

Comparison of SD28WK with ZDSD-SVD

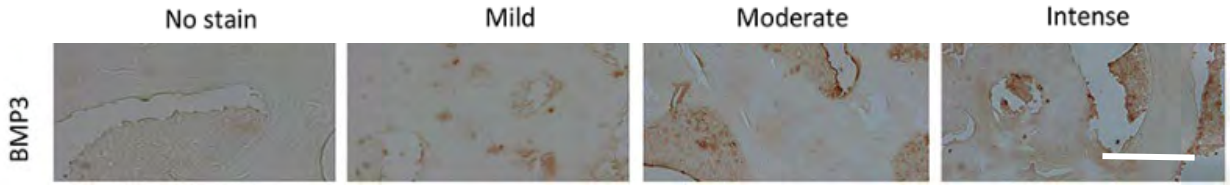


Figure 5.14: Femur BMP3 immunopositivity grading. Scale bar represents 100µm and applies all photomicrographs.

5.2.13 BMP3 expression in the neck of 20-week-old and 28 week old rats

Majority of the SD20WK controls (n=4; 66.78%) had mild immunopositivity while 2 rats (33.33%) had no detectable immunopositivity for BMP3. In the ZDSD20WK, majority of rats exhibited mild immunopositivity (n=5; 83.30%) and only 1 animal had moderate immunopositivity (16.70%) (Table 5.4 and Fig 5.14). Similarities were observed between the SD20WK and ZDSD20WK (p=0.069). The SD28WK controls, majority of the rats exhibited mild immunopositivity (n=6; 85.78%), one animal (16.78%) had moderate immunopositivity (Table 5.4 and Fig 5.14). The age matched ZDSD28WK-MOD had more rats (n=5; 55.67%) with moderate immunopositivity while 4 rats (44.44%) showed mild immunopositivity. The ZDSD28WK-SVD had a majority of rats (n=5; 83.33%) with mild immunopositivity and 1 animal exhibiting moderate immunopositivity (16.78%) (Table 5.4 and Fig 5.14). Similarities were observed between SDs and ZDSD28WK-SVD but not the ZDSD28WK-MOD (p=0.234; p=0.005, respectively) (Table 5.6). No age differences

were observed between SDs (p=0.461) as well as the all ZDSD groups (p=0.0.118; p=1.000, respectively) (Table 5.4).

Table 5.4: Femoral neck BMP3 immunopositivity

Femur neck BMP3

Group		No stain		Mild		Moderate		Intense		p value
	N	Count	%	Count	%	Count	%	Count	%	
SD20WK	6	2	33.33	4	66.78	0	0	0	0	p=0.069
ZDSD20WK	6	0	0	5	83.33	1	16.78	0	0	
SD28WK	7	1	14.3	6	85.78	0	0	0	0	
ZDSD28WK-MOD	9	0	0	4	44.44	5	55.67	0	0	p=0.005
ZDSD28WK-SVD	6	0	0	5	83.33	1	16.78	0	0	#p=0.234

Comparison of SD28WK with ZDSD-SVD

5.2.6 Percentage estimate of cells expressing AGE in the femoral head of 20 and 28-week-old rats

SD20WK (mean=31.00%±9.98) presented a smaller proportion of AGE positive cells compared to ZDSD20WK (mean=55.83% ±9.26) in the femoral head (p<0.001) (Figs. 5.15 and 5.16 a-d). Again at 28 weeks, a smaller proportion of these cells occurred in the SD28WK controls (mean=29.57% ±6.64) compared to the ZDSD28WK-MOD (mean=66.99% ±15.56) and ZDSD28WK-SVD (mean=67.86%±12.40) (p<0.001 for both comparisons) (Figs. 5.15 and 5.16 e-j). There were no age differences observed for both SD controls (p=0.573) and ZDSDs (p=0.742; p=0.668) in this femoral region (Fig. 5.15).

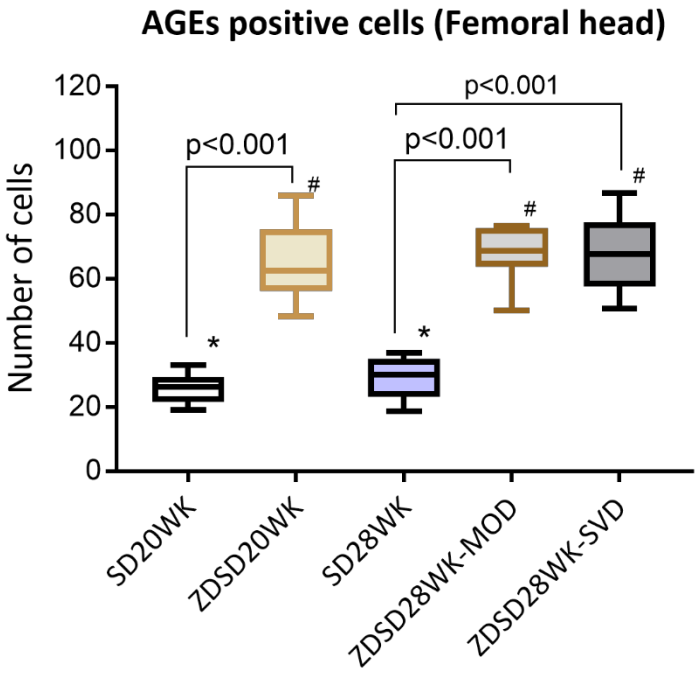


Figure 5.15: Advanced glycation end products (AGEs) immunopositive cells quantity in the femoral head. Box-and-whisker plots of AGEs cell estimation in various study groups. The line inside the box represents the mean, whereas the bottom and top lines of the box show the 25th and 75th percentiles, respectively. The whiskers below and above the box show the minimum and maximum values, respectively.

SD20WK and SD28WK, Sprague Dawley rats aged 20 and 28 weeks, respectively. ZDSD20WK, ZDSD28WK-MOD and ZDSD28WK-SVD, Zucker Diabetic Sprague Dawley rats aged 20 weeks, and aged 28 weeks moderately diabetic and severely diabetic, respectively. *; p=0.573 and #; p=0.742; p=0.668 comparing ZDSD20WK against the ZDSD28WK-MOD and ZDSD28WK-SVD, respectively.

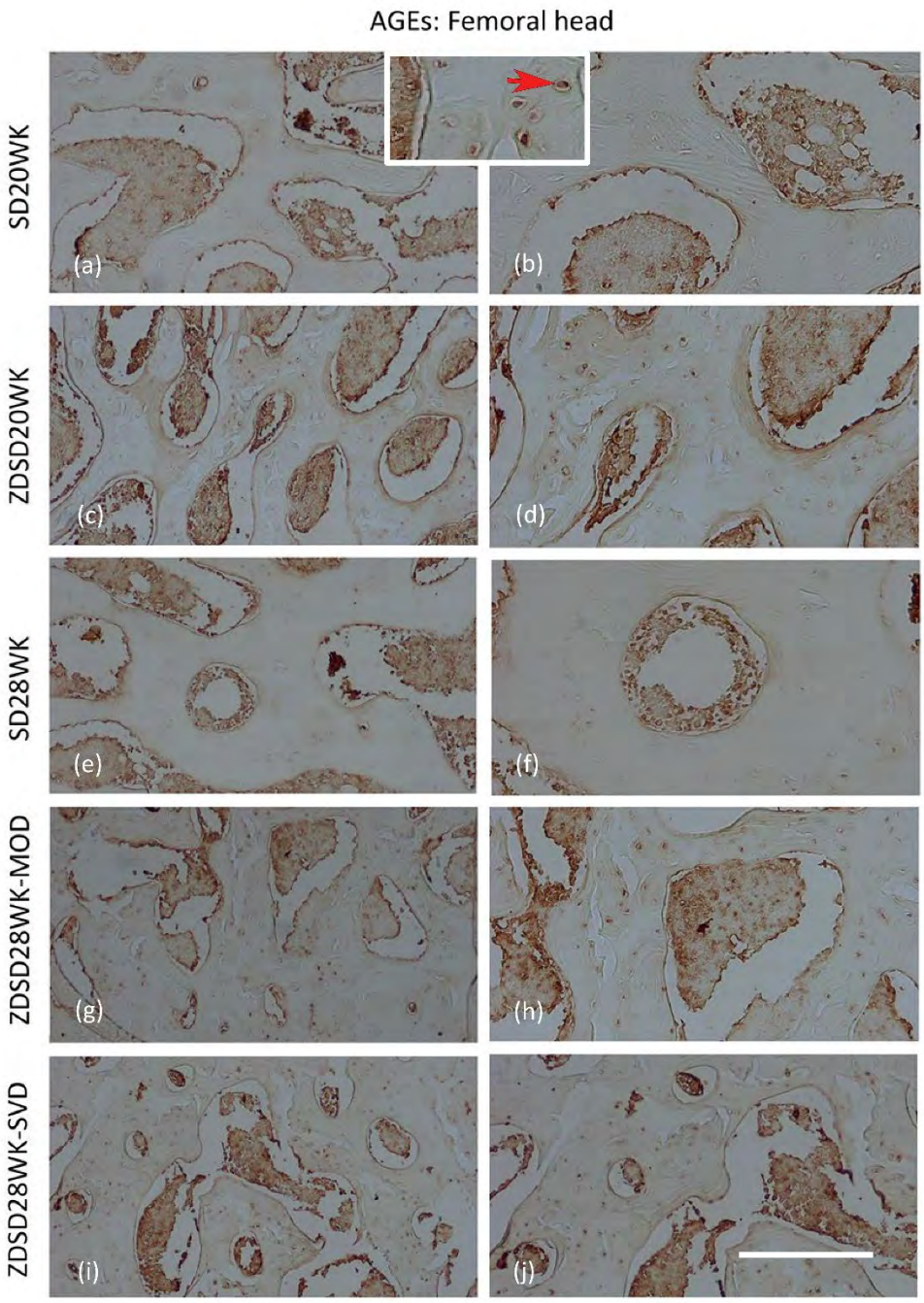


Figure 5.16 Femoral head: AGEs immunopositive cells. Immunopositive cells are depicted by arrows in the insert and are found throughout a-j. Scale bar represents 100µm and applies all photomicrographs

5.2.7 Percentages estimate of cells expressing AGE in the femoral neck of 20 and 28-week-old rats

In the femoral neck, the ZDSD20WK (mean=34.36% ±4.27) exhibited a higher AGEs proportion compared to the SD20WK controls (mean=13.06% ±3.95) ($p<0.001$) (Figs. 5.17 and 5.16 a-d). Similarly at 28 weeks, SD28WK controls (mean=14.31% ±3.99) expressed a larger proportion of AGE positive cells compared to the ZDSD28WK-MOD (mean=46.41% ±4.49) and the ZDSD28WK-SVD (mean=51.10% ±9.93) ($p<0.001$) (Figs. 5.17 and 5.16 e-j). Age differences were observed in the ZDSD groups, with an increased proportion of AGEs at 28-weeks ($p<0.001$) but not in the SD control group ($p=0.911$) (Fig. 5.17).

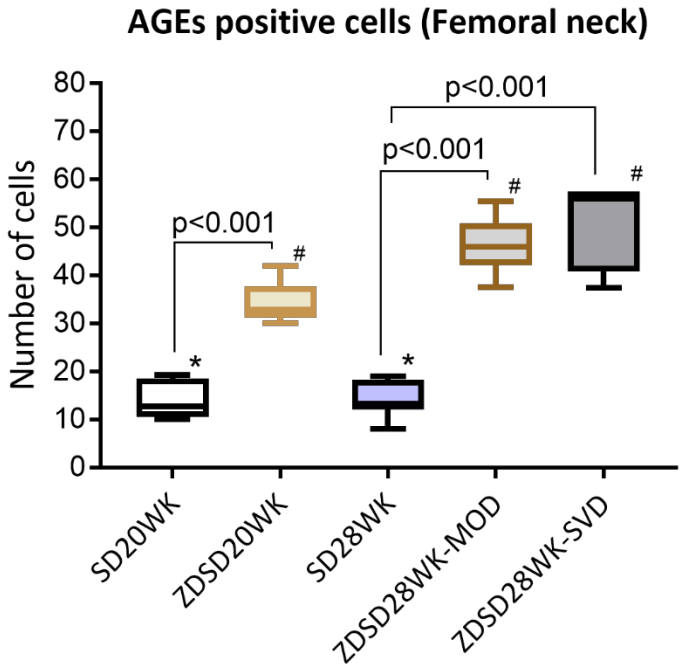


Figure 5.17: Advanced glycation end products (AGEs) immunopositive cells quantity in the femoral neck. Box-and-whisker plots of AGEs cell estimation in various study groups. The line inside the box represents the mean, whereas the bottom and top lines of the box show the 25th and 75th percentiles, respectively. The whiskers below and above the box show the minimum and maximum values, respectively.

SD20WK and SD28WK, Sprague Dawley rats aged 20 and 28 weeks, respectively. ZDSD20WK, ZDSD28WK-MOD and ZDSD28WK-SVD, Zucker Diabetic Sprague Dawley rats aged 20 weeks, and aged 28 weeks moderately diabetic and severely diabetic, respectively. *; p=0.573 and #; p=0.742; p=0.668 comparing ZDSD20WK against the ZDSD28WK-MOD and ZDSD28WK-SVD, respectively.

5.2.8 AGE expression in the femoral head of 20-week-old rats and 28 week old rats

All (n=6; 100%) SD20WK exhibited mild expression of extracellular AGEs, while majority of the ZDSD20WK (n=5; 83.33%) showed mild immunopositivity with only 1 animal (16.70%) with moderate immunopositivity (Table 5.5 and Fig 5.18). There were similarities between the SD20WK and ZDSD20WK (p=0.609) (Table 5.1). Again at 28 weeks, all SD28WK (n=7; 100%) had mild immunopositivity while the ZDSD28WK-MOD, 2 rats (22.22%) exhibited mild immunopositivity, 4 rats (44.44%) had moderate immunopositivity, with 3 rats (33.33%) showing intense immunopositivity (Table 5.5 and Fig 5.18). The ZDSD28WK-SVD had half the rats (50%) exhibiting intense immunopositivity, with 2 rats (33.33%) and only one animal (16.67%) showing moderate and mild expression respectively (Table 5.5 and Fig 5.18). Statistical significance was observed between the SD28WK controls and both diabetic groups (p<0.001) (Table 5.1). There were age differences between ZDSDs groups (p=.0.003; p=0.001 respectively), but not the SD controls (p=1.000) (Table 5.5).

Table 5.5: Femoral head AGEs immunopositivity

Femur Head AGE

Group	No stain			Mild		Moderate		Intense		p value
	N	Count	%	Count	%	Count	%	Count	%	
SD20WK	6	0	0	6	100	0	0	0	0	p=0.609
ZDSD20WK	6	0	0	5	83.33	1	16.7	0	0	
SD28WK	7	0	0	7	100	0	0	0	0	
ZDSD28WK	9	0	0	2	22.22	4	44.44	3	33.33	p<0.001
ZDSD28WKOVERT	6	0	0	1	16.7	2	33.33	3	50	#p<0.001

Comparison of SD28WK with ZDSD-SVD

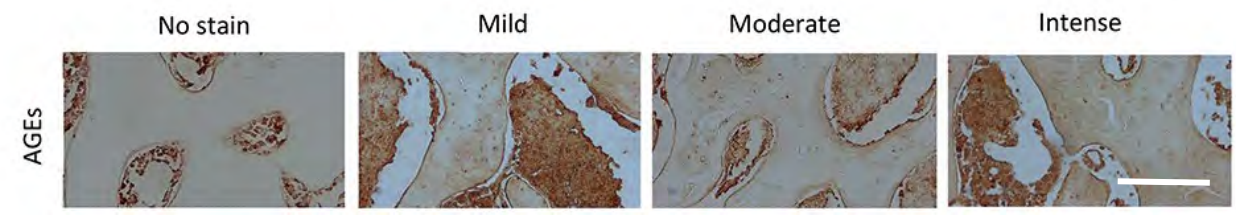


Figure 5.18: Femur AGEs immunopositivity grading. Scale bar represents 100µm and applies all photomicrographs

All 6 rats (100%) presented with mild immunopositivity for AGEs in the SD20WK controls and ZDSD20WK (n=6; 100%) (p=1.000). At 28 weeks, all SD28WK controls (n=7; 100%) had a mild expression, whereas majority of diabetic ZDSDs (n=4; 44.44%) had moderate immunopositivity with 2 rats exhibiting intense immunopositivity while only 2 rats (22.22%) had mild immunopositivity (Table 5.6 and Fig 5.18). Most of the ZDSD28WK-SVD (n=4; 66.67%) exhibited intense immunopositivity with the remaining 2 rats (33.33%) showing moderate immunopositivity (Table 5.6 and Fig 5.18). A comparison between the SD28WK with the ZDSD28WK-MOD and ZDSD28WK-SVD, indicates statistical significance (p=0.001; p<0.001 respectively) (Table 5.6). Age differences were not observed between SD controls (p=1.000) but were apparent in the ZDSD28WK-MOD and ZDSD28WK-SVD (p=0.001; p<0.001) (Table 5.6).

Table 5.6: Femoral neck AGEs Immunopositivity

Femur neck AGE

Group		No stain		Mild		Moderate		Intense		
	N	Count	%	Count	%	Count	%	Count	%	p value
SD20WK	6	0	0	6	100	0	0	0	0	p=1.00
ZDSD20WK	6	0	0	6	100	0	0	0	0	
SD28WK	7	1	0	7	100	0	0	0	0	
ZDSD28WK-MOD	9	0	0	3	33.3	4	44.44	2	22.22	p=0.001
ZDSD28WK-SVD	6	0	0	0	0	2	33.33	4	66.7	#p<0.001

Comparison of SD28WK with ZDSD-SVD

5.3 DISCUSSION

The ZDSD rat seems to be increasingly adopted as a translational model of T2D. However, diabetic skeletopathy investigations using ZDSDs are scarce and this study is among the few. this study interrogate the hypothesis that T2D increases bone adiposity (Piccinin and Khan, 2014; Kim and Schafer, 2016; Ferland-McCollough et al., 2018)(Piccinin and Khan, 2014; Kim and . To achieve this, adipocytes were quantified in the femoral head and neck. We found that ZDSD groups had higher adipocyte numbers. We then employed immunolabeling methods for detection of ALP (osteoblasts) and TRAP (osteocytes) positive cells to evaluate the balance in the quantity of these cells involved in bone remodeling. More TRAP immunopositive cells were found in the ZDSD, with fewer ALP immunopositive cells. To understand the role of cytokines in regulating the quantities of osteoblasts and osteocytes in the ZDSD rat bone, the study assessed the expression of one osteogenic cytokine (TGFB1) as well as an antagonist (BMP3). The ZDSD groups had less osteogenic cytokine (TGFB1) expression, with more of the antagonist (BMP3) expression. Finally, the study quantified AGEs immuno-positive bone cells together with AGEs extracellular expression in the femoral head neck. This showed that T2D increases the number of AGEs immuno-positive cells as well as its extracellular expression.

Adiposity in the femoral head and neck

T2D was found to contribute towards bone marrow adiposity (Kim and Schafer, 2016) in both humans (Sheu et al., 2017) and animal models (Devlin et al., 2014). This contributes to skeletopathy through the development of adipogenic cell lines and suppression of osteogenic cell lineages (Gillet et al., 2017; Ferland-McCollough et al., 2018). In the present study all ZDSDs exhibited higher adipocyte numbers in the femoral head, but not in the femoral neck. This observation confirms that T2D increases the accumulation of adipocytes in the femoral head, and possibly contributes to increased bone fragility reported in T2D (Kim and Schafer, 2016; Gillet et al., 2017; Ferland-McCollough et al., 2018). Although the femoral neck has the highest fracture risk, our observations suggest that T2D induced adiposity is not a contributory factor to the increased susceptibility of the femoral neck to fracture (Moseley, 2012; Valderrabano and Linares, 2018). Age differences were observed, with older rats (28 weeks) recording more

adipocytes numbers in the femoral head but not in the femoral neck. This observation suggests that age, hyperglycemia encourages femoral head trabeculae bone adiposity at disease onset and latter stages of diabetes T2D (Kim and Schafer, 2016; Gillet et al., 2017; Ferland-McCollough et al., 2018).

TRAP as a marker for osteocytes

TRAP is typically used as a reliable marker for osteoclasts and osteoclast-precursors (Nakano et al., 2004). However, recent studies show that osteocytes express this bone matrix catabolic enzyme during bone remodeling (Nakano et al., 2004; Qing et al., 2012; Kaya et al., 2017). Recent literature has established that osteocytes in their various developmental stages also express TRAP (Kaya et al., 2017), including at their apoptotic phase (Nakano et al., 2004). Considering this, the present study used TRAP immunopositivity as a maker for osteocytes. Osteocytes are involved in bone matrix resorption in two ways as follows: (i) TRAP produced by osteocytes directly resorbs bone matrix (ii), apoptotic osteocytes attract osteoclast precursors to their immediate environment. This ability to express TRAP enables osteocytes to participate in bone remodeling via a network of canaliculi and gap junctions. This network is reduced in T2D while remodeling is accentuated therefore increasing the propensity to fracture (Burger, 1998; Kaya et al., 2017; Picke et al., 2019).

TRAP positive osteocytes in the femoral head and neck

In the femoral head, ZDSDs had more TRAP immnopositive cells irrespective of age. This suggests that active bone remodeling by osteocytes occurs throughout the diabetic state in the femoral head. In contrast, the femoral neck, exhibited similarities in the number of TRAP positive cells irrespective of age, except for the overt ZDSDs that had more TRAP immuno-positive cells at 28 weeks. This suggests that bone remodeling may be accentuated by the presence of hyperglycemia and coupled with ageing in the femoral neck. This finding may possibly explain the higher prevalence of femoral neck fractures than femoral head fractures in T2D (Moseley, 2012; Valderrabano and Linares, 2018).

In both the SD and ZDSD femoral head and neck, TRAP positive cells decreased with age except for the overt ZDSD femoral neck where there was an increase. The age-related reduced numbers of TRAP immunopositive cells in SD controls and ZDSDs, could be attributed to normal physiologic cell apoptosis or it could be diabetes induced. Increased osteocyte apoptosis was reported in T2D (Picke et al., 2019) although it also occurs as a normal physiological process in bone homeostasis (Plotkin et al., 2019).

ALP positive osteoblasts in the femoral head and neck

Osteoblasts express the osteogenic enzyme ALP, which is also used as a bone turnover marker. Its function is to synthesize collagen, secrete osteoid and mineralize the organic matrix (Čepelak and Čvorišćec, 2009; Bhattarai et al., 2014; Florencio-Silva et al., 2015). In the present study, ALP immunopositive cells were fewer in the ZDSDs in both the femoral head and neck, in all age groups. No age-related changes were observed in ALP positive cells throughout the duration of the diabetic state in both femoral regions studied. This study confirms our hypothesis that T2D compromises osteoblastogenesis in the femoral head and neck, at all stages of the diabetic state. Our finding possibly explains the reduced osteoid volume and increased bone fragility found in T2D subjects (Ahmad et al., 2003; Blakytny et al., 2011; Hamann et al., 2011; Picke et al., 2019). IHC studies on distal femurs of insulin resistant ZDF rat models reported suboptimal matrix mineralization and reduced osteoblast numbers (Ahmad et al., 2003; Blakytny et al., 2011; Hamann et al., 2011). The results of our study on the ZDSD rat femur are aligned to these findings.

AGEs immunopositive bone cells and extracellular AGE expression in the femoral head and neck

T2D exacerbates the expression of intracellular and extracellular AGEs in various tissues including bone tissue (Goldin et al., 2006). AGEs are incorporated into the intracellular domain and alter intracellular signaling processes that encode for osteoblast, osteoclast, and osteocyte functions, adversely affecting bone turnover and bone quality (Kislinger et al., 1999; Singh et al., 2014; Creecy et al., 2016; Plotkin et al., 2019). Within the extracellular matrix, AGEs crosslink bone matrix collagen fibrils and negatively affect the binding of collagen to adhesive matrix molecules

(Goldin et al., 2006), leading to increased bone fragility (Creecy et al., 2016). The ZDSDs have a higher percentage of AGEs immuno-positive cells in the head and neck, for all groups, with the older rats showing more immuno-positive cells. This finding suggests that T2D facilitates intracellular AGEs accumulation at disease onset and throughout the disease. This intracellular AGEs accumulation compromises osteogenic cell lines, therefore, compromises bone turnover and bone quality (Kislinger et al., 1999; Singh et al., 2014; Creecy et al., 2016; Plotkin et al., 2019). Younger ZDSDs show a similar ECM expression of AGEs to their controls in both regions, while older rats show stronger expression with age, more especially the overtly diabetic group that exhibited intense immunopositivity at 28 weeks. This study confirms an age dependent intracellular and extracellular AGE accumulation in T2D that is accentuated by overt hyperglycemia. This could possibly explain the AGEs induced susceptibility of diabetic bone to fracture as reported previously (Goldin et al., 2006; Singh et al., 2014).

Expression of the osteogenic cytokine, TGFβ1

TGFβ1 is an osteogenic cytokine that exists as an extracellular complex that is translocated into the intracellular domain to regulate bone cell differentiation and function to maintain skeletal integrity (Ehnert et al., 2010; Yang et al., 2014; Wu et al., 2016). The ZDSDs exhibited less expression of extracellular TGFβ1 than controls in all age groups and regions. This observation indicates that T2D reduces the expression of extracellular TGFβ1 irrespective of age. This reduced extracellular expression could potentially compromise availability of the cytokine intracellularly. If correct, this may affect osteoblast numbers and function, leading to increased fracture risk associated with T2D (Wang et al., 2018). Age differences were observed in ZDSDs in the femoral head where older (28 weeks) rats exhibit a reduced expression. In the femoral neck, age differences were observed in the diabetic group but not the overtly diabetic group. These observations imply that reduced expression of TGFβ1 becomes more pronounced with age in the femoral head. However, in the femoral neck, this reduced expression is experienced at disease onset and much later in the disease possibly contributing to the increased fracture risk of the femoral neck (Valderrabano and Linares, 2018).

Expression of the anti-osteogenic cytokine, BMP3

BMP-3 is an anti-osteogenic cytokine that is secreted by osteoblasts and osteocytes, and it negatively regulates osteoblastogenesis by inhibiting osteoblast differentiation (Wu et al., 2016; Kokabu and Rosen, 2018). Its effect manifests as reduced BMD, smaller trabeculae volume and thinner cortical bone (Gamer et al., 2009; Horbelt et al., 2012), therefore, increased bone fragility. Increased bone extracellular BMP3 expression in a mouse model led to spontaneous fractures while adult BMP3 knockout mice had increased bone mass (Kokabu and Rosen, 2018). Majority of diabetic ZDSDs express more BMP3 in the head than the neck at 28 weeks. This finding suggests that T2D facilitates accumulation of the anti-osteogenic cytokine BMP3 much earlier in the femoral head than the neck. No age differences were observed for both regions. Our study demonstrates that T2D facilitates the accumulation of BMP3 at disease onset and latter stages of the disease, for both regions. This BMP3 accumulation possibly compromises bone turnover and (Kokabu and Rosen, 2018), and subsequent skeletal fragility (Gamer et al., 2009; Horbelt et al., 2012; Wu et al., 2016). BMP3 knockout mice were found to negatively affect osteoblastogenesis leading to increased bone fracture risk (Gazzerro and Canalis, 2006; Kokabu and Rosen, 2018).

5.3.1 Conclusions

This study has shown that diabetes increases adiposity in the ZDSD rat femoral head and neck. The high TRAP immunopositivity in the femoral neck ZDSD-28WK rats supports the commonly known high fracture risk in this bone region. On the other hand, fewer ALP immunopositive cells occurred in the ZDSDs, therefore, this study confirms our hypothesis that T2D compromises osteolysis and osteoblastogenesis in the femoral head and neck, at all stages of the diabetic state. The femoral neck exhibited reduced TGFB1 expression in both age groups showing that the reduction is experienced at disease onset and much later in the disease, possibly contributing to femoral neck weakness. We found that T2D increases the number of AGEs immuno-positive cells as well as its extracellular expression in the ZDSD rat femur. Our overall finding mean that osteoblast and osteocyte numbers are regulated by TGFβ1 and BMP3 in the ZDSD rat femur with

the influence of AGEs. In addition, our study demonstrates that T2D facilitates the accumulation of BMP3 at disease onset and latter stages of the disease, for both regions.

Chapter 6

Interaction of AGEs with TGFβ1 and its antagonist BMP3 in diabetes affects osteoblastogenesis and osteolysis in the Zuker Diabetic Sprague Dawley rat humerus head

TABLE OF CONTENTS

6.0 Introduction 140

6.1 MATERIALS AND METHODS 142

6.1.1 Rats 142

6.1.2 Termination and bone harvesting 142

6.1.3 Tissue processing for immunohistochemical techniques 142

6.1.4 Haematoxylin and Eosin (H&E) stain 142

6.1.5 Immunohistochemistry for TRAP, ALP, BMP3, TGFβ1, AGE in the head of the humerus 143

6.1.6 Photography, quantification, and immunopositivity intensity of ROI (region of interest) 144

6.1.7 Data analysis 144

6.2 Results 145

6.2.1 Humerus head general histological appearance 145

6.2.1 Estimation of osteocyte quantity in the humerus head of 20 and 28-week-old rats 147

Cells expressing TRAP (Osteocytes) 147

6.2.2 Estimation of osteoblast quantity in the humerus head of 20 and 28-week-old rats 149

Cells expressing ALP (Osteoblasts) 149

6.2.7 BMP3 expression in the humerus of 20 week old and 28 week old rats 152

6.2.5 AGE expression in the extracellular matrix of the humerus head in 20 and 28-week-old rats 155

6.3 Discussion 156

Anti-osteoblastogenic effects of adipocytes 156

Osteoblastogenesis and osteolysis 156

Interaction of AGEs with TGFβ1 and its antagonist BMP3 157

6.4 Conclusion 158

6.0 INTRODUCTION

The endocrinology of type 2 diabetes (T2D) and its predisposing factors to have been studied extensively while its skeletal effects have received negligible research (Del Prato, 2009). Fractures in T2D are exacerbated by hyperglycemia and disease progression (Devlin et al., 2014). Proximal humerus fractures (PHF) account for 4 to 10% of all fractures, constituting the 2nd most common fractures of the upper arm (Chu et al., 2004; Iglesias-Rodriguez et al., 2021), and the 3rd commonest fracture site after the proximal femur and distal radius (Chen et al., 2021). A study on the humerus of female T2D Goto-Kakizaki rats demonstrated that fracture risk in T2D varies with specific sub regions in bones (Ahmad et al., 2003). This prompted our study to focus on the proximal humerus head of the Zuker Diabetic Sprague Dawley (ZDSD) rat.

The cellular and molecular association between PHF and T2D has not been fully elucidated. However, previous studies suggest that T2D induces osteopenia (Chu et al., 2004) that compromises bone turnover (Martinez-Huedo et al., 2017; Schousboe et al., 2022), as well as an imbalance between pro and anti-osteogenic cytokines (Seibel, 2005; Sassi et al., 2018). Reduced bone turnover is directly linked to altered bone cell numbers and their function (Neer et al., 2001; Seibel, 2005; Feng and McDonald, 2011).

TRAP as contained in osteocytes, participates in osteolysis in response to pathologic conditions such as T2D (Qing et al., 2012; Dole et al., 2017). Additionally, TRAP positive osteocytes, also found in elevated levels in T2D, attract osteoclast precursors to their vicinity, accelerating bone matrix resorption and increasing bone fragility (Burger, 1998; Bellido, 2014). Osteoblasts secrete osteoid and mineralize the organic matrix under the influence of ALP (Bhattarai et al., 2014). Studies on the femur of the Zucker Diabetic Fatty rat (ZDF), found impaired osteoblast differentiation, reduced osteoblast numbers and less matrix mineralization in diabetes (Ahmad et al., 2003; Blakytny et al., 2011; Hamann et al., 2011). Therefore, in the present study, it was postulated that reduced osteoblast numbers and increased expression of TRAP immune-positive cells in diabetic ZDSDs.

The extracellular bone matrix cytokine TGFβ1 (Ehnert et al., 2010; Wu et al., 2016) is responsible for regulating differentiation, proliferation, and migration of osteoprogenitor cells (Jian et al.,

2006; Jepsen et al., 2015). In contrast, BMP3 is antagonistic to the TGFβ1 functions (Wu et al., 2016). In addition, T2D facilitates accumulation of extracellular AGEs that adversely crosslink bone matrix collagen, compromising skeletal integrity (Creecy et al., 2016). This occurs by inhibiting osteoblast differentiation and proliferation, induction of osteoblast apoptosis while increasing osteoclastic and osteocytic bone catabolism - all this increases skeletal fragility (Sanguineti et al., 2014; Yamamoto and Sugimoto, 2016; Singh et al., 2018; Plotkin et al., 2019). Relatively recent studies show that increased skeletal fragility in T2D is exacerbated by bone marrow adiposity due to the differentiation of skeletal stem cells into adipogenic cell lines instead of osteogenic cell lines (Gillet et al., 2017; Ferland-McCollough et al., 2018).

The ZDSD rat is increasingly being adopted as a translational model of T2D, although skeletal studies are scanty in respect of this model. In this study will start by assessing bone samples for adipocyte accumulation. We will then quantify the bone turnover cells namely, osteocytes and osteoblasts using TRAP and ALP as cell markers respectively. Expression of the pro-osteogenic cytokine TGFβ1 (Yang et al., 2014), together with the anti-osteogenic cytokine BMP3 (Wu et al., 2016), will be investigated, as they are reported to be altered in T2D (Sassi et al., 2018). The extent of glycation end-product accumulation will be assessed by quantifying AGEs immunopositive bone cells together with its extracellular expression.

6.1 MATERIALS AND METHODS

6.1.1 Rats

Rats were handled as described in section 2.1.2.

6.1.2 Termination and bone harvesting

Rats were injected with a lethal intraperitoneal dose of phenobarbital, then immersed in 10% buffered formalin. Abdominal and limb incisions were made, to facilitate penetration of the formalin fixative. Anterior left and right limbs were removed, and muscles were cleaned out of the humerus. Individual bones were then stored in 10% buffered formalin to continue fixation until further processing. Left humeri were used for immunohistochemical investigations.

6.1.3 Tissue processing for immunohistochemical techniques

Bone samples were fixed in 10% buffered formalin for a minimum of 14 days, then decalcified in 20% w/v ethylenediaminetetraacetic acid (EDTA, pH 7.4) for 10 days in an incubator with regular gentle shaking at 45˚C. The bones were then rinsed, and their proximal epiphysis severed about 3mm below the intertubercular groove, then immersed in 10% buffered formalin for 24 hours before processing for histology. An automatic processor (Citadel 2000, Thermo Fischer Scientific) was used to take the samples through ascending grades of ethanol prior to embedding in paraffin wax. During embedding, bone samples were orientated longitudinally to minimize differences in the sectioning angle. Bone sections were cut at 5µm thickness using a microtome (Leica RM2125 RTS, Leica Biosystems, USA) and mounted on silane-coated glass slides. Three sections per slide were mounted. Section sequences were mounted in order for specific stains, namely; Hematoxylin and Eosin to assess humerus head and morphology, and to quantify adipocyte numbers; Immunolocalization of TRAP, ALP, BMP3, TGFβ1 and AGEs for the same region.

6.1.4 Haematoxylin and Eosin (H&E) stain

This method is also used to determine normal tissue structure (Totty, 2002). Sections were dewaxed in xylene for 10 minutes and hydrated by passing through 3 changes (1 minute each) of absolute alcohol followed by 90% and 70% alcohol (1 minute each) and eventually into running

tap water for 1 minute. The sections were then stained for 10 min in haematoxylin, differentiated in periodic acid for 10 seconds, rinsed in tap water for a minute, blued in Scott's tap water for 2 minutes, and rinsed again in tap water. The cytoplasm was stained with eosin by immersing the sections in 70% alcohol followed by eosin for 2 minutes. The sections were then dehydrated in increasing concentrations of alcohol before they were mounted in entellen.

6.1.5 Immunohistochemistry for TRAP, ALP, BMP3, TGFβ1, AGE in the head of the humerus

Immunohistochemistry was conducted using the anti-TRAP antibody (ab185716) for osteocytes detection, anti-ALP antibody (ab108337) for osteoblasts and anti-AGE antibody (ab23722) advanced glycation end products, anti-BMP3 antibody (ab134724) and anti-TGF beta 1 antibody (ab92486). All antibodies were sourced from Abcam. Sections were placed in an incubator at 40^0C for 30 minutes and then deparaffinized and rehydrated in a series of graded alcohols. They were then immersed in a citrate buffer (pH=6) and placed in a water bath set at 60^0C for 24 hours, to facilitate antigen removal. After 24 hours sections were cooled at room temperature for 20 minutes then rinsed 3 x 5minutes times in PBS (pH=7.4). Endogenous peroxidase was blocked with 1% hydrogen peroxide (H_2O_2) and then the sections were washed in PBS 3 x 5 minutes. Sections were transferred to a perspex plate and incubated with the primary antibodies at appropriate dilutions (TRAP; 1: 100, ALP; 1:200, AGE; 1: 10 000, TGFβ1, 1:400, BMP3 1: 75) and placed at 4^0C overnight. After 24 hours, sections were left outside the fridge for 20 minutes to reach room temperature before washing in PBS 3 x 5 minutes. They were then soaked in biotinylated secondary antibody (Biotinylated Goat Anti-Rabbit IgG (H+L) (ab64256) for 10 minutes, and again washed in PBS 3 x 5 minutes. Sections were then incubated in streptavidin HRP for 10 minutes (ab64269) to reduce background immunopositivity and to enhance the binding of the antibodies. This was followed by 3 x 5 minutes rinses in PBS (pH=7.4). Sections were then incubated with 3-3' di-aminobenzidine (DAB) working solution while monitoring colour development under a light microscope. Once optimal immunopositivity was achieved the sections were, rinsed in running tap water for 5 minutes, then dehydrated through graded alcohol, cleared in xylene and eventually mounted in entellen.

6.1.6 Photography, quantification, and immunopositivity intensity of ROI (region of interest)

A light microscope (Zeiss Axioscope 2 plus) fitted with an Axiocam HRC digital camera connected to a PC was used to take photomicrographs of the stained slides. Anatomical landmarks were determined for the humerus head, using the H&E stained slides, to create consistency in quantification and immunopositivity analysis. Nonadjacent fields were selected, two above and two below the epiphyseal growth plate (Fig. 6.1). Photomicrographs were imported into Fiji Image-J software (National Institute of Health USA) for further analysis. TRAP positive osteocytes (Nakano et al., 2004; Dole et al., 2017), ALP positive osteoblasts (Miao and Scutt, 2002; Hawthorne et al., 2013), AGEs positive bone cells and adipocytes were identified as specified in previous literature (Ferland-McCollough et al., 2018). Cells were counted manually. Immunolocalization for anti-AGEs antibody, anti-BMP3 antibody, and anti-TGFβ1 antibody was performed. These were graded as no stain, mild, moderate, and intense immunopositivity (Fig. 6.2)

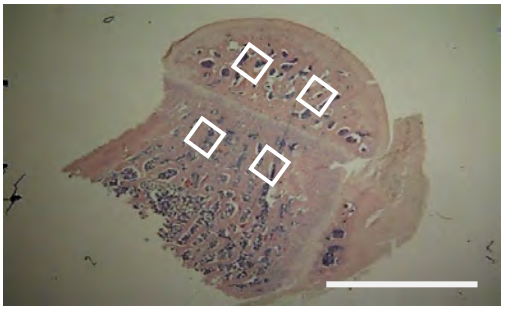


Figure 6.1: Head of the humerus regions of interest. Scale bar = 100µm. Original magnification: 50×

6.1.7 Data and statistical analysis

The data were managed in Microsoft Excel Office 365 (Microsoft Corporation) and all data were analyzed using SPSS® version 28 (IBM®). The data was tested for normality using the Shapiro Wilks test, the data was found to be normally distributed, and a One-Way ANOVA with LSD post-hoc test was applied for multiple group comparisons. Ordinal data for immunopositivity intensity

were assigned grading scales of no stain (0), mild (1), moderate (2) and intense (3). Data were given as means and standard deviation. Significance level was set at $p < 0.05$.

6.2 RESULTS

6.2.1 Humerus head general histological appearance

Controls exhibited normal bone marrow cells (Fig. 6.2 a and c) as opposed to diabetic groups that had extensive adipocyte infiltration (Fig. 6.2 b, d and e)**.** The ZDSD20WK (mean±SD=77.57±8.30) presented significantly higher adipocyte numbers compared to their SD20WK controls (mean±SD =14.83±3.19) ($p<0.001$) (Fig. 6.3). Similarly, ZDSD28WK-MOD (mean±SD =108.89±6.05) and ZDSD28WK-SVD (mean=100±5.04) showed significantly more adipocytes compared to their SD28WK controls (mean±SD =17.86±1.07) ($p<0.001$) (Figs .6.2 and Fig.6.3). Similarities in adipocyte quantity were observed in the SD controls at 20 and 28-weeks ($p=0.327$). In contrast, ZDSD28WK-MOD and ZDSD28WK-SVD had significantly more adipocytes at 28-weeks than the ZDSD20WK ($p<0.001$ for both comparisons) (Fig. 6.3).

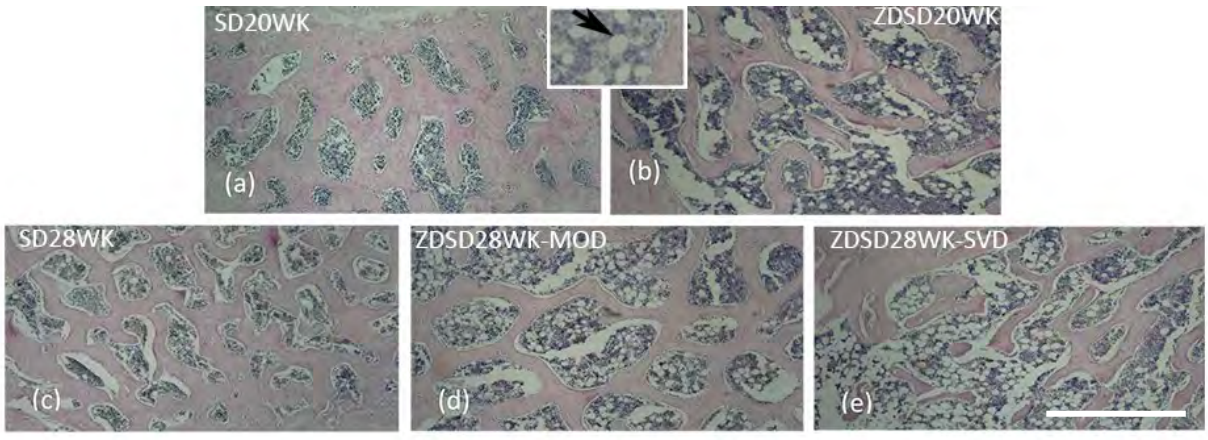


Figure 6.2: General histology and relative adipocyte infiltration in the humerus head. Adipocytes are the large round cells with a clear cytoplasm as depicted by the arrow in the insert. Scale bar represents 100µm and applies to a-e.

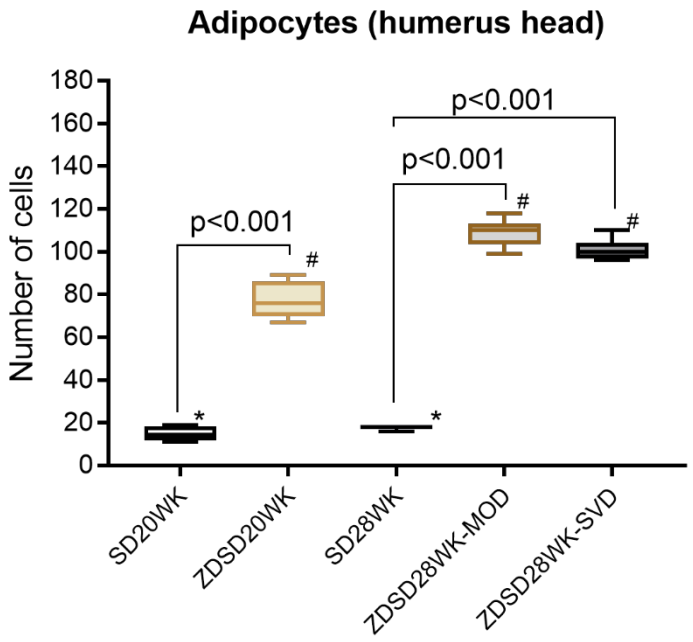


Figure: 6.3 Number of adipocytes in the humerus head. Box-and-whisker plots of adipocyte quantity in various study groups. The line inside the box represents the mean, whereas the bottom and top lines of the box show the 25th and 75th percentiles, respectively. The whiskers below and above the box show the minimum and maximum values, respectively.

SD20WK and SD28WK; Sprague Dawley rats aged 20 and 28 weeks, respectively. ZDSD20WK, ZDSD28WK-MOD and ZDSD28WK-SVD; Zucker Diabetic Sprague Dawley rats aged 20 weeks, and aged 28 weeks moderately diabetic and severely diabetic, respectively. *; p=0.327 and #; p<0.001 for both, comparing ZDSD20WK against ZDSD28WK-MOD and ZDSD28WK-SVD.

6.2.1 Estimation of osteocyte quantity in the humerus head of 20 and 28-week-old rats

Cells expressing TRAP (Osteocytes)

Higher TRAP positive cell numbers were observed in the ZDSD20WK (mean±SD =106.73±15.54) compared to their SD20WK controls (mean±SD =77.39±3.27) (p=0.007) (Figs. 6.4 and 6.5 a-d). The same pattern was observed when comparing SD28WK controls (mean=71.83±20.31) to their age matched ZDSD28WK-MOD (mean±SD=110.69±20.95) and ZDSD28WK-SVD (mean±SD =98.68±22.63) (p=0.001; p<0.001 respectively) (Figs. 6.4 and 6.5 e-j). No age differences were observed for SD controls when comparing 20 and 28-week groups (p=0.589), the ZDSD groups were also similar when comparing these two age groups (p=0.671; p=0.435) (Fig. 6.4).

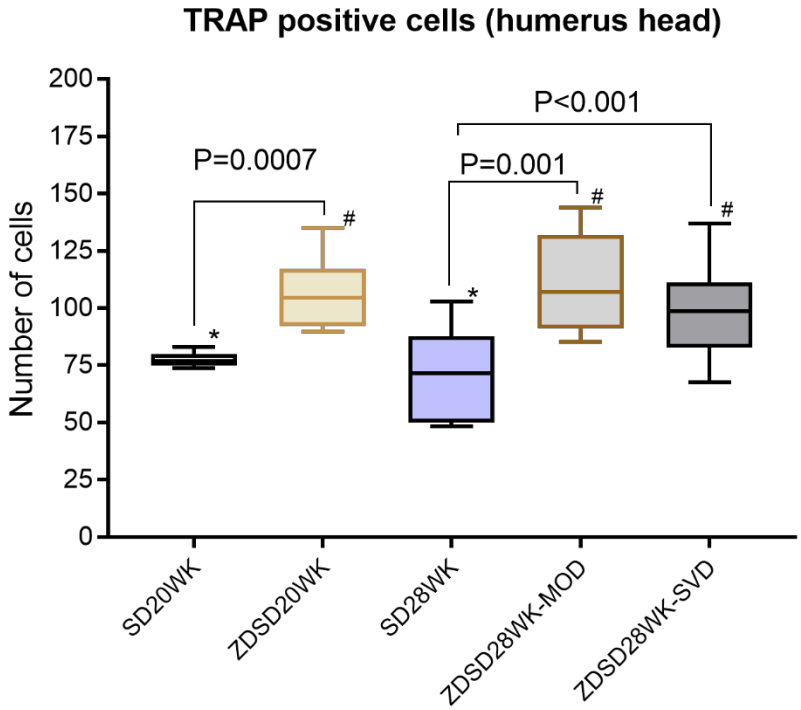


Figure 6.4: TRAP immunopositive cells quantity in the humerus head. Box-and-whisker plots of osteoblast estimation in various study groups. The line inside the box represents the mean, whereas the bottom and top lines of the box show the 25th and 75th percentiles, respectively. The whiskers below and above the box show the minimum and maximum values, respectively.
SD20WK and SD28WK; Sprague Dawley rats aged 20 and 28 weeks, respectively. ZDSD20WK, ZDSD28WK-MOD and ZDSD28WK-SVD; Zucker Diabetic Sprague Dawley rats aged 20 weeks, and aged 28 weeks moderately diabetic and severely diabetic, respectively. *; p<0.001 and #; p=0.512; p=0.510 comparing ZDSD20WK against ZDSD28WK-MOD and ZDSD28WK-SVD respectively.

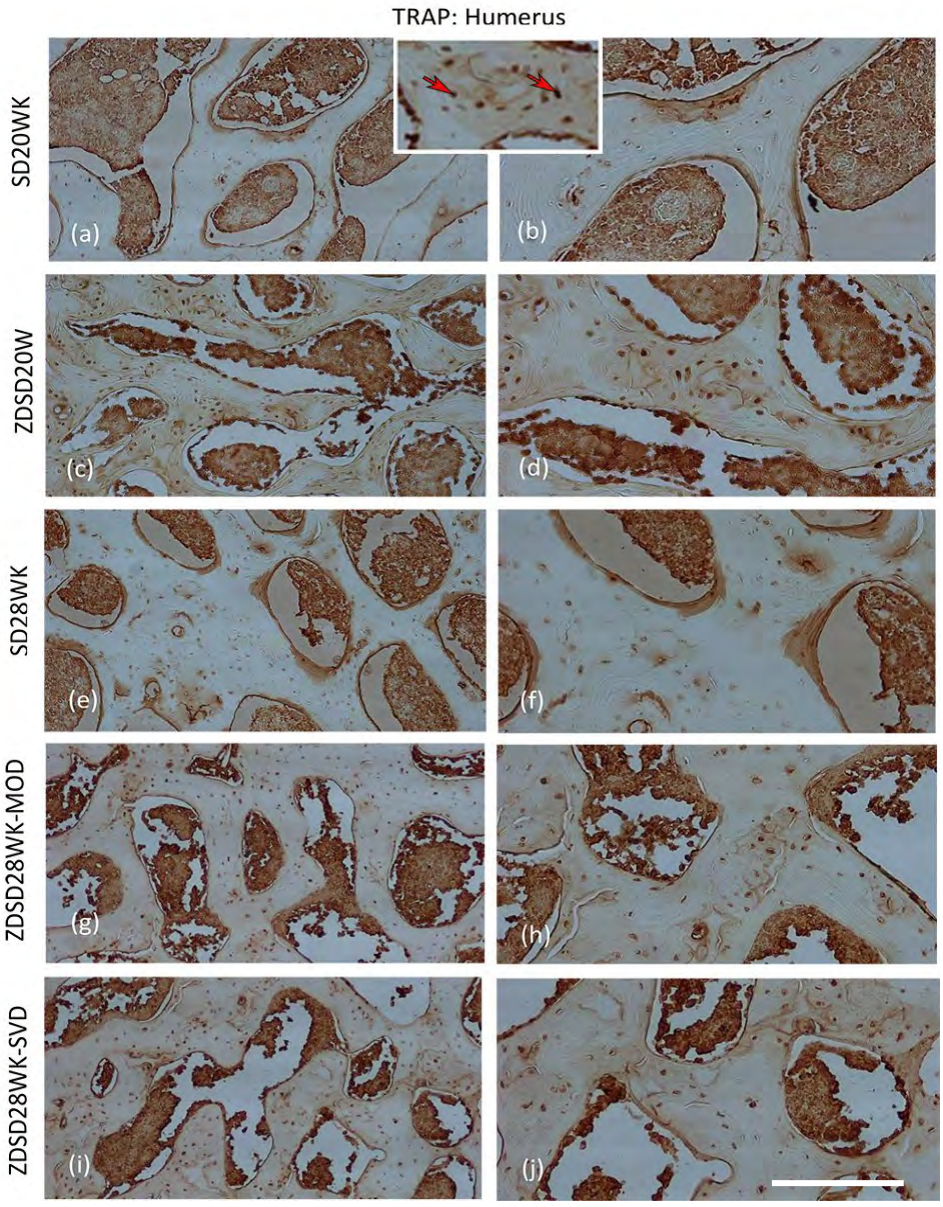


Figure 6.5: Humerus TRAP Immunopositive osteocytes. The osteocytes are embedded in the bone matrix as depicted by the arrows in the insert and are found throughout a-j. Scale bar represents 100µm and applies all photomicrographs.

6.2.2 Estimation of osteoblast quantity in the humerus head of 20 and 28-week-old rats

Cells expressing ALP (Osteoblasts)

More ALP positive cells were observed in SD20WK controls (mean±SD =33.44±7.05) compared to ZDSD20WK (mean±SD =9.15±2.61) ($p<0.001$) (Figs. 6.6 and Fig 6.7 a-d). A similar pattern was observed at 28 weeks where the SD28WK controls (mean±SD =14.77±3.97) exhibited significantly greater numbers compared to ZDSD28WK-MOD (mean±SD =9.15±2.61) and ZDSD28WK-SVD (mean±SD =6.56±0.54) ($p<0.001$ for both comparisons) (Figs. 6.6 and 6.7 e-J). The SD controls exhibited higher numbers of ALP positive cells at 20 weeks compared to 28 weeks ($p<0.001$). Similarities were observed between the ZDSD20WK and ZDSD28WK-MOD and ZDSD28WK-SVD ($p=0.512$; $p=0.510$, respectively) (Fig.6.6).

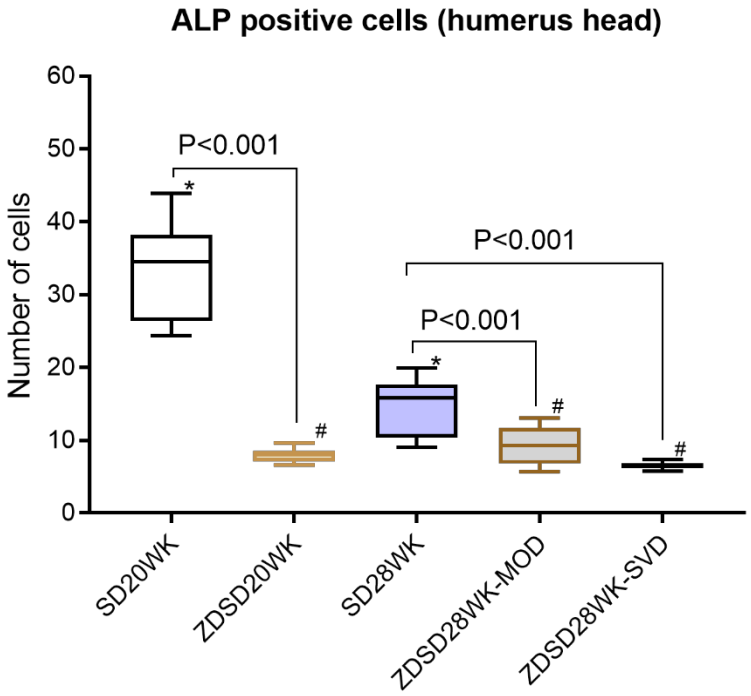


Figure 6.6: ALP immunopositive cells quantity in the humerus head. Box-and-whisker plots of osteoblast quantity in various study groups. The line inside the box represents the mean, whereas the bottom and top lines of the box show the 25th and 75th percentiles, respectively. The whiskers below and above the box show the minimum and maximum values, respectively.
SD20WK and SD28WK; Sprague Dawley rats aged 20 and 28 weeks, respectively. ZDSD20WK, ZDSD28WK-MOD and ZDSD28WK-SVD; Zucker Diabetic Sprague Dawley rats aged 20 weeks, and aged 28 weeks moderately diabetic and severely diabetic, respectively. *; $p=0.327$ and #; $p<0.001$ for both, comparing ZDSD20WK against ZDSD28WK-MOD and ZDSD28WK-SVD.

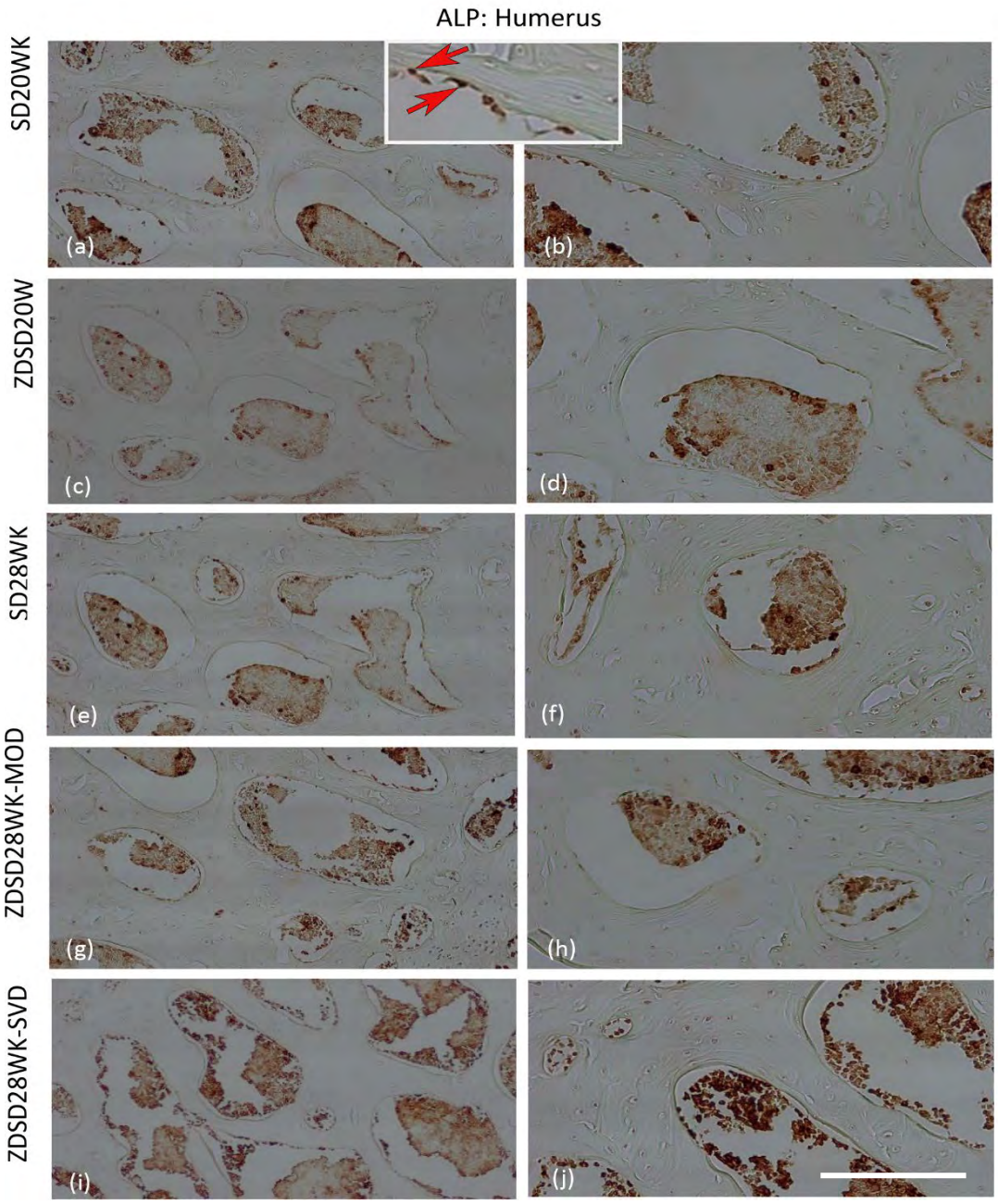


Figure 6.7: Humerus ALP Immunopositive osteoblasts. The osteoblasts lining bone marrow spaces are depicted by arrows in the insert and are found throughout a-j. Scale bar represents 100µm and applies all photomicrographs.

6.2.6 TGFβ1 expression in the humerus head of 20 and 28-week-old rats

All the ZDSD20WK (n=7; 100%) had mild immunopositivity for TGFβ1, whereas SD20WK controls exhibited an equal distribution of mild, moderate and intense immunopositivity (n=2; 33.33%, respectively), with statistical significance (p=0.004) (Table 6.1 and Fig 6.8). The ZDSD28WK-MOD and ZDSD28WK-SVD, majority of rats (n=6; 66.70, n=5; 83.33% respectively) exhibited mild immunopositivity. The remaining ZDSD28WK-MOD (n=3; 33.33%) and ZDSD28WK-SVD (n=1; 16.7%) had moderate immunopositivity. The SD28WK controls exhibited mild, moderate and intense immunopositivity (n=3; 42.9%, n=3; 42.9%, n=1; 14.3% respectively). Similarities were observed between the SD28WK controls, ZDSD28WK-MOD and ZDSD28WK-SVD ZDSDs (p=0.206; p=0.103 respectively) (Table 6.1 and Fig 6.8). No age differences were observed between the SDs (p=0.387) or ZDSDs (p=0.267; p=0.612) (Table 6.1).

Table 6.1: Humerus TGFβ1 Immunopositivity

TGFβ1

Group		No stain		Mild		Moderate		Intense		p value
	N	Count	%	Count	%	Count	%	Count	%	
SD20WK	6	0	0	2	33.33	2	33.33	2	33.33	p=0.004
ZDSD20WK	7	0	0	7	100	0	0	0	0	
SD28WK	7	0	0	3	42.9	3	42.9	1	14.3	
ZDSD28WK-MOD	9	0	0	6	66.7	3	33.33	0	0	p=0.203
ZDSD28WK-SVD	6	0	0	5	83.33	1	16.7	0	0	#P=0.103

Comparison of SD28WK with ZDSD28WK-SVD

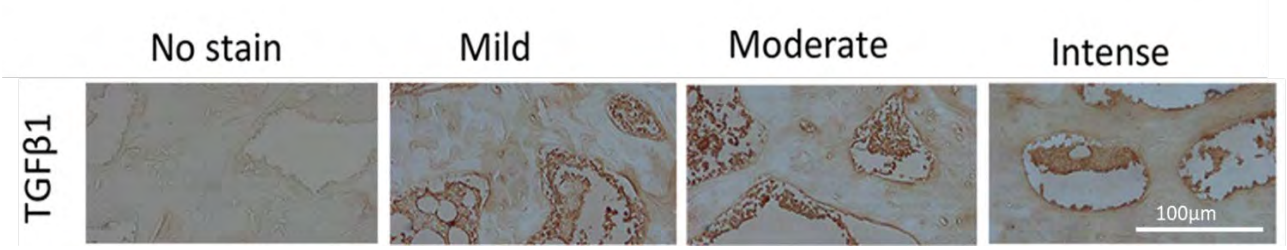


Figure 6.8: Humerus TGFβ1 Immunopositivity graded. The grading was based on staining intensity.

6.2.7 BMP3 expression in the humerus of 20 and 28 week old rats

Majority of ZDSD20WK (n=6; 85.70) exhibited moderate immunopositivity for BMP3, with 1 animal (14.30%) having mild immunopositivity, while with SD20WK controls, 4 rats (66.70%) had mild immunopositivity and 2 rats (33.33%) had zero immunopositivity. The SD20WK controls and ZDSD20WK show statistical significance ($p<0.001$) (Table 6.2 and Fig 6.9). At 28 weeks, all ZDSD28WK-SVD (n=6; 100%) exhibit intense immunopositivity, the ZDSD28WK-MOD exhibit mild and moderate immunopositivity (n=4; 44.44%, n=5; 55.56% respectively). The majority of SD28WK controls (n=6; 85.70%) had mild immunopositivity with only 1 animal (14.30%) exhibiting zero immunopositivity. Significant differences were observed between the SD28WK controls and both groups of ZDSDs ($p=0.002$; $p<0.001$ respectively) (Table 6.2 and Fig 6.9). Similarities were observed in SD20WK and SD28WK ($p=0.420$), again between ZDSD20WK and ZDSD28WK-MOD) ($p=0.164$), but not the ZDSD28WK-SVD ($p<0.001$) (6.2).

Table 6.2: Humerus BMP3 Immunopositivity

BMP3 Humerus head

Group	No stain			Mild		Moderate		Intense		p value
	N	Count	%	Count	%	Count	%	Count	%	
SD20WK	6	2	33.33	4	66.7	0	0	0	0	p<0.001
ZDSD20WK	7	0	0	1	14.3	6	85.7	0	0	
SD28WK	7	1	14.3	6	85.7	0	0	0	0	
ZDSD28WK-MOD	9	0	0	4	44.4	5	55.6	0	0	p=0.002
ZDSD28WK-SVD	6	0	0	0	0	0	0	6	100	#p<0.001

Comparison of SD28WK with ZDSD28WK-SVD

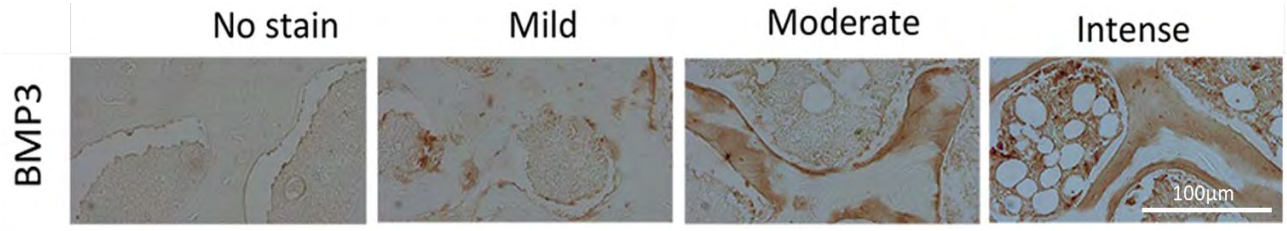


Figure 6.9: Humerus BMP3 Immunopositivity graded. The grading was based on staining intensity.

6.2.4 Percentage estimate of cells expressing AGEs in the humerus head of 20- and 28-week-old rats

The ZDSD20WK (mean=65.09±2.98) displayed significantly higher AGEs positive cell numbers compared to SD20WK controls (mean=14.73±6.93) (p<0.001) (Fig 6.10 and Fig 6.11). This significance trend also occurred at 28 weeks, with ZDSD28WK-MOD (mean=65.06±7.84) and ZDSD28WK-SVD (mean=58.90±9.04) displaying higher numbers compared to SD28WK controls (mean=29.00±2.49) (p<0.001 for both comparisons) (Fig 6.10 and Fig 6.11). The SDs had age differences, with more AGEs positive cells observed at 28 than 20 weeks (p=0.005). In contrast, similarities were observed in ZDSD20WK in the diabetic as well as ZDSD28WK-SVD at 28 weeks of age (p=0.999; p=0.197 respectively) (Fig 6.10).

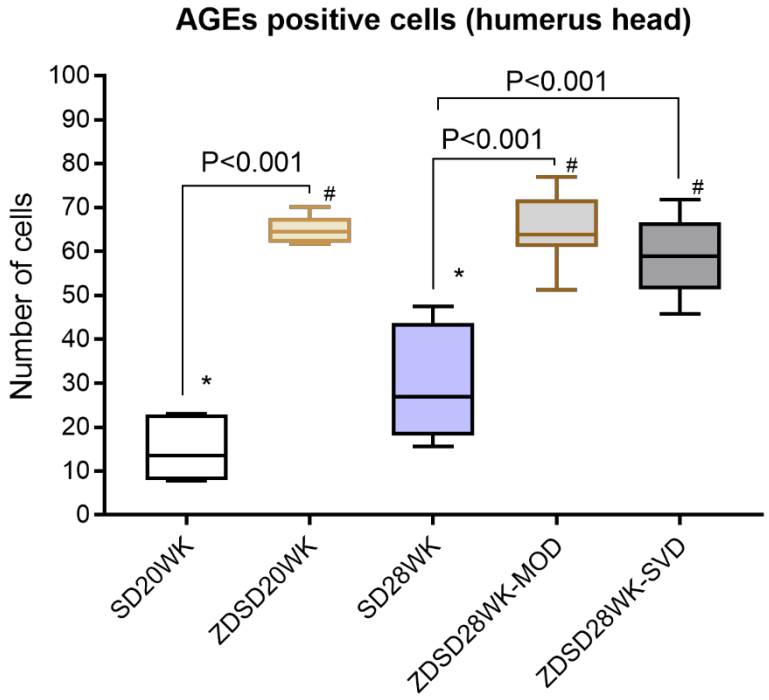


Figure 6.10: AGEs immunopositive cells in the humerus head. Box-and-whisker plots of AGEs cells estimation in various study groups. The line inside the box represents the mean, whereas the bottom and top lines of the box show the 25th and 75th percentiles, respectively. The whiskers below and above the box show the minimum and maximum values, respectively.
SD20WK and SD28WK; Sprague Dawley rats aged 20 and 28 weeks, respectively. ZDSD20WK, ZDSD28WK-MOD and ZDSD28WK-SVD; Zucker Diabetic Sprague Dawley rats aged 20 weeks, and aged 28 weeks moderately diabetic and severely diabetic, respectively. *; p=0.005 and #; p=0.999; p=0.197 comparing ZDSD20WK against ZDSD28WK-MOD and ZDSD28WK-SVD, respectively.

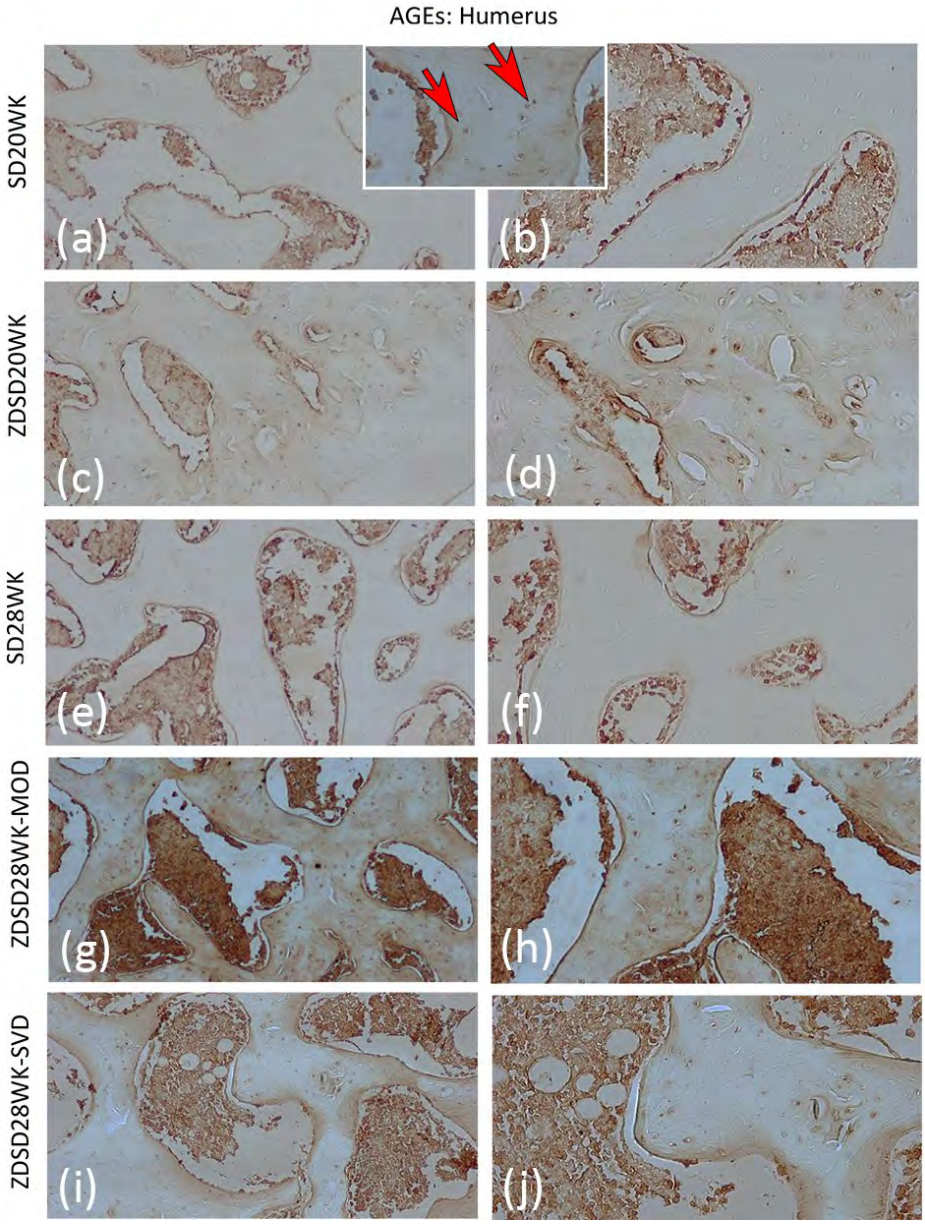


Figure 6.11: Humerus AGEs Immunopositivity. Immunopositive cells are depicted by arrows in the insert and are found throughout a-j. Scale bar represents 100µm and applies all photomicrographs.

6.2.5 AGE expression in the extracellular matrix of the humerus head in 20 and 28-week-old rats

All SD20WK (n=6; 100%) had mild immunopositivity for AGEs, the majority of ZDSD20WK (n=6; 85.70%) exhibited mild immunopositivity, only 1 animal (14.30%) had zero immunopositivity. Similarities were observed between the SD20WK and ZDSD20WK (p=0.575). Majority of SD28WK (n=5; 71.40%) exhibited mild immunopositivity while the rest of the rats had an equal distribution of moderate and zero immunopositivity (n=1; 14.3% respectively) (Table 6.3 and Fig 6.12). Majority of the ZDSD28WK-MOD (n=6; 66.70%) exhibited moderate immunopositivity, with 3 rats (33.33%) that had mild immunopositivity. Again the majority of ZDSD28WK-SVD (n=4; 66.70%) had moderate immunopositivity, with 2 rats (33.33%) that exhibited intense immunopositivity (Table 6. and Fig 6.12). Similarities were observed between both SD20WK and SD28WK (p=0.420), and ZDSD20WK with ZDSD28WK-MOD (p=0.164), but not the ZDSD28WK-SVD (p<0.001) (Table 6.3).

Table 6.3: Humerus AGEs Immunopositivity

Humerus head AGEs

Group		No stain		Mild		Moderate		Intense		p value
	N	Count	%	Count	%	Count	%	Count	%	
SD20WK	6	0	0	6	100	0	0	0	0	p=0.575
ZDSD20WK	7	1	14.3	6	85.7	0	0	0	0	
SD28WK	7	1	14.3	5	71.4	1	14.3	0	0	
ZDSD28WK-MOD	9	0	0	3	33.33	6	66.7	0	0	p=0.001
ZDSD28Wk-SVD	6	0	0	0	0	4	66.7	2	33.33	#p<0.001

Comparison of SD28WK with ZDSD28WK-SVD

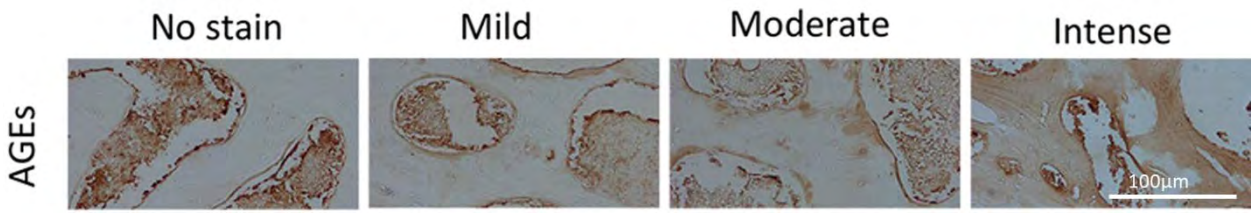


Figure 6.12: Humerus AGEs immunopositivity grading. The grading was based on staining intensity.

6.3 DISCUSSION

Quantification of adipocytes revealed increased adiposity in the ZDSDs similar to other rat (Kim and Schafer, 2016), and human studies (Ferland-McCollough et al., 2018). TRAP and ALP immunopositive cells quantities showed that T2D promotes osteolysis and inhibits osteoblastogenesis in ZDSD rats. To understand the role of cytokines in the ZDSD rat skeletal elements, were assessed the expression of one osteogenic cytokine (TGFB1) as well as an antagonist (BMP3). The ZDSDs had more BMP3 expression and relatively less TGFβ1. This shows that T2D affects bone cells though suppression TGFβ1 expression while its antagonist (BMP3) is elevated.

Anti-osteoblastogenic effects of adipocytes

Multiple studies have elucidated how T2D contributes to increased bone marrow adiposity. This adipogenic influence of T2D on mesenchymal stem cell (MSC) enhances the development of adipocytogenic cell lines while suppressing osteogenic cell lines (Piccinin and Khan, 2014; Kim and Schafer, 2016; Ferland-McCollough et al., 2018; Rharass and Lucas, 2018). These marrow adipocytes secrete the hormone adiponectin that is anti-osteoblastogenic, pro-osteoclastogenic and promotes osteoblast apoptosis (Rharass and Lucas, 2018; Singh et al., 2018). This could partially explain the susceptibility of bones to fracture in diabetes (Gillet et al., 2017; Ferland-McCollough et al., 2018). In the present study, the ZDSDs exhibited higher adipocyte numbers compared to age matched controls, with more adipocytes recorded at 28 weeks than 20 weeks. Our observation implies that that age and T2D contribute to increased bone marrow adiposity (Kim and Schafer, 2016) in the head of the humerus. This could possibly accentuate the increased risk to fracture of the proximal humerus.

Osteoblastogenesis and osteolysis

To evaluate the proposition that osteocytes are active (Bellido, 2014; Dole et al., 2017; Kaya et al., 2017), and not dormant as previously thought (Plotkin et al., 2019), these cells were immuno-labeled using the anti-TRAP antibody. TRAP is typically used as an osteoclast marker; however, recent studies have shown that osteocytes express the bone matrix catabolic enzyme TRAP as

they engage in osteolysis or peri lacuna-canaliculi remodeling (Dole et al., 2017; Kaya et al., 2017). This causes direct resorption and deposition of the bone matrix in osteocytes' immediate environment in response to pathologic conditions like T2D (Nakano et al., 2004; Qing et al., 2012; Dole et al., 2017; Kaya et al., 2017). In the present study, significantly more TRAP immunopositive osteocytes were observed in the ZDSDs and their age matched controls in alignment with previous research (Picke et al., 2019). These TRAP immunopositive cells trigger processes that attract osteoclast precursors to their vicinity, leading to increased bone matrix resorption (Burger, 1998; Bellido, 2014), thus contributing to osteolysis. Additionally, our observation of no differences in 20 and 28-week-old ZDSDs TRAP expression suggests that high TRAP expression is possibly maintained as diabetes progresses, potentially immunopositivity osteolysis. This could explain the bone fragility manifested in T2D (Burger, 1998; Bellido, 2014; Picke et al., 2019).

Osteoblastic ALP promotes osteoid formation and bone mineralization (Bhattarai et al., 2014). It is used as a bone turnover marker in the diagnosis of bone disease (Čepelak and Čvorišćec, 2009; Bhattarai et al., 2014; Florencio-Silva et al., 2015). Studies on animal models of T2D have reported impaired osteoblast differentiation, reduced osteoblast numbers and poor matrix mineralization in T2D. This is thought to lead to increased bone fragility (Ahmad et al., 2003; Blakytny et al., 2011; Hamann et al., 2011). In the present study, ZDSDs had fewer ALP positive osteoblasts, with no age differences. This finding supports the proposition that T2D inhibits osteoblastogenesis, from the early stages of the disease including its advanced stages. This may further explain the known bone fragility in T2D, and the possibility that it may start at early stages of the disease, at least at cellular level.

Interaction of AGEs with TGFβ1 and its antagonist BMP3

Type 2 diabetes increases the expression of AGEs both intracellularly and in the ECM (Goldin et al., 2006). This AGEs accumulation increases with age and diabetes progression (Goldin et al., 2006; Singh et al., 2014). It adversely affects intracellular signalling molecules that encode for osteoblast, osteoclast, and osteocyte functions (Kislinger et al., 1999; Singh et al., 2014; Creecy et al., 2016; Picke et al., 2019). In the present study, an increased accumulation of intracellular

and extracellular AGEs in ZDSDs compared to their age matched controls was observed, with no age differences in all groups. A possibility exists that this high AGEs accumulation could interfere with the TGFβ1 receptors, preventing entry of the extracelullar TGFβ1 into the cells, thereby interfering with the osteoblastogenic role of this cytokine.

While TGFβ1 expression was not significantly different between older rat groups (28 weeks) whereas the 20 weeks ZDSDs had significantly less expression of this cytokine. The present study refers to the secreted cytokine rather than intracellular TGFβ1. Therefore, the extracellular TGFβ1 amounts may not be directly engaged in the cellular activities such as the well-known transcription for osteoprogenitor cell differentiation and function (Ehnert et al., 2010). A possibility exists that the AGEs accumulation may block the interaction of TGFβ1 with cellular components required for osteoblastogeneis gene encoding (Singh et al., 2014).

In both age groups of our study, ZDSDs exhibited either moderate or intense BMP3 immunopositivity, with no immunopositivity in the controls. These observations suggest that T2D reduces the expression of BMP3, and possibly suppresses osteoblast function (Gazzerro and Canalis, 2006; Wu et al., 2016). In support of this proposition, previous research report increased osteoblast activity in BMP3 null mice (Gazzerro and Canalis, 2006). Notably, intense immunopositivity was observed in the overtly diabetic group, possibly suggesting that BMP-3 over expression may be associated with excessive hyperglycemia. Increased BMP3 expression manifests as reduced BMD, reduced trabeculae volume and thinner cortical bone (Gazzerro and Canalis, 2006; Horbelt et al., 2012).

6.4 Conclusion

We found that diabetes affected osteoblastogenesis as measured by ALP positive cells and bone marrow adipocytes. TRAP positive osteocytes numbers were increased in the presence of T2D, suggesting an increased osteolysis. The ZDSD groups had less osteogenic cytokine (TGFB1) expression, with more of the antagonist (BMP3) expression. We also found that T2D increases the number of AGEs immuno-positive cells, as well as its extracellular expression, thus providing

a conducive environment for the interaction of the osteogenic cytokine and its antagonist to suppress osteoblastogenesis. ZDSD groups had higher adipocyte numbers therefore increased marrow adiposity in T2D. We conclude that the ZDSD rat can be used as a translational model for diabetic skeletopathy at cellular and molecular level, and it can be extrapolated to humans after consideration of other factors like, basal metabolism, age, sex and skeletal loading patterns.

Chapter 7

General discussion and conclusion

7.0 GENERAL DISCUSSION AND CONCLUSION

This study was aimed at characterizing T2D induced skeletopathy in the Zucker Diabetic Sprague Dawley (ZDSD) rat using the femur and humerus. These bones were assessed from rats terminated at 2 time points namely, age of 20 and 28 weeks to evaluate the effect of disease duration. We confirmed successful induction of diabetes by monitoring weekly body mass, fasting blood glucose, and conducting fasting oral glucose tolerance tests (OGTTs) every 2 weeks, in addition to triglycerides measurements. Serum insulin concentration was quantified by ELISA as well as a hormone involved in bone homeostasis, osteocalcin. The assessment of oxidative stress was done by determining malondialdehyde (MDA) serum levels using ELISA. The biomechanical strength was analyzed by 3-point bending tests using a universal tensile tester whereas trabecular morphometric parameters, midshaft cortical bone and medullary area were analyzed using Three Dimensional Micro-focus X-ray Computed Tomography (Micro CT).

The diabetic state manifested as reduced weight, elevated fasting blood glucose, abnormal OGTTs, elevated insulin, triglyceride and MDA levels. Levels of the osteoregulatory hormone osteocalcin were also increased. Diabetic bones exhibited poor loading when subjected to 3-point bending tests until fracture, such as maximum force, break force, and maximum time. The bones did not perform well when evaluated for stiffness and elastic modulus. These two parameters evaluate the ability of bone to absorb forces per unit area. Following Micro-CT evaluation, trabecular morphometric parameters such as medulluary canal area, TbTh, TbN were reduced in the presence of diabetes.

Histological analysis of bone trabecular morphology and adiposity was performed using hematoxylin and Eosin (H&E) stain. Immunohistochemical expression of the osteogenic growth factor, TGF-β1 and its antagonist, BMP-3, were evaluated to understand whether T2D compromises bone quality through altering cytokine expression. To assess osteolysis and osteogenesis, osteocytes and osteoblasts were immunolabelled using the anti-TRAP and anti-ALP antibodies, respectively. Immunolocalization of AGEs was conducted to investigate their role in diabetic skeletopathy.

In both the femur and humerus, bone mass was lower in the diabetic rats irrespective of age or duration of diabetes. Bone mass reflects osseous tissue content, which in turn is controlled by the activity of osteoblasts and osteoclasts. In the present study, fewer osteoblasts were found in both bones among diabetics. This could partly explain the lower bone mass reported in this study. Quantification of TRAP immunopositive cells showed more cells expressing this enzyme in the diabetic groups irrespective of age of, disease severity or duration in the present study. This further explained the loss of bone mass in the diabetic rats. The osteolytic ability of TRAP positive cells is a major factor in depletion of bone mass.

In the present study, both the femur and humerus had lower BV/TV at 20 weeks and lower BV/TV in the humerus of 28-week-old the severely diabetic rats. Although this parameter showed these differences in the way the femur and humerus were affected, it remains a demonstration of the detrimental effect of hyperglycemia on bone. This is an important finding as our study used both the femur and humerus. Had this study used only the femur, it would have underestimated the effects of diabetes on skeletal elements. Our study shows that diabetes affects various bones differently.

Most osteometric measurements showed a reduction in bone size in the diabetic groups. This is consistent with previous studies (Reinwald et al., 2009; Creecy et al., 2016). While osteometric measurents give an estimation of bone size, they do not account for the geometric, non-linear nature of bone phenotype. To address this shortcoming, for the first time Micro CT was used to estimate bone size (BV) in the femur and humerus of ZDSD rats. We found that bone tissue volume (BV) was lower in the diabetic rats irrespective of age or duration of diabetes in both the femur and humerus.

Again, it is , herein, for the first-time report on the robusticity index of the femur and humerus in ZDSD rats. We found low robusticity in the diabetic rats irrespective of age or disease severity. Our study found that both the femur and humerus had lower maximum force and break force as

well as less time to fracture among the 28-week ZDSDs. This demonstrates bone weakness among diabetics. It appears that the robusticity could have been a crucial factor as long thin bones would be weaker than short wider bones. This finding is corroborated by the observed wider medullary canals with smaller cortical area in diabetic rats, particularly in the femur.

We found that diabetes altered trabecular microarchitecture for both the femoral head and neck as well as the humerus. This is demonstrated by the observed increased trabeculae spacing, reduced trabeculae numbers and diminished trabeculae thickness. This is possibly due to reduced osteoblastogenesis. We found increased adiposity in the femoral head, neck and humerus. Adipogenesis is common under chronic hyperglycemic conditions such as in diabetes (Devlin et al., 2014; Sheu et al., 2017), and it usually occurs with suppression of osteogenesis (Kim and Schafer, 2016; Gillet et al., 2017; Ferland-McCollough et al., 2018). We propose that these disturbances in the balance of trabecular microarchitectural parameters may be a consequence of suppressed osteogenesis. This is further corroborated by a reduced expression of the osteogenic cytokine, TGF-beta1 and an increased expression of the anti-osteogenic cytokine BMP-3.

We found reduced insulin levels, elevated blood glucose, and poor glucose handling as shown by OGTT findings. Hyperglycemia causes an increased expression of intracellular and extracelullar AGEs (Sanguineti et al., 2014; Yamamoto and Sugimoto, 2016; Singh et al., 2018; Plotkin et al., 2019) as observed in the present study, in both the femur and humerus. Hyperglycemia precipitates MDA accumulation as a result of oxidative stress (Jaganjac et al., 2013; Wang et al., 2018). MDA is an anti-osteoblastogenic agent ((Slatter et al., 2000; Negre-Salvayre et al., 2010; Ayala et al., 2014). The elevated MDA in the present study may have contributed to reduced osteogenesis. This may further explain the weaker bones in diabetic rats as evidenced by older 28-week ZDSD that had lower values for yield force, causing the bones to bend less under load, and therefore prone to fracture. Diabetes also reduced the amount of load that could be absorbed per unit area in ZDSD bones, as exhibited by the low elastic modulus.

Limitations

1. Only male rats were used, therefore the findings may not apply to females
2. This is a rat study; therefore, the results must be applied with caution to humans
3. Osteocalcin was not divided the carboxylated and undercarboxylated form
4. A lager sample size may yield different results

7.1 CONCLUSIONS

1. We have successfully induced diabetes in a relatively new polygenetic model of T2D as per various markers of T2D (loss of body mass, abnormal OGTTs and FBG, reduced insulin levels).

2. Type 2 diabetes affects femoral osteometry, mid-diaphyseal loading, and trabeculae microarchitectural parameters, resulting in weaker bones. These perturbations occur early and late in the disease and accentuated by the hyperglycemia.

3. Aspects of femoral parameters most affected by age, diabetes, and its duration are bicondylar width, TbN, femoral mass, femoral neck superoinferior diameter and maximum time(s) as depicted by discriminant function analysis.

4. Our findings from osteometry, 3-point bending tests and Micro CT support that diabetes weakens the humerus in the presence of T2D. Animal age and the duration of T2D also contribute to weaker bones.

5. Discriminant function analysis showed that epicondylar breadth, midshaft anteroposterior diameter, bone length, Robusticity Index, and TbN were the main factors influenced by age, diabetes, and its duration in the humerus.

6. Type 2 diabetes increases adiposity in both the humerus as well as the femoral head and neck, while reducing osteoblastogenesis as exhibited by lower ALP

7. Type 2 diabetes compromises osteolysis and osteoblastogenesis at all stages of the diabetic state, as shown by high TRAP immunopositivity, fewer ALP immunopositive cells.

8. Type 2 diabetes causes reduced expression of TGFβ1 and increases the expression of BMP3, to negatively affect osteoblast and osteocyte numbers in the femoral head and neck, at disease onset and latter stages of the disease with an associated AGEs immuno-positive cell as well as its extracellular accumulation and high MDA serum levels

9. We also found that T2D increases the number of AGEs immuno-positive cells, as well as its extracellular expression, thus providing a conducive environment for the interaction of the osteogenic cytokine (TGFβ1) and its antagonist (BMP3) to suppress osteoblastogenesis in the humerus.

10. We conclude that the ZDSD rat can be used as a translational model to study diabetic skeletopathy at cellular, molecular and bone phenotype level, and it can be extrapolated to humans after consideration of other factors like, basal metabolism, age, sex and skeletal loading patterns.

REFERENCES

Abubakar I, Tillmann T, Banerjee A. 2015. Global, regional, and national age-sex specific all-cause and cause-specific mortality for 240 causes of death, 1990-2013: a systematic analysis for the Global Burden of Disease Study 2013. Lancet 385:117-171.

Adeva-Andany MM, Martínez-Rodríguez J, González-Lucán M, Fernández-Fernández C, Castro-Quintela E. 2019. Insulin resistance is a cardiovascular risk factor in humans. Diabetes & Metabolic Syndrome: Diabetes Metab Syndr 13:1449-1455.

Ahmad T, Ohlsson C, Saaf M, Ostenson CG, Kreicbergs A. 2003. Skeletal changes in type-2 diabetic Goto-Kakizaki rats. J Endocrinol 178:111-116.

Al-Rubeaan K, Al-Manaa HA, Khoja TA, Ahmad NA, Al-Sharqawi AH, Siddiqui K, Alnaqeb D, Aburisheh KH, Youssef AM, Al-Batel A. 2015. Epidemiology of abnormal glucose metabolism in a country facing its epidemic: SAUDI-DM study. J Diabetes 7:622-632.

Alberti KG. 2009. International diabetes federation task force on epidemiology and prevention; hational heart, lung, and blood institute; American heart association; world heart federation; international atherosclerosis society; international association for the study of obesity: harmonizing the metabolic syndrome: a joint interim statement of the international diabetes federation task force on epidemiology and prevention; national heart, lung, and blood institute; American heart association; world heart federation; international atherosclerosis society; and international association for the study of obesity. Circulation 120:1640-1645.

Allan FN. 1972. Diabetes before and after insulin. Medical history 16:266-273.

Aronoff SL, Berkowitz K, Shreiner B, Want L. 2004. Glucose metabolism and regulation: beyond insulin and glucagon. Diabetes Spectr 17:183-190.

Arredondo A. 2014. Type 2 diabetes and health care costs in Latin America: exploring the need for greater preventive medicine. BMC Med 12:136.

Association AD. 2010. Standards of medical care in diabetes—2010. Diabetes care 33:S11-S61.

Ayala A, Munoz MF, Arguelles S. 2014. Lipid peroxidation: production, metabolism, and signaling mechanisms of malondialdehyde and 4-hydroxy-2-nonenal. Oxid Med Cell Longev 2014:360438.

Bahamonde ME, Lyons KM. 2001. BMP3: to be or not to be a BMP. JBJS 83:S56-S62.

Bellido T. 2014. Osteocyte-driven bone remodeling. Calcif Tissue Int 94:25-34.

Bertram MY, Jaswal AV, Van Wyk VP, Levitt NS, Hofman KJ. 2013. The non-fatal disease burden caused by type 2 diabetes in South Africa, 2009. Glob Health Action 6:19244.

Bhattarai T, Bhattacharya K, Chaudhuri P, Sengupta P. 2014. Correlation of common biochemical markers for bone turnover, serum calcium, and alkaline phosphatase in post-menopausal women. Malays J Med Sci 21:58-61.

Blakytny R, Spraul M, Jude EB. 2011. Review: The diabetic bone: a cellular and molecular perspective. Int J Low Extrem Wounds 10:16-32.

Blaslov K, Naranda FS, Kruljac I, Renar IP. 2018. Treatment approach to type 2 diabetes: Past, present and future. World J Diabetes 9:209-219.

Boden G, Laakso M. 2004. Lipids and glucose in type 2 diabetes: what is the cause and effect? Diabetes care 27:2253-2259.

Bonds DE, Larson JC, Schwartz AV, Strotmeyer ES, Robbins J, Rodriguez BL, Johnson KC, Margolis KL. 2006. Risk of fracture in women with type 2 diabetes: the Women's Health Initiative Observational Study. J Clin Endocrinol Metab 91:3404-3410.

Booth SL, Centi A, Smith SR, Gundberg C. 2013. The role of osteocalcin in human glucose metabolism: marker or mediator? Nat Rev Endocrinol 9:43-55.

Bouxsein ML, Boyd SK, Christiansen BA, Guldberg RE, Jepsen KJ, Müller R. 2010. Guidelines for assessment of bone microstructure in rodents using micro–computed tomography. J Bone Miner Res 25:1468-1486.

Bradshaw D, Norman R, Pieterse D, Levitt NS, South African Comparative Risk Assessment Collaborating G. 2007. Estimating the burden of disease attributable to diabetes in South Africa in 2000. S Afr Med J 97:700-706.

Burger E. 1998. Mechanotransduction in bone-role of the lacuno-canalicular network. FASEB J 13:1243-1250.

Care D. 2019. Standards of medical care in diabetes 2019. Diabetes Care 42:S124-138.

Castrillón J, Moral J, De Luis D, Rey J, Rodrıguez D, Sagrado M. 2011. Structural study using micro-CT of the femur of Goto-Kakizaki rats, experimental model for non-overweight type 2 diabetes. Rev Osteoporos Metab Miner 3:95-100.

Čepelak I, Čvorišćec D. 2009. Biochemical markers of bone remodeling–review. Biochemia Medica 19:17-35.

Chandrasekera PC, Pippin JJ. 2014. Of rodents and men: species-specific glucose regulation and type 2 diabetes research. ALTEX 31:157-176.

Chapurlat RD, Confavreux CB. 2016. Novel biological markers of bone: from bone metabolism to bone physiology. Rheumatology (Oxford) 55:1714-1725.

Chen Y, Lin C, Huang X, Lin F, Luo X. 2021. Comparison of treatment results between surgical and conservative treatment of distal radius fractures in adults: A meta-analysis of randomized controlled trials. Acta Orthop Traumatol Turc 55:118-126.

Cho NH, Shaw JE, Karuranga S, Huang Y, da Rocha Fernandes JD, Ohlrogge AW, Malanda B. 2018. IDF Diabetes Atlas: Global estimates of diabetes prevalence for 2017 and projections for 2045. Diabetes Res Clin Pract 138:271-281.

Chu SP, Kelsey JL, Keegan TH, Sternfeld B, Prill M, Quesenberry CP, Sidney S. 2004. Risk factors for proximal humerus fracture. Am J Epidemiol 160:360-367.

Cipriani C, Colangelo L, Santori R, Renella M, Mastrantonio M, Minisola S, Pepe J. 2020. The interplay between bone and glucose metabolism. Front Endocrinol 11:122.

Cousin E, Duncan BB, Stein C, Ong KL, Vos T, Abbafati C, Abbasi-Kangevari M, Abdelmasseh M, Abdoli A, Abd-Rabu R, Abolhassani H, Abu-Gharbieh E, Accrombessi MMK, Adnani QES, Afzal MS, Agarwal G, Agrawaal KK, Agudelo-Botero M, Ahinkorah BO, Ahmad S, Ahmad T, Ahmadi K, Ahmadi S, Ahmadi A, Ahmed A, Ahmed Salih Y, Akande-Sholabi W, Akram T, Al Hamad H, Al-Aly Z, Alcalde-Rabanal JE, Alipour V, Aljunid SM, Al-Raddadi RM, Alvis-Guzman N, Amini S, Ancuceanu R, Andrei T, Andrei CL, Anjana RM, Ansar A, Antonazzo IC, Antony B, Anyasodor AE, Arabloo J, Arizmendi D, Armocida B, Artamonov AA, Arulappan J, Aryan Z, Asgari S, Ashraf T, Astell-Burt T, Atorkey P, Atout MMdW, Ayanore MA, Badiye AD, Baig AA, Bairwa M, Baker JL, Baltatu OC, Banik PC, Barnett A, Barone MTU, Barone-Adesi F, Barrow A, Bedi N, Belete R, Belgaumi UI, Bell AW, Bennett DA, Bensenor IM, Beran D, Bhagavathula AS, Bhaskar S, Bhattacharyya K, Bhojaraja VS, Bijani A, Bikbov B, Birara S, Bodolica V, Bonny A, Brenner H, Briko NI, Butt ZA, Caetano dos Santos FL, Cámera LA, Campos-Nonato IR, Cao Y, Cao C, Cerin E, Chakraborty PA, Chandan JS, Chattu VK, Chen S, Choi J-YJ, Choudhari SG, Chowdhury EK, Chu D-T, Corso B, Dadras O, Dai X, Damasceno AAM, Dandona L, Dandona R, Dávila-Cervantes CA, De Neve J-W, Denova-Gutiérrez E, Dhamnetiya D, Diaz D, Ebtehaj S, Edinur HA, Eftekharzadeh S, El Sayed I, Elgendy IY, Elhadi M, Elmonem MA, Faisaluddin M, Farooque U, Feng X, Fernandes E, Fischer F, Flood D, Freitas M, Gaal PA, Gad MM, Gaewkhiew P, Getacher L, Ghafourifard M, Ghanei Gheshlagh R, Ghashghaee A, Ghith N, Ghozali G, Gill PS, Ginawi IA, Glushkova EV, Golechha M, Gopalani SV, Guimarães RA, Gupta RD, Gupta R, Gupta VK, Gupta VB, Gupta S, Habtewold TD, Hafezi-Nejad N, Halwani R, Hanif A, Hankey GJ, Haque S, Hasaballah AI, Hasan SS, Hashi A, Hassanipour S, Hay SI, Hayat K,

Heidari M, Hossain MBH, Hossain S, Hosseini M, Hoveidamanesh S, Huang J, Humayun A, Hussain R, Hwang B-F, Ibitoye SE, Ikuta KS, Inbaraj LR, Iqbal U, Islam MS, Islam SMS, Islam RM, Ismail NE, Isola G, Itumalla R, Iwagami M, Iyamu IO, Jahani MA, Jakovljevic M, Jayawardena R, Jha RP, John O, Jonas JB, Joo T, Kabir A, Kalhor R, Kamath A, Kanchan T, Kandel H, Kapoor N, Kayode GA, Kebede SA, Keshavarz P, Keykhaei M, Khader YS, Khajuria H, Khan MAB, Khan MN, Khan M, Khater AM, Khoja TAM, Khubchandani J, Kim MS, Kim YJ, Kimokoti RW, Kisa S, Kisa A, Kivimäki M, Korshunov VA, Korzh O, Koyanagi A, Krishan K, Kuate Defo B, Kumar GA, Kumar N, Kusuma D, La Vecchia C, Lacey B, Larsson AO, Lasrado S, Lee W-C, Lee CB, Lee PH, Lee SWH, Li M-C, Lim SS, Lim L-L, Lucchetti G, Majeed A, Malik AA, Mansouri B, Mantovani LG, Martini S, Mathur P, McAlinden C, Mehedi N, Mekonnen T, Menezes RG, Mersha AG, Miao Jonasson J, Miazgowski T, Michalek IM, Mirica A, Mirrakhimov EM, Mirza AZ, Mithra P, Mohammadian-Hafshejani A, Mohammadpourhodki R, Mohammed A, Mokdad AH, Molokhia M, Monasta L, Moni MA, Moradpour F, Moradzadeh R, Mostafavi E, Mueller UO, Murray CJL, Mustafa A, Nagel G, Nangia V, Naqvi AA, Nayak BP, Nazari J, Ndejjo R, Negoi RI, Neupane Kandel S, Nguyen CT, Nguyen HLT, Noubiap JJ, Nowak C, Oancea B, Odukoya OO, Oguntade AS, Ojo TT, Olagunju AT, Onwujekwe OE, Ortiz A, Owolabi MO, Palladino R, Panda-Jonas S, Pandi-Perumal SR, Pardhan S, Parekh T, Parvizi M, Pepito VCF, Perianayagam A, Petcu I-R, Pilania M, Podder V, Polibin RV, Postma MJ, Prashant A, Rabiee N, Rabiee M, Rahimi-Movaghar V, Rahman MA, Rahman MM, Rahman M, Rahmawaty S, Rajai N, Ram P, Rana J, Ranabhat K, Ranasinghe P, Rao CR, Rao S, Rawaf S, Rawaf DL, Rawal L, Renzaho AMN, Rezaei N, Rezapour A, Riahi SM, Ribeiro D, Rodriguez JAB, Roever L, Rohloff P, Rwegerera GM, Ryan PM, Saber-Ayad MM, Sabour S, Saddik B, Saeedi Moghaddam S, Sahebkar A, Sahoo H, Saif-Ur-Rahman KM, Salimzadeh H, Samaei M, Sanabria J, Santric-Milicevic MM, Sathian B, Sathish T, Schlaich MP, Seidu A-A, Šekerija M, Senthil Kumar N, Seylani A, Shaikh MA, Shamshad H, Shawon MSR, Sheikhbahaei S, Shetty JK, Shiri R, Shivakumar KM, Shuval K, Singh JA, Singh A, Skryabin VY, Skryabina AA, Sofi-Mahmudi A, Soheili A, Sun J, Szerencsés V, Szócska M, Tabarés-Seisdedos R, Tadbiri H, Tadesse EG, Tariqujjaman M, Thankappan KR, Thapar R, Thomas N, Timalsina B, Tobe-Gai R, Tonelli M, Tovani-Palone MR, Tran BX, Tripathy JP, Tudor Car L, Tusa BS, Uddin R, Upadhyay E, Valadan Tahbaz S, Valdez PR, Vasankari TJ, Verma M, Villalobos-Daniel VE, Vladimirov SK, Vo B, Vu GT, Vukovic R, Waheed Y, Wamai RG, Werdecker A, Wickramasinghe ND, Winkler AS, Wubishet BL, Xu X, Xu S, Yahyazadeh Jabbari SH, Yatsuya H, Yaya S, Yazie TSY, Yi S, Yonemoto N, Yunusa I, Zadey S, Zaman SB, Zamanian M, Zamora N, Zastrozhin MS, Zastrozhina A, Zhang Z-J, Zhong C, Zmaili M, Zumla A, Naghavi M, Schmidt MI. 2022. Diabetes mortality and trends before 25 years of age: an analysis of the Global Burden of Disease Study 2019. Lancet Diabetes Endocrinol 10:177-192.

Creecy A, Uppuganti S, Merkel AR, O'Neal D, Makowski AJ, Granke M, Voziyan P, Nyman JS. 2016. Changes in the Fracture Resistance of Bone with the Progression of Type 2 Diabetes in the ZDSD Rat. Calcif Tissue Int 99:289-301.

D'Adamo E, Caprio S. 2011. Type 2 diabetes in youth: epidemiology and pathophysiology. Diabetes Care 34 Suppl 2:S161-165.

Del Prato S. 2009. Role of glucotoxicity and lipotoxicity in the pathophysiology of Type 2 diabetes mellitus and emerging treatment strategies. Diabet Med 26:1185-1192.

Del Rio D, Stewart AJ, Pellegrini N. 2005. A review of recent studies on malondialdehyde as toxic molecule and biological marker of oxidative stress. Nutr Metab Cardiovasc Dis 15:316-328.

Devlin MJ, Van Vliet M, Motyl K, Karim L, Brooks DJ, Louis L, Conlon C, Rosen CJ, Bouxsein ML. 2014. Early-onset type 2 diabetes impairs skeletal acquisition in the male TALLYHO/JngJ mouse. Endocrinology 155:3806-3816.

Dobnig H. 2006. Type2 diabetes mellitus in nursing home patients : effects on bone tuneover, bone mass, and fracture risk. J Clin Endocrinol Metab 91:3276-3278.

DOBSON M. 1967. throughout his hospital stay. All seven patients did. JAMA 201:291-296.
Dole NS, Mazur CM, Acevedo C, Lopez JP, Monteiro DA, Fowler TW, Gludovatz B, Walsh F, Regan JN, Messina S. 2017. Osteocyte-intrinsic TGF-β signaling regulates bone quality through perilacunar/canalicular remodeling. Cell reports 21:2585-2596.
Ducy P. 2020. Bone Regulation of Insulin Secretion and Glucose Homeostasis. Endocrinology 161.
Ehnert S, Baur J, Schmitt A, Neumaier M, Lucke M, Dooley S, Vester H, Wildemann B, Stöckle U, Nussler AK. 2010. TGF-β1 as possible link between loss of bone mineral density and chronic inflammation. PloS one 5:e14073.
Emmerson BR, Varacallo M, Inman D. 2022. Hip Fracture Overview. In: StatPearls. Treasure Island (FL): StatPearls Publishing.
Fairfield H, Falank C, Harris E, Demambro V, McDonald M, Pettitt JA, Mohanty ST, Croucher P, Kramer I, Kneissel M, Rosen CJ, Reagan MR. 2018. The skeletal cell-derived molecule sclerostin drives bone marrow adipogenesis. J Cell Physiol 233:1156-1167.
Fajardo RJ, Karim L, Calley VI, Bouxsein ML. 2014. A review of rodent models of type 2 diabetic skeletal fragility. J Bone Miner Res 29:1025-1040.
Feng X, McDonald JM. 2011. Disorders of bone remodeling. Annu Rev Pathol 6:121-145.
Ferland-McCollough D, Maselli D, Spinetti G, Sambataro M, Sullivan N, Blom A, Madeddu P. 2018. MCP-1 feedback loop between adipocytes and mesenchymal stromal cells causes fat accumulation and contributes to hematopoietic stem cell rarefaction in the bone marrow of patients with diabetes. Diabetes 67:1380-1394.
Ferron M, Lacombe J. 2014. Regulation of energy metabolism by the skeleton: osteocalcin and beyond. Arch Biochem Biophys 561:137-146.
Florencio-Silva R, Sasso GRdS, Sasso-Cerri E, Simões MJ, Cerri PS. 2015. Biology of bone tissue: structure, function, and factors that influence bone cells. Biomed Res Int 2015.
Forestier-Zhang L, Bishop N. 2016. Bone strength in children: understanding basic bone biomechanics. Arch Dis Child Educ Pract Ed 101:2-7.
Fulzele K, Clemens TL. 2012. Novel functions for insulin in bone. Bone 50:452-456.
Gamer LW, Cox K, Carlo JM, Rosen V. 2009. Overexpression of BMP3 in the developing skeleton alters endochondral bone formation resulting in spontaneous rib fractures. Dev Dyn 238:2374-2381.
Garber AJ, Handelsman Y, Einhorn D, Bergman DA, Bloomgarden ZT, Fonseca V, Garvey WT, Gavin JR, Grunberger G, Horton ES. 2008. Diagnosis and management of prediabetes in the continuum of hyperglycemia—when do the risks of diabetes begin? A consensus statement from the American College of Endocrinology and the American Association of Clinical Endocrinologists. Endocr Pract 14:933-946.
Gazzerro E, Canalis E. 2006. Bone morphogenetic proteins and their antagonists. Rev Endocr Metab Disord 7:51-65.
Gillet C, Dalla Valle A, Gaspard N, Spruyt D, Vertongen P, Lechanteur J, Rigutto S, Dragan ER, Heuschling A, Gangji V, Rasschaert J. 2017. Osteonecrosis of the Femoral Head: Lipotoxicity Exacerbation in MSC and Modifications of the Bone Marrow Fluid. Endocrinology 158:490-502.
Giugliano D, Ceriello A, Esposito K. 2008. Glucose metabolism and hyperglycemia. Am J Clin Nutr 87:217S-222S.
Goettsch C, Iwata H, Aikawa E. 2014. Parathyroid hormone: critical bridge between bone metabolism and cardiovascular disease. In: Am Heart Assoc. p 1333-1335.
Goldin A, Beckman JA, Schmidt AM, Creager MA. 2006. Advanced glycation end products: sparking the development of diabetic vascular injury. Circulation 114:597-605.
Gougeon R. 2013. Insulin resistance of protein metabolism in type 2 diabetes and impact on dietary needs: a review. Can J Diabetes 37:115-120.
Gullberg B, Johnell O, Kanis JA. 1997. World-wide projections for hip fracture. Osteoporos Int 7:407-413.

Hamann C, Goettsch C, Mettelsiefen J, Henkenjohann V, Rauner M, Hempel U, Bernhardt R, Fratzl-Zelman N, Roschger P, Rammelt S. 2011. Delayed bone regeneration and low bone mass in a rat model of insulin-resistant type 2 diabetes mellitus is due to impaired osteoblast function. Am J Physiol Endocrinol 301:E1220-E1228.

Hawthorne AC, Xavier SP, Okamoto R, Salvador SL, Antunes AA, Salata LA. 2013. Immunohistochemical, tomographic, and histological study on onlay bone graft remodeling. Part III: allografts. Clinical oral implants research 24:1164-1172.

Henneicke H, Gasparini SJ, Brennan-Speranza TC, Zhou H, Seibel MJ. 2014. Glucocorticoids and bone: local effects and systemic implications. Trends Endocrinol Metab 25:197-211.

Himsworth HP. 1936. Diabetes mellitus. Its differentiation into insolin-sensitive and insulin-insensitive types. Lancet 230:127-130.

Holt RI. 2004. Diagnosis, epidemiology and pathogenesis of diabetes mellitus: an update for psychiatrists. Br J Psychiatry Suppl 47:S55-63.

Horbelt D, Denkis A, Knaus P. 2012. A portrait of Transforming Growth Factor beta superfamily signalling: Background matters. Int J Biochem Cell Biol 44:469-474.

Hsu JT, Fuh LJ, Tu MG, Li YF, Chen KT, Huang HL. 2013. The effects of cortical bone thickness and trabecular bone strength on noninvasive measures of the implant primary stability using synthetic bone models. Clin Implant Dent Relat Res 15:251-261.

Huang S, Kaw M, Harris M, Ebraheim N, McInerney M, Najjar S, Lecka-Czernik B. 2010. Decreased osteoclastogenesis and high bone mass in mice with impaired insulin clearance due to liver-specific inactivation to CEACAM1. Bone 46:1138-1145.

Hurtado MD, Vella A. 2019. What is type 2 diabetes? Medicine 47:10-15.

Iglesias-Rodriguez S, Dominguez-Prado DM, Garcia-Reza A, Fernandez-Fernandez D, Perez-Alfonso E, Garcia-Pineiro J, Castro-Menendez M. 2021. Epidemiology of proximal humerus fractures. J Orthop Surg Res 16:402.

Im J-A, Yu B-P, Jeon JY, Kim S-H. 2008. Relationship between osteocalcin and glucose metabolism in postmenopausal women. Clinica chimica acta 396:66-69.

Iwaniec UT, Turner RT. 2016. Influence of body weight on bone mass, architecture and turnover. J Endocrinol 230:R115-130.

Jaganjac M, Tirosh O, Cohen G, Sasson S, Zarkovic N. 2013. Reactive aldehydes–second messengers of free radicals in diabetes mellitus. Free Radic Res 47:39-48.

Janghorbani M, Van Dam RM, Willett WC, Hu FB. 2007. Systematic review of type 1 and type 2 diabetes mellitus and risk of fracture. Am J Epidemiol 166:495-505.

Janssens K, ten Dijke P, Janssens S, Van Hul W. 2005. Transforming growth factor-beta1 to the bone. Endocr Rev 26:743-774.

Jepsen KJ, Silva MJ, Vashishth D, Guo XE, van der Meulen MC. 2015. Establishing biomechanical mechanisms in mouse models: practical guidelines for systematically evaluating phenotypic changes in the diaphyses of long bones. J Bone Miner Res 30:951-966.

Jian H, Shen X, Liu I, Semenov M, He X, Wang X-F. 2006. Smad3-dependent nuclear translocation of β-catenin is required for TGF-β1-induced proliferation of bone marrow-derived adult human mesenchymal stem cells. Genes Dev 20:666-674.

Jorgens V. 2006. Oskar Minkowski (1858-1931). An outstanding master of diabetes research. HORMONES-ATHENS- 5:310.

Junqueira L, Carneiro J. 2003. Basic Histology, 10th Edn, Lange Edition. McGraw Hill 16:340.

Kahn SE. 2003. The relative contributions of insulin resistance and beta-cell dysfunction to the pathophysiology of Type 2 diabetes. Diabetologia 46:3-19.

Kanazawa I. 2015. Osteocalcin as a hormone regulating glucose metabolism. World J Diabetes 6:1345.

Karim L, Rezaee T, Vaidya R. 2019. The Effect of Type 2 Diabetes on Bone Biomechanics. Curr Osteoporos Rep 17:291-300.

Kaya S, Basta-Pljakic J, Seref-Ferlengez Z, Majeska RJ, Cardoso L, Bromage TG, Zhang Q, Flach CR, Mendelsohn R, Yakar S, Fritton SP, Schaffler MB. 2017. Lactation-Induced Changes in the Volume of Osteocyte Lacunar-Canalicular Space Alter Mechanical Properties in Cortical Bone Tissue. J Bone Miner Res 32:688-697.

Kemink SA, Hermus AR, Swinkels LM, Lutterman JA, Smals AG. 2000. Osteopenia in insulin-dependent diabetes mellitus; prevalence and aspects of pathophysiology. J Endocrinol Invest 23:295-303.

Kierszenbaum AL, Tres L. 2015. Histology and Cell Biology: an introduction to pathology E-Book: Elsevier Health Sciences.

Kim TY, Schafer AL. 2016. Diabetes and Bone Marrow Adiposity. Curr Osteoporos Rep 14:337-344.

Kislinger T, Fu C, Huber B, Qu W, Taguchi A, Du Yan S, Hofmann M, Yan SF, Pischetsrieder M, Stern D. 1999. N ε-(carboxymethyl) lysine adducts of proteins are ligands for receptor for advanced glycation end products that activate cell signaling pathways and modulate gene expression. J Biol Chem 274:31740-31749.

Kohei K. 2010. Pathophysiology of type 2 diabetes and its treatment policy. JMAJ 53:41-46.

Kokabu S, Rosen V. 2018. BMP3 expression by osteoblast lineage cells is regulated by canonical Wnt signaling. FEBS Open Bio 8:168-176.

Kotha SP, Guzelsu N. 2007. Tensile behavior of cortical bone: dependence of organic matrix material properties on bone mineral content. J Biomech 40:36-45.

Kowalski GM, Bruce CR. 2014. The regulation of glucose metabolism: implications and considerations for the assessment of glucose homeostasis in rodents. American journal of physiology Endocrinology and metabolism 307:E859-871.

Lakhtakia R. 2013. The history of diabetes mellitus. Sultan Qaboos Univ Med J 13:368-370.

Lee NK, Sowa H, Hinoi E, Ferron M, Ahn JD, Confavreux C, Dacquin R, Mee PJ, McKee MD, Jung DY, Zhang Z, Kim JK, Mauvais-Jarvis F, Ducy P, Karsenty G. 2007. Endocrine regulation of energy metabolism by the skeleton. Cell 130:456-469.

Lekkala S, Taylor EA, Hunt HB, Donnelly E. 2019. Effects of Diabetes on Bone Material Properties. Curr Osteoporos Rep 17:455-464.

Leppanen O, Sievanen H, Jokihaara J, Pajamaki I, Jarvinen TL. 2006. Three-point bending of rat femur in the mediolateral direction: introduction and validation of a novel biomechanical testing protocol. J Bone Miner Res 21:1231-1237.

Leung K, Fung K, Sher A, Li C, Lee K. 1993. Plasma bone-specific alkaline phosphatase as an indicator of osteoblastic activity. J Bone Joint Surg Am 75:288-292.

Li X, Weng H, Reece EA, Yang P. 2011. SOD1 overexpression in vivo blocks hyperglycemia-induced specific PKC isoforms: substrate activation and consequent lipid peroxidation in diabetic embryopathy. Am J Obstet Gynecol 205:84 e81-86.

Lin DPL, Dass CR. 2018. Weak bones in diabetes mellitus - an update on pharmaceutical treatment options. J Pharm Pharmacol 70:1-17.

Manyema M, Veerman JL, Chola L, Tugendhaft A, Labadarios D, Hofman K. 2015. Decreasing the Burden of Type 2 Diabetes in South Africa: The Impact of Taxing Sugar-Sweetened Beverages. PLoS One 10:e0143050.

Margolis DS, Kim D, Szivek JA, Lai LW, Lien YH. 2006. Functionally improved bone in calbindin-D28k knockout mice. Bone 39:477-484.

Martin RM, Correa PH. 2010. Bone quality and osteoporosis therapy. Arq Bras Endocrinol Metabol 54:186-199.

Martinez-Huedo MA, Jiménez-García R, Mora-Zamorano E, Hernández-Barrera V, Villanueva-Martinez M, Lopez-de-Andres A. 2017. Trends in incidence of proximal humerus fractures, surgical

procedures and outcomes among elderly hospitalized patients with and without type 2 diabetes in Spain (2001–2013). BMC Musculoskelet Disord 18:1-11.

Massaous J, Hata A. 1997. TGF-β signalling through the Smad pathway. Trends in cell biology 7:187-192.

Matzelle MM, Shaw AT, Baum R, Maeda Y, Li J, Karmakar S, Manning CA, Walsh NC, Rosen V, Gravallese EM. 2016. Inflammation in arthritis induces expression of BMP3, an inhibitor of bone formation. Scand J Rheumatol 45:379-383.

McCalden RW, McGeough JA, Court-Brown CM. 1997. Age-related changes in the compressive strength of cancellous bone. The relative importance of changes in density and trabecular architecture. J Bone Joint Surg Am 79:421-427.

Miao D, Scutt A. 2002. Histochemical localization of alkaline phosphatase activity in decalcified bone and cartilage. J Histochem Cytochem 50:333-340.

Minkowski O. 1890. Diabetes mellitus nach Pankreasexstirpation. Arch Exp Path Pharm 26:371-387.

Mohan V, Sandeep S, Deepa R, Shah B, Varghese C. 2007. Epidemiology of type 2 diabetes: Indian scenario. Indian J Med Res 125:217-230.

Monzem S, Gohin S, Yague Ballester R, Lopes de Souza R, Meeson R, Pitsillides AA. 2022. An examination of two different approaches for the study of femoral neck fracture: Towards a more relevant rodent model. Proc Inst Mech Eng H 236:199-207.

Morigny P, Houssier M, Mouisel E, Langin D. 2016. Adipocyte lipolysis and insulin resistance. Biochimie 125:259-266.

Morton GJ, Schwartz MW. 2011. Leptin and the central nervous system control of glucose metabolism. Physiol Rev 91:389-411.

Moseley KF. 2012. Type 2 diabetes and bone fractures. Curr Opin Endocrinol Diabetes Obes 19:128-135.

Nakano Y, Toyosawa S, Takano Y. 2004. Eccentric localization of osteocytes expressing enzymatic activities, protein, and mRNA signals for type 5 tartrate-resistant acid phosphatase (TRAP). J Histochem Cytochem 52:1475-1482.

Nakrani MN, Wineland RH, Anjum F. 2020. Physiology, glucose metabolism.

Neer RM, Arnaud CD, Zanchetta JR, Prince R, Gaich GA, Reginster JY, Hodsman AB, Eriksen EF, Ish-Shalom S, Genant HK, Wang O, Mitlak BH. 2001. Effect of parathyroid hormone (1-34) on fractures and bone mineral density in postmenopausal women with osteoporosis. N Engl J Med 344:1434-1441.

Negre-Salvayre A, Auge N, Ayala V, Basaga H, Boada J, Brenke R, Chapple S, Cohen G, Feher J, Grune T, Lengyel G, Mann GE, Pamplona R, Poli G, Portero-Otin M, Riahi Y, Salvayre R, Sasson S, Serrano J, Shamni O, Siems W, Siow RC, Wiswedel I, Zarkovic K, Zarkovic N. 2010. Pathological aspects of lipid peroxidation. Free Radic Res 44:1125-1171.

Oei L, Zillikens MC, Dehghan A, Buitendijk GH, Castaño-Betancourt MC, Estrada K, Stolk L, Oei EH, van Meurs JB, Janssen JA. 2013. High bone mineral density and fracture risk in type 2 diabetes as skeletal complications of inadequate glucose control: the Rotterdam Study. Diabetes care 36:1619-1628.

Organization WH. 2006. Definition and diagnosis of diabetes mellitus and intermediate hyperglycaemia: report of a WHO/IDF consultation.

Ozougwu J, Obimba K, Belonwu C, Unakalamba C. 2013. The pathogenesis and pathophysiology of type 1 and type 2 diabetes mellitus. J Physiol Pathophysiol 4:46-57.

Patel M, Pandya A, Singel T. Study of Robusticity Index of Femur in Gujarat Region.

Paul B, Snyder S. 2010. The unusual amino acid L-ergothioneine is a physiologic cytoprotectant. Cell Death Differ 17:1134-1140.

Peterson RG, Jackson CV, Zimmerman K, de Winter W, Huebert N, Hansen MK. 2015. Characterization of the ZDSD Rat: A Translational Model for the Study of Metabolic Syndrome and Type 2 Diabetes. J Diabetes Res 2015:487816.

Pheiffer C, Pillay-van Wyk V, Joubert JD, Levitt N, Nglazi MD, Bradshaw D. 2018. The prevalence of type 2 diabetes in South Africa: a systematic review protocol. BMJ Open 8:e021029.

Piccinin MA, Khan ZA. 2014. Pathophysiological role of enhanced bone marrow adipogenesis in diabetic complications. Adipocyte 3:263-272.

Picke AK, Campbell G, Napoli N, Hofbauer LC, Rauner M. 2019. Update on the impact of type 2 diabetes mellitus on bone metabolism and material properties. Endocr Connect 8:R55-R70.

Piotrowska K, Tarnowski M. 2021. Bone Marrow Adipocytes—Role in Physiology and Various Nutritional Conditions in Human and Animal Models. Nutrients 13:1412.

Plotkin LI, Essex AL, Davis HM. 2019. RAGE Signaling in Skeletal Biology. Curr Osteoporos Rep 17:16-25.

Polonsky KS. 2012. The past 200 years in diabetes. N Engl J Med 367:1332-1340.

Prisby RD, Swift JM, Bloomfield SA, Hogan HA, Delp MD. 2008. Altered bone mass, geometry and mechanical properties during the development and progression of type 2 diabetes in the Zucker diabetic fatty rat. J Endocrinol 199:379-388.

Qing H, Ardeshirpour L, Pajevic PD, Dusevich V, Jahn K, Kato S, Wysolmerski J, Bonewald LF. 2012. Demonstration of osteocytic perilacunar/canalicular remodeling in mice during lactation. J Bone Miner Res 27:1018-1029.

Raggatt LJ, Partridge NC. 2010. Cellular and molecular mechanisms of bone remodeling. J Biol Chem 285:25103-25108.

Reaven GM. 2005. Why Syndrome X? From Harold Himsworth to the insulin resistance syndrome. Cell Metab 1:9-14.

Reddy GK, Stehno-Bittel L, Hamade S, Enwemeka CS. 2001. The biomechanical integrity of bone in experimental diabetes. Diabetes Res Clin Pract 54:1-8.

Reinwald S, Peterson RG, Allen MR, Burr DB. 2009. Skeletal changes associated with the onset of type 2 diabetes in the ZDF and ZDSD rodent models. American journal of physiology Endocrinology and metabolism 296:E765-774.

Rharass T, Lucas S. 2018. MECHANISMS IN ENDOCRINOLOGY: Bone marrow adiposity and bone, a bad romance? Eur J Endocrinol 179:R165-R182.

Saeedi P, Petersohn I, Salpea P, Malanda B, Karuranga S, Unwin N, Colagiuri S, Guariguata L, Motala AA, Ogurtsova K, Shaw JE, Bright D, Williams R, Committee IDFDA. 2019. Global and regional diabetes prevalence estimates for 2019 and projections for 2030 and 2045: Results from the International Diabetes Federation Diabetes Atlas, 9(th) edition. Diabetes Res Clin Pract 157:107843.

Sanguineti R, Puddu A, Mach F, Montecucco F, Viviani GL. 2014. Advanced glycation end products play adverse proinflammatory activities in osteoporosis. Mediators Inflamm 2014:975872.

Sassi F, Buondonno I, Luppi C, Spertino E, Stratta E, Di Stefano M, Ravazzoli M, Isaia G, Trento M, Passera P, Porta M, Isaia GC, D'Amelio P. 2018. Type 2 diabetes affects bone cells precursors and bone turnover. BMC Endocr Disord 18:55.

Scheen AJ. 2003. Pathophysiology of type 2 diabetes. Acta Clin Belg 58:335-341.

Schousboe JT, Morin SN, Kline GA, Lix LM, Leslie WD. 2022. Differential risk of fracture attributable to type 2 diabetes mellitus according to skeletal site. Bone 154:116220.

Schwartz AV. 2003. Diabetes Mellitus: Does it Affect Bone? Calcif Tissue Int 73:515-519.

Seibel MJ. 2005. Biochemical markers of bone turnover: part I: biochemistry and variability. Clin Biochem Rev 26:97-122.

Sheu Y, Amati F, Schwartz AV, Danielson ME, Li X, Boudreau R, Cauley JA, Osteoporotic Fractures in Men Research G. 2017. Vertebral bone marrow fat, bone mineral density and diabetes: The Osteoporotic Fractures in Men (MrOS) study. Bone 97:299-305.

Singh L, Tyagi S, Myers D, Duque G. 2018. Good, Bad, or Ugly: the Biological Roles of Bone Marrow Fat. Curr Osteoporos Rep 16:130-137.

Singh S, Kumar D, Lal AK. 2015. Serum osteocalcin as a diagnostic biomarker for primary osteoporosis in women. J Clin Diagnostic Res 9:RC04.

Singh VP, Bali A, Singh N, Jaggi AS. 2014. Advanced glycation end products and diabetic complications. Korean J Physiol Pharmacol 18:1-14.

Slatter DA, Bolton CH, Bailey AJ. 2000. The importance of lipid-derived malondialdehyde in diabetes mellitus. Diabetologia 43:550-557.

Starup-Linde J, Vestergaard P. 2016. Biochemical bone turnover markers in diabetes mellitus - A systematic review. Bone 82:69-78.

Sun H, Saeedi P, Karuranga S, Pinkepank M, Ogurtsova K, Duncan BB, Stein C, Basit A, Chan JCN, Mbanya JC, Pavkov ME, Ramachandaran A, Wild SH, James S, Herman WH, Zhang P, Bommer C, Kuo S, Boyko EJ, Magliano DJ. 2022. IDF Diabetes Atlas: Global, regional and country-level diabetes prevalence estimates for 2021 and projections for 2045. Diabetes Res Clin Pract 183:109119.

Sun K, Semba RD, Fried LP, Schaumberg DA, Ferrucci L, Varadhan R. 2012. Elevated Serum Carboxymethyl-Lysine, an Advanced Glycation End Product, Predicts Severe Walking Disability in Older Women: The Women's Health and Aging Study I. J Aging Res 2012:586385.

Tang Y, Wu X, Lei W, Pang L, Wan C, Shi Z, Zhao L, Nagy TR, Peng X, Hu J, Feng X, Van Hul W, Wan M, Cao X. 2009. TGF-beta1-induced migration of bone mesenchymal stem cells couples bone resorption with formation. Nat Med 15:757-765.

Thomas CJ, Cleland TP, Sroga GE, Vashishth D. 2018. Accumulation of carboxymethyl-lysine (CML) in human cortical bone. Bone 110:128-133.

Thrailkill KM, Lumpkin Jr CK, Bunn RC, Kemp SF, Fowlkes JL. 2005. Is insulin an anabolic agent in bone? Dissecting the diabetic bone for clues. Am J Physiol Endocrinol 289:E735-E745.

Tiwari BK, Pandey KB, Abidi AB, Rizvi SI. 2013. Markers of Oxidative Stress during Diabetes Mellitus. J Biomark 2013:378790.

Turner CH, Burr DB. 1993. Basic biomechanical measurements of bone: a tutorial. Bone 14:595-608.

Tyrovola JB, Odont X. 2015. The “mechanostat theory” of frost and the OPG/Rankl/RANK system. J Cell Biochem 116:2724-2729.

Uppuganti S, Granke M, Makowski AJ, Does MD, Nyman JS. 2016. Age-related changes in the fracture resistance of male Fischer F344 rat bone. Bone 83:220-232.

Valderrabano RJ, Linares MI. 2018. Diabetes mellitus and bone health: epidemiology, etiology and implications for fracture risk stratification. Clin Diabetes Endocrinol 4:9.

Vestergaard P, Rejnmark L, Mosekilde L. 2009. Diabetes and its complications and their relationship with risk of fractures in type 1 and 2 diabetes. Calcif Tissue Int 84:45-55.

Vijan S. 2010. In the clinic. Type 2 diabetes. Ann Intern Med 152:ITC31-15; quiz ITC316.

Wang WD, Cheng BZ, Kang WB, Zheng RW, Cai YL, Wang XJ. 2018. Investigation for TGF-beta1 expression in type 2 diabetes and protective effects of TGF-beta1 on osteoblasts under high glucose environment. Eur Rev Med Pharmacol Sci 22:6500-6506.

Wu M, Chen G, Li YP. 2016. TGF-beta and BMP signaling in osteoblast, skeletal development, and bone formation, homeostasis and disease. Bone Res 4:16009.

Xu L, Porter NA. 2015. Free radical oxidation of cholesterol and its precursors: Implications in cholesterol biosynthesis disorders. Free Radic Res 49:835-849.

Yamamoto M, Sugimoto T. 2016. Advanced Glycation End Products, Diabetes, and Bone Strength. Curr Osteoporos Rep 14:320-326.

Yang Y, Zhang N, Lan F, Van Crombruggen K, Fang L, Hu G, Hong S, Bachert C. 2014. Transforming growth factor-beta 1 pathways in inflammatory airway diseases. Allergy 69:699-707.

Yeni YN, Dong XN, Fyhrie DP, Les CM. 2004. The dependence between the strength and stiffness of cancellous and cortical bone tissue for tension and compression: extension of a unifying principle. Biomed Mater Eng 14:303-310.

Zaccardi F, Webb DR, Yates T, Davies MJ. 2016. Pathophysiology of type 1 and type 2 diabetes mellitus: a 90-year perspective. Postgrad Med J 92:63-69.

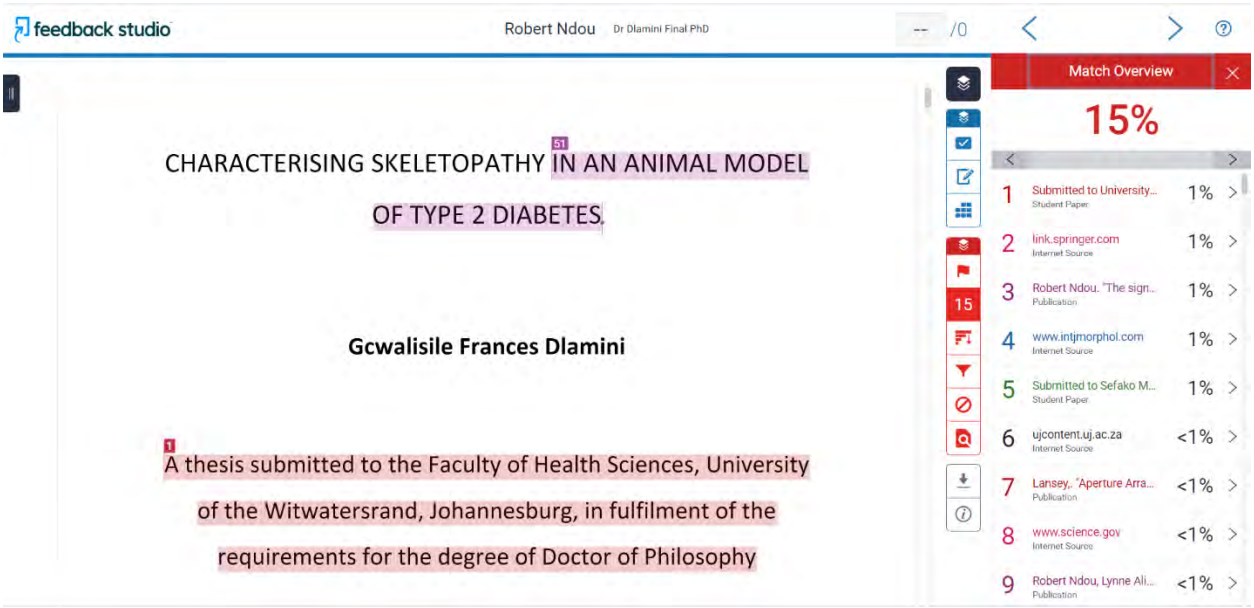
Zajac J, Shrestha A, Patel P, Poretsky L. 2010. The main events in the history of diabetes mellitus. In: Principles of diabetes mellitus: Springer. p 3-16.

Zheng W, Wang SY. 2001. Antioxidant activity and phenolic compounds in selected herbs. J Agric Food Chem 49:5165-5170.

Zheng Y, Ley SH, Hu FB. 2018. Global aetiology and epidemiology of type 2 diabetes mellitus and its complications. Nat Rev Endocrinol 14:88-98.

APPENDIX A

Turnitin in Report



Appendix B

Ethics

STRICTLY CONFIDENTIAL

ANIMAL ETHICS SCREENING COMMITTEE (AESC)

CLEARANCE CERTIFICATE NO. 2015/07/28/C

APPLICANT: Dr R Ndou

SCHOOL: School of Anatomical Sciences
DEPARTMENT:
LOCATION:

PROJECT TITLE: Bone integrity and health in type 2 diabetes using a rat model (Zucker Fatty Rat)

Number and Species

20 Male Zucker Fatty Rats

Approval was given for the use of animals for the project described above at an AESC meeting held on 2015/07/28. This approval remains valid until 2017/08/13.

The use of these animals is subject to AESC guidelines for the use and care of animals, is limited to the procedures described in the application form and is subject to any additional conditions listed below:

None

Signed: _____ (Chairperson, AESC) Date: 21st August 2015

I am satisfied that the persons listed in this application are competent to perform the procedures therein, in terms of Section 23 (1) (c) of the Veterinary and Para-Veterinary Professions Act (19 of 1982)

Signed: _____ (Registered Veterinarian) Date: 21 August 2015

cc: Supervisor: N/A
Director: CAS

Works 2000/lain0015/AESCCert.wps